



WPI

Opportunities and Challenges of Low-Carbon Hydrogen via Metallic Membrane Reactors

by

Kourosh Kian

A Dissertation

Submitted to the Faculty of

Worcester Polytechnic Institute

In partial fulfillment of the requirements for the

Degree of Doctor of Philosophy

in

Chemical Engineering

May 2020

APPROVED BY:

Dr. Jennifer Wilcox, Academic Advisor
Chemical Engineering Department, WPI

Dr. Nikolaos K. Kazantzis, Committee Member
Chemical Engineering Department, WPI

Dr. John A. Bergendahl, Committee Member
Department of Civil and Environmental Engineering, WPI

Dr. Simona Liguori, Co-Advisor
Chemical Engineering Department, WPI

Dr. Michael T. Timko, Committee Member
Chemical Engineering Department, WPI

Dr. Fereshteh Rashidi, Committee Member,
Pall Corporation

Dr. Susan C. Roberts, Head of Chemical
Engineering Department, WPI

Dedication

Dedication

I would love to dedicate this work to the stars of my life, to my family! To my mother, my lovely sister and my two adorable brothers, and to the hero of my life, my late father. I want you to know that I love you from the bottom of my heart. There is not a single day that passes by and I do not think of you. You have always been there for me during these hard times. When the storms settle, you have always been the only ones I could find next to me! I wish you were here and could celebrate this moment with me. Nevertheless, your love is always present in my life and I always feel it!

Acknowledgements

First and foremost, I would like to thank my advisor, Professor Jennifer Wilcox for her unconditional support during this PhD journey. The years that I have been working under the supervision of Dr. Wilcox have been such fruitful years that have shaped both my personality, and intellectual thinking abilities. I have had the great and unique opportunities to travel across the world and learn from the experts in the academic, industry, business, and policy environments. I have been able to publish my work in very prestigious peer reviewed journals during these years. I had the opportunity to contribute as an author to some very important scientific reports including the recent report published by National Petroleum Council on carbon capture, use, and storage. It is needless to say that all these priceless opportunities have only been available to me because of the support I received from my advisor and the encouragement she gave me during this time. And for all of these, I am sincerely grateful to you from the bottom of my heart Jen.

I would like to extend my very special appreciation to my co-advisor and my mentor, Dr. Simona Liguori. I am not exaggerating by any means by saying this work was impossible without Simona's help, support, training, and passion for this work. There were so many instances of hopelessness and despair, the stormy days, desperate trials which led to nowhere, the long days of trying and getting no results in the lab! The moments that one can seriously doubt themselves and their abilities, the moments that a researcher is ready to give up! In those moments, having someone like Simona to talk to and ask for help can make a big difference. Simona, you might think it was not important, but sharing the personal stories of your PhD work with me, telling me about your struggles, and in the end, encouraging me that I could do this task, had such remarkable impact on my performance and inspired me to keep trying. We have had a very wonderful journey together. Yes, sometime the roads were a little bumpy and frustrating for both of us but in the end, what is left in my heart for you, is only love and respect.

I would like to sincerely thank my committee members: Dr. Nikolaos K. Kazantzis, Dr. Michael T. Timko, Dr. John A. Bergendahl, and Dr. Fereshteh Rashidi who have been very

Acknowledgements

supportive and helpful during these strange times that we are dealing with Covid-19. My interactions with every single one of you have been very memorable and I have learned significantly from the conversations that I have had with you all during this time. The advice and encouragement I received from all my committee members is exemplary and I am humble and grateful for all your support.

I would like to extend my gratefulness to Dr. Aaron Deskins, Dr. Nikolaos K. Kazantzis, Dr. Terri Camesano, and Dr. Susan Roberts for their exceptional support to make my move to WPI as smooth as possible. More specifically, the phenomenal support of Nick, Aaron, and Terri for transferring my credit hours and making it possible to graduate on time has been priceless. I have nothing but love and respect for you all. Thank you for everything.

I would like to acknowledge the support of two very special individuals who changed my life for good and in some ways, they are the main reason I got to know Jen and work in her group. Dr. Richard Esposito and Pamela Tomski. I had the opportunity to work as an intern with Richard and participated in a summer program that was managed by Pam: Research Experience in Carbon Sequestration (RECS). The experience I gained from working with Pam and Richard is priceless and I am so humble to have them as mentors and friends in my life. Thank you, Pam, thank you Richard, your friendship is such a blessing for me!

I would like to acknowledge the constant intellectual and emotional support I received from my colleagues during this journey. During those dark times, you were the only ones that could understand my struggle and I am really indebted to you all for constant encouragement. Caleb Woodall, H el ene Pilorg e, Nora Buggy, Christopher Caskey, Sina Soltanmohammad, James Crawford, Kasra Taghikhani, Maksim Vasilev Tyufekchiev, Ben Kolosz, Noah McQueen, thank you for everything! I can say without any hesitations that I had a lot of fun with you guys. The time we spent together playing games, watching movies, and doing some other intellectual activities were the highlights of my days!

I would like to sincerely thank Dr. Sina Soltanmohammad, Dr. Boquan Li, Dr. Alex Maag, Dr. Kenneth Xerxes Steirer, and Dr. Gary Zito for both training me on how to use the XRD

Acknowledgements

and SEM equipment and with their help with data acquisition and analysis. I would like to sincerely acknowledge the invaluable support from WPI staff including Dr. Geoffrey Tompsett for his help with the adsorption experiments. I would also like to sincerely appreciate Tom Partington for his invaluable help and support during this study. A lot of the experiments I performed in this work were not even possible without Tom's help.

I would like to acknowledge those wonderful people who worked so hard behind the scenes, who helped me on a daily basis, and went above and beyond to provide me with the necessities required for my research activities: Leslie Brodeur and Tiffany Royal, thank you for all the logistic and emotional support during this time. Your unconditional support and lovely words made a big difference on those hard days.

Also, a good portion of this PhD work was conducted in Colorado School of Mines. I made such great friends during the time in Golden Colorado, and I would like to sincerely thank all the faculty and staff in the Department of Chemical and Biological Engineering in Colorado School of Mines who supported me during my journey. It was such a precious experience and I learned a lot from professors Carolyn Koh, Ning Wu, Kevin Cash, Keith Neeves, and John Jechura. The intellectual interactions that I had with all of you have changed my perspective toward research and have left an enduring legacy on my view toward life. In addition, the daily support that I received from Jennie Gambach, Kim Luzeckyj, and Mike Stadick were priceless; you are so precious, and I am always grateful to you.

Abstract

The industrial sector is one of the largest emitters of CO₂ and a great potential for retrofitting with carbon capture systems. In this work the performance of a palladium-based membrane reactor at 400 °C and operating pressures between 100-400 kPa have been studied in terms of methane conversion, hydrogen recovery, hydrogen purity, and CO₂ emission. It is found that the MR has the potential to produce high purity hydrogen while the methane conversion values could be as high as 40% at very moderate operating conditions and without using any sweep gases.

The H₂ permeation and separation properties of two Pd-based composite membranes were evaluated and compared at 400 °C and at a pressure range of 150 kPa to 600 kPa. One membrane was characterized by an approximately 8 μm-thick palladium (Pd)-gold (Au) layer deposited on an asymmetric microporous Al₂O₃ substrate; the other membrane consisted of an approximately 11 μm-thick pure palladium layer deposited on a yttria-stabilized zirconia (YSZ) support. At 400 °C and with a trans-membrane pressure of 50 kPa, the membranes showed a H₂ permeance of $8.42 \times 10^{-4} \text{ mol/m}^2 \cdot \text{s} \cdot \text{Pa}^{0.5}$ and $2.54 \times 10^{-5} \text{ mol/m}^2 \cdot \text{s} \cdot \text{Pa}^{0.7}$ for Pd-Au and Pd membranes, respectively. Pd-Au membrane showed infinite ideal selectivity to H₂ with respect to He and Ar at 400 °C and a trans-membrane pressure of 50 kPa, while the ideal selectivities for the Pd membrane under the same operating conditions were much lower. Furthermore, the permeation tests for ternary and quaternary mixtures of H₂, CO, CO₂, CH₄, and H₂O were conducted on the Pd/YSZ membrane. The H₂ permeating flux decreased at the conclusion of the permeation tests for all mixtures. This decline however, was not permanent, i.e., H₂ permeation was restored to its initial value after treating the membrane with H₂ for a maximum of 7 h. The effects of gas hourly space velocity (GHSV) and the steam-to-carbon (S/C) ratio on H₂ permeation were also investigated using simulated steam methane reforming mixtures. It was found that H₂ permeation is highest at the greatest GHSV, due to a decline in the concentration polarization effect. Variations in S/C ratio however, showed no significant effect on the H₂ permeation. The permeation characteristics for the Pd/YSZ membrane were also investigated at temperatures ranging from 350 to 400 °C. The pre-exponential factor and

Abstract

apparent activation energy were found to be $5.66 \times 10^{-4} \text{ mol/m}^2 \cdot \text{s} \cdot \text{Pa}^{0.7}$ and 12.8 kJ/mol, respectively. Scanning Electron Microscope (SEM) and X-ray diffraction (XRD) analyses were performed on both pristine and used membranes, and no strong evidence of the formation of Pd-O or any other undesirable phases was observed.

The permeation tests with pure hydrogen and inert gases indicate that the MR is highly selective toward hydrogen and the produced hydrogen is an ultrahigh purity grade. The carbon capture experiments in the work consists of dehydrating the retentate stream and redirecting it to a 13X packed bed before analyzing the stream via mass spectrometry. The carbon capture studies reveal that approximately 5.96 mmole CO₂ (or 262.25 mg of CO₂) can be captured per g of 13X.

In this study, SEM-EDS, and XRD technics have been used to characterize the crystallography and morphology of the membrane surface. These material characterization techniques reveal that the surface of the membrane has gone through significant oxidation during the steam methane reforming reaction, although this oxidation is only limited to the few nanometers of depth through the surface of the palladium membrane.

Table of Contents

Dedication.....	i
Acknowledgements	ii
Abstract.....	v
Table of Contents	vii
Abbreviations.....	xi
Greek symbols.....	xv
List of Tables	xvi
List of Figures	xvii
Chapter 1 - Introduction	20
1.1 Research Objectives	21
1.2 Impacts	22
1.3 Organization of Dissertation.....	22
References.....	24
Chapter 2 - Literature Review.....	26
2.1 Hydrogen Properties.....	26
2.1.1 Physical and atomic properties of hydrogen.....	26
2.1.2 Chemical properties of hydrogen.....	28
2.2 Hydrogen Production	29
2.2.1 Laboratory methods for hydrogen production.....	29
2.2.2 Industrial methods for hydrogen production	30
2.3 Climate Change, Global Energy Demand, and Hydrogen Economy.....	35
2.4 Current status of hydrogen production, purification, and usage.....	40
2.4.1 Economics and scale	40
2.4.2 Current industrial production and separation technologies	45

Table of Contents

2.4.3	Hydrogen use and the role of metallic membranes.....	49
2.5	Metallic membranes and recent progress	54
2.5.1	Metallic membranes and hydrogen permeation.....	54
2.5.2	Pd-alloy membranes and costs.....	57
2.5.3	Non-Pd membranes.....	61
2.5.4	Efficient material screening.....	63
2.5.5	Theoretical studies on metallic membrane materials.....	65
2.6	Metallic membrane opportunities for next-generation applications	66
2.6.1	Small-scale industrial applications.....	66
2.6.2	Power generation and large-scale hydrogen production	67
2.6.3	Hydrogen transportation and carbon dioxide capture via membrane technology.....	69
2.7	Challenges for Pd membrane applications	71
2.7.1	Structural and chemical stability of Pd	71
2.7.2	The effect of poisoning on the performance of Pd-based MRs	73
2.7.3	Pd availability	74
2.7.4	Technical challenges and uncertainties for Pd membrane scale-up.....	75
2.7.5	Cost of Pd membrane scale-up	77
2.7.6	Hydrogen storage	78
	References.....	81
	Chapter 3 - Experimental and Methodology.....	106
3.1	Methodology.....	106
3.1.1	Equipment calibration	106
3.2	Experimental design.....	111
3.2.1	Permeation studies	111

Table of Contents

3.2.2	SMR reaction studies	114
3.2.3	Carbon capture experiments	118
3.3	Material characterization	122
	References.....	123
Chapter 4 - Hydrogen Permeation in Pd-based MRs		124
4.1	Introduction.....	124
4.2	Materials and Methods	130
4.2.1	Pd-Based Membrane	130
4.2.2	Procedure.....	131
4.2.3	Materials	134
4.3	Results and Discussion.....	135
4.3.1	Membrane Permeation Tests	135
4.3.2	Scanning Electron Microscope (SEM) Tests.....	157
4.3.3	X-ray Diffraction (XRD) Tests.....	160
	References.....	163
Chapter 5 - Carbon Capture and Hydrogen Production via MRs		171
5.1	Introduction.....	171
5.1.1	Membrane reactor for SMR.....	172
5.1.2	Principles of Pd-based MR	173
5.1.3	Operating parameters of a MR.....	175
5.1.4	CO ₂ capture.....	176
5.2	Experimental Methodology and Materials	179
5.2.1	Pd-based Membrane.....	179
5.2.2	Permeation tests	179
5.2.3	SMR reactions.....	182

Table of Contents

5.2.4	The use of 13X for capturing CO ₂ produced by SMR reaction in the MR183	
5.2.5	Membrane characterization	186
5.2.6	Materials	187
5.3	Results and Discussion	188
5.3.1	Hydrogen permeation	188
5.3.2	Steam Methane Reforming Reaction	190
5.3.3	Breakthrough analysis	201
5.3.4	Membrane integrity and characterization	204
	References	212
	Chapter 6 - Technoeconomic Analysis	217
	References	234
	Chapter 7 - Conclusions and Recommendations	239

Abbreviations

A_{active}	active surface area of the membrane [m^2]
A_{cs}	molecular cross-sectional area of the adsorbate molecules [m^2]
AR	air reactor
BCC	body-centered cubic
BECCS	bioenergy with carbon capture and storage
BET	Brunauer–Emmett–Teller
CAC	cost of CO_2 avoided [$\text{\$}\cdot\text{tonne}^{-1}$]
CAES	compressed air energy storage
CAPEX	capital expenditure [$\text{\$}$]
CCUS	carbon capture, utilization, and storage
CLC	chemical looping combustion
CO_2e	CO_2 equivalent [tonne]
CR	conventional reactor
d	interplane spacing [m]
D_{H}	diffusivity of hydrogen [$\text{m}^2\cdot\text{s}^{-1}$]
DOE	Department of Energy
DR	Dubinin–Radushkevich
E_0	characteristic energy of a standard adsorbate [$\text{J}\cdot\text{mol}^{-1}$]
E_{a}	apparent activation energy [$\text{J}\cdot\text{mol}^{-1}$]
EIA	International Energy Agency
E_1	activation energy barrier [$\text{J}\cdot\text{mol}^{-1}$]
E_{L}	energy associated with condensation to a liquid phase [$\text{J}\cdot\text{mol}^{-1}$]
EDS	energy dispersive spectroscopy
ESR	ethanol steam reforming
F	Faraday constant [$9.6485\times 10^4 \text{ C}\cdot\text{mol}^{-1}$]
FCC	face-centered cubic
FCI	fixed capital investment
FR	fuel reactor

Abbreviations

FTR	fired tubular reforming
GHG	greenhouse gas
HDI	human development index
HFC	hydrofluorocarbons
HFCV	hydrogen fuel cell vehicle
HPP	hydrogen purity of permeate
HR	hydrogen recovery
HTS	high temperature shift
IAMs	integrated assessment models
ICE	internal combustion engines
IGCC	integrated gasification combined cycle
IPCC	intergovernmental panel on climate change
IRR	internal rate of return
J_{H_2}	hydrogen permeating flux [$\text{mol}\cdot\text{m}^{-2}\cdot\text{s}^{-1}$]
K	equilibrium constant
k_a	rate constant for adsorption
k_d	rate constant for desorption
L_{active}	active length of the membrane [m]
LCOH	levelized cost of hydrogen [$\text{\$}\cdot\text{Nm}^{-3}$]
LTS	low temperature shift
m	mass of the adsorbent [kg]
MA-CLR	membrane assisted chemical looping reforming
MDEA	methyl-di-ethanolamine
MEA	mono-ethanolamine
MMBtu	million British thermal units [Btu]
MPS	microwave plasma source
MR	membrane reactor
MS	mass spectrometer
MW	molecular weight [$\text{g}\cdot\text{mol}^{-1}$]
N	Avogadro's number [6.023×10^{23} molecules $\cdot\text{mole}^{-1}$]
NGCC	natural gas combined cycle

Abbreviations

NPV	net present value [\\$]
OD	outer diameter [m]
p	absolute pressure [Pa]
P2H	power-to-hydrogen
P2M	power-to-methane
P2X	power-to-x
p_{c1}	probability of fluid particles condensing upon collision with layer1
p_{c2}	probability of fluid particles condensing upon collision with layer 2
Pd	palladium
Pe^0	pre-exponential factor [$\text{mol}\cdot\text{m}^{-1}\cdot\text{s}^{-1}\cdot\text{Pa}^{-0.5}$]
PEC	photoelectrochemical
Pe_{H2}	permeability of the membrane toward hydrogen [$\text{mol}\cdot\text{m}^{-1}\cdot\text{s}^{-1}\cdot\text{Pa}^{-0.5}$]
PEM	proton exchange membrane
PEMFC	proton exchange membrane fuel cell
PGMs	platinum-group metals
$p_{H2,perm}$	partial pressure of hydrogen in the permeate side [Pa]
$p_{H2,ret}$	partial pressure of hydrogen in the retentate side [Pa]
PHS	pumped hydro energy storage
ppm	parts per million
P_s	standard pressure [Pa]
PSA	pressure swing adsorption
PSS	porous stainless steel
PTFE	polytetrafluoroethylene
PV-E	photovoltaic electrolysis
Q_{CH4}^{IN}	molar flow rate of methane entering the reactor [$\text{mol}\cdot\text{s}^{-1}$]
Q_{CH4}^{OUT}	molar flow rate of methane leaving the reactor [$\text{mol}\cdot\text{s}^{-1}$]
Q_F	feed volumetric flow rate at standard conditions [$\text{m}^3\cdot\text{s}^{-1}$]
$Q_{H2}^{Permeate}$	molar flow rate of hydrogen in the permeate side [$\text{mol}\cdot\text{s}^{-1}$]
$Q_{H2}^{Retentate}$	molar flow rate of hydrogen on the retentate side [$\text{mol}\cdot\text{s}^{-1}$]
$Q_{Total}^{Permeate}$	total molar flow rate of all gaseous species on the permeate side [$\text{mol}\cdot\text{s}^{-1}$]
R	universal gas constants [$\text{J}\cdot\text{mol}^{-1}\cdot\text{K}^{-1}$]

Abbreviations

RD&D	research, design, and development
S	apparent surface area [m ²]
SAR	steam alcohol reforming
S _H	selectivity of hydrogen
SMR	steam-methane reforming
SOEC	solid oxide electrolysis cells
SWOT	strengths, weaknesses, opportunities, threats
t	time [s]
T	absolute temperature [K]
T&D	transmission and distribution
t _b	breakthrough time [s]
TCI	total capital investment [\$]
TRL	technology readiness level
T _s	standard temperature [K]
t _{ss}	stoichiometric (steady state) time [s]
V	volume [m ³]
v ₁	vibrational frequency of the adsorbate normal to layer 1 [Hz]
v ₂	vibrational frequency of the adsorbate normal to layer 2 [Hz]
W	mass of adsorbed gas per gram of sample [g]
WACC	weighted average cost of capital
WGS	water-gas shift
W _m	mass of adsorbed gas per gram of sample for complete monolayer coverage [g]
X _{CH₄}	methane conversion
X _{CO}	carbon monoxide conversion
XRD	X-ray diffraction
y	mole fraction
y _{CO₂}	mole fraction of carbon dioxide

Greek symbols

α	ideal selectivity
β	affinity coefficient
δ	membrane thickness [m]
ε	porosity
η	viscosity
θ	X-ray glancing angle [Radians]
λ	wavelength [m]
μ_k	shape factor associated with Knudsen flow
μ_m	micrometer
μ_v	shape factor associated with viscous flow
φ	fraction of the bed volume saturated at breakthrough
ϕ	ratio of the number of occupied adsorption sites to the number of available adsorption sites

List of Tables

- Table 2-1. Physical properties of hydrogen (adapted from [1])
- Table 2-2. Comparison of Hydrogen Separation Technologies[67,68]
- Table 2-3. Specific energy density of various fuels (adapted from [1])
- Table 2-4. Comparison between various methods for energy storage (adapted from the 2015 IEA report: Technology Roadmap: Hydrogen and Fuel Cells) [101]
- Table 2-5. U.S. DOE 2015 targets for hydrogen separation and purification by dense metallic membranes[132]
- Table 2-6. Properties of the Pd-based membranes available in the open literature
- Table 2-7. Properties of the group V metal-based membranes available in the open literature
- Table 2-8. Volumetric energy density of various fuels (adapted from [1])
- Table 3-1 Calibration parameters for various MFCs
- Table 4-1 Gas mixtures fed into the Pd and Pd-Au MRs at 400 °C for permeation tests.
- Table 4-2 Gas mixtures fed into the Pd and Pd-Au MRs at 400 °C for permeation tests.
- Table 4-3 Ideal Selectivity of H₂ with respect to He and Ar under various pressures at 400 °C for composite Pd and Pd-Au membranes.
- Table 4-4 XRD analysis for Pd and Pd-Au MRs at 400 °C.
- Table 5-1. Dimensions of the MR used for SMR reactions
- Table 5-2. Parameters used in BET method calculations
- Table 5-3. BET adsorption data for CO₂ at 273.15K
- Table 5-4. BET adsorption data for N₂ at 77.35K
- Table 5-5. Parameters used in DR method calculations
- Table 5-6. DR adsorption data for CO₂ at 273.15 K
- Table 5-7. DR adsorption data for N₂ at 77.35 K
- Table 5-8. EDS peaks and compositions for intact and used membranes
- Table 5-9. XRD analysis of the Pd-based MR
- Table 6-1. Benefits, Drawbacks and Costs of different Hydrogen Production Technologies

List of Figures

Figure 2-1. Comparison of the per capita electricity consumption for various nations with different HDI

Figure 2-2. Breakdown of global energy-related CO₂e emissions in 2016: a) Emissions associated with each sector¹; b) Emissions associated with the transport sub-sector by mode² (¹ Others include domestic waterborne, pipeline, and HFC & indirect N₂O; ² Due to lack of information on other nations, the transport sub-sector represents only the U.S. emission values) [6,7]

Figure 2-3. Breakdown of the global hydrogen market sectors (left) and further breakdown of chemical industry sector (right). [33]

Figure 2-4. Conventional steam reforming process with multiple stages for H₂ production.

Figure 2-5. Share of hydrogen consumption in various industries (adapted from [1])

Figure 2-6. Abundance and cost of the most commonly used metals for the fabrication of Pd-based membranes (Each price is referred to 2019. Price of titanium is based on TiO₂ with a minimum purity of 95%; price of yttrium is based on yttrium metal with minimum purity of 99.9%; price of vanadium is based on the vanadium pentoxide)

Figure 2-7. Hydrogen permeability through Pd alloy membranes at 350 °C and 2.2 MPa (adapted from Knapton assuming hydrogen as an ideal gas and atmospheric pressure on the permeate side)[135]

Figure 3-1. MFC calibration for CH₄

Figure 3-2. MS calibration for the CH₄/Ar pair

Figure 3-3. Image of the Pd membrane and membrane module

Figure 3-4. Schematic of the MR setup

Figure 3-5. Schematic of the MR setup with inclusion of zeolite 13X for CO₂ capture

Figure 3-6. Isothermal CO₂ adsorption based on the Langmuir model

Figure 4-1 Schematic of the experimental setup.

Figure 4-2 Permeating flux of H₂ vs. trans-membrane pressure at 400°C and various values of n for (a) Pd membrane (b) Pd-Au membrane.

Figure 4-3 Arrhenius plot representing the permeation flux of pure H₂ in a Pd/Al₂O₃ at a trans-membrane pressure of 100 kPa.

List of Figures

Figure 4-4 Influence of temperature on the (a) permeating flux of H₂ (b) ideal selectivity of H₂ to Ar.

Figure 4-5 Influence of inert gases on the permeation flux of H₂ in (a) Pd/YSZ and (b) Pd-Au/Al₂O₃ membranes.

Figure 4-6 Influence of feed flow rate on the permeation flux of H₂ in (a) Pd/YSZ and (b) Pd-Au/Al₂O₃ membranes.

Figure 4-7. Influence of impurities on the permeation flux of H₂ in (a) Pd/YSZ and (b) Pd-Au/Al₂O₃ membranes.

Figure 4-8 H₂ permeation flux in ternary gas mixtures using Pd/YSZ membrane.

Figure 4-9 H₂ permeation flux in simulated SMR stream using Pd/YSZ membrane.

Figure 4-10 Influence of GHSV on the H₂ permeating flux using Pd/YSZ membrane.

Figure 4-11 Influence of S/C ratio on the H₂ permeating flux using Pd/YSZ membrane.

Figure 4-12 SEM image of the Pd-Au membrane before (a,b) and after the permeation tests (c,d).

Figure 4-13 SEM image of the Pd membrane after the permeation tests at various magnifications: (a) X500 (b) X2,000 and (c) X25,000

Figure 4-14 EDS analysis of the surface composition for Pd (a,c), and Pd-Au (b,d) membranes.

Figure 4-15 XRD analysis of Pd/YSZ and Pd membranes after the permeation tests.

Figure 5-1. Schematic of a MR for SMR or SAR process (taken from Anzelmo et al.) [18]

Figure 5-2. Schematic of the experimental setup (a); image of the MR used for SMR studies (b)

Figure 5-3. Permeation flux of H₂ vs. trans-membrane pressure at 400°C and various values of n

Figure 5-4. Effect of the reaction pressure on methane conversion

Figure 5-5. Effect of the reaction pressure on hydrogen recovery

Figure 5-6. Adsorption isotherms for CO₂ (at 273.15K) and N₂ (at 77.35K)

Figure 5-7. DR adsorption isotherms for CO₂ (at 273.15K) and N₂ (at 77.35K)

Figure 5-8. breakthrough curve for CO₂ adsorption on 13X at atmospheric pressure and 298.15K

Figure 5-9. MR Pd-13 after the conclusion of the SMR reaction

List of Figures

Figure 5-10. SEM images of the intact membrane MR that has not been exposed to SMR reactions

Figure 5-11. SEM images of the MR after the conclusion of the SMR reaction

Figure 5-12. EDS analysis of the a) intact and b) used MRs

Figure 5-13. XRD analysis of the a) intact and b) used MRs

Figure 6-1. Schematic of an MR for SMR or SAR process (taken from Anzelmo et al.)

Figure 6-2. Hydrogen production cost and price sensitivity of various technologies (adapted from the 2019 IEA report: The Future of Hydrogen: Seizing today's opportunities)

Figure 6-3. CO₂ emissions associated with various technologies for hydrogen production (adapted from the 2019 IEA report: The Future of Hydrogen: Seizing today's opportunities)

Chapter 1 - Introduction

Non-renewable fossil fuels comprise 80% of the energy portfolio in the U.S. [1] Burning fossil fuels releases significant amounts of CO₂ into the atmosphere. Climate change effects can be mitigated through the development of state-of-the-art carbon capture technologies, reduction of fossil fuel consumption by utilizing more efficient industrial processes, switching to less carbon-intensive fuels, and the use of renewable carbon-free energy resources.[2] Hydrogen can be used as a replacement fuel for gasoline to help mitigate the Greenhouse Gas (GHG) effects and improve air quality. This change from gasoline-fueled to hydrogen-fueled vehicles or for a stationary system can be the pivotal element of the transformation of the world's transportation system. Unfortunately, hydrogen does not occur naturally. However, steam methane reforming (SMR) remains the most widely used industrial process for hydrogen generation which accounts for 50% of the global hydrogen production.[3] SMR takes place under very harsh operating conditions (i.e., 800 - 1000 °C and 1.5 - 2.0 MPa) due to thermodynamic constraints. Generated hydrogen is later separated and purified by several steps among them pressure swing adsorption (PSA) process is a highly energy-intensive process.[4] The membrane reactor (MR) technology is an alternative method that can be used to perform the SMR reaction at milder operating temperatures. MR combines the advantages of catalytic reactors such as catalyst bed uniformity, and improved heat and mass transfer rates, with the advantages of selective membranes to increase methane conversion and hydrogen recovery. Specifically, by placing a metallic membrane inside the reactor, hydrogen is continuously removed from the reaction zone (retentate side) through the membrane.[5] The continuous withdrawal of hydrogen shifts the reaction toward further production of hydrogen according to Le Chatelier's principle.[6] A membrane with infinite permeability toward hydrogen will allow for a collection of a pure stream of hydrogen on the permeate side. Collecting pure hydrogen on the permeate side, will cause the partial pressure of CO₂ to increase in the retentate side and decrease the minimum thermodynamic work required for CO₂ capture.[7] All of these advantages will allow for simultaneous production of a highly concentrated stream of hydrogen and separation of CO₂ in one single unit. As a result, a significant reduction in capital and operational costs of reforming and capture processes

may occur. Palladium-based (Pd) metallic membranes are the best candidates for the production of high purity hydrogen due to their ‘*infinite*’ selectivity towards hydrogen permeation.[8] However, the high cost of Pd (\$15,400 per pound [9]) makes it unattractive for industrial-scale applications.[10] Furthermore, pure Pd-membrane is susceptible to poisoning due to existence of impurities in the feed stream such as H₂S, CO, and CO₂. Alloying Pd with Transition Metals (TM, e.g., Ag, Au, Cu, Mo, Ta, Y) can significantly decrease the membrane cost while maintaining the features of the membrane and improve its resistivity against the impurities. [11] In particular, composite membranes consisting of Pd-Cu, Pd-Ag, and Pd-Au have been studied intensively due to their significant resistance against sulfidization [12-14].

1.1 Research Objectives

The research presented in this dissertation was undertaken to investigate the performance of the Pd-based membrane reactors for production of green hydrogen and capture of carbon dioxide. The specific objectives of this research can be summarized as following:

- Objective 1: Study of the performance of Pd and Pd/Au membranes under various operating conditions and in the presence of other reaction gases
- Objective 2: Study of the performance of Pd and Pd/Au membranes at various temperatures ranging from 350 to 450 °C and various operating pressures ranging from 150 kPa to 600 kPa, in terms of the hydrogen permeating flux and formation of undesirable phases due to membrane poisoning.
- Objective 3: Investigating the influence of various gaseous compounds, specifically He, Ar, N₂, CH₄, CO₂, CO, and superheated steam, on the hydrogen permeating flux
- Objective 4: Experimental investigation of four major mechanisms that adversely affect the hydrogen permeating flux, namely: concentration polarization, dilution, depletion, and competitive adsorption on the Pd surface
- Objective 5: Conducting the SMR reaction in Pd-based MR

Introduction

- Objective 6: Identifying the optimal operating conditions of the SMR reaction in terms of methane conversion, and hydrogen recovery, and hydrogen purity
- Objective 7: Investigation of the potential for CO₂ capture in a MR system under the optimal operating condition (identified in objective 6)
- Objective 8: Technoeconomic analysis of MR system for simultaneous hydrogen production and carbon capture

1.2 Impacts

The MR technology has proven to be able to produce high-purity hydrogen streams at lower operating temperatures and pressures compared with traditional reactors that can be used as a carbon-free fuel in hydrogen-fuel cell vehicles. In addition, promoting carbon capture technology via membrane separation is a significant contribution of this work, which helps to mitigate CO₂ emissions associated with industrial SMR.

1.3 Organization of Dissertation

This PhD dissertation is composed of seven chapters. Chapter 1 lays out the introduction and motivation behind this work. In Chapter 2 a deep and thorough evaluation of the Pd-based membranes and MRs is undertaken. This chapter could be used as a standalone document to familiarize the interested audience to the field. In Chapter 3 the methodology, equipment, and techniques used in each step of this research are explained in detail.

Chapter 4 discusses in detail how the permeation tests were conducted and explains the theoretical reasons why various reaction gases may impede the permeating flux of hydrogen in a MR system. This chapter is one of the few experimental works that fundamentally evaluates the four famous mechanisms for hindering of hydrogen flux. Objectives 1 through 4 which were mentioned earlier, are met and explained in Chapter 4.

In Chapter 5 the details of the SMR reaction and the influence of operating conditions on the performance of MR in terms of methane conversion, hydrogen recovery, and hydrogen

Introduction

purity are discussed, and the optimal operating conditions based on these metrics are identified. Next, the carbon capture experiments, and subsequent results are using solid sorbents (zeolite 13X) are discussed. Objectives 5 through 7 are met and explained in Chapter 5.

Chapter 6 examines the hydrogen economy as it relates to carbon capture, not from a technical perspective, but rather, through a technical and economic lens. In this chapter, the technoeconomic evaluation of MR for hydrogen production and carbon capture are presented and the role of hydrogen in our future energy portfolio is discussed.

Finally, Chapter 7 discussed the major findings and conclusion of this work and proposes some recommendations for future work.

References

- [1] Annual Energy Outlook, Energy Information Administration (EIA), U.S. Department of Energy, Washington, D.C., (2014).
- [2] S. Plasynski, J. Litynski, H. McIlvried, R. Srivastava, Progress and new developments in carbon capture and storage, *Critical Reviews in Plant Science*, 28 (2009) 123-138.
- [3] A. Iulianelli, S. Liguori, J. Wilcox, A. Basile, Advances on methane steam reforming to produce hydrogen through membrane reactors technology: A review, *Catalysis Reviews*, 58 (2016) 1-35.
- [4] B. Anzelmo, On-board Hydrogen Production from Natural Gas Via a Metallic Pd-based Membrane Reactor, in, Stanford University, 2016.
- [5] A.-E.M. Adris, A fluidized bed membrane reactor for steam methane reforming: experimental verification and model validation, in, University of British Columbia, 1994.
- [6] M. Sjardin, K.J. Damen, A. Faaij, Techno-economic prospects of small-scale membrane reactors in a future hydrogen-fuelled transportation sector, *Energy*, 31 (2006) 2523-2555.
- [7] J. Wilcox, Carbon capture, Springer Science & Business Media, 2012.
- [8] G.S. Burkhanov, N.B. Gorina, N.B. Kolchugina, N.R. Roshan, D.I. Slovetsky, E.M. Chistov, Palladium-based alloy membranes for separation of high purity hydrogen from hydrogen-containing gas mixtures, *Platinum Metals Review*, 55 (2011) 3-12.
- [9] APMEX Gold and Silver Prices in USA, <https://www.apmex.com/spotprices/palladium-price>, (2017).
- [10] Metal prices in the United States through 2010: U.S. Geological Survey Scientific Investigations Report, U.S. Geological Survey, (2013).
- [11] M. Dolan, Non-Pd BCC alloy membranes for industrial hydrogen separation, *Journal of Membrane Science*, 362 (2010) 12-28.
- [12] F. Borgognoni, S. Tosti, M. Vadrucci, A. Santucci, Pure hydrogen production in a Pd–Ag multi-membranes module by methane steam reforming, *International journal of hydrogen energy*, 36 (2011) 7550-7558.

Introduction

[13] A. Brunetti, A. Caravella, E. Drioli, G. Barbieri, Process Intensification by Membrane Reactors: High-Temperature Water Gas Shift Reaction as Single Stage for Syngas Upgrading, *Chemical Engineering & Technology*, 35 (2012) 1238-1248.

[14] T. Peters, M. Stange, H. Klette, R. Bredesen, High pressure performance of thin Pd–23% Ag/stainless steel composite membranes in water gas shift gas mixtures; influence of dilution, mass transfer and surface effects on the hydrogen flux, *Journal of membrane science*, 316 (2008) 119-127.

Chapter 2 - Literature Review

This chapter provides a thorough overview of hydrogen properties, the technologies used to produce hydrogen, and the opportunities and challenges of metallic membranes for hydrogen production. The comprehensive literature review presented in this chapter along with some of the results obtained in Chapter 6, have been accepted as a peer reviewed article in the journal of “Progress in Energy and Combustion Science” under the title “**Opportunities and Challenges of Low-Carbon Hydrogen via Metallic Membranes**”.

2.1 Hydrogen Properties

In order to produce hydrogen through industrial processes, or to utilize hydrogen as a fuel (energy carrier) one needs to understand its physiochemical properties for better design and safe handling of the appropriate production units or storage facilities. This section gives an overall overview of hydrogen, its applications, and some of its more important chemical and physical properties.

2.1.1 Physical and atomic properties of hydrogen

Hydrogen is the lightest element on the periodic table with an atomic number of 1. The word “hydrogen” is derived from Greek words *hydro* meaning water and *genes* meaning forming. Hydrogen was first discovered and collected as a unique gas by Robert Boyle in 1671 through dissolving iron in diluted hydrochloric acid. However, the English chemist Henry Cavendish was the one who first discovered and recognized hydrogen as an element in 1766.

Hydrogen is the simplest element in the periodic table which is made up of a nucleus with a positively charged proton and only one electron. Depending on the number of neutrons in the nucleus, hydrogen can have three different isotopes namely protium, deuterium, and tritium. Protium (^1H) has a nucleus which consists of only one proton and its abundance in the nature is more than 99.985%. Deuterium (^2H or D_2) is the heavy and stable isotope of

Literature Review

hydrogen which has a nucleus that consists of one proton and one neutron and is approximately 0.015% abundant in the nature. Tritium (^3H or T) is the unstable and radioactive isotope of hydrogen which is very rare in nature however can be artificially produced within a nuclear reactor. Tritium's nucleus has one proton and two neutrons.

Hydrogen is a colorless, odorless, and non-poisoning gas at room temperature and under atmospheric pressure. Hydrogen is a highly reactive atoms since there is only a single electron orbiting its nucleus. As a result, hydrogen exists in nature only in the form of hydrogen molecules H_2 . Hydrogen has a very high adsorption capacity, and is highly soluble in water, alcohol, and ether. Hydrogen has a boiling point of $-252.8\text{ }^\circ\text{C}$ below which it becomes an odorless, transparent liquid. Liquid hydrogen is not corrosive but is considerably reactive. The physical properties of hydrogen are summarized in Table 2-1.

Table 2-1. Physical properties of hydrogen (adapted from [1])

Property	Value
Molecular weight	2.016 g/mol
Melting point	$-259\text{ }^\circ\text{C}$
Liquid density (at 1.013 bar and boiling point)	70.973 kg/m^3
Boiling point (1.013 bar)	$-252.8\text{ }^\circ\text{C}$
Latent heat of vaporization (at 1.013 bar and boiling point)	454.3 kJ/kg
Critical temperature	$-240\text{ }^\circ\text{C}$
Critical pressure	12.98 bar
Critical density	30.09 kg/m^3
Triple point temperature	$-259.3\text{ }^\circ\text{C}$
Triple point pressure	0.072 bar
Gas density (at 1.013 bar and boiling point)	1.312 kg/m^3
Gas density (at 1.013 bar and $15\text{ }^\circ\text{C}$)	0.085 kg/m^3
Compressibility (Z) factor (at 1.013 bar and $15\text{ }^\circ\text{C}$)	1.001
Specific gravity (at 1.013 bar and $21\text{ }^\circ\text{C}$)	0.0696
Specific heat capacity at constant pressure (C_p) (at 1.0 bar and $25\text{ }^\circ\text{C}$)	0.029 kJ/(mol.K)
Specific heat capacity at constant volume (C_v) (at 1.0 bar and $25\text{ }^\circ\text{C}$)	0.021 kJ/(mol.K)
Viscosity (at 1.013 bar and $15\text{ }^\circ\text{C}$)	0.0000865 poise
Thermal conductivity (at 1.013 bar and $0\text{ }^\circ\text{C}$)	168.35 mW/(m.K)
Solubility in water (at 1.013 bar and $0\text{ }^\circ\text{C}$)	0.0214 vol/vol
Concentration in air (at 1.013 bar and $0\text{ }^\circ\text{C}$)	0.00005 vol.%
Autoignition temperature	$560\text{ }^\circ\text{C}$
Flame temperature	$2318\text{ }^\circ\text{C}$

2.1.2 Chemical properties of hydrogen

Hydrogen is not very reactive at room temperature and atmospheric pressure. However, at high temperatures, hydrogen becomes very reactive and the molecular hydrogen dissociates into its atoms. Atomic hydrogen on the other hand, is highly reactive and a very strong reducing agent even at room temperature. Due to the high reactivity of its nature, hydrogen can form compounds with *all* the known elements except for the noble gases. Hydrogen has an electronegativity of 2.2 which enables it to act as an electron receiver when reacting with the metals such as Na, and Ca to form ionic salt compounds or metal hydrides. It can also act as an electron donor when reacting with non-metal elements such as S, N, and halogens and forms covalent bonds. Hydrogen can also form a wide variety of organic compounds when reacting with carbon. The high ability of hydrogen to form such a wide variety of compounds can be explained by its unique $1s^1$ electron configuration. This half-full valence shell will allow hydrogen to receive one electron and become H^- , the hydride ion, which can readily form salts when reacting with group 1 and group 2 metals such as Na, and Ca or donate one electron and become H^+ , which can strongly attract halogen atoms and form acids. In addition, hydrogen can share one electron of its valence shell with other atoms such as carbon in the form of covalent bonds.

One of the most important properties of hydrogen is its ability to provide very strong intermolecular attraction forces called hydrogen bonds. Hydrogen bonding occurs between the molecules containing hydrogen, where the hydrogen atom is directly attached to a small, highly electronegative atoms such as oxygen, nitrogen, or fluorine. Although the hydrogen bond is only 5% as strong as the covalent bond, bonding of large number of molecules together via the hydrogen bonds can create a very strong molecular organisms such as proteins and nucleic acids. This unique property of hydrogen is used in various industrial applications in order to produce useful products such as the formation of salts known as metal hydrides, reduction of metal oxides to produce pure metals, catalytic reduction of nitrogen in the Haber-Bosch process to produce ammonia, reduction of halogens to produce hydrogen halides or acids, etc.

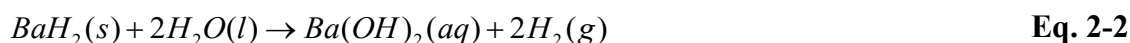
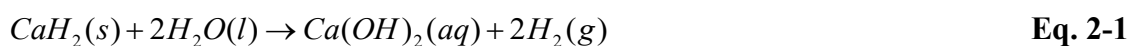
2.2 Hydrogen Production

Hydrogen is the most abundant element in the universe making up approximately 90% of its atoms. Hydrogen nuclei combine with each other in the stars, including in the earth's sun, in a very high-energy nuclear reaction and form helium atoms. This nuclear reaction is responsible for the significant heat and light emitting from the stars. Despite its abundance in the universe, hydrogen is rarely found in the pure form on earth. The reason why hydrogen cannot be found freely in nature are twofold. First, hydrogen is extremely light, and it easily escapes the earth's atmosphere. Second, hydrogen is extraordinarily reactive and has a high affinity to form more stable chemical compounds such as water, minerals, hydrocarbons, etc. Hence, for industrial and commercial applications, hydrogen must be produced using other techniques such as water electrolysis or steam reforming. Hydrogen can be produced through very simple processes on a lab scale or through more complicated processes in an industrial setting.

2.2.1 Laboratory methods for hydrogen production

The most common methods for production of hydrogen in a laboratory are the following:

- Reaction of a metal hydride with water:



Reaction of certain metals with dilute sulfuric acid or hydrochloric acid:



Reaction of a strong base in aqueous solution with aluminum:



2.2.2 Industrial methods for hydrogen production

There are numerous methods for industrial production of liquid and gaseous hydrogen. Depending on factors such as availability of raw materials, the market demand, cost, availability of the underlying technologies, etc. These methods could be categorized into two major groups: fossil-based hydrogen and hydrogen from renewable energy.

2.2.2.1 Production of hydrogen from fossil resources

Fossil fuels such as coal, oil, and natural gas have played an important role in the development of nations after the industrial revolution. In this section, the methods for the production of hydrogen using fossil fuels are briefly described.

2.2.2.1.1 Coal gasification and steam reforming of natural gas

The most widely methods for production of hydrogen are gasification of coke or combustion of natural gas, or other light hydrocarbons such as methane, ethane, and propane, with steam in the presence of a catalyst.



Coal gasification and steam reforming of natural gas occur at temperatures ranging between 1,100-1,300 °C and 700-925 °C respectively. These reactions are strongly endothermic, and the heat of reaction is provided by combustion of the fossil fuels. The conversion of coke and natural gas can be increased by sending the CO to another reactor, called water gas shift (WGS) reactor. WGS reaction is performed over iron or cobalt based catalysts at approximately 400 °C as shown in Eq. 2-8.



In the final stage, the exit stream of the reaction is sent to the purifying unit where hydrogen is separated from CO₂ using one of the various techniques such as pressure swing adsorption (PSA), wet scrubbing, membrane technologies, cryogenic distillation, etc. The details of steam methane reforming are explained in Chapter 5.

2.2.2.1.2 Partial oxidation of hydrocarbons

Partial oxidation is the process of converting the heavy hydrocarbons such as naphtha, petroleum coke, or coal into a mixture of H₂, CO, and CO₂ using superheated steam and reduced amount of oxygen. The external energy required for this process can be obtained through the combustion of the feedstock. Hydrogen yield can be maximized by utilizing a WGS as explained before in the steam reforming process. The overall efficiency of the partial oxidation process could be as high as 50%.

2.2.2.1.3 Thermal decomposition/cracking of methane

Thermal cracking of methane is an endothermic process in which methane gas is decomposed into carbon and hydrogen as following:



In this process, a mixture of methane/air heats a furnace to temperatures around 1,400 °C. at this point, the flame is shut off and the furnace is allowed to cool down to temperatures around 800 °C while methane is constantly decomposing into hydrogen gas and carbon black. Carbon black can be separated from the hydrogen which can be used as a fuel, a filler in the tire industry, or as a reducing material in the metallurgic industries. The main

Literature Review

advantage of the thermal cracking of methane over the SMR process is the significant reduction in CO₂ emissions.

2.2.2.1.4 Petroleum refining

Hydrogen can be collected from a wide range of chemical reactions in the petroleum refining processes in the forms of purge gas, tail gas, and fuel gas. For instance, in the process of converting hexane to benzene, hydrogen can be collected according to the following reaction:



2.2.2.1.5 Ammonia decomposition

Ammonia molecules can be broken down into their building components, namely hydrogen and nitrogen in a catalytic reaction at temperatures as high as 1,000 °C according to the following reaction:



The reaction products are molecular hydrogen and atomic nitrogen which can be used as a protective atmosphere for applications in the metal industry such as brazing or bright annealing.

2.2.2.1.6 Water electrolysis

Electrolysis of water is a process that uses electricity to transform water into its building elements, namely hydrogen and oxygen. This process, is composed of the following two half reactions:

Literature Review



The overall chemical reaction for water electrolysis can be written as a combination of the two half-reactions as follows:[2,3]



Depending on the type of electrolyte used in the electrolysis cells, various types of electrolyzer can be used for this process. Some of the more widely used electrolyzers used in the water electrolysis process are alkaline electrolyzers, polymer electrolyte membrane electrolyzers, solid oxide electrolyzers, seawater electrolyzers, and solar powered electrolyzers.

2.2.2.2 Production of hydrogen from renewable resources

All the conventional technologies for production of hydrogen from fossil fuel feedstocks have serious environmental and health impacts including air and water pollution, ozone depletion, climate change and global warming. Hence, scientists are constantly looking for new ways of producing hydrogen to mitigate these negative impacts.

Furthermore, rising energy prices have attracted alternative and cheaper renewable energies that could help shifting the global energy portfolio toward a more sustainable and less carbon intensive energy mix. However, one of the greatest shortfalls of electric energy is the inability to store large quantities of electricity in an effective and economically viable way. As a result of this, the full capacity of renewable energies such as wind and solar, have never been fully realized. There are some methods to store electric energy such as electric battery packs, flywheels pneumatic, and hydraulic storage methods. However, all these methods consume a lot of energy during the conversion cycles and impose pertinent

Literature Review

environmental risks. However, the renewable electric energy from wind, solar, nuclear, and biomass sources can be efficiently stored in the form of “renewable hydrogen”.

2.3 Climate Change, Global Energy Demand, and Hydrogen Economy

The generation of carbon-free electricity and the production of low-carbon fuels are urgent needs that must be addressed as the global concentration of anthropogenic carbon dioxide (CO₂) emissions is rapidly increasing. According to the most recent report published by the International Energy Agency (IEA) in 2018, the global energy-related CO₂ emissions increased by 1.7% compared to 2017 and rose to the historic high value of 33.1 Gt CO₂. [4]

Although CO₂ emissions from all sectors increased consistently, the power sector alone accounted for two-thirds of emission growth. The amount of CO₂ emissions by burning coal for power generation exceeded 10 Gt. Notably, only three countries, China, India, and the U.S., were responsible for more than 85% of the net emission increases in 2018. For China and India this can be attributed to their constant economic development. For the U.S. however, other than a steady increase in oil consumption and higher economic growth in 2018, other factors such as changes in energy policy and withdrawal from the Paris Agreement may play a role in the increase of emissions. [5] Nevertheless, longer term emission studies could reveal the magnitude and importance of the impact that such a change in U.S. policy will have in terms of the nation's CO₂ emissions.

One method of forecasting the CO₂ emissions of various countries is by examining their Human Development Index (HDI) and per capita electricity consumption. The HDI analysis of various countries shows that there is a direct relationship between the energy consumption of a nation and its HDI. As shown in Figure 2-1, the countries that have an HDI value of more than 0.9 consume the greatest energy per capita. For example, China and India consume 4,292 and 818 kWh/year-person, respectively, while this number is close to 12,000 kWh/year-person for the U.S. The minimum energy requirement for a country to have an HDI of at least 0.9 is approximately 5,000 kWh/year-person, which is associated with the U.K.; therefore, if all the developed countries in the world with an HDI of 0.9 and above reduce their electricity consumption to 5,000 kWh/year-person and only India and China increase theirs to the same amount, this results in a net annual increase of

2.4 Gt in CO₂ emissions. Hence, as long as countries rely on fossil fuels for generating their electricity without implementing carbon capture and sequestration units, the global CO₂ emissions are only going to rise in the coming decades.

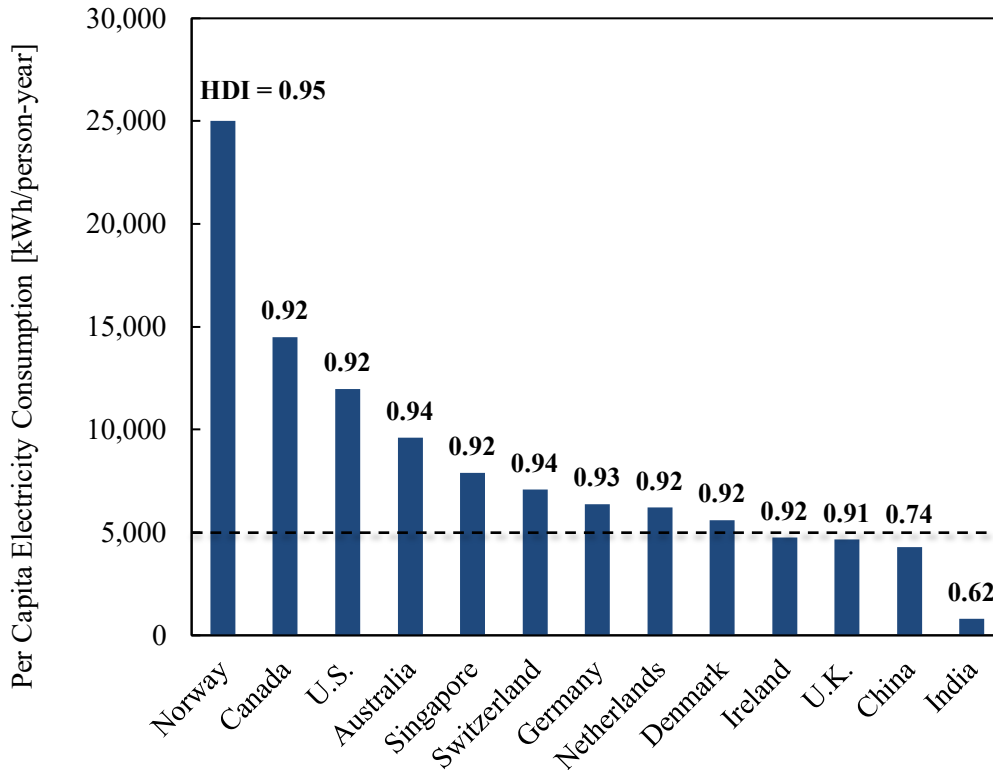


Figure 2-1. Comparison of the per capita electricity consumption for various nations with different HDI

Despite constant improvements in fuel efficiency, development of less carbon intensive biofuels, developments in hybrid and electric vehicles, and more stringent environmental policies, global CO₂ emissions from transport sector increased by 2% in 2016 compared to the previous year. Figure 2-2-a shows the CO₂ equivalent (CO₂e) emissions by each sector worldwide and Figure 2-2-b further breaks down the emissions associated with each mode of the transportation sector for U.S. emissions only due to lack of information on other nations. Although the U.S. had the greatest transport emissions in 2016, the rate of increase of the emissions from this sector are significantly higher in Asia with an alarming rate of 4.5%.

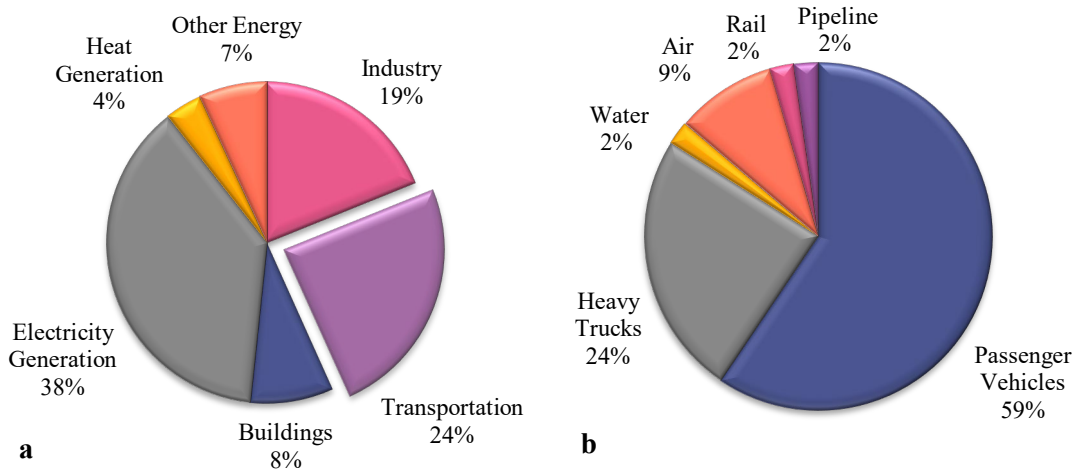


Figure 2-2. Breakdown of global energy-related CO₂e emissions in 2016: a) Emissions associated with each sector¹; b) Emissions associated with the transport sub-sector by mode² (¹ Others include domestic waterborne, pipeline, and HFC & indirect N₂O; ² Due to lack of information on other nations, the transport sub-sector represents only the U.S. emission values) [6,7]

Electricity & heat generation, transportation, and industrial sectors together produce more than 80% of the energy-related CO₂ emissions. In the transportation sector alone, CO₂ emissions increased by an annual global average rate of 2.5% between 2010 and 2015.[8] In 2016, the transportation sector emitted approximately 8 GtCO₂ which accounted for roughly 25% of total global emissions (up from 23% in 2012). This number is 71% larger than the sector’s emissions in 1990 (2.8 Gt CO₂) and 19% larger than the sector’s emissions in 2010 (6.7 Gt CO₂). Nearly 74% of the transportation-related emissions are sourced exclusively from road vehicles.[6] As shown in Figure 2-2, this number is even larger for the U.S. In the U.S. the total CO₂ emissions associated with passenger vehicles and heavy trucks is approximately 83%.[7] Without the implementation of significant mitigation policies, CO₂ emissions from the transportation sector are projected to reach 9.3-12 GtCO₂/yr by 2050 which will be an increase between 16-50% compared to 2016.[9]

The solutions proposed for mitigating climate change effects are deployment of low-carbon fuels and improving the efficiency of current technologies for energy conversion. Hydrogen fuels from low-carbon energy resources are viewed as a promising long-term

Literature Review

option for tackling CO₂ emissions from distributed sources. The use of hydrogen as an alternative fuel in the industrial, residential, and transportation sectors can help to achieve these goals. In particular, the use of hydrogen fuel cell vehicles (HFCVs) has the potential to virtually eliminate CO₂ emissions from tailpipes. If only 25% of vehicles were replaced by HFCVs, overall emissions from the transportation sector could be reduced by 10% [10] and curtail the emissions of NO_x and SO_x and particulate matter by 70-80%.[11] Moreover, hydrogen can be used to supply a proton exchange membrane fuel cell (PEMFC) to generate electricity, which only produces water as a byproduct.[12]

Until the 1960s hydrogen was used in the form of town gas for street lighting and also as a source of energy for heating, cooking, and lighting homes.[11] Today, the same concept can be extended to use the on demand renewably generated hydrogen for powering a single family home with near zero emissions and noise-free fuel.[13] According to a recent work by Stern[13], a large 160-cell hydrogen generator can be employed to provide the total required energy for a single family home including power for appliances, lighting, electronics, and electric heat pumps for heating and cooling. A similar generator could be used to support the energy requirements of a small commercial entity such as a bank or pharmacy.

Currently, hydrogen is primarily produced from fossil fuels such as natural gas and consequently, CO₂ is generated and subsequently released into the atmosphere due to the process. However, sustainable hydrogen production combined with carbon capture, utilization, and storage (CCUS) technology could be a possible strategy for addressing CO₂ generated from the transportation sector.[14] For instance, using an alternative technology to SMR with pressure swing adsorption (PSA) for H₂ production such as a membrane reactor (MR) has the potential to lead to H₂ production on demand with subsequent CO₂ storage on the vehicle. [15,16]

Over the past 60 years, MR technology for H₂ production has advanced significantly. The rapid growth of research in this area can be judged by a significant increase in citations in recent years. As a special field of interest, metallic membranes, specifically Pd and its

Literature Review

alloys, have been heavily investigated in the hydrogen separation field due to their peculiar characteristic to allow for only hydrogen permeation making possible to produce a stream up to 99.999+% purity. [17–19]

These advantageous characteristics could make metallic membranes and MRs suitable for onsite hydrogen production and separation to satisfy distributed hydrogen demands for mobile and small-scale systems. However, despite several decades of research, most metallic membranes have remained at the pilot scale due to uncertain economic feasibility and competitiveness at a large scale. Although the scientific literature on this topic is exceptionally rich, only few scientific studies have focused on the analysis of the costs, opportunities and challenges associated with industrial feasibility. Therefore, the aim of this review is to assess the potential and feasibility of metallic membranes and MRs toward utilization for hydrogen separation and production at high purity as well as to highlight the challenges that need to be overcome for accelerating widespread hydrogen use. Moreover, a comparison between metallic membranes and alternative hydrogen production and separation technologies is presented and discussed.

2.4 Current status of hydrogen production, purification, and usage

2.4.1 Economics and scale

According to a recent study by Dou et al., the global hydrogen market was estimated at \$80 billion in 2015 and is expected to rise up to \$1.6 trillion by 2050. Additionally, the study predicts that the market infrastructure will rise to \$300 billion in 2030 and remain stable at this value until 2050.[20] The primary market driver for the hydrogen economy is expected to come from HFCVs at a market value of \$1 trillion in 2050, while the market value of stationary hydrogen power generation is expected to rise to \$200 billion during the same timeframe.

Another potential area that could drive the hydrogen market in the near future is the concept of power-to-x (P2X). P2X can be defined as processes for conversion of electricity, specifically electricity that is generated from renewable energy resources such as wind or solar, into various products and/or applications to chemically store the electric energy during the low demand times and either use the products as feedstock for the production of other chemicals or convert them back to electricity during the peak demand periods. The letter “X” in the terminology could refer to gas, chemicals, fuel, methane, methanol, hydrogen, etc.[21–23] Among the P2X technologies, power-to-hydrogen (P2H) process is one of the most attractive one where renewable or “green” hydrogen can be produced through water electrolysis with renewable electricity. Hence, P2H could be the crucial link which closes the gap between renewable electricity generation and large scale electricity storage.[21] It should be noted that P2H can be considered a low carbon energy concept, only if the electricity used in this process is supplied from non-fossil based and renewable energy resources such as wind or solar. In doing so, P2X can be considered as an approach that incorporates renewable energy into sectors such as transportation and industry.

However, it should be noted that although P2H technologies have the potential to lower the carbon emissions, there are other environmental concerns associated with these chains

that need to be taken into account. For instance, these technologies require significant amount of materials such as steel, nickel, and polytetrafluoroethylene (PTFE)ⁱ for use in electrolysis electrodes. Although not explicitly limited to the P2X technologies, there are other major environmental concerns that require further attention when considering P2X chains. Hence, the implementation of P2X, like any other new technology, should be guided by accurate sustainability assessments taking into account the environmental concerns such as ozone depletion, acidification, and human toxicity.[22] Another challenge associated with the P2H technologies is the difficulty for storage and transport of hydrogen. This challenge could be addressed by producing hydrogen in the proximity of chemical plants where it can be used as a feedstock for production of other chemicals such as ammonia. Roughly 60% of the global hydrogen market share will be in North America, Europe, and China by 2050.[20]

Currently, the use of hydrogen in the electricity and transportation sectors in the U.S. is still developing. However, the expectations for its evolution and utilization in the short term are evident in the stated objectives of the Hydrogen and Fuel Cells Program funded by the U.S. Department of Energy (U.S. DOE). Funding in this area reached a peak of approximately \$270 million in 2008, with a low of \$109 million in 2014. For the fiscal year 2017, the research budget saw an increase to \$122 million.[24] The aim of the program is to fund research and development efforts to assess the viability of widespread implementation of fuel cell technologies and a hydrogen energy infrastructure, ultimately in an effort to reduce the use of fossil fuels, mitigate greenhouse gas (GHG) emissions, and improve air quality.[24]

The global demand for hydrogen is expected to remain constant up to 2025 at the current rate of 3.5% per year.[25] The current annual hydrogen production capacity in U.S. refineries is approximately 15.8 million tonnes. Of this volume, 3.3 million tonnes is captive by-product hydrogen and 2 million tonnes is combusted for heat generation. Hence, the total hydrogen capacity in the U.S. from conventional captive (hydrogen that is

ⁱ It should be noted that PTFE is not required for all electrolysis techniques.

Literature Review

produced for internal use on the same site, such as oil refineries) and merchant (hydrogen that is produced by a producer and sold as a commodity and delivered to the consumer by pipeline, bulk tank or cylinder) markets is approximately 11 million tonnes per year.[26] Nearly 95% of this amount is produced by the SMR process.[27] Globally, approximately 50 million tonnes of hydrogen is produced each year.[28,29] Roughly 48% comes from SMR, 30% from petroleum reforming, 18% from coal gasification, and 4% from water electrolysis.[30]

Hydrogen can be used in industrial processes for ammonia and methanol synthesis, fossil fuel hydrocracking, metal production, or as a fuel for HFCVs and rockets.[20,28] Approximately 55% of global hydrogen production is used in ammonia plants and 35% in petroleum refining industries. The other end-use sectors include the electronics industry, metal/glass industries, the food industry, pharmaceuticals, etc.[31,32] The breakdown of the hydrogen market end-use is shown in Figure 2-3.

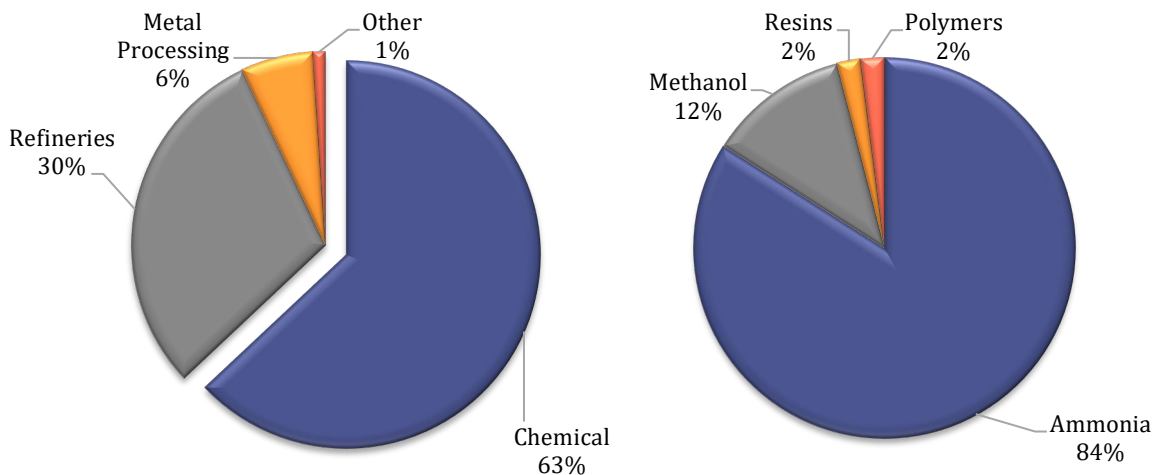


Figure 2-3. Breakdown of the global hydrogen market sectors (left) and further breakdown of chemical industry sector (right). [33]

The chemical manufacturing sector has a market share of approximately 63%. Synthesis of ammonia requires high volumes of hydrogen and this process alone uses more than half of the hydrogen market share. Refineries have the second largest market share. In the last

Literature Review

two decades, refineries have become net hydrogen consumers [31,34,35] with typical capacities from 10,000 to 100,000 m³/h,[36] accounting for 30% of the total hydrogen market. Hydrogen is required for many operations in petrochemical processing such as hydrotreating (where it is used for hydrodesulphurization, hydroisomerization and hydrogenation of aromatics and olefins) and hydrocracking (where it breaks down large hydrocarbons into smaller, and higher-value molecules).[37] Until recently, hydrogen was available internally to industrial processes as a co-product from catalytic reforming of aromatics.[34,35] Today there is stricter control of gasoline aromatic composition, and therefore less hydrogen is produced within refineries, limiting its availability.[34,36,38] Ultimately, this has catalyzed the push for refiners to increase the efficiency of their hydrogen production systems.

Approximately 64% of hydrogen consumed in the industrial sector is “captive” hydrogen which is produced and consumed on-site. Furthermore, the hydrogen that is produced as a by-product of industrial processes, is also commercialized, and makes up 27% of the hydrogen market.[39]

Based on today’s method of production, hydrogen does not represent a shift away from fossil fuels, nor does it present itself as a complete solution to climate change.[11,28] In order to address climate change concerns, alternative methods for hydrogen production such as electrolysis and photovoltaic water splitting, with renewable sources of electricity, can be used to produce hydrogen rather than producing hydrogen using fossil fuels such as natural gas. However, some of these methods consume significant amount of electricity, could suffer from toxicityⁱⁱ of the generated products, and others such as photovoltaic water splitting, have low efficiency and have a very high production cost compared with the reforming process.[40] Nevertheless, there is ongoing research for alternative methods and devices to produce high-purity hydrogen, such as the new method and device invented by Ham et al., to produce hydrogen in a dry reforming process using available methane and

ii This could be an issue in photo-reduction technologies, the products that are generated in photo arsenic electrodes.[40]

Literature Review

CO₂ in biogas.[41] Moreover, a significant infrastructure expansion would be valuable toward supporting its use as a transportation or grid fuel.[42,43]

One of the biggest challenges that the hydrogen economy faces is the imbalance between hydrogen supply and demand. The current global production volumes of hydrogen cannot support a smooth transition from internal combustion engine vehicles to HFCVs. More specifically, in order to replace all the gasoline engine vehicles in the U.S. solely by HFCVs, the daily amount of produced hydrogen should be approximately 0.34 million tonnes or 124 million tonnes per year. This value is more than twice the current hydrogen that is consumed on a global scale and more than 10 times the current annual U.S. production.[28]

The other significant challenge is hydrogen delivery and transportation. Although hydrogen can “potentially” be transported via pipelines like natural gas, the pipelines used for natural gas transport are not suitable for hydrogen delivery due to serious challenges arising from hydrogen leakage and metal embrittlement under the high-pressure conditions required.[28] Furthermore, 1.2% of hydrogen energy will be used every 150 km to power the compressors which is 4 times the amount of natural gas used for the same purpose, i.e. 0.3%.[44] High costs of pipeline delivery and distribution, material handling losses, increased traffic congestion, and safety issues associated with highly flammable and explosive hydrogen gas are some of the biggest concerns that will need to be addressed thoroughly for successful deployment of hydrogen energy.[28,44,45]

A SWOT (strengths, weaknesses, opportunities, threats) analysis of hydrogen energy in China indicates the strengths of a hydrogen economy include:[46]

- Abundant resources to produce hydrogen from: coal, oil, natural gas, biomass, wastewater, wind, hydropower, solar etc.
- Great development potential (transportation and communication)
- Environmental benefits (as the greatest CO₂ emitter, China needs to reform its energy structure toward more renewable and clean resources to address the ever-increasing problem of the air pollution in its major cities)

In the same report, the weaknesses of hydrogen energy are listed as following:

- High cost
- Lack of key technologies (China currently lacks the state-of-the-art technologies and infrastructures to use renewable sources such as wind and solar for hydrogen production)
- Lack of the appropriate infrastructure (refueling and transportation infrastructure are missing)

Although this SWOT analysis is performed for the Chinese market, many of its elements such as abundance, environmental friendliness, costs, and lack of infrastructure are valid for other countries as well, including the U.S.

2.4.2 Current industrial production and separation technologies

The SMR is currently the dominant industrial method for hydrogen production where methane and steam react over a catalyst to produce a mixture of H_2 and CO_2 . [15,47–56] SMR has developed into specifically tailored processes, consisting of a conventional reformer followed by two water-gas shift (WGS) reactors (i.e., high temperature shift (HTS) and low temperature shift (LTS)) and equipment for H_2 separation and purification, with PSA being the dominant technique. Figure 2-4 shows a schematic of the entire process.

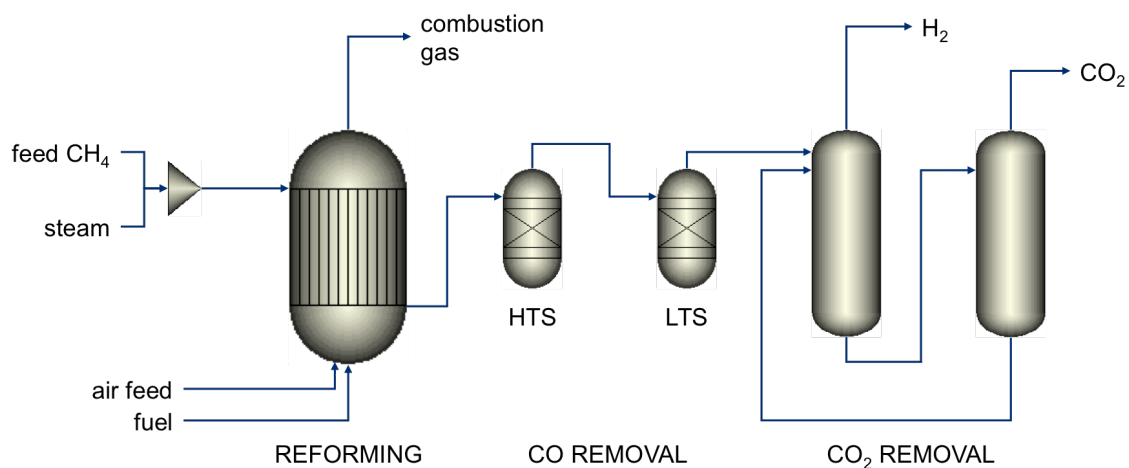


Figure 2-4. Conventional steam reforming process with multiple stages for H_2 production.

Literature Review

The reaction between methane and steam takes place in the reformer at harsh operating conditions due to the endothermic nature of the reaction. Specifically, the operating temperature and pressure ranges between 800 °C to 1000 °C and 15 to 20 bar, respectively.[57]



The stream exiting the reformer contains a hydrogen-rich gas mixture with substantial CO content (generally higher than 5 vol.%),[58] which may be suppressed by the WGS reaction:



This reaction takes place in two reactors arranged in series since it is an exothermic reaction promoted at low temperature, but kinetically-limited at temperatures below *ca.* 200 °C.[59] Therefore, the first reactor (HTS) operates at high temperature between 310-450 °C and uses a high-temperature catalyst such as chromium-promoted iron oxide to favor the kinetics.[60] The second reactor (LTS) operates at low temperature in the range of 190 to 250 °C and uses a low-temperature catalyst of copper-promoted zinc oxide.[61] The outlet stream from the LTS reactor contains 86% H₂, 12% CO₂, 0.3-1% CO and 1.6% CH₄ on a dry basis.[62,63] Therefore, in order to obtain high-grade hydrogen, different separation/purification steps using diverse technology can be used, as shown in Table 2-2. Each technology is chosen according to the hydrogen purity requirements for any specific process. For instance, cryogenic distillation, which uses the difference in boiling point temperatures of the species is a very energy intensive process[64] due to operating at very low temperatures and therefore does not allow for significant hydrogen purification[65] However, cryogenic separation processes have very better economies of scale compared to the other separation methods and can produce separate hydrocarbon streams rich in C₄⁺, ethane, propane, etc.[66]

Table 2-2. Comparison of Hydrogen Separation Technologies[67,68]

Technique	Description	T [°C]	H ₂ -feed	H ₂ purity	H ₂ recovery	Drawbacks	Benefits
PSA	Selective adsorption of compounds from a gas stream	80-180	Any H ₂ rich gas	99.999	70-85	Around 20% of H ₂ is lost in the operation Energy intensive	High H ₂ purity >99.99%
Cryogenic distillation	Partial condensation of gas mixtures at low temperatures	-180	Petrochemical and refinery off-gases	90-98	95	Relatively low H ₂ purity Energy intensive	Better economies of scale
Dense Pd-alloy membrane	Selective diffusion of hydrogen through a Pd-based alloy membrane	300-450	Any H ₂ containing stream	99.999	Up to 99	High cost Low mechanical resistance	High purity H ₂ stream H ₂ recovery up to 99%
Polymeric membrane	Differential rate of diffusion of gases through a permeable membrane	25-100	Refinery off-gases and ammonia purge gas	92-98	>85	Relatively low H ₂ purity	Low cost
Metal hydride separation	Reversible reaction of hydrogen with metals to form hydrides	>RT	Ammonia purge gas	99	75-95	Relatively low H ₂ recovery	High H ₂ purity
Solid polymer electrolyte cell	Electrolytic passage of hydrogen ions across a solid polymer membrane	RT	H ₂ produced by thermo-chemical cycles	99.8	95	Sluggish anode reaction coupled with the inefficient cathode reaction (low overall cell performance)	High H ₂ purity ≈99.8% High H ₂ recovery ≈95%

Palladium-based membrane technology allows for high recovery and high purity of hydrogen. The primary challenges associated with Pd-based membranes for H₂ production include their low tolerance for H₂S and unsaturated hydrocarbons, high cost on a large scale due to the price of Pd, and low mechanical resistance.[69] Today, the most extensively used technology for large-scale production is the PSA process.[65] The PSA technology allows for variation in H₂ purity making it tunable for a wide range of industrial applications.[57] Sorbents that are commonly used include activated carbon, silica gel, alumina and zeolite.[70–72] The PSA process operates at approximately 20-25 bar [73,74]

Literature Review

and has a hydrogen separation efficiency of 85-90%. [75] Moreover, PSA technology has the ability to process large capacities of feed gas, i.e., on the order of 100,000 m³/h [76] while maintaining a hydrogen purity of 99.999+%. [73] More specifically, a 100,000 m³/h unit would produce 78,000 tonnes of H₂ per year, which amounts to approximately 0.2% of annual global H₂ production.ⁱⁱⁱ While PSA has many benefits, it has the drawback of relatively low hydrogen recovery (approximately 70%)^{iv}. [77] The savings associated with using a dense Pd membrane and achieving a hydrogen recovery of 99% are worth noting. By using this technology, 36% less natural gas can be used to produce the same amount of hydrogen, resulting in an annual savings of 11,000 tonnes of natural gas and \$2MM per PSA unit. Furthermore, more than 31,000 of CO₂ emissions could be avoided annually.^v

Recent studies have investigated alternative solutions to the conventional system, such as the adoption of membrane technology applied to the SMR reaction. [78–94] It has been demonstrated that the use of a hydrogen permeability-selective MR such as Pd-based MRs [65,95] could allow for working at milder operating conditions and enhancing the performance of the SMR reaction, while additionally collecting high-purity hydrogen. [96] The interest in MR technology has grown due to its potential to provide significant process improvements such as operational simplicity, compatibility between different membrane operations in integrated systems, low energy requirements and environmental compatibility. Membrane technology provides process intensification by combining reaction and separation steps in a single device, while simultaneously achieving higher conversions and efficiencies compared to conventional separation and reaction operations. [97]

iii Assume the operation is 24 hours per day, 365 days per year.

iv Hydrogen recovery is lower compared to other hydrogen separation techniques as a fraction of hydrogen is lost in the purging step. [68]

v Assumptions: Natural gas is considered pure methane; PSA (90% conversion, 70% recovery); Membrane (99% conversion, 99% recovery); price of natural gas set at 3.268 \$/MMBtu; Standard conditions are assumed to be 15.56 °C and 1.01325 bar; carbon emissions associated with burning natural gas are assumed to be 0.0053 tonnes of CO₂/therm

2.4.3 Hydrogen use and the role of metallic membranes

Hydrogen's clean combustion and high energy density (hydrogen has the highest mass energy density in all types of fossil fuels, 120 MJ/kg at its lower limit heating value) make it very attractive for sustainable development.[20] As a clean fuel, hydrogen can be used in cogeneration systems for industries and households to mitigate air pollution associated with other combustion fuels.[20] Most of the applications of hydrogen stem from its reactivity rather than its physical properties.

Hydrogen is the essential feedstock for various industrial applications some of which are: catalytic hydrogenation of unsaturated vegetable oils in food and beverage industry, catalytic reduction of nitrogen in Haber-Bosch process to produce ammonia, as a feedstock in the synthesis of methanol, hydrogen peroxide, hydrochloric acid, polymers, and solvents, in the refining industry to break down and convert the heavy unsaturated compounds into lighter hydrocarbons, as a fuel for rockets in the space programs, as a fuel in hydrogen fuel cell vehicles, etc. Various applications of hydrogen are shown in Figure 2-5.

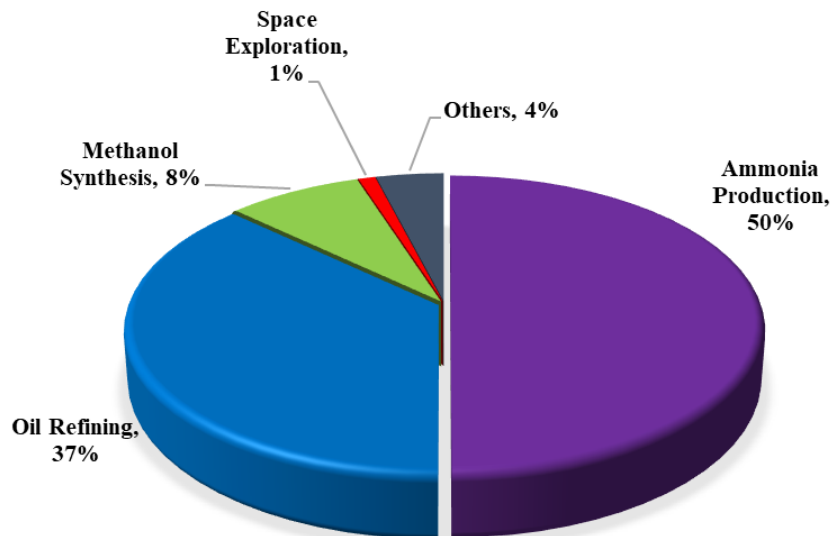


Figure 2-5. Share of hydrogen consumption in various industries (adapted from [1])

There have been significant debates in the recent decades about the “fuel of future” and as a result, “hydrogen economy” has gained significant attention amongst the scientists. Some of the unique physical and chemical properties of hydrogen that make it plausible for hydrogen to be the potential fuel of the future are as follows: the combustion hydrogen with oxygen will produce water and releases heat, hydrogen has the highest energy density per unit of mass compared to any other combustible fuel (Table 2-3), the combustion of hydrogen has no adverse environmental impact and emits no carbon dioxide, hydrogen can be produced from renewable sources such as bio-ethanol and electrolysis of water, and finally, hydrogen has a broad flammable range which makes it a suitable fuel for various applications. Hydrogen is an energy carrier like electricity, however, unlike electricity, great amount of energy can be stored in the form of hydrogen for future use or be moved from the production site to the consumption location.

Table 2-3. Specific energy density of various fuels (adapted from [1])

Fuel	Energy density (MJ/kg)
Gasoline	42.7
Diesel	42.5
Crude oil	46.1
Ethanol	26.8
Methanol	19.7
Natural gas	47.7
Methane	50
Propane	46.3
Hydrogen	120

One area that has been very attractive and has created significant momentum for research and development projects in the past 20 years [98] is the use of hydrogen in the HFCVs. HFCVs could be attractive to the customers as they combine the benefits of electric vehicles, like quietness and efficiency, with those of the internal combustion engine (ICE) vehicles, such as refueling time and driving range. Given the 700 bar on-board hydrogen storage requirement, a HFCV can be refueled within 3-5 minutes, which is enough for driving 400-500 km.[99] The energy conversion efficiency of HFCVs can be as high as

Literature Review

40-60%^{vi} while only 10-15% of the gasoline in the conventional ICE is converted to traction energy.[100]

Table 2-4 shows a comparison between energy storage capacity, discharge time, and siting of hydrogen and other forms of energy storage. As can be seen, hydrogen is superior to all other forms of energy storage from both storage capacity and discharge duration.

Table 2-4. Comparison between various methods for energy storage (adapted from the 2015 IEA report: Technology Roadmap: Hydrogen and Fuel Cells) [101]

Technology	Storage capacity	Discharge duration	Siting
Supercapacitors	10kW-10MW	Seconds	T&D
Flywheel	10kW-10MW	Seconds-minutes	T&D
Battery	1kW-100MW	Seconds-hours	End-user, T&D, Generation
Pumped Hydro Energy Storage (PHS)	100MW-1GW	Seconds-weeks	Generation
Compressed Air Energy Storage (CAES)	10MW-100MW	Minutes-days	T&D, generation
Hydrogen	10MW-1GW	Hours-season	T&D, generation

However, the fundamental issues stemming from the low volumetric energy density of hydrogen gas, make the development of HFCVs a challenging task. Hydrogen has a significantly lower volumetric fuel density compared to gasoline and diesel oil, which makes its delivery more difficult and costly. The feasible modes of transportation for hydrogen are via tube trailers, tanker trucks and pipelines. The only delivery method that makes hydrogen emission-free is pipeline transport, which has significant environmental footprints.[102]

One of the most important challenges that keeps HFCVs from being commercially available is the cost associated with onboard storage of hydrogen. A HFCV requires 4-7 kg of hydrogen to drive a distance of 480 km. Currently, a carbon-fiber composite tank pressurized to 700 bar is the best storage material for passenger vehicles which costs approximately \$3,000 with today's technology.[103]

^{vi} Efficiencies are based on higher heating values (HHV). It should be noted that for a power-to-fuel scenario where electricity is transformed into hydrogen, which is then used in a HFCV, the overall efficiency from well to wheel could be as low as 20-30% due to the losses in each conversion step from electricity to hydrogen and back to electricity.[101] In such scenarios, electric vehicles may be a better alternative to the HFCVs if the electricity is provided by renewable sources.

One technology that may make a significant difference in making the hydrogen economy a reality in the coming decades is SMR combined with MR technology. This, however, requires major breakthroughs in membrane technology development. Industrial interest towards membrane technology has grown over the years. Currently, metallic membranes are already being used on an industrial scale in the semiconductor industry to produce high-purity hydrogen.[104] Commercial polymeric membranes have been effectively employed since 1979[105] and currently compete with PSA and cryogenic separation on an industrial scale for recovering hydrogen from refineries, ammonia plants, and petrochemical manufacturing.[106–108] Polymeric membranes achieve high hydrogen purity reaching 95%, as reported in Table 2-2, which is usually adequate[109] for most petroleum refining applications. Nevertheless, for some catalytic processes such as ammonia synthesis and for supplying fuel cells, e.g., PEMFCs, ultrahigh purity hydrogen of 99.99+% is required.[110] For these applications, Pd-based membranes could be employed due to their complete selectivity towards hydrogen permeation with respect other gases.

The performance of Pd-based alloy membranes has more recently been enhanced by decreasing the thickness of the metallic layer. The transition from a thick, unsupported membrane to a thin, supported membrane has led to economic benefits and higher-purity hydrogen in the permeate. Despite recent improvements, they are still affected by relatively high cost due to membrane production and operation, especially at industrial scales,[109] and compared to the polymeric membranes they are expected to be one to three orders of magnitude more expensive per unit surface area.[107] For example, spiral-wound turnkey membrane skids used in natural gas processing plants cost \$500/m²^{vii},[111] while the cost of one 50 μm-thick Pd membrane, would be *ca.* \$5,500/m²^{viii}. [112] Nevertheless, at the same pressure gradient, Pd-based membranes are characterized by superior selectivity and permeability, which can be *ca.* 1000-10,000 times higher than polymeric membranes.[113]

viiPolymer membrane cost was converted from 12.5 million dollars (2007 USD) for 25,000 m². [111]

viiiCost of Pd was chosen for the cheapest price in 2010, and 10% of preparation cost is included.[112]

Literature Review

Therefore, the cost of metallic membranes based on the same amount of hydrogen permeating flux would yield a competitive result in comparison to polymeric membranes.

One of the obstacles that Pd-based membranes could face at industrial scale is their inability to produce high flow rates of hydrogen compared with PSA technology which currently produces hydrogen flow rates as high as 10,000-100,000 m³/h,[36] on a large-scale industrial basis. This problem inherently stems from the challenges associated with scaling up the MR technology. Although the process capacity may be expanded with additional membrane units to increase the hydrogen flow rate, it is not cost-effective for Pd-based membranes. However, Pd-based membranes may be suitable for small applications where the benefits of their performance outweigh the membrane cost.[107] Such applications, some of which are under development, include semiconductor manufacturing[114,115] and hydrogen fuel cells[116].

2.5 Metallic membranes and recent progress

2.5.1 Metallic membranes and hydrogen permeation

Membranes used for H₂ separation can be divided into four categories based on the materials used in their fabrication: polymeric, metallic, carbon, and ceramic. Polymeric membranes are organic while the other three classifications are considered inorganic membranes.[65] Dense metallic membranes such as Pd and Pt as well as the metallic elements of groups III-V are of special interest due to their capability to produce pure H₂ in one single separation step with a low energy penalty.[117] The best candidates are Pd-based metallic membranes for producing high-purity hydrogen due to their “infinite” selectivity towards H₂ permeation.[118] Hydrogen permeation through Pd is governed by the solution-diffusion mechanism which takes place in six steps: [119,120].

Hydrogen transport through the Pd membrane can be either surface-limited or diffusion-limited. In thick membranes ($\delta > 100 \mu\text{m}$), the rate-limiting step is usually the diffusion of hydrogen atoms through the bulk of Pd[121], while in thin membranes ($\delta < 1 \mu\text{m}$) and at high operating pressures the rates of surface reactions dictate the rate of transport.[112,121] However, it is worth mentioning that at low temperatures the associative desorption of hydrogen atoms from the Pd surface become the rate-determining step, while at very low hydrogen partial pressures ($\ll 1 \text{ bar}$), the adsorption of hydrogen atoms onto the Pd surface might become the rate-limiting step.[122,123]

When the limiting step is hydrogen diffusion, the hydrogen permeating flux through the dense Pd-based membrane can be expressed by Sieverts-Fick’s law.

$$J_{H_2} = P e_{H_2} \frac{\left(P_{H_2,ret}^{0.5} - P_{H_2,perm}^{0.5} \right)}{\delta} \quad \text{Eq. 2-18}$$

Literature Review

where J_{H_2} is the hydrogen permeating flux through the membrane, Pe_{H_2} is the permeability of the membrane, $p_{H_2,ret}^{0.5}$ and $p_{H_2,perm}^{0.5}$ are the partial pressure of hydrogen in the retentate and permeate sides, respectively, and δ is the membrane thickness.

Permeability is an intrinsic property of the membrane and is independent of the thickness of the membrane or the partial pressure of hydrogen. In some instances, the “permeance” is used to characterize its performance and is defined as the ratio of permeability over thickness:

$$P_{H_2} = \frac{Pe_{H_2}}{\delta} = \frac{J_{H_2}}{(p_{H_2,ret}^{0.5} - p_{H_2,perm}^{0.5})} \quad \text{Eq. 2-19}$$

It is worth noting that permeance is mainly used to characterize a thin metallic film deposited on a porous support, while permeability is generally used for characterization of unsupported membranes.[112] The membrane permeability is a function of temperature and may be described by an Arrhenius-type relationship[80,124–127]:

$$Pe_{H_2} = Pe_{H_2}^0 \exp\left(-\frac{E_a}{RT}\right) \quad \text{Eq. 2-20}$$

Where $Pe_{H_2}^0$ is the pre-exponential factor, E_a is the apparent activation energy, R is the universal gas constant, and T is the absolute temperature. Combining Eq. 2-18 and Eq. 2-20 yields the Richardson’s equation[126,127]:

$$J_{H_2} = Pe_{H_2}^0 \exp\left(-\frac{E_a}{RT}\right) \frac{(p_{H_2,ret}^{0.5} - p_{H_2,perm}^{0.5})}{\delta} \quad \text{Eq. 2-21}$$

This relationship highlights the proportionality of the hydrogen permeating flux to the membrane thickness, hydrogen partial pressure, and temperature, which need to be optimized to obtain a high hydrogen permeating flux.

Although the Sieverts-Fick's law is fairly simple, there are numerous studies that undermine its validity and use the general empirical form where the hydrogen permeating flux is proportional to the partial pressure of hydrogen to the power of n,[96,121,126,128]

$$J_{H_2} = P e_H \frac{(P_{H_2,ret}^n - P_{H_2,perm}^n)}{\delta} \quad \text{Eq. 2-22}$$

The empirical exponent n in Eq. 2-22 is a dependent factor which determines the correlation between the hydrogen permeating flux and the driving force (partial pressure of hydrogen on the retentate and permeate sides). The value of n, varies between 0.5 and 1.0 [90], and is usually evaluated using nonlinear regression technics.[129]. Although controversial, the value of n has been used as a benchmark to determine the rate controlling steps. The deviation of n values from 0.5 may be explained by the deviation of the hydrogen solubility from the values proposed by Sieverts' law, which may results from incorrect assumptions of the rate-determining steps, non-ideality of interstitial hydrogen diffusivity, or crystallographic phase transition. [126] In addition, a deviation from 0.5 indicates that the permeation of hydrogen may be influenced by a combination of other factors such as Pd surface impurities, bulk defects, i.e., organic contaminants from fabrication or pinholes, respectively.[108,130]

Eq. 2-22 is usually used to evaluate the permeation characteristics of composite membranes, which consist of a thin Pd-layer deposited on a porous support. Porous supports are typically porous stainless steel (PSS) or ceramic.[131] The benefits in the use of a PSS support are the mechanical and chemical resistance, the thermal expansion being similar to Pd and ease in implementing it within a module. However, they suffer from intermetallic diffusion, rough surface area, and broad pore size distribution, which makes the deposition of a thin dense layer difficult. On the contrary, ceramic supports offer narrow pore size distribution, stability over a wide range of temperatures, and they are chemically inert. Nevertheless, they suffer from differing thermal expansion coefficients, high costs and difficulty in implementing within a module.[67,131]

A common characteristic of Pd-based membranes is their ability to be completely hydrogen permeability-selective with respect to all the other gases. The parameter commonly used to evaluate this feature is the ideal selectivity (α), which is defined as the ratio between the permeance of hydrogen to the permeance of a secondary gas [124]:

$$\text{Ideal Selectivity } (\alpha_{H_2/i}) = \frac{P_{H_2}}{P_i} \quad \text{Eq. 2-23}$$

The benchmark for the development of hydrogen selective membranes and hydrogen production technologies is set by the U.S. DOE. Performance targets for dense metallic membranes are summarized in Table 2-5.

Table 2-5. U.S. DOE 2015 targets for hydrogen separation and purification by dense metallic membranes[132]

Performance criteria	Target
Flux	1.135 mol.m ⁻² .s ⁻¹ (300 Scfh.ft ⁻²)
Cost of membrane	< 5400 \$ per m ² (< 500 \$ per ft ²)
Durability	> 5 years
H ₂ recovery	90 %
Hydrogen purity	99.99%

2.5.2 Pd-alloy membranes and costs

Alloy-based membranes have gained increasing interest due to their improved properties compared to pure Pd such as sulfur resistivity, thermal stability, and enhanced hydrogen permeability, as well as their generally lower material cost and decreased embrittlement tendency.[112,133,134] The abundance and cost of various metals that are commonly used to fabricate Pd-based alloy membranes for the purpose of hydrogen production are shown in Figure 2-6. Furthermore, the permeability of these Pd alloy membranes at 350 °C and 2.2 MPa are depicted in Figure 2-7. From these graphs it can be inferred that, alloying Pd with other metals offers a reasonable compromise between the material cost of the membrane and the permeability of hydrogen through the membrane.

Literature Review

One of the most widely used Pd alloy membranes that has shown high permeability and stability is the Pd_{77%}Ag_{23%} membrane.[135]

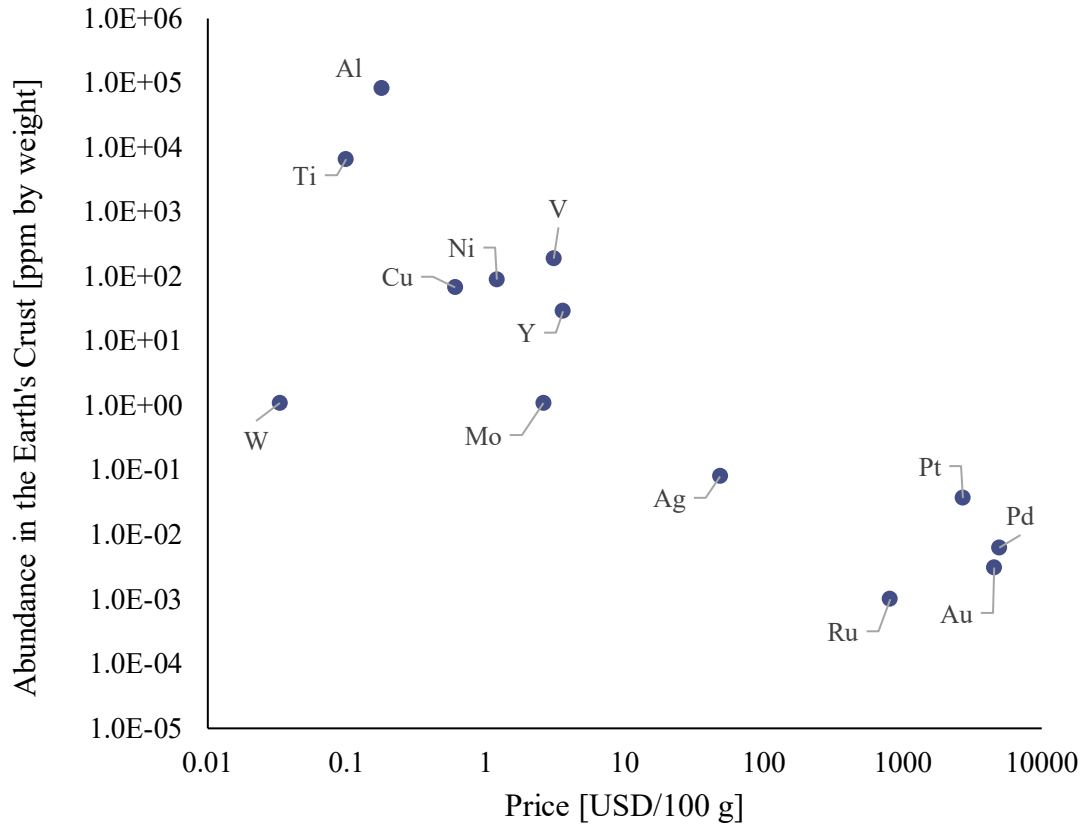


Figure 2-6. Abundance and cost of the most commonly used metals for the fabrication of Pd-based membranes (Each price is referred to 2019. Price of titanium is based on TiO₂ with a minimum purity of 95%; price of yttrium is based on yttrium metal with minimum purity of 99.9%; price of vanadium is based on the vanadium pentoxide)

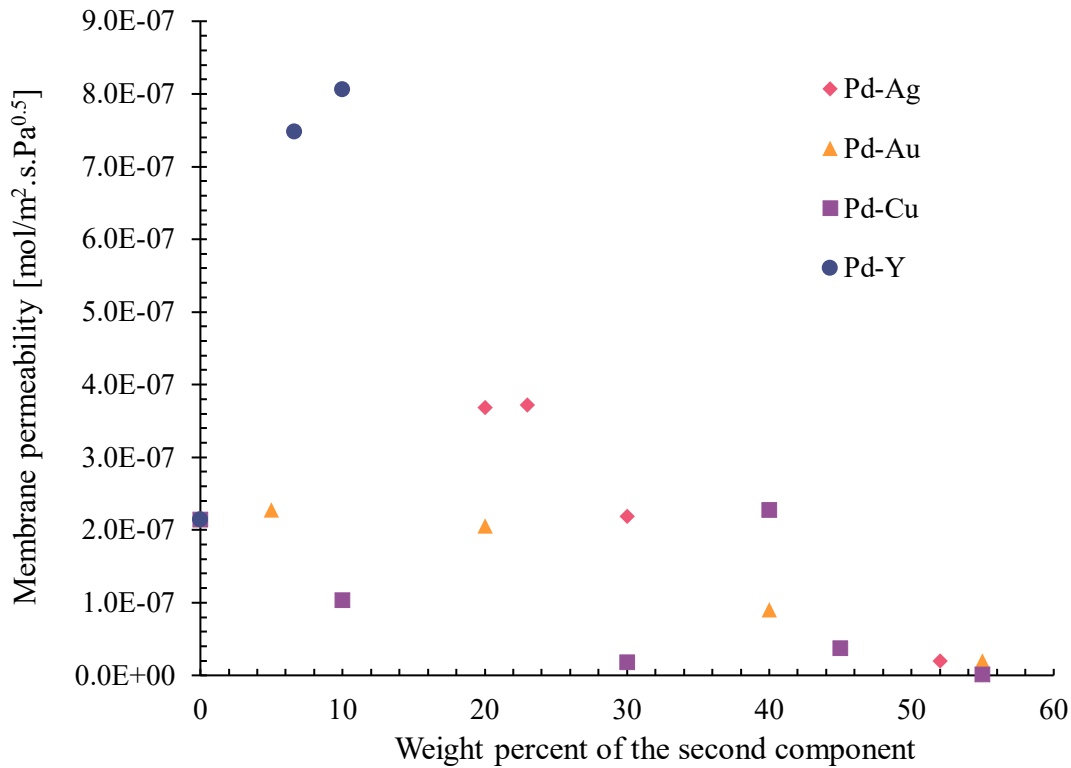


Figure 2-7. Hydrogen permeability through Pd alloy membranes at 350 °C and 2.2 MPa (adapted from Knapton assuming hydrogen as an ideal gas and atmospheric pressure on the permeate side)[135]

The hydrogen permeabilities of various Pd-based membranes reported in recent literature are shown in Table 2-6. Since the permeability depends not only on the type of alloy but also on their composition, fabrication methods, and testing procedures, comparing permeabilities across different studies provides only an approximate trend. The most widely studied Pd-based alloy membranes are Pd-Ag, some of which are applied to MR technology.[136–138] In general, Pd-Ag membranes provide 1.5-2 times higher hydrogen permeability compared to pure Pd due to their increased hydrogen solubility. In addition, Pd-Ag membranes have demonstrated higher resistance against hydrogen embrittlement.

Aside from enhancing membrane transport properties, another purpose of alloying is to improve chemical stability against sulfur contamination. The Pd-Cu alloy has achieved higher tolerance against sulfur contamination, with the permeability similar or slightly lower than that of pure Pd. The face-centered cubic (FCC) phase of the Pd-Cu alloy containing 30-60 wt.% Cu has been found to have increased tolerance against sulfur

Literature Review

poisoning compared to the body-centered cubic (BCC) phase, in which hydrogen permeability has been found to remain constant at 1000 ppm H₂S exposure.[139] The extent of sulfur tolerance varies among the various studies reported in the literature. For instance, a concentration of 300 ppm of H₂S completely inhibited hydrogen permeation through Pd-Cu membranes while only 100 ppm of H₂S inhibited permeation in pure Pd membranes.[140] In addition, 80%, 20% and 1% loss in hydrogen permeation were reported for various Pd-Cu membranes at 50 ppm, 20 ppm and 5 ppm H₂S, respectively.[141–143] Since these experimental results are compiled from different studies, the effect of H₂S concentration may not appear as a quantitative correlation with the decrease in permeation, but the overall trend qualitatively shows the inhibition effect of H₂S. In addition, Pd-Au alloy membranes with low Au compositions (<10 wt%) have also exhibited enhanced sulfur resistance.[144] The hydrogen permeation dropped to 15% of the initial flux at 55 ppm H₂S, but soon recovered to 65% with hydrogen purging, whereas the hydrogen permeation through a pure Pd membrane was reduced to 7% under the same H₂S concentration without recovery after 20 hours of purging under hydrogen.[145] Another promising alloy exhibiting sulfur resistance is Pd-Pt. However, a content of Pt between 10 and 30 wt% exhibited decreased permeability (i.e., 20-60% of the permeability of pure Pd), while demonstrating improved sulfur tolerance; for instance, 30% permeation loss was reported at 1000 ppm H₂S at 400 °C.[146,147] Without bulk sulfide formation, the permeability of sulfur-tolerant membranes can be partially or fully recovered after flushing with a pure hydrogen stream.[141,144,145,148] In order to achieve higher hydrogen permeability while maintaining sulfur resistance, alloys with more than two elements have also been investigated, including Pd-Ag-Cu[149–151], Pd-Ag-Au[144,152], and Pd-Au-Pt[153]. Permeabilities of these ternary alloys are also listed in Table 2-6.

Table 2-6. Properties of the Pd-based membranes available in the open literature

Pd-based metallic system**	Membrane thickness (μm)	Temperature ($^{\circ}\text{C}$)	Permeability ($10^{-9} \text{ mol m}^{-1} \text{ s}^{-1} \text{ Pa}^{-0.5}$)	Selectivity	Reference
Pd disk	14.6	400	9.6	205 (H_2/N_2)	[154]
Pd disk	12.1	400	13.5	172 (H_2/N_2)	[154]
Pd disk	5.2	400	11.7	infinite	[153]
Pd/ Al_2O_3	5	300	7.1*	>1,000 (H_2/N_2)	[155]
Pd-Ag23%/PSS	2.8	400	18	2,900	[156]
Pd-Ag23%/PSS, oxidized	2.8	400	41	2,900	[156]
Pd-Ag12%/Al $_2$ O $_3$	11	550	11.1*	2,000 (H_2/N_2)	[157]
Pd-Ag25% disk, oxidized	25	300	11.8	infinite	[158]
Pd-Cu9%/Pd-Ag23%/PSS	40	280	17.7	700 (H_2/N_2)	[143]
Pd-Cu41% disk	16.7	400	13.3	105 (H_2/N_2)	[154]
Pd-Cu34%/PSS	20	350	4.86*	high (H_2/CO_2)	[159]
Pd-Cu18wt% /Al $_2$ O $_3$	11.4	450	2.63*	high	[141]
Pd-Au15%/Al $_2$ O $_3$	2.5	500	11.8*	1,400 (H_2/N_2)	[160]
Pd-Au10% disk	25	300	9.4	infinite	[158]
Pd-Au10% disk	25	400	14.5	infinite	[153]
Pd-Au10% disk	25	400	18.2	infinite	[153]
Pd-Pt9%	6.8	400	5.55	4,465	[147]
Pd-Pt26%	12.1	400	2.92	13,393	[147]
Pd-Au10%-Pt10%	25	400	6.14	infinite	[153]
Pd-Au10%-Pt10%	25	400	14.1	infinite	[153]

* Values converted from the given information in the reference

** Values represent composition in alloy systems in wt.%

2.5.3 Non-Pd membranes

Non-precious metal alloys for hydrogen separation have been studied as a way to reduce the use of precious metals. A range of hydrogen permeabilities for non-Pd membranes from the literature is listed in Table 2-7. The alloy $\text{Zr}_{36}\text{Ni}_{64}$ was the first amorphous metal alloy membrane introduced by Hara et al., demonstrating 12 \times lower hydrogen flux with 31 \times reduced cost than a $\text{Pd}_{77}\text{Ag}_{23}$ membrane.[161] Hydrogen permeabilities tend to increase along with a Zr content in amorphous metal alloys.[162,163] Superior hydrogen permeability may also be achieved by using crystalline alloys of early transition metals with the BCC structure, such as the Group 5 metals (e.g., V, Nb, and Ta).[164–166] It should be noted that the presence of a catalytic Pd layer is often required for such high permeation levels of hydrogen through these metals. Group 5 metals have high surface resistance for hydrogen entry and exit[165], but a thin Pd layer (several hundred

Literature Review

nanometers) coated upon the surfaces of those metals allows for rapid hydrogen dissociation and subsequent bulk diffusion. Some Zr-Ni amorphous alloys have reactive surfaces, which allow for hydrogen dissociation thereby eliminating the use of precious metals.[161]

The increased permeability of the crystalline and amorphous metal alloys can be largely attributed to their high hydrogen solubility.[112] However, the high solubility is often correlated to the susceptibility of potential hydrogen embrittlement. As the hydrogen concentration rises, the precipitation of new hydride phases occurs, and the stress along phase boundaries potentially increases, leading to defects and cracks in metals.[167] To reduce the embrittlement induced by this dual phase, alloying with less hydrogen-soluble metals, such as Ni, has been reported in the literature.[168–172] It was found that the presence of the less hydrogen-soluble additive metals suppresses the formation of the hydride phases, thereby limiting hydrogen embrittlement. Another important property of membrane material is the thermal stability for high-temperature operation. The thermal stability may be enhanced when a refractory metal (e.g., Nb, Ta, Mo, or W) is contained in alloys.[173] Even though these non-Pd membranes are at a premature stage compared to the Pd-based membranes, more research should continue since the impact of these new membranes on cost reduction could be very significant and more advanced membrane properties (e.g., permeability, chemical and thermal stability) may be achieved.

Table 2-7. Properties of the group V metal-based membranes available in the open literature

Composition (at.%)	Membrane thickness (μm)	Temperature ($^{\circ}\text{C}$)	Permeability ($10^{-9} \text{ mol m}^{-1} \text{ s}^{-1} \text{ Pa}^{-0.5}$)	Reference
V	2000	400 - 450	30	[165]
V ₉₀ Pd ₁₀	107	400	38.6	[174]
V ₉₅ Ni ₅	1000	400	190	[175]
V ₈₅ Ni ₁₅	1000 - 1133	300	40	[175]
V ₉₀ Al ₁₀	1500 - 1800	400	130	[176]
V ₈₀ Al ₂₀	1500 - 1800	400	37-60	[176]
V ₈₅ Ni _{10.5} Al _{4.5}	1500-2000	350	62.9	[172]
V ₉₀ Ti ₁₀	500	400	270	[177]
V ₈₅ Ti ₁₅	600	438	360	[177]
V ₉₉ Y ₁	500	400	148	[178]
V ₉₅ W ₅	500	500	80.4*	[171]
V ₉₅ W ₅ Mo ₅	500	500	74.1*	[179]
Nb	< 2000	420	360	[166]
Nb ₉₅ Ru ₅	450-500	500	127*	[180]
Nb ₉₅ W ₅	450-500	500	178*	[180]
Nb ₉₀ W ₅ Mo ₅	500	500	121*	[181]
Ni ₆₀ Nb ₄₀ (amorphous)	30 - 40	400	2	[182]
Nb ₃₉ Ti ₃₁ Ni ₃₀ (eutectic)	550 - 750	400	19.3	[183]
Ni ₆₅ Nb ₂₅ Zr ₁₀ (amorphous)	30 - 40	400	5	[182]
(Ni _{0.6} Nb _{0.4}) ₇₀ Zr ₃₀ (amorphous)	54	450	14	[184]
Nb ₄₂ Ni ₃₂ Zr ₂₀ Co ₆ (amorphous)	50	400	14	[185]
Nb ₄₂ Ni ₄₀ Zr ₁₂ Co ₆ (amorphous)	50	400	6.9	[185]
(Ni _{0.6} Nb _{0.3} Ta _{0.1}) ₇₀ Zr ₃₀ (amorphous)	65	400	9.8	[184]
Ta	< 2000	420	145	[166]
Ta	1000	350	19.2	[186]
Ta	400	350	63.8	[186]

* Values converted from the given information in the reference

2.5.4 Efficient material screening

Various metallic membrane materials have been used and tested as discussed previously in sections 3.2 and 3.3. Despite the existence of a vast amount of experimental data on membrane fabrication and permeation tests, a direct, quantitative comparison of the properties among various membranes from different studies is often difficult and at times not possible due to differing measurement conditions and different units used among the various studies. It may be useful if studies could apply a standard measure of sulfur tolerance among different membranes; for example, it could be a fraction of permeation loss at a H₂S concentration of 500 ppm compared to the original permeance in the absence of H₂S. This availability of well-organized standard lab-scale data across various research

Literature Review

groups may accelerate further development of the new membranes through efficient communication and accurate comparisons, preventing duplicated experiments on the same or less desirable membrane materials.

Finding an optimal alloy and its composition through experiments is challenging since there are a limited number of tests that can be carried out within a reasonable time frame while using finite resources. In addition to individual experimental tests to inform the design of an optimal membrane, high-throughput material screening has been attempted, in which alloys of multiple compositions are created and characterized on a small scale for efficient analyses.[187,188]

Another method for efficient material screening is based on a computational approach, which does not involve collecting experimental data. Membrane properties, such as permeability, phase stability, and sulfur resistance, have been simulated through computational modeling. First-principles calculations combined with statistical mechanics methods have been used to predict hydrogen solubility and diffusivity to determine the permeability of Pd-based[189–191] and amorphous metal-based[192–194] membranes. This computational approach enables searching through a vast range of material compositions to select new membrane materials having enhanced permeability. Hao and Sholl have shown that the predictions often agree with experimentally measured permeabilities to within an order of magnitude; however, considering that the experimental permeability can vary significantly depending on microstructure variations even within the same alloy compositions[96,108,195], this may not always be the case. The accuracy of predictions varies across different metal-hydrogen systems, as do the models used in the simulations. These computational approaches suffer from intrinsic errors associated with the approximate nature of potentials that describe interactions among electrons or atoms, with which we solve equations of motion (Newton's equation for molecular dynamics calculations, or approximations to Schrödinger's equation for electronic structure calculations) pertaining to many-body systems to obtain ground-state energies and optimized geometries.[196] In addition, the errors may result from numerical approximations in solving those equations. Therefore, one should be careful in making

comparisons, and it is more appropriate, in general, to compare trends between experimental and theoretical properties of materials rather than between particular experimental data points and the corresponding theoretical predictions.

2.5.5 Theoretical studies on metallic membrane materials

Electronic structure calculations have provided mechanistic understanding of hydrogen-metal interactions, which cannot be easily demonstrated experimentally. Theoretical studies have revealed that hydrogen binding in subsurface layers of a metallic lattice results in a very stable state in most transition metals and that overcoming an activation barrier is often required for subsequent diffusion.[197] Hydrogen diffusion in the bulk phase between two interstitial sites, i.e., octahedral and tetrahedral sites, also involves an activation barrier[198] and possibly charge state variations between charged and neutral states.[199] In fact, a high charge density associated with hydrogen in metals may be correlated to strong hydrogen absorption, for instance, in the case of hydrogen in Group 5 metals and their alloys.[200] The phase stability of virtual alloy membrane materials has been evaluated by comparing alloy formation energies, segregation energies, and charge interactions.[201,202] Phase diagrams of Pd-based alloys in the presence of hydrogen or sulfur have been estimated by rigorous thermodynamic modeling combined with first-principles calculations, thereby further assessing the thermodynamic stability of materials under given temperature and pressure conditions.[203,204] The interaction between sulfur and membrane surfaces has been investigated through first-principles calculations that have provided the sulfur adsorption energy, release temperature, and segregation tendency of sulfur compounds.[202,205] Electronic coupling between the sulfur p-orbital and the metal d-band (valence electronic state of transition metals) was found to be the primary mode of interaction correlating directly to the sulfur adsorption strength.[205,206] Therefore, tuning the sulfur affinity through alloying of metals with different d-band centers (along the energy state with respect to Fermi-level) may be possible. A fundamental understanding of the interactions between membrane materials and gases may aid in the design of new materials with optimal properties and further may lead to the discovery of advanced membrane materials.

2.6 Metallic membrane opportunities for next-generation applications

2.6.1 Small-scale industrial applications

For smaller and emerging hydrogen markets such as the semiconductor and fuel cell industries, the use of Pd-based membranes is appropriate due to the scales and purity requirements. First, these applications are small- to medium-scale with capacities ranging from 5 to 1,000 m³/h,[36] more than 100 times smaller than large-scale applications such as refining and ammonia production. The inherent compactness of membrane units would enable on-site production of hydrogen for applications on these scales. Alternatively, distributed small-scale users can source hydrogen from large-scale plants at a reasonable production cost[36], but the high cost of distribution would make this option less attractive. The distribution cost of hydrogen is 15 times higher than that of liquid hydrocarbon fuels on a mass basis primarily due to higher pumping costs.[27] If CCUS is considered, CO₂ distribution to sequestration sites would contribute to the cost of small-scale production units. In this case, Sjardin et al. concluded from a techno-economic study that at a hydrogen production scale below 40 MW (*ca.* 12,300 m³/h^{ix}), MRs with CCUS (\$19/GJ) would become competitive with centralized H₂ production (\$18/GJ).[207] On-site hydrogen production would also provide self-sufficient supply and further circumvent delivery delays as well as issues with storage safety. Nevertheless, higher production costs due to smaller product sizes and safety concerns over local production and handling of hydrogen as an explosive gas should be taken into consideration.[28] Secondly, fuel cell and semiconductor applications require hydrogen of very high purities. In semiconductor manufacturing, hydrogen is used as a carrier gas for trace doping elements[19], and hydrogen of near absolute purity (99.999999%) is needed.[19,109] For PEMFCs, CO impurities in the hydrogen feed could strongly adsorb onto the catalyst, leading to catalyst deactivation and cell performance deterioration.[18,208,209] A CO concentration of as low

^{ix} Converted based on the higher heating value of hydrogen as used in Ref. [262] and the molar volume of an ideal gas at 298 K.

as 2 ppm has been recommended by the U.S. DOE for hydrogen used in onboard vehicle fuel cells[18], which corresponds to a hydrogen purity of 99.999+%. Such high purities are readily available from dense Pd-based membranes, which have a theoretically complete selectivity towards hydrogen.[18,207,210]

2.6.2 Power generation and large-scale hydrogen production

A foreseeable large-scale application of hydrogen is to be used as a low-carbon energy resource for electricity generation. This would differ from the current use of hydrogen, which is as a coolant for turbo generators.[211–215] When used as a fuel gas, high-pressure hydrogen[216] with a purity of less than 80% [109,217] is favored for conventional gas turbines. This hydrogen purity is necessary for maintaining a moderate flame temperature[111,218] to suppress NO_x formation in the combustion chamber[73,111,218], as current NO_x reduction technology in gas turbines cannot be used for hydrogen combustion.[73] If pre-combustion CO₂ capture is considered for H₂/CO₂ separation, membrane technology may be employed. In this case, a nitrogen or steam sweep gas can be used to increase the separation driving force by decreasing the permeate-side hydrogen partial pressure[73,216,218] in addition to reducing the required membrane surface area.[218] The sweep gas will also act as a diluent to control the flame temperature and reduce NO_x levels[111,218] as previously discussed. Since high purity is not a requirement for power generation, highly selective Pd-based membranes would lose their advantage compared to other membrane materials. For example, it has been estimated that a H₂/CO₂ selectivity ranging from 20 to 60 and a H₂/N₂ selectivity from 130 to 870 would be sufficient for integrated gasification combined cycle (IGCC) plants.[216] The more stringent H₂/N₂ selectivity is needed to prevent back-diffusion of N₂ into the CO₂-rich stream to meet the specifications for CO₂ pipeline transport and sequestration.[216] These selectivity requirements allow for a wider range of materials to be used, such as ceramic and polymeric membranes.[216]

Although the high operating temperature of Pd-based membranes, e.g., 300-600 °C, is compatible with exhaust streams of power plant applications, the high temperature range

Literature Review

is not unique to metallic membranes. For example, an operating temperature of 400 °C is accessible to microporous silica hydrogen-selective membranes[65,109] or even some high-temperature polymeric hydrogen-selective membranes. A common disadvantage of the hydrogen-selective membrane technology for turbine applications is that the hydrogen product exits the membrane from the low-pressure permeate side, which makes recompression necessary thereby imposing additional costs.[107,108,219,220]

Other separation technologies such as physical absorption, e.g., Selexol, have also been studied for pre-combustion CO₂ capture. The high partial pressure of CO₂ after the WGS reactor makes physical absorption of CO₂ a suitable approach for capturing carbon.[73] Computational modeling studies have shown that Pd-based membranes do not have a distinct advantage over physical absorption in terms of plant efficiency and costs. For example, Chiesa et al. concluded that an IGCC system with a Pd₆₀Cu₄₀ MR is more efficient by nearly 1.7% than a reference IGCC plant using Selexol for carbon capture.[218] Amelio et al. found that a Pd-Ag membrane-based IGCC plant has a slightly lower efficiency than an IGCC plant using a Selexol separation process. The reason for this lower efficiency is due to the fact that the membrane-based IGCC system consumes a larger fraction of its generated power for CO₂ compression and for producing steam as a sweep gas for the MR system. However, it is worth noting that the investment cost and the cost of electricity in the membrane-based system are 4% and 1.4% lower than the reference case, respectively.[221] Rezvani et al. found that the overall efficiency of IGCC with CO₂ capture using a Pd-Ag membrane is 3.7% higher than using Selexol, and the investment cost of the membrane system is 1.6% lower than the Selexol system. The results of these techno-economic studies are subject to assumptions on separation efficiencies, capital and operating costs, and even regulations on CO₂ capture, and therefore should be interpreted and compared with caution. Lab- and pilot-scale experimental studies will be needed to fully understand the potential opportunities and issues of applying Pd-based membranes in electricity generation with pre-combustion carbon capture.

In addition to electricity, hydrogen can be co-produced from coal- or natural gas-based processes. For instance, PSA can be integrated with the shift reactor for bulk hydrogen

recovery in the range of 70-85% and for high-purity hydrogen production[73,222], and this concept would be similar to the large-scale hydrogen production method conventionally employed. Techno-economic studies have shown that, similar to the case of electricity generation from an IGCC plant, Pd-based membranes may only offer modest efficiency improvements and cost savings compared to PSA or physical absorption. For example, Kreutz et al. assessed hydrogen production from coal gasification with Pd₆₀Cu₄₀ membranes and found that using Selexol for CO₂ capture and subsequent PSA for hydrogen purification that the former case offers a less than 1% reduction in capital costs, but that the hydrogen production cost is 2% greater.[223]

In theory, these metallic membranes for hydrogen production have a place within large-scale systems. However, experimental testing has yet to reinforce these claims. Until large-scale testing occurs, hydrogen production membranes will remain experimental in scale.

2.6.3 Hydrogen transportation and carbon dioxide capture via membrane technology

In the transportation sector, hydrogen can be used as a fuel for either adapted hydrogen internal combustion engines (ICEs) or onboard HFCV. Even when hydrogen is produced from SMR without CCUS, up to a 40% reduction in greenhouse gas emissions can be achieved in transportation due to the higher efficiency of a HFCV over a conventional gasoline-powered ICE vehicle.[27] Although the initial attention on HFCVs has shifted to other low-carbon transportation solutions such as biofuel and electric cars[224], steady research, design, and development (RD&D) progress has been made by leading international car and energy companies.[225] One of the remaining challenges is a lack of hydrogen fuel infrastructure.[225] In the meantime, on-site natural gas reforming at refueling stations could be a viable near- to medium-term solution[103,207], especially when low-cost natural gas is available.[103] Additionally, Pd-based MRs may be considered for distributed hydrogen production for application to the transportation sector. For instance, MRs can be used to produce hydrogen on a small scale (between 2-4 MW) at the refueling stations integrated with the existing natural gas infrastructure. [207]

Another option would be onboard hydrogen production for fuel cells. For this application, high-purity hydrogen has to be produced within highly space-compact devices, and traditional purification facilities would not be able to meet this requirement due to their complexity and size.[226] In this case, MRs would be advantageous for onboard applications given their ability to produce high-purity hydrogen within a small volume. In particular, the MR concept may potentially reduce the reactor volume by a factor of 10 to 100 compared to conventional SMR and the subsequent WGS reaction.[227] Another benefit of the MR is its high conversion efficiencies.

This onboard technology for transportation would have an MR on the vehicle, which would produce hydrogen for power (fuel cell or ICE) and temporarily store CO₂. The CO₂ sourced from the high-pressure side of the membrane would be stored outside of the membrane unit, and the compression energy would be provided by the original fuel source, i.e., compressed natural gas. Upon refueling, the temporarily stored CO₂ would be removed from the vehicle and subsequently used in a secondary market. In the case of small-scale hydrogen production with CO₂ capture, the trade-off between H₂ distribution to users and CO₂ transport to centralized facilities for usage should be balanced.

In 2004, the U.S. DOE investigated funding future research related to onboard fuel reforming and made a no-go decision. The investigation team believed the milestones could be met, but that the milestones could not be met in the timeframe allotted by the administration at that time. The original timeframe of 2030 was pushed up to 2015, thereby overpromising the potential onboard reforming technology at that time. Although the independent panel recommended a no-go decision, they also made a number of specific recommendations that, if implemented, would effectively continue support of onboard fuel processing RD&D.[228]

2.7 Challenges for Pd membrane applications

2.7.1 Structural and chemical stability of Pd

As mentioned briefly in section 3, one of the major challenges associated with the mechanical stability of pure Pd membranes arises from hydrogen embrittlement. The absorption of hydrogen into the Pd structure can induce the α -to- β phase transition at relatively low temperatures.[19] Palladium hydride (Pd-H) can exist as two distinct phases, α and β . The α phase is a solid solution while within the β phase, the H atoms are ordered within octahedral interstitial sites.[112] The distinct feature of the Pd-H phase diagram is that there is a miscibility gap where α and β phases coexist. The highest temperature beyond which the β phase cannot form is referred to as the “critical point”. The critical point is estimated to be approximately 298 °C and 2 MPa.[132,229] The existence of α and β phases depend on the atomic ratio of Pd to H. The α phase appears at concentrations of atomic hydrogen below Pd-H_{0.02}, while only the β phase exists at H concentrations higher than Pd-H_{0.58}. At H concentrations within Pd-H_{0.02-0.58} both phases coexist.[134] The X-ray powder diffraction (XRD) results reveal that, at room temperature, both the α and β phases of Pd-H alloys are FCC solid solutions and have lattice parameters greater than those of pure Pd.[230] The nucleation of β -hydride from the α phase will cause severe lattice strains which lead to membrane embrittlement after numerous α - β phase transitions.[195] The coexistence of two phases may lead to significant volume expansion and hence membrane failure. Therefore, it is crucial to operate the MR at temperatures above the critical temperature.[229]

The effect of hydrogen embrittlement on the integrity of the membrane has been studied extensively.[183,184,231,232] Embrittlement is simply defined as the weakening of the membrane metal structure due to the diffusion and permeation of H atoms in the lattice structure.[112] Kolachev has listed eight main mechanisms responsible for the embrittlement-induced failure of metallic membranes which can be categorized by two types.[232] Embrittlement of the first type is caused by the sources that are initially present in the metal structure and before application of stresses. This type of embrittlement

Literature Review

becomes more pronounced as the strain rate in the metal structure increases and is irreversible in nature. The embrittlement of the second type is caused by sources in the metal structure that only appear as the hydrogen concentration increases during the plastic deformation. Plastic deformation is defined as the “permanent distortion that occurs when a material is subjected to tensile, compressive, bending, or torsion stresses that exceed its yield strength and cause it to elongate, compress, buckle, bend, or twist”. [233]

The embrittlement of the first type may be caused by the:

- Formation of gaseous reaction products between the hydrogen atoms and impurities in the metal structure
- The formation and accumulation of molecular hydrogen in the discontinuities of the metal structures such as micro-shrinkage cavities or gas holes
- Formation of hydride precipitates
- Formation of dissolved hydrogen

The embrittlement of the second type can be caused by the:

- Decomposition of unstable solid solutions influenced by stresses
- Interaction of H atoms with moving dislocations
- Directional diffusion of H atoms due to nonuniform external elastic, thermal, and electric fields

Although the development of an embrittlement-resistant Pd-based MR is a challenge, this phenomenon and its adverse effects may be diminished by careful and accurate modeling and prediction of the temperature profile inside an MR, cautious selection of operating conditions, avoiding to apply pressure pulses, and optimizing membrane-support interactions.[112,234] Moreover, the embrittlement phenomena can be reduced or avoided by alloying pure Pd with different metals, as reported in section 3.

2.7.2 The effect of poisoning on the performance of Pd-based MRs

The surface of a Pd membrane is susceptible to contamination by chemical components in the gas stream, such as sulfur and carbon impurities. Hydrogen sulfide, at concentrations as low as 5-10 ppm, readily adsorbs onto the Pd surface leading to the formation of a strong metal-sulfur bond and, as a result, hydrogen dissociation may be substantially inhibited due to the lack of active sites available on the surface.[142,235,236] This surface inhibition may be the dominant mechanism of sulfur poisoning, but severe sulfur exposure may lead to bulk sulfide formation causing irreversible damage to the membrane.[237] This could be a significant drawback in the case of utilizing the syngas from coal gasification or natural gas reforming, which commonly contains concentrations from hundreds of ppm to several percent H₂S. [238,239] In order to reduce the sulfur content suitable for Pd-based membrane operation, pre-desulfurization may be required. Sulfur-resistant alloy membrane materials may also alleviate the impact of sulfur, as discussed previously in section 3.2. In addition to the sulfur poisoning, the formation and deposition of carbon in high-temperature catalytic applications such as methane reforming or dehydrogenation may lead to defects thereby shortening the membrane lifetime.[34,210]

Other compounds have also been reported that could lead to the poisoning of the Pd-based membrane and MRs and hindering of the hydrogen permeation. Carbon monoxide, steam, hydrocarbons, chlorine and mercury are the compounds/elements reported in the literature which may decrease the hydrogen permeating flux in a Pd-based MR. CO may compromise the permeating flux of hydrogen via two different mechanisms depending on the operating temperatures. At lower temperatures, the main mechanism for reducing hydrogen flux is the adsorption of CO molecules onto the Pd surface where they compete with hydrogen atoms for the active sites.[124,240] At higher temperatures the catalytic decomposition of CO molecules and carbon deposition on the Pd surface is the main mechanism for hampering the hydrogen permeation.[240] Some studies suggest that electronegative atoms such as chlorine and oxygen may act as a “poison” for the adsorption of the electropositive molecules such as hydrogen by “electronically” blocking the surrounding area next to the hydrogen molecules and preventing them from getting access to the active sites.[241]

Water vapor molecules can also poison the Pd surface and hinder the permeating flux of hydrogen, however, compared with CO molecules, water vapor has a more adverse effect.[124,236] At low temperatures the adsorption of water on the metal surface occurs due to physisorption of water dipoles on the Pd surface. At higher temperatures, however, dissociative chemisorption of water vapor molecules on the solid surface is the governing mechanism controlling the adsorption. Although the number of adsorbed water molecules decreases with increasing the temperature, the decomposition rate of the adsorbed molecules increases at elevated temperatures. This means that the dissociation of water molecules into hydrogen and oxygen atoms and the recombination of these atoms to reform the water molecules could potentially poison the Pd surface with the adsorbed oxygen atoms as explained by Heras et al.[242]

2.7.3 Pd availability

Although Pd-based membranes may be promising alternatives to PSA and cryogenic distillation for H₂ separation on small to medium scales, their success for large industrial scales is still uncertain due to the availability of Pd. Palladium is a precious metal that is finite and should be used sparingly in application. The global supply of Pd in 2012 was 186 tonnes, which still fell short of the demand in the same year of 242 tonnes.[243].

Primarily, Pd is used as a catalyst for automobile emission controls, electrical and electronic equipment, dental prostheses, and jewelry. In 2014, approximately 65% of the global Pd was used in the automobile industry and 14% in the electrical and electronic equipment sector.[244,245] The global Pd production in 2017 was around 225 tones. Only five countries account for more than 95% of the global Pd production, i.e., South Africa, Russia, U.S., Canada, and Zimbabwe.[246]

The 2019 U.S. Geological Survey mineral commodity summaries report estimates that the total global resources of the platinum-group metals (PGMs) are more than 100,000 tonnes. In particular, more than 75% of all produced Pd comes from two countries, i.e., Russia (38%) and South Africa (39%).[247]

The availability of Pd with regard to large-scale applications such as IGCC power plants has been discussed in detail by Helmi et al.[243] A key conclusion from their study is that given the scale of membrane material requirements predicted from modeling studies, even a rather optimistic assumption of membrane thickness would result in 1.2 to 9 tonnes of palladium for a single power plant with the electricity production capacity of 1 GWe. For example, Galuszka estimated that 1.2 tonnes of Pd would be required to supply hydrogen to a 1000 ton/day methanol synthesis plant from methane reforming using a 10- μm Pd coating on an Al_2O_3 supported tubular membrane filled with 5% Pd/ Al_2O_3 catalyst.[34] Helmi and coworkers estimated that approximately 2 tonnes of Pd would be needed for a 386-MW IGCC plant, given a thickness of 10 μm . [243] Membrane thickness, permeance, and composition all affect estimated Pd requirements but do not impact the amount required beyond an order of magnitude.[243]

To alleviate the concern of diminishing world Pd resources and provide a confident source well into the future[248], Pd may be recycled from a spent MR, similar to the automotive industry's recycling of metals from catalytic converters.[249] The average recycling rate of PGMs in chemical and petrochemical industries is 76%, and a feasible Pd recovery of 60% may be plausible with negligible cost.[207]

2.7.4 Technical challenges and uncertainties for Pd membrane scale-up

In addition to material availability, scale-up potential on the order of 1.5 million m^3/day may be another limiting factor preventing wider application of Pd-based membranes. Process-scale analysis from the literature has reported that Pd-based metallic membranes may not satisfy the production rate on a large scale for economic industrial hydrogen production while meeting the purity criteria.[216] Despite the promising progress observed in emerging small-scale membrane units,[69] it remains unclear whether thin, defect-free, and stable Pd-based membranes can be economically mass-produced; therefore, much RD&D is still needed in this area.[34,73,207,210,218]

Literature Review

Reducing the membrane thickness is a key factor in making Pd-based membranes cost-effective.[18,207,210] For example, it has been predicted that a membrane thickness below 20 μm could make Pd-based MRs competitive with traditional WGS reactors[18], yet today commercially-available membranes are 20-50 μm thick, and thinner membranes of 2-5 μm are only produced on the laboratory scale.[207] In order to support a thin metal layer, a high-quality porous substrate (e.g., a small pore size with a narrow pore size distribution) is required. In fact, this substrate becomes 50 times more expensive than the cost of the thin layer of Pd.[250] Therefore, for the composite membranes to be economically viable on an industrial scale, not only does the cost of the thin metallic layer need to be reduced but also the porous support.[195]

Enhanced permeability and reduced material cost may be achieved through investigation of new materials such as alloys, Earth-abundant metals, or amorphous metals, as discussed in section 3. Using new membrane materials or substrates combined with suitable fabrication methods could also alleviate instability against chemical impurities and thermal impacts. The high cost of Pd may be avoided by using Earth-abundant Group 5 metals, which cost approximately 1,000 times less than Pd at approximately \$15 per kg, compared with that of Pd which is more than \$49,000 per kg.

In addition to improved performance and lower costs, long-term stability and durability against aggressive chemical environments, high-pressure conditions, and thermal cycling are critical to scale-up and remain to be demonstrated for commercialization purposes.[210,218] The integration of catalysts into the membrane unit would add another layer of vulnerability-depending on how the catalyst is embedded, complete replacement of the module may be necessary if the catalyst fails.[251] It is therefore necessary to develop the ability to repair the membrane during operation for commercial application[34], which is currently done for commercial polymeric membranes.[34,210] Other scale-up challenges that need to be addressed include difficulties in sealing,[34,210,252] lack of pilot-scale performance data[252], and the need for material and design optimization to balance the reaction productivity and membrane flux.[34]

2.7.5 Cost of Pd membrane scale-up

Relevant to both the scale and material availability are economic considerations. Membranes are limited when it comes to economies of scale[34,251] and consequently have minor benefits of scale-up due to their modular nature.[207] The capital cost of membrane systems scales less than linearly with increasing plant size.[253] Assuming that Pd membranes have a module cost of \$1,500/ft² (\$16,146/m²)[109], based on the membrane surface area estimates by Chiesa and coworkers (~34,000 m²)[218], a capital investment of \$548 million would be needed for the membrane unit at a 420-MW IGCC plant. By comparison, the total capital investment for post-combustion amine absorption units in natural gas combined cycle (NGCC) plants has been estimated to be \$0.7-1.0 million/MW[254–256]^x, and that for physical absorption units (Selexol) for IGCC plants \$1.2(2007)-2.9(2006) million/MW.[255,257–259]^{xi} Whether it is justified to invest in metallic membrane-based carbon capture will depend on the trade-off between cost and required performance[34] and the adoption of a national policy framework on CO₂ emissions. Some authors have suggested that the cost of Pd membranes and their production will decrease as cumulative production increases.[260] For example, Iaquaniello and coworkers forecast that the cost of Pd-based membranes will be reduced from *ca.* \$112,432/m² ^{xii} at a cumulative production of 1000 m² to *ca.* \$1,253/m² when cumulative production reaches 10,000,000 m² worldwide.[260] However, if one assumes a membrane thickness of 10 μm, 10,000,000-m² of production would equate to 1,200 tonnes of Pd, which is more than five times the global mine production of palladium in 2018.[261] Given the already unstable Pd market[34,243], the effect of this large production on the price of Pd as well as whether the concept of economies associated with “learning by doing” would hold in this case remains uncertain.

^x The capital cost in Damen et al., 2007 was converted using the 2007 yearly average exchange rate of 1.370412. The inflation adjusted range will be \$0.87-1.24 million/MW in 2019.

^{xi} The inflation adjusted range will be \$1.48-2.90 million/MW in 2019

^{xii} Converted using the weighted average exchange rate of 1.392705 for EURUSD in 2011; same for the cost at 10,000,000-m² of cumulative production.

2.7.6 Hydrogen storage

Regardless of the production technology, one of the major challenges that needs to be addressed in the development of hydrogen fuel cells in specific and hydrogen economy in general, is the ability to store hydrogen in a safe, efficient, compact, and economic way. This problem arises from the fact the very low volumetric energy density of hydrogen, although the specific energy density of hydrogen is the highest. The volumetric energy density of various fuels has been compared in Table 2-8.

Table 2-8. Volumetric energy density of various fuels (adapted from [1])

Fuel	(BTU/ft³) @ STP	(BTU/ft³) @ 1,000 psi	(BTU/ft³) @ 5,000 psi	(BTU/ft³) @ 10,000 psi
Gasoline (liquid)	894,740	894,740	894,740	894,740
Propane (liquid)	782,000	782,000	782,000	782,000
Propane (gas)	2,450	175,000	-	-
Methane	985	70,357	-	-
Hydrogen	320	22,857	114,300	230,000

Due to the very low volumetric energy density of hydrogen, most of the hydrogen plants are constructed near to the final point of use such as the petroleum refineries and ammonia plants. As it can be seen in Table 2-8, even at the very high pressure of 5,000 psi, a hydrogen pipeline can only carry 12.8% of the equivalent energy of a gasoline pipeline. Due to these problems and cost considerations, it is recommended that rather than transporting hydrogen via pipelines, it would be more practical and economically viable to build the hydrogen fueling stations near the production sites.

Furthermore, the hydrogen fuel cell vehicles should have a driving range of at least 300 miles in order to be competitive with other technologies such as electric vehicles and internal combustion engine automobiles. In order to achieve this goal, a HFCV requires approximately 4-5 kg of hydrogen stored onboard. Storage of such quantity of hydrogen in a safe and operational manner requires addressing significant economic and engineering challenges.

Literature Review

Hydrogen can be stored as a gas, liquid, or solid state. Storage of hydrogen as a gas has been done successfully for many decades. However, this method is limited to the transportation of small amount of gas which are transported via gas cylinders over short distances for various industrial and research applications. For HFCVs however, there are still significant challenges to manufacture light weight, high resistance storage tanks at low cost. More specifically, the materials used for hydrogen storage tanks need to be significantly improved for this purpose. Hydrogen molecule is the smallest molecule on the periodic table which has a significant diffusion rate in the solid materials such as steel that is used in storage tanks. The penetrated hydrogen can react with the carbon present in the carbon steel and create hydrogen induced cracks which compromise the integrity of the storage tank. Most high-pressure hydrogen storage tanks operate at 350 bar while some advance composite materials can operate at pressures up to 700 bar and temperatures between -30 to 50 °C.

Hydrogen can also be stored as a liquid at temperatures as low as 20 K (-253 °C) and pressures as low as a few bars. There are some problems with the storage of hydrogen in liquid state though some of which are: a great amount of energy is required to cool down hydrogen to such low temperatures, the high cost of manufacturing the super-insulated storage tank, lack of safe and reliable infrastructure for transportation and fueling, and extra safety measures for filling and withdrawing of fuel such as purging with Nitrogen before refueling to avoid entry of the air into the tank and consequent explosion.

Hydrogen can also be stored in solid state using chemical reactions. Various metals such as palladium, titanium, iron, manganese, nickel, and chromium along with their alloys can react with hydrogen to form metal hydrides. Metal hydrides are of great interest for hydrogen storage in HFCVs due to their high volumetric density. Hydrogen can be absorbed onto the surface of a metal or an alloy according to the following exothermic reaction :



Literature Review

Where AB_z is an alloy, A is usually an early transition metal, rare earth metal or magnesium which form stable hydrides, B is a metal which does not form a stable hydride such as Ni, Co, Cr, Fe, Mn, or Al, and ΔH is the heat that is released upon reaction. In order to release hydrogen from its absorbed state, a small amount of heat will be supplied to the metal hydride which will shift the reaction to the left according to the Le Chatelier's principle. This reaction is conducted over the surface of an alloy which is placed into a pressurized vessel in just a few minutes. Although metal hydrides have shown a great potential for onboard hydrogen storage, they still are in the development phase to meet the desired hydrogen capacity and overcome the thermodynamic and kinetic challenges. There are other methods to store hydrogen in the solid state such as alkali metal hydrides, and carbon nanotubes which are still in the research and development phase.

References

- [1] Press RJ, Santhanam KS V., Miri MJ, Bailey A V., Takacs GA. Introduction to Hydrogen Technology .By Roman J. Press, K. S. V. Santhanam, Massoud J. Miri, Alla V. Bailey, and Gerald A. Takacs. John Wiley & Sons, Inc.; 2008.
- [2] Zeng K, Zhang D. Recent progress in alkaline water electrolysis for hydrogen production and applications. *Prog Energy Combust Sci* 2010;36:307–26. doi:10.1016/j.pecs.2009.11.002.
- [3] Hosseini SE, Wahid MA. Hydrogen production from renewable and sustainable energy resources: Promising green energy carrier for clean development. *Renew Sustain Energy Rev* 2016;57:850–66. doi:10.1016/j.rser.2015.12.112.
- [4] International Energy Agency (IEA). Global energy & CO₂ status report. 2018.
- [5] Jackson RB, Le Quéré C, Andrew RM, Canadell JG, Korsbakken JI, Liu Z, et al. Global energy growth is outpacing decarbonization. *Environ Res Lett* 2018;13. doi:10.1088/1748-9326/aaf303.
- [6] International Energy Agency (IEA). CO₂ Emissions from Fuel Combustion 2018 Highlights. vol. 1. OECD; 2018. doi:10.1787/co2_fuel-2014-en.
- [7] Davis SC, Boundy RG. Transportation Energy Data Book. vol. 37. Oak Ridge National Laboratory; 2019.
- [8] International Energy Agency (IEA). Tracking Clean Energy Progress 2017, “Energy Technology Perspectives 2017 Excerpt Informing Energy Sector Transformations.” Paris: International Energy Agency; 2017.
- [9] Intergovernmental Panel on Climate Change, IPCC. Climate Change 2014: Mitigation of Climate Change. Cambridge, United Kingdom and New York, NY, USA: 2014. doi:10.1017/CBO9781107415416.
- [10] Dincer I, Acar C. Innovation in hydrogen production. vol. 42. Elsevier Ltd; 2017. doi:10.1016/j.ijhydene.2017.04.107.
- [11] BALL M, WIETSCHEL M. The future of hydrogen – opportunities and challenges. *Int J Hydrogen Energy* 2009;34:615–27. doi:10.1016/j.ijhydene.2008.11.014.
- [12] Bose S, Kuila T, Nguyen TXH, Kim NH, Lau K, Lee JH. Polymer membranes for

- high temperature proton exchange membrane fuel cell: Recent advances and challenges. *Prog Polym Sci* 2011;36:813–43.
doi:10.1016/j.progpolymsci.2011.01.003.
- [13] Stern AG. A new sustainable hydrogen clean energy paradigm. *Int J Hydrogen Energy* 2018;43:4244–55. doi:10.1016/j.ijhydene.2017.12.180.
- [14] Pacala S, Socolow R. Stabilization wedges: Solving the climate problem for the next 50 years with current technologies. *Science (80-)* 2004;305:968–72.
doi:10.1126/science.1100103.
- [15] Kalamaras CM, Efstathiou AM. Hydrogen Production Technologies: Current State and Future Developments. *Conf Pap Energy* 2013;2013:1–9.
doi:10.1155/2013/690627.
- [16] MURADOV N, VEZIROLU T. From hydrocarbon to hydrogen?carbon to hydrogen economy. *Int J Hydrogen Energy* 2005;30:225–37.
doi:10.1016/j.ijhydene.2004.03.033.
- [17] Han J, Kim I-S, Choi K-S. High purity hydrogen generator for on-site hydrogen production. *Int J Hydrogen Energy* 2002;27:1043–7. doi:10.1016/S0360-3199(02)00003-4.
- [18] Mendes D, Mendes A, Madeira LM, Iulianelli A, Sousa JM, Basile A. The water-gas shift reaction: from conventional catalytic systems to Pd-based membrane reactors—a review. *Asia-Pacific J Chem Eng* 2010;5:111–37.
- [19] Philpott JE. Hydrogen diffusion technology. *Platin Met Rev* 1985;29:12–6.
- [20] Dou Y, Sun L, Ren J, Dong L. Opportunities and Future Challenges in Hydrogen Economy for Sustainable Development. *Hydrog. Econ. Supply Chain. Life Cycle Anal. Energy Transit. Sustain.*, Elsevier; 2017, p. 277–305. doi:10.1016/B978-0-12-811132-1.00010-9.
- [21] Schiebahn S, Grube T, Robinius M, Tietze V, Kumar B, Stolten D. Power to gas: Technological overview, systems analysis and economic assessment for a case study in Germany. *Int J Hydrogen Energy* 2015;40:4285–94.
doi:10.1016/j.ijhydene.2015.01.123.
- [22] Koj JC, Wulf C, Zapp P. Environmental impacts of power-to-X systems - A review of technological and methodological choices in Life Cycle Assessments.

Literature Review

- Renew Sustain Energy Rev 2019;112:865–79. doi:10.1016/j.rser.2019.06.029.
- [23] Buffo G, Marocco P, Ferrero D, Lanzini A, Santarelli M. Power-to-X and power-to-power routes. *Sol. Hydrog. Prod.*, Elsevier; 2019, p. 529–57. doi:10.1016/b978-0-12-814853-2.00015-1.
- [24] U.S. Department of Energy. Hydrogen & Fuel Cells Program 2018. <https://www.hydrogen.energy.gov/budget.html>.
- [25] Freedonia Group. World Hydrogen Industry Study with Forecasts for 2018 & 2023. Cleveland, OH: 2018.
- [26] Lee D-Y, Elgowainy AA, Dai Q. Life Cycle Greenhouse Gas Emissions of By-product Hydrogen from Chlor-Alkali Plants. Argonne, IL (United States): Argonne National Lab.(ANL), Argonne, IL (United States); 2017. doi:10.2172/1418333.
- [27] Lattin WC, Utgikar VP. Transition to hydrogen economy in the United States: A 2006 status report. *Int J Hydrogen Energy* 2007;32:3230–7. doi:10.1016/j.ijhydene.2007.02.004.
- [28] Armaroli N, Balzani V. The Hydrogen Issue. *ChemSusChem* 2011;4:21–36. doi:10.1002/cssc.201000182.
- [29] Mueller-Langer F, Tzimas E, Kaltschmitt M, Peteves S. Techno-economic assessment of hydrogen production processes for the hydrogen economy for the short and medium term. *Int J Hydrogen Energy* 2007;32:3797–810. doi:10.1016/j.ijhydene.2007.05.027.
- [30] Konieczny A, Mondal K, Wiltowski T, Dydo P. Catalyst development for thermocatalytic decomposition of methane to hydrogen. *Int J Hydrogen Energy* 2008;33:264–72. doi:10.1016/J.IJHYDENE.2007.07.054.
- [31] RAMACHANDRAN R, Menon RK. An overview of industrial uses of hydrogen. *Int J Hydrogen Energy* 1998;23:593–8. doi:10.1016/S0360-3199(97)00112-2.
- [32] Chaubey R, Sahu S, James OO, Maity S. A review on development of industrial processes and emerging techniques for production of hydrogen from renewable and sustainable sources. *Renew Sustain Energy Rev* 2013;23:443–62. doi:10.1016/j.rser.2013.02.019.
- [33] The Linde Group. Production and Utilization of Green Hydrogen. 2013.
- [34] Armor JN. Applications of catalytic inorganic membrane reactors to refinery

- products. *J Memb Sci* 1998;147:217–33. doi:10.1016/S0376-7388(98)00124-0.
- [35] Courty PR, Chauvel A. Catalysis, the turntable for a clean future. *Catal Today* 1996;29:3–15. doi:10.1016/0920-5861(95)00253-7.
- [36] Rostrup-Nielsen T. Manufacture of hydrogen. *Catal Today* 2005;106:293–6. doi:10.1016/j.cattod.2005.07.149.
- [37] Alfke G, Irion WW, Neuwirth OS. Oil refining. *Ullmann's Encycl. Ind. Chem.*, vol. 25, Weinheim, Germany: Wiley-VCH Verlag Gmb H & Co. KGaA; 2012.
- [38] Adris AM, Pruden BB, Lim CJ, Grace JR. On the Reported Attempts to Radically Improve the Performance of the Steam Methane Reforming Reactor. *Can J Chem Eng* 1996;74:177–86.
- [39] Fraile D, Lanoix J-C, Maio P, Rangel A, Torres A. Overview of the market segmentation for hydrogen across potential customer groups, based on key application areas. *CertifHy Proj* 2015:1–32.
- [40] da Silva Veras T, Mozer TS, da Costa Rubim Messeder dos Santos D, da Silva César A. Hydrogen: Trends, production and characterization of the main process worldwide. *Int J Hydrogen Energy* 2017;42:2018–33. doi:10.1016/j.ijhydene.2016.08.219.
- [41] Ham HC, Kwon BW, Lee CH, Joohyeng OH, Jang SC, Choi S-H, et al. High purity hydrogen production device and high purity hydrogen production method 2019.
- [42] Agnolucci P. Hydrogen infrastructure for the transport sector. *Int J Hydrogen Energy* 2007;32:3526–44. doi:http://dx.doi.org/10.1016/j.ijhydene.2007.02.016.
- [43] HUGO A, RUTTER P, PISTIKOPOULOS S, AMORELLI A, ZOIA G. Hydrogen infrastructure strategic planning using multi-objective optimization. *Int J Hydrogen Energy* 2005;30:1523–34. doi:10.1016/j.ijhydene.2005.04.017.
- [44] Wilson J, Burgh G. *Energizing our future: Rational choices for the 21st century.* John Wiley & Sons; 2007.
- [45] Olah GA. *Beyond oil and gas : the methanol economy .* Weinheim, Germany: Wiley-VCH; 2018.
- [46] Ren J, Gao S, Liang H, Tan S, Dong L. *The Role of Hydrogen Energy.* *Hydrog. Econ.*, Elsevier; 2017, p. 1–33. doi:10.1016/B978-0-12-811132-1.00001-8.

- [47] Soltani R, Rosen MA, Dincer I. Assessment of CO₂ capture options from various points in steam methane reforming for hydrogen production. *Int J Hydrogen Energy* 2014;39:20266–75. doi:10.1016/j.ijhydene.2014.09.161.
- [48] Faraji S, Sotudeh-Gharebagh R, Mostoufi N. Hydrogen recovery from refinery off-gases. *J Appl Sci* 2005;5:459–64.
- [49] Boyano A, Blanco-Marigorta AM, Morosuk T, Tsatsaronis G. Exergoenvironmental analysis of a steam methane reforming process for hydrogen production. *Energy* 2011;36:2202–14. doi:10.1016/j.energy.2010.05.020.
- [50] Johansson D, Franck P-Å åke, Berntsson T. Hydrogen production from biomass gasification in the oil refining industry - A system analysis. *Energy* 2012;38:212–27. doi:10.1016/j.energy.2011.12.011.
- [51] Maqbool W, Park SJ, Lee ES. Steam Methane Reforming of Natural Gas with Substantial Carbon Dioxide Contents—Process Optimization for Gas-to-Liquid Applications. *Appl. Mech. Mater.*, vol. 548, Trans Tech Publ; 2014, p. 316–20.
- [52] Nieva MA, Villaverde MM, Monzón A, Garetto TF, Marchi AJ. Steam-methane reforming at low temperature on nickel-based catalysts. *Chem Eng J* 2014;235:158–66. doi:10.1016/j.cej.2013.09.030.
- [53] MURADOV N, VEZIROGLU T. “Green” path from fossil-based to hydrogen economy: An overview of carbon-neutral technologies. *Int J Hydrogen Energy* 2008;33:6804–39. doi:10.1016/j.ijhydene.2008.08.054.
- [54] Muradov NZZ, Veziroğlu TNN. From hydrocarbon to hydrogen–carbon to hydrogen economy. *Int J Hydrogen Energy* 2005;30:225–37. doi:10.1016/j.ijhydene.2004.03.033.
- [55] Lee D, Cha K, Kim H-S, Park C, Kim Y. Syngas and hydrogen production via stepwise methane reforming over Cu-ferrite/YSZ. *Int J Energy Res* 2014;38:1522–30. doi:10.1002/er.3159.
- [56] Spath PL, Mann MK. Life cycle assessment of hydrogen production via natural gas steam reforming. National Renewable Energy Laboratory Golden, CO; 2000.
- [57] Barelli L, BIDINI G, Gallorini F, SERVILI S. Hydrogen production through sorption-enhanced steam methane reforming and membrane technology: A review. *Energy* 2008;33:554–70. doi:10.1016/j.energy.2007.10.018.

Literature Review

- [58] Barelli L, Bidini G, Gallorini F, Servili S. Hydrogen production through sorption-enhanced steam methane reforming and membrane technology: A review. *Energy* 2008;33:554–70. doi:10.1016/J.ENERGY.2007.10.018.
- [59] Chen Z, Po F, Grace JR, Lim CJ, Mahecha-Botero A, Rakib M, et al. Sorbent-enhanced/membrane-assisted steam-methane reforming. *Chem Eng Sci* 2008;63:170–82. doi:10.1016/j.ces.2007.09.031.
- [60] Rhodes C, Peter Williams B, King F, Hutchings GJ. Promotion of Fe₃O₄/Cr₂O₃ high temperature water gas shift catalyst. *Catal Commun* 2002;3:381–4. doi:10.1016/S1566-7367(02)00156-5.
- [61] Ratnasamy C, Wagner JP. Water Gas Shift Catalysis. *Catal Rev* 2009;51:325–440. doi:10.1080/01614940903048661.
- [62] Luengnaruemitchai A, Osuwan S, Gulari E. Comparative studies of low-temperature water–gas shift reaction over Pt/CeO₂, Au/CeO₂, and Au/Fe₂O₃ catalysts. *Catal Commun* 2003;4:215–21. doi:10.1016/S1566-7367(03)00036-0.
- [63] Basile A, Iulianelli A, Tong J. *Compendium of Hydrogen Energy: Hydrogen Production and Purification*. Boston, MA: Elsevier; 2015.
- [64] Hinchliffe AB, Porter KE. A Comparison of Membrane Separation and Distillation. *Chem Eng Res Des* 2000;78:255–68. doi:10.1205/026387600527121.
- [65] Adhikari S, Fernando S. Hydrogen membrane separation techniques. *Ind Eng Chem Res* 2006;45:875–81. doi:10.1021/ie050644l.
- [66] Bernardo P, Jansen JC. Polymeric membranes for the purification of hydrogen. *Compend. Hydrog. Energy*, Elsevier; 2015, p. 419–43. doi:10.1016/b978-1-78242-361-4.00014-5.
- [67] Iulianelli A, Liguori S, Wilcox J, Basile A. Advances on methane steam reforming to produce hydrogen through membrane reactors technology: A review. *Catal Rev - Sci Eng* 2016;58:1–35. doi:10.1080/01614940.2015.1099882.
- [68] Grashoff GJ, Pilkington CE, Corti CW. The purification of hydrogen. *Platin Met Rev* 1983;27:157–69.
- [69] Gallucci F, Fernandez E, Corengia P, van Sint Annaland M. Recent advances on membranes and membrane reactors for hydrogen production. *Chem Eng Sci* 2013;92:40–66. doi:10.1016/j.ces.2013.01.008.

Literature Review

- [70] Yong Z, Mata V, Rodrigues AE. Adsorption of Carbon Dioxide on Basic Alumina at High Temperatures. *J Chem Eng Data* 2000;45:1093–5. doi:10.1021/je000075i.
- [71] Lopes FVS, Grande CA, Ribeiro AM, Loureiro JM, Evaggelos O, Nikolakis V, et al. Adsorption of H₂, CO₂, CH₄, CO, N₂ and H₂O in Activated Carbon and Zeolite for Hydrogen Production. *Sep Sci Technol* 2009;44:1045–73. doi:10.1080/01496390902729130.
- [72] Malek A, Farooq S. Hydrogen purification from refinery fuel gas by pressure swing adsorption. *AIChE J* 1998;44:1985–92. doi:10.1002/aic.690440906.
- [73] Damen K, Troost M van, Faaij A, Turkenburg W. A comparison of electricity and hydrogen production systems with CO₂ capture and storage. Part A: Review and selection of promising conversion and capture technologies. *Prog Energy Combust Sci* 2006;32:215–46. doi:10.1016/j.pecs.2005.11.005.
- [74] Amphlett JC, Mann RF, Peppley BA. On board hydrogen purification for steam reformation/PEM fuel cell vehicle power plants. *Int J Hydrogen Energy* 1996;21:673–8. doi:10.1016/0360-3199(95)00131-X.
- [75] Kreutz T, Williams R, Consonni S, Chiesa P, Consonni S, Kreutz T, et al. Co-production of hydrogen, electricity and CO₂ from coal with commercially ready technology. Part A: Performance and emissions. *Int J Hydrogen Energy* 2005;30:747–67. doi:10.1016/j.ijhydene.2004.08.002.
- [76] Collodi G, Wheeler F. Hydrogen Production via Steam Reforming with CO₂ Capture. *4th Int Conf Saf Environ Process Ind* 2010;10.
- [77] Huang Q, Malekian A, Eić M, Q H, A M, M. E. Optimization of PSA process for producing enriched hydrogen from plasma reactor gas. *Sep Purif Technol* 2008;62:22–31. doi:doi.org/10.1016/j.seppur.2007.12.017.
- [78] Kikuchi E. Membrane reactor application to hydrogen production. *Catal Today* 2000;56:97–101. doi:10.1016/S0920-5861(99)00256-4.
- [79] Kikuchi E. Palladium/ceramic membranes for selective hydrogen permeation and their application to membrane reactor. *Catal Today* 1995;25:333–7. doi:10.1016/0920-5861(95)00085-T.
- [80] Iulianelli A, Manzolini G, De Falco M, Campanari S, Longo T, Liguori S, et al. H₂ production by low pressure methane steam reforming in a Pd-Ag membrane

- reactor over a Ni-based catalyst: Experimental and modeling. *Int J Hydrogen Energy* 2010;35:11514–24. doi:DOI: 10.1016/j.ijhydene.2010.06.049.
- [81] Ligthart DDAJM, Pieterse JAZZAZ, Hensen EJMMJM. The role of promoters for Ni catalysts in low temperature (membrane) steam methane reforming. *Appl Catal a-General* 2011;405:108–19. doi:10.1016/j.apcata.2011.07.035.
- [82] Lin YM, Liu SL, Chuang CH, Chu YT. Effect of incipient removal of hydrogen through palladium membrane on the conversion of methane steam reforming: Experimental and modeling. *Catal. Today*, vol. 82, Elsevier; 2003, p. 127–39. doi:10.1016/S0920-5861(03)00212-8.
- [83] Sarić M, van Delft YCC, Sumbharaju R, Meyer DFF, de Groot A. Steam reforming of methane in a bench-scale membrane reactor at realistic working conditions. *Catal Today* 2012;193:74–80. doi:10.1016/j.cattod.2012.04.009.
- [84] Simakov DSASA, Sheintuch M. Model-based optimization of hydrogen generation by methane steam reforming in autothermal packed-bed membrane reformer. *AIChE J* 2011;57:525–41. doi:10.1002/aic.12265.
- [85] Tong J, Matsumura Y. Effect of catalytic activity on methane steam reforming in hydrogen-permeable membrane reactor. *Appl Catal A Gen* 2005;286:226–31. doi:10.1016/j.apcata.2005.03.013.
- [86] Tong J, Matsumura Y, Suda H, Haraya K. Experimental Study of Steam Reforming of Methane in a Thin (6 μm) Pd-Based Membrane Reactor. *Ind Eng Chem Res* 2005;44:1454–65. doi:10.1021/ie049115s.
- [87] Lin Y-M, Lee G-LG-L, Rei M-HM-H. An integrated purification and production of hydrogen with a palladium membrane-catalytic reactor. *Catal Today* 1998;44:343–9. doi:10.1016/S0920-5861(98)00208-9.
- [88] Oklany JSS, Hou K, Hughes R. A simulative comparison of dense and microporous membrane reactors for the steam reforming of methane. *Appl Catal A* 1998;170:13–22. doi:10.1016/S0926-860X(98)00027-1.
- [89] Boeltken T, Wunsch A, Gietzelt T, Pfeifer P, Dittmeyer R. Ultra-compact microstructured methane steam reformer with integrated Palladium membrane for on-site production of pure hydrogen: Experimental demonstration. *Int J Hydrogen Energy* 2014;39:18058–68. doi:10.1016/j.ijhydene.2014.06.091.

Literature Review

- [90] Basile A, Campanari S, Manzolini G, Iulianelli A, Longo T, Liguori S, et al. Methane steam reforming in a Pd–Ag membrane reformer: An experimental study on reaction pressure influence at middle temperature. *Int J Hydrogen Energy* 2011;36:1531–9. doi:10.1016/j.ijhydene.2010.10.101.
- [91] Chen Y, Wang Y, Xu H, Xiong G. Efficient production of hydrogen from natural gas steam reforming in palladium membrane reactor. *Appl Catal B Environ* 2008;81:283–94. doi:10.1016/j.apcatb.2007.10.024.
- [92] De Falco M, Iaquaniello G, Salladini A. Experimental tests on steam reforming of natural gas in a reformer and membrane modules (RMM) plant. *J Memb Sci* 2011;368:264–74. doi:10.1016/j.memsci.2010.11.050.
- [93] Dittmar B, Behrens A, Schödel N, Rüttinger M, Franco T, Straczewski G, et al. Methane steam reforming operation and thermal stability of new porous metal supported tubular palladium composite membranes. *Int J Hydrogen Energy* 2013;38:8759–71. doi:10.1016/j.ijhydene.2013.05.030.
- [94] Hwang K-RRR, Lee C-BBB, Ryi S-KKK, Lee S-WWW, Park J-SSS. A multi-membrane reformer for the direct production of hydrogen via a steam-reforming reaction of methane. *Int J Hydrogen Energy* 2012;37:6601–7. doi:10.1016/j.ijhydene.2012.01.022.
- [95] Steward SA, Laboratory LLN. Review of Hydrogen Isotope Permeability Through Materials. Lawrence Livermore National Laboratory; 1983.
- [96] Yun S, Ted Oyama S. Correlations in palladium membranes for hydrogen separation: A review. *J Memb Sci* 2011;375:28–45. doi:10.1016/j.memsci.2011.03.057.
- [97] Adris A-EM. A fluidized bed membrane reactor for steam methane reforming: experimental verification and model validation. University of British Columbia, 1994.
- [98] Andújar JM, Segura F. Fuel cells: History and updating. A walk along two centuries. *Renew Sustain Energy Rev* 2009;13:2309–22. doi:10.1016/J.RSER.2009.03.015.
- [99] Ball M, Weeda M. The hydrogen economy – Vision or reality? *Int J Hydrogen Energy* 2015;40:7903–19. doi:10.1016/j.ijhydene.2015.04.032.

Literature Review

- [100] Emadi A, Rajashekara K, Williamson SSS, Lukic SMM. Topological overview of hybrid electric and fuel cell vehicular power system architectures and configurations. *IEEE Trans Veh Technol* 2005;54:763–70. doi:10.1109/TVT.2005.847445.
- [101] Körner A, Tam C, Bennett S, Gagné JF. Technology roadmap-hydrogen and fuel cells. Int Energy Agency Paris, Fr 2015.
- [102] Dougherty W, Kartha S, Rajan C, Lazarus M, Bailie A, Runkle B, et al. Greenhouse gas reduction benefits and costs of a large-scale transition to hydrogen in the USA. *Energy Policy* 2009;37:56–67. doi:10.1016/J.ENPOL.2008.06.039.
- [103] Chu S, Majumdar A. Opportunities and challenges for a sustainable energy future. *Nature* 2012;488:294–303. doi:10.1038/nature11475.
- [104] Lin YS, Buxbaum RE. METAL MEMBRANES: MEMBRANE SEPARATIONS. *Encycl. Sep. Sci.*, San Diego, CA: Elsevier; 2000, p. 3365–72. doi:10.1016/B0-12-226770-2/05301-1.
- [105] Baker RW. *Membrane Technology and Applications*. 3rd ed. Oxford: Wiley-Blackwell; 2012.
- [106] Edlund D. Hydrogen membrane technologies and application in fuel processing. *Hydrog Syngas Prod Purif Technol* 2009;357–84.
- [107] Koros WJ, Mahajan R. Pushing the limits on possibilities for large scale gas separation: which strategies? *J Memb Sci* 2000;175:181–96. doi:10.1016/S0376-7388(00)00418-X.
- [108] Paglieri SN, Way JD. INNOVATIONS IN PALLADIUM MEMBRANE RESEARCH. *Sep Purif Methods* 2002;31:1–169. doi:10.1081/SPM-120006115.
- [109] Ockwig NW, Nenoff TM. Membranes for Hydrogen Separation. *Chem Rev* 2007;107:4078–110. doi:10.1021/cr0501792.
- [110] SJARDIN M, Damen K, FAAIJ A. Techno-economic prospects of membrane reactors in a future hydrogen-driven transportation sector. vol. 31. Elsevier; 2005. doi:10.1016/B978-008044704-9/50375-X.
- [111] Merkel TC, Zhou M, Baker RW. Carbon dioxide capture with membranes at an IGCC power plant. *J Memb Sci* 2012;389:441–50. doi:10.1016/j.memsci.2011.11.012.

- [112] Dolan MD. Non-Pd BCC alloy membranes for industrial hydrogen separation. *J Memb Sci* 2010;362:12–28. doi:10.1016/j.memsci.2010.06.068.
- [113] Wilcox J, Haghpanah R, Rupp EC, He J, Lee K. Advancing Adsorption and Membrane Separation Processes for the Gigaton Carbon Capture Challenge. *Annu Rev Chem Biomol Eng* 2014;5:479–505. doi:10.1146/annurev-chembioeng-060713-040100.
- [114] Zeng G, Goldbach A, Xu H. Defect sealing in Pd membranes via point plating. *J Memb Sci* 2009;328:6–10. doi:10.1016/j.memsci.2008.11.053.
- [115] Moss TS, Peachey NM, Snow RC, Dye RC. Multilayer metal membranes for hydrogen separation. *Int J Hydrogen Energy* 1998;23:99–106. doi:10.1016/S0360-3199(97)00030-X.
- [116] Ogden JM. Review of small stationary reformers for hydrogen production. Rep to Int Energy Agency 2001:1–64.
- [117] Conde JJ, Maroño M, Sánchez-Hervás JM. Pd-Based Membranes for Hydrogen Separation: Review of Alloying Elements and Their Influence on Membrane Properties. *Sep Purif Rev* 2017;46:152–77. doi:10.1080/15422119.2016.1212379.
- [118] Catalano J, Giacinti Baschetti M, Sarti GC. Influence of the gas phase resistance on hydrogen flux through thin palladium–silver membranes. *J Memb Sci* 2009;339:57–67. doi:10.1016/J.MEMSCI.2009.04.032.
- [119] Yan S, Maeda H, Kusakabe K, Morooka S. Thin Palladium Membrane Formed in Support Pores by Metal-Organic Chemical Vapor Deposition Method and Application to Hydrogen Separation. vol. 33. 1994.
- [120] Rahimpour MR, Samimi F, Babapoor A, Tohidian T, Mohebi S. Palladium membranes applications in reaction systems for hydrogen separation and purification: A review. *Chem Eng Process Process Intensif* 2017;121:24–49. doi:10.1016/j.cep.2017.07.021.
- [121] Morreale BD, Ciocco M V., Enick RM, Morsi BI, Howard BH, Cugini A V., et al. The permeability of hydrogen in bulk palladium at elevated temperatures and pressures. *J Memb Sci* 2003;212:87–97. doi:10.1016/S0376-7388(02)00456-8.
- [122] Guazzone F. Engineering of substrate surface for the synthesis of ultra-thin composite Pd and Pd-Cu membranes for H₂ Separation 2005.

Literature Review

- [123] Ward TL, Dao T. Model of hydrogen permeation behavior in palladium membranes. *J Memb Sci* 1999;153:211–31. doi:10.1016/S0376-7388(98)00256-7.
- [124] Kian K, Woodall C, Wilcox J, Liguori S. Performance of Pd-Based Membranes and Effects of Various Gas Mixtures on H₂ Permeation. *Environments* 2018;5:128. doi:10.3390/environments5120128.
- [125] San Marchi C, Somerday B, Robinson S. Permeability, solubility and diffusivity of hydrogen isotopes in stainless steels at high gas pressures. *Int J Hydrogen Energy* 2007;32:100–16. doi:10.1016/j.ijhydene.2006.05.008.
- [126] Deveau ND, Ma YH, Datta R. Beyond Sieverts' law: A comprehensive microkinetic model of hydrogen permeation in dense metal membranes. *J Memb Sci* 2013;437:298–311. doi:10.1016/j.memsci.2013.02.047.
- [127] Vadrucci M, Borgognoni F, Moriani A, Santucci A, Tosti S. Hydrogen permeation through Pd-Ag membranes: Surface effects and Sieverts' law. *Int J Hydrogen Energy* 2013;38:4144–52. doi:10.1016/j.ijhydene.2013.01.091.
- [128] Caravella A, Barbieri G, Drioli E. Concentration polarization analysis in self-supported Pd-based membranes. *Sep Purif Technol* 2009;66:613–24. doi:10.1016/j.seppur.2009.01.008.
- [129] Caravella A, Scura F, Barbieri G, Drioli E. Sieverts law empirical exponent for PD-based membranes: Critical analysis in pure H₂ permeation. *J Phys Chem B* 2010;114:6033–47. doi:10.1021/jp1006582.
- [130] Guazzone F, Engwall EE, Ma YH. Effects of surface activity, defects and mass transfer on hydrogen permeance and n-value in composite palladium-porous stainless steel membranes. *Catal Today* 2006;118:24–31. doi:10.1016/J.CATTOD.2005.12.010.
- [131] Liguori S, Iulianelli A, Dalena F, Pinacci P, Drago F, Broglia M, et al. Performance and long-term stability of Pd/PSS and Pd/Al₂O₃ membranes for hydrogen separation. *Membranes (Basel)* 2014;4:143–62. doi:10.3390/membranes4010143.
- [132] Arratibel Plazaola A, Pacheco Tanaka D, Van Sint Annaland M, Gallucci F. Recent Advances in Pd-Based Membranes for Membrane Reactors. *Molecules* 2017;22:51. doi:10.3390/molecules22010051.

- [133] Okazaki J, Ikeda T, Tanaka DAP, Sato K, Suzuki TM, Mizukami F. An investigation of thermal stability of thin palladium–silver alloy membranes for high temperature hydrogen separation. *J Memb Sci* 2011;366:212–9. doi:10.1016/J.MEMSCI.2010.10.011.
- [134] Baloyi LN, North BC, Langmi HW, Bladergroen BJ, Ojumu T V. The production of hydrogen through the use of a 77 wt% Pd 23 wt% Ag membrane water gas shift reactor. *South African J Chem Eng* 2016;22:44–54. doi:10.1016/j.sajce.2016.11.001.
- [135] Knapton AG. Palladium alloys for hydrogen diffusion membranes. *Platin Met Rev* 1977;21:44–50.
- [136] Peters TA, Stange M, Klette H, Bredesen R. High pressure performance of thin Pd–23%Ag/stainless steel composite membranes in water gas shift gas mixtures; influence of dilution, mass transfer and surface effects on the hydrogen flux. *J Memb Sci* 2008;316:119–27. doi:10.1016/j.memsci.2007.08.056.
- [137] Borgognoni F, Tosti S, Vadrucci M, Santucci A. Pure hydrogen production in a Pd-Ag multi-membranes module by methane steam reforming. *Int J Hydrogen Energy* 2011;36:7550–8. doi:10.1016/j.ijhydene.2011.03.120.
- [138] Brunetti A, Caravella A, Drioli E, Barbieri G. Process Intensification by Membrane Reactors: High-Temperature Water Gas Shift Reaction as Single Stage for Syngas Upgrading. *Chem Eng Technol* 2012;35:1238–48. doi:10.1002/ceat.201100641.
- [139] Morreale BD, Ciocco M V., Howard BH, Killmeyer RP, Cugini A V., Enick RM. Effect of hydrogen-sulfide on the hydrogen permeance of palladium-copper alloys at elevated temperatures. *J Memb Sci* 2004;241:219–24. doi:10.1016/j.memsci.2004.04.033.
- [140] Kulprathipanja A, Alptekin GO, Falconer JL, Way JD. Pd and Pd-Cu membranes: Inhibition of H₂ permeation by H₂S. *J Memb Sci* 2005;254:49–62. doi:10.1016/j.memsci.2004.11.031.
- [141] Pomerantz N, Ma YH. Effect of H₂S on the Performance and Long-Term Stability of Pd/Cu Membranes. *Ind Eng Chem Res* 2009;48:4030–9. doi:10.1021/ie801947a.

- [142] Mundschau M V., Xie X, Evenson IV CR, Sammells AF. Dense inorganic membranes for production of hydrogen from methane and coal with carbon dioxide sequestration. *Catal Today* 2006;118:12–23.
doi:10.1016/j.cattod.2006.01.042.
- [143] Gharibi H, Saadatinasab M, Zolfaghari A. Hydrogen permeability and sulfur tolerance of a novel dual membrane of PdAg/PdCu layers deposited on porous stainless steel. *J Memb Sci* 2013;447:355–61. doi:10.1016/j.memsci.2013.07.037.
- [144] Braun F, Tarditi AM, Miller JB, Cornaglia LM. Pd-based binary and ternary alloy membranes: Morphological and perm-selective characterization in the presence of H₂S. *J Memb Sci* 2014;450:299–307. doi:10.1016/j.memsci.2013.09.026.
- [145] Chen C-H, Ma YH. The effect of H₂S on the performance of Pd and Pd/Au composite membrane. *J Memb Sci* 2010;362:535–44.
doi:10.1016/j.memsci.2010.07.002.
- [146] Howard BH, Morreale BD. Effect of H₂S on performance of Pd₄Pt alloy membranes. *Energy Mater* 2008;3:177–85.
doi:10.1179/174892309X12519750237717.
- [147] Lewis AE, Kershner DC, Paglieri SN, Slepicka MJ, Way JD. Pd–Pt/YSZ composite membranes for hydrogen separation from synthetic water–gas shift streams. *J Memb Sci* 2013;437:257–64. doi:10.1016/j.memsci.2013.02.056.
- [148] Gade SK, DeVoss SJ, Coulter KE, Paglieri SN, Alptekin GO, Way JD. Palladium–gold membranes in mixed gas streams with hydrogen sulfide: Effect of alloy content and fabrication technique. *J Memb Sci* 2011;378:35–41.
doi:10.1016/j.memsci.2010.11.044.
- [149] Nayebossadri S, Speight J, Book D. Effects of low Ag additions on the hydrogen permeability of Pd–Cu–Ag hydrogen separation membranes. *J Memb Sci* 2014;451:216–25. doi:10.1016/j.memsci.2013.10.002.
- [150] Tarditi AM, Braun F, Cornaglia LM. Novel PdAgCu ternary alloy: Hydrogen permeation and surface properties. *Appl Surf Sci* 2011;257:6626–35.
doi:10.1016/j.apsusc.2011.02.089.
- [151] Tarditi AM, Cornaglia LM. Novel PdAgCu ternary alloy as promising materials for hydrogen separation membranes: Synthesis and characterization. *Surf Sci*

- 2011;605:62–71. doi:10.1016/j.susc.2010.10.001.
- [152] Braun F, Miller JB, Gellman AJ, Tarditi AM, Fleutot B, Kondratyuk P, et al. PdAgAu alloy with high resistance to corrosion by H₂S. *Int J Hydrogen Energy* 2012;37:18547–55. doi:10.1016/j.ijhydene.2012.09.040.
- [153] Coulter KE, Way JD, Gade SK, Chaudhari S, Alptekin GO, DeVoss SJ, et al. Sulfur tolerant PdAu and PdAuPt alloy hydrogen separation membranes. *J Memb Sci* 2012;405–406:11–9. doi:10.1016/j.memsci.2012.02.018.
- [154] Gade SK, Thoen PM, Way JD. Unsupported palladium alloy foil membranes fabricated by electroless plating. *J Memb Sci* 2008;316:112–8. doi:10.1016/j.memsci.2007.08.022.
- [155] Pacheco Tanaka DA, Llosa Tanco MA, Nagase T, Okazaki J, Wakui Y, Mizukami F, et al. Fabrication of Hydrogen-Permeable Composite Membranes Packed with Palladium Nanoparticles. *Adv Mater* 2006;18:630–2. doi:10.1002/adma.200501900.
- [156] Peters TA, Stange M, Bredesen R. On the high pressure performance of thin supported Pd–23%Ag membranes—Evidence of ultrahigh hydrogen flux after air treatment. *J Memb Sci* 2011;378:28–34. doi:10.1016/j.memsci.2010.11.022.
- [157] Nair BKR, Choi J, Harold MP. Electroless plating and permeation features of Pd and Pd/Ag hollow fiber composite membranes. *J Memb Sci* 2007;288:67–84. doi:10.1016/j.memsci.2006.11.006.
- [158] Zhang K, Gade SK, Way JD. Effects of heat treatment in air on hydrogen sorption over Pd–Ag and Pd–Au membrane surfaces. *J Memb Sci* 2012;403–404:78–83. doi:10.1016/j.memsci.2012.02.025.
- [159] Chen W-H, Hsu P-C. Hydrogen permeation measurements of Pd and Pd–Cu membranes using dynamic pressure difference method. *Int J Hydrogen Energy* 2011;36:9355–66. doi:10.1016/j.ijhydene.2011.04.141.
- [160] Shi L, Goldbach A, Xu H. High-flux H₂ separation membranes from (Pd/Au)_n nanolayers. *Int J Hydrogen Energy* 2011;36:2281–4. doi:10.1016/j.ijhydene.2010.11.056.
- [161] Hara S, Sakaki K, Itoh N, Kimura H-M, Asami K, Inoue A. An amorphous alloy membrane without noble metals for gaseous hydrogen separation. *J Memb Sci*

- 2000;164:289–94. doi:10.1016/S0376-7388(99)00192-1.
- [162] Yamaura S, Sakurai M, Hasegawa M, Wakoh K, Shimpo Y, Nishida M, et al. Hydrogen permeation and structural features of melt-spun Ni–Nb–Zr amorphous alloys. *Acta Mater* 2005;53:3703–11. doi:10.1016/j.actamat.2005.04.023.
- [163] Dolan M, Dave N, Morpeth L, Donelson R, Liang D, Kellam M, et al. Ni-based amorphous alloy membranes for hydrogen separation at 400°C. *J Memb Sci* 2009;326:549–55. doi:10.1016/j.memsci.2008.10.030.
- [164] Phair JW, Donelson R. Developments and Design of Novel (Non-Palladium-Based) Metal Membranes for Hydrogen Separation. *Ind Eng Chem Res* 2006;45:5657–74. doi:10.1021/ie051333d.
- [165] Buxbaum RE, Marker TL. Hydrogen transport through non-porous membranes of palladium-coated niobium, tantalum and vanadium. *J Memb Sci* 1993;85:29–38. doi:10.1016/0376-7388(93)85004-G.
- [166] Buxbaum RE, Kinney AB. Hydrogen Transport through Tubular Membranes of Palladium-Coated Tantalum and Niobium. *Ind Eng Chem Res* 1996;35:530–7. doi:10.1021/ie950105o.
- [167] Bair J, Asle Zaeem M, Tonks M. A review on hydride precipitation in zirconium alloys. *J Nucl Mater* 2015;466:12–20.
- [168] Nishimura C, Komaki M, Amano M. HYDROGEN PERMEATION CHARACTERISTICS OF VANADIUM-NICKEL ALLOYS. *Mater Trans Jim* 1991;32:501–7.
- [169] Dolan MD, Song G, Liang D, Kellam ME, Chandra D, Lamb JH. Hydrogen transport through V85Ni10M5 alloy membranes. *J Memb Sci* 2011;373:14–9. doi:10.1016/j.memsci.2011.02.028.
- [170] Amano M, Komaki M, Nishimura C. Hydrogen permeation characteristics of palladium-plated V-Ni alloy membranes. *J Less Common Met* 1991;172–174:727–31. doi:10.1016/0022-5088(91)90196-B.
- [171] Yukawa H, Nambu T, Matsumoto Y. V–W alloy membranes for hydrogen purification. *J Alloys Compd* 2011;509:S881–4. doi:10.1016/j.jallcom.2010.09.161.
- [172] Ozaki T, Zhang Y, Komaki M, Nishimura C. Hydrogen permeation characteristics

Literature Review

- of V–Ni–Al alloys. *Int J Hydrogen Energy* 2003;28:1229–35. doi:10.1016/S0360-3199(02)00251-3.
- [173] Dolan MD, Dave NC, Ilyushechkin AY, Morpeth LD, McLennan KG. Composition and operation of hydrogen-selective amorphous alloy membranes. *J Memb Sci* 2006;285:30–55. doi:10.1016/j.memsci.2006.09.014.
- [174] Paglieri SN, Wermer JR, Buxbaum RE, Ciocco M V, Howard BH, Morreale BD. Development of membranes for hydrogen separation: Pd coated V–10Pd. *Energy Mater* 2008;3:169–76. doi:10.1179/174892409X427931.
- [175] Dolan MD, McLennan KG, Way JD. Diffusion of Atomic Hydrogen through V–Ni Alloy Membranes under Nondilute Conditions. *J Phys Chem C* 2012;116:1512–8. doi:10.1021/jp208691x.
- [176] Zhang Y, Ozaki T, Komaki M, Nishimura C. Hydrogen permeation characteristics of vanadium–aluminium alloys. *Scr Mater* 2002;47:601–6. doi:10.1016/S1359-6462(02)00218-X.
- [177] Roark SE, Mackay R, Mundschau M V. Dense, layered membranes for hydrogen separation, 2006.
- [178] Magnone E, Jeon SI, Park JH, Fleury E. Hydrogen Permeation Properties and Chemical Stability of Novel Pd-Free Alloy Membranes Based on the V–Y System. *Chem Eng Technol* 2012;35:469–72. doi:10.1002/ceat.201100456.
- [179] Yukawa H, Tsukada C, Nambu T, Matsumoto Y. Hydrogen solubility and permeability of V–W–Mo alloy membrane for hydrogen separation and purification. *J Alloys Compd* 2013;580:S386–90. doi:10.1016/j.jallcom.2013.03.144.
- [180] Yukawa H, Zhang GX, Watanabe N, Morinaga M, Nambu T, Matsumoto Y. Analysis of hydrogen diffusion coefficient during hydrogen permeation through niobium and its alloys. *J Alloys Compd* 2009;476:102–6. doi:10.1016/j.jallcom.2008.08.054.
- [181] Awakura Y, Nambu T, Matsumoto Y, Yukawa H. Hydrogen solubility and permeability of Nb–W–Mo alloy membrane. *J Alloys Compd* 2011;509:S877–80. doi:10.1016/j.jallcom.2010.10.133.
- [182] Yamaura S, Shimpo Y, Okouchi H, Nishida M, Kajita O, Kimura H, et al.

- Hydrogen permeation characteristics of melt-spun Ni-Nb-Zr amorphous alloy membranes. *Mater Trans* 2003;44:1885–90.
- [183] Hashi K, Ishikawa K, Matsuda T, Aoki K. Microstructures and hydrogen permeability of Nb-Ti-Ni alloys with high resistance to hydrogen embrittlement. *Mater Trans* 2005;46:1026–31.
- [184] Paglieri SN, Pal NK, Dolan MD, Kim S-M, Chien W-M, Lamb J, et al. Hydrogen permeability, thermal stability and hydrogen embrittlement of Ni–Nb–Zr and Ni–Nb–Ta–Zr amorphous alloy membranes. *J Memb Sci* 2011;378:42–50. doi:<http://dx.doi.org/10.1016/j.memsci.2011.04.049>.
- [185] Ding HY, Zhang W, Yamaura SI, Yao KF. Hydrogen Permeable Nb-Based Amorphous Alloys with High Thermal Stability. *Mater Trans* 2013;54:1330–4. doi:10.2320/matertrans.MF201310.
- [186] Rothenberger KS, Howard BH, Killmeyer RP, Cugini A V, Enick RM, Bustamante F, et al. Evaluation of tantalum-based materials for hydrogen separation at elevated temperatures and pressures☆. *J Memb Sci* 2003;218:19–37. doi:10.1016/S0376-7388(03)00134-0.
- [187] Westerwaal RJ, den Besten C, Slaman M, Dam B, Nanu DE, Böttger AJ, et al. High throughput screening of Pd-alloys for H₂ separation membranes studied by hydrogenography and CVM. *Int J Hydrogen Energy* 2011;36:1074–82. doi:10.1016/j.ijhydene.2010.10.014.
- [188] Priyadarshini D, Kondratyuk P, Picard YN, Morreale BD, Gellman AJ, Miller JB. High-Throughput Characterization of Surface Segregation in Cu x Pd 1– x Alloys. *J Phys Chem C* 2011;115:10155–63. doi:10.1021/jp201793d.
- [189] Kamakoti P. Prediction of Hydrogen Flux Through Sulfur-Tolerant Binary Alloy Membranes. *Science (80-)* 2005;307:569–73. doi:10.1126/science.1107041.
- [190] Semidey-Flecha L, Sholl DS. Combining density functional theory and cluster expansion methods to predict H₂ permeance through Pd-based binary alloy membranes. *J Chem Phys* 2008;128:144701. doi:10.1063/1.2900558.
- [191] Sonwane CG, Wilcox J, Ma YH. Achieving optimum hydrogen permeability in PdAg and PdAu alloys. *J Chem Phys* 2006;125:184714. doi:10.1063/1.2387166.
- [192] Hao S, Sholl DS. Using first-principles calculations to accelerate materials

- discovery for hydrogen purification membranes by modeling amorphous metals. *Energy Environ Sci* 2008;1:175. doi:10.1039/b806909n.
- [193] Hao S, Sholl DS. Comparison of first principles calculations and experiments for hydrogen permeation through amorphous ZrNi and ZrNiNb films. *J Memb Sci* 2010;350:402–9. doi:10.1016/j.memsci.2010.01.017.
- [194] Hao S, Sholl DS. Rapid prediction of hydrogen permeation through amorphous metal membranes: an efficient computational screening approach. *Energy Environ Sci* 2013;6:232–40. doi:10.1039/C2EE23180H.
- [195] Ma YH. *Composite Pd and Pd/Alloy Membranes*, Springer; 2009, p. 241–54.
- [196] Sholl DSS, Steckel JAA. *Density Functional Theory: A Practical Introduction*. John Wiley & Sons, Inc., Inc.: John Wiley & Sons, Inc.; 2009.
- [197] Ferrin P, Kandoi S, Nilekar AU, Mavrikakis M. Hydrogen adsorption, absorption and diffusion on and in transition metal surfaces: A DFT study. *Surf Sci* 2012;606:679–89. doi:10.1016/j.susc.2011.12.017.
- [198] Kamakoti P. A comparison of hydrogen diffusivities in Pd and CuPd alloys using density functional theory. *J Memb Sci* 2003;225:145–54. doi:10.1016/j.memsci.2003.07.008.
- [199] Koroteev YM, Gimranova O V, Chernov IP. Hydrogen migration in palladium: First-principles calculations. *Phys Solid State* 2011;53:896–900. doi:10.1134/S1063783411050143.
- [200] Aboud S, Wilcox J. A Density Functional Theory Study of the Charge State of Hydrogen in Metal Hydrides. *J Phys Chem C* 2010;114:10978–85. doi:10.1021/jp911811r.
- [201] Gao MC, Ouyang L, Doğan ÖN. First principles screening of B2 stabilizers in CuPd-based hydrogen separation membranes: (1) Substitution for Pd. *J Alloys Compd* 2013;574:368–76. doi:10.1016/j.jallcom.2013.05.126.
- [202] Løvvik OM, Peters TA, Bredesen R. First-principles calculations on sulfur interacting with ternary Pd–Ag–transition metal alloy membrane alloys. *J Memb Sci* 2014;453:525–31. doi:10.1016/j.memsci.2013.11.035.
- [203] Huang W, Opalka SM, Wang D, Flanagan TB. Thermodynamic modelling of the Cu–Pd–H system. *Calphad* 2007;31:315–29. doi:10.1016/j.calphad.2007.02.002.

- [204] Hu R, Gao MC, Doğan ÖN, King P, Widom M. Thermodynamic modeling of the Pd–S system supported by first-principles calculations. *Calphad* 2010;34:324–31. doi:10.1016/j.calphad.2010.07.002.
- [205] Ozdogan E, Wilcox J. Investigation of H₂ and H₂S Adsorption on Niobium- and Copper-Doped Palladium Surfaces. *J Phys Chem B* 2010;114:12851–8. doi:10.1021/jp105469c.
- [206] Opalka SM, Løvvik OM, Emerson SC, She Y, Vanderspurt TH. Electronic origins for sulfur interactions with palladium alloys for hydrogen-selective membranes. *J Memb Sci* 2011;375:96–103. doi:10.1016/j.memsci.2011.03.018.
- [207] Sjardin M, Damen KJ, Faaij APC. Techno-economic prospects of small-scale membrane reactors in a future hydrogen-fuelled transportation sector. *Energy* 2006;31:2523–55. doi:10.1016/j.energy.2005.12.004.
- [208] Majlan EH, Wan Daud WR, Iyuke SE, Mohamad AB, Kadhum AAH, Mohammad AW, et al. Hydrogen purification using compact pressure swing adsorption system for fuel cell. *Int J Hydrogen Energy* 2009;34:2771–7. doi:10.1016/j.ijhydene.2008.12.093.
- [209] Sharma SD. Gas Cleaning: Pressure Swing Adsorption. *Encycl. Electrochem. Power Sources*, vol. 3, Elsevier; 2009, p. 335–49. doi:10.1016/B978-044452745-5.00307-5.
- [210] Lu GQ, Diniz da Costa JC, Duke M, Giessler S, Socolow R, Williams RH, et al. Inorganic membranes for hydrogen production and purification: A critical review and perspective. *J Colloid Interface Sci* 2007;314:589–603. doi:10.1016/j.jcis.2007.05.067.
- [211] Klempner G, Kerszenbaum I. Operation and maintenance of large turbo-generators. vol. 14. John Wiley & Sons; 2004.
- [212] Lambrecht D, Weghaupt E. Electric machines, particularly turbogenerators, having liquid cooled rotors 1976.
- [213] Nagano S, Kitajima T, Yoshida K, Kazao Y, Kabata Y, Murata D, et al. Development of world's largest hydrogen-cooled turbine generator. *IEEE Power Eng. Soc. Summer Meet.*, vol. 2, IEEE; 2002, p. 657–63. doi:10.1109/PESS.2002.1043376.

- [214] Tari M, Yoshida K, Sekito S, Allison J, Brutsch R, Lutz A, et al. A high voltage insulating system with increased thermal conductivity for turbo generators. Proc. Electr. Insul. Conf. Electr. Manuf. Coil Wind. Technol. Conf. (Cat. No.03CH37480), IEEE; 2003, p. 613–7. doi:10.1109/EICEMC.2003.1247959.
- [215] Weili L, Jichao H, Feiyang H, Xingfu Z, Yihuang Z, Yong L. Influence of the End Ventilation Structure Change on the Temperature Distribution in the End Region of Large Water–Hydrogen–Hydrogen Cooled Turbogenerator. IEEE Trans Energy Convers 2013;28:278–88. doi:10.1109/TEC.2013.2253104.
- [216] Ku AY, Kulkarni P, Shisler R, Wei W. Membrane performance requirements for carbon dioxide capture using hydrogen-selective membranes in integrated gasification combined cycle (IGCC) power plants. J Memb Sci 2011;367:233–9. doi:10.1016/j.memsci.2010.10.066.
- [217] Marano JJ, Ciferino JP. Integration of Gas Separation Membranes with IGCC Identifying the right membrane for the right job. Energy Procedia 2009;1:361–8. doi:10.1016/J.EGYPRO.2009.01.049.
- [218] Chiesa P, Kreutz TG, Lozza GG. CO₂ Sequestration From IGCC Power Plants by Means of Metallic Membranes. J Eng Gas Turbines Power 2007;129:123. doi:10.1115/1.2181184.
- [219] Dittmeyer R, Höllein V, Daub K. Membrane reactors for hydrogenation and dehydrogenation processes based on supported palladium. J Mol Catal A Chem 2001;173:135–84. doi:10.1016/S1381-1169(01)00149-2.
- [220] DOCEKAL J. Hydrogen production from hydrocarbons. Int J Hydrogen Energy 1986;11:709–14. doi:10.1016/0360-3199(86)90139-4.
- [221] Amelio M, Morrone P, Gallucci F, Basile A. Integrated gasification gas combined cycle plant with membrane reactors: Technological and economical analysis. Energy Convers Manag 2007;48:2680–93. doi:10.1016/j.enconman.2007.04.023.
- [222] Sircar S, Waldron WE, Rao MB, Anand M. Hydrogen production by hybrid SMR-PSA-SSF membrane system. Sep Purif Technol 1999;17:11–20. doi:10.1016/S1383-5866(99)00021-0.
- [223] KREUTZ T, WILLIAMS R, SOCOLOW R, CHIESA P, LOZZA G. Production of Hydrogen and Electricity from Coal with CO₂ Capture. In: Gale J, Kaya Y, editors.

- Greenh. Gas Control Technol. - 6th Int. Conf., vol. 1, Kyoto, Japan, Japan: Elsevier; 2003, p. 141–7. doi:10.1016/B978-008044276-1/50023-4.
- [224] Tollefson J. Hydrogen vehicles: fuel of the future? *Nat News* 2010;464:1262–4.
- [225] Eberle U, Müller B, von Helmolt R. Fuel cell electric vehicles and hydrogen infrastructure: status 2012. *Energy Environ Sci* 2012;5:8780. doi:10.1039/c2ee22596d.
- [226] Lin Y-M. Process development for generating high purity hydrogen by using supported palladium membrane reactor as steam reformer. *Int J Hydrogen Energy* 2000;25:211–9. doi:10.1016/S0360-3199(99)00047-6.
- [227] Brunetti A, Barbieri G, Drioli E. Membrane reactors in hydrogen production. In: Drioli E, Barbieri G, editors. *Membr. Eng. Treat. Gases, Vol. 2 Gas-separation Probl. Comb. with Membr. React.*, Cambridge, UK, UK: The Royal Society of Chemistry; 2011.
- [228] U.S. Department of Energy. On-board fuel processing: Go/no-go decision 2004.
- [229] Alique D, Martinez-Diaz D, Sanz R, Calles JA. Review of supported pd-based membranes preparation by electroless plating for ultra-pure hydrogen production. vol. 8. *Multidisciplinary Digital Publishing Institute (MDPI)*; 2018. doi:10.3390/membranes8010005.
- [230] King HW, Manchester FD. A low-temperature x-ray diffraction study of Pd and some Pd-H alloys. *J Phys F Met Phys* 1978;8:15–26. doi:10.1088/0305-4608/8/1/007.
- [231] Bockris JO, Subramanyan PK. Hydrogen Embrittlement and Hydrogen Traps. *J Electrochem Soc* 1971;118:1114–9. doi:10.1149/1.2408257.
- [232] Kolachev BA, Gabidullin RM. Forms of the manifestation of hydrogen embrittlement in metals and alloys. *Sov Mater Sci* 1977;12:463–8. doi:10.1007/BF00728177.
- [233] Pfeifer M. *Degradation and Reliability of Materials. Mater. Enabled Des.*, Elsevier; 2009, p. 161–87. doi:10.1016/B978-0-7506-8287-9.00006-9.
- [234] Iulianelli A, Ghasemzadeh K, Basile A. Progress in Methanol Steam Reforming Modelling via Membrane Reactors Technology. *Membranes (Basel)* 2018;8:65. doi:10.3390/membranes8030065.

Literature Review

- [235] Mckinley DL. Metal alloy for hydrogen separation and purification 1967.
- [236] Gao HY, Lin YS, Li YD, Zhang BQ. Chemical stability and its improvement of palladium-based metallic membranes. *Ind Eng Chem Res* 2004;43:6920–30. doi:10.1021/ie049722f.
- [237] Dunleavy JK. Sulfur as a catalyst poison. *Platin Met Rev* 2006;50:110–110. doi:10.1595/147106706X111456.
- [238] Douglas RA. Hydrogen sulfide oxidation by naphthoquinone complexes the hiperion process. *Am Chem Soc, Div Fuel Chem* 1990;35:136–49.
- [239] Porter JH. Gas well sulfur removal by diffusion through polymeric membranes 1970.
- [240] Li H, Goldbach A, Li W, Xu H. PdC formation in ultra-thin Pd membranes during separation of H₂/CO mixtures. *J Memb Sci* 2007;299:130–7. doi:10.1016/j.memsci.2007.04.034.
- [241] Lang ND, Holloway S, Nørskov JK. Electrostatic adsorbate-adsorbate interactions: The poisoning and promotion of the molecular adsorption reaction. *Surf Sci* 1985;150:24–38. doi:10.1016/0039-6028(85)90208-0.
- [242] Heras JM, Estiú G, Viscido L. The interaction of water with clean palladium films: A thermal desorption and work function study. *Appl Surf Sci* 1997;108:455–64. doi:10.1016/S0169-4332(96)00686-1.
- [243] Helmi A, Gallucci F, van Sint Annaland M. Resource scarcity in palladium membrane applications for carbon capture in integrated gasification combined cycle units. *Int J Hydrogen Energy* 2014;39:10498–10506. doi:10.1016/J.IJHYDENE.2014.05.009.
- [244] Takahashi T, Iwata K, Tanaka S, Takashima N, Ikawa T, Takahashi S. Lifecycle of palladium in Japan: for setting clearance levels of 107 Pd. *J Nucl Sci Technol* 2018;55:822–7. doi:10.1080/00223131.2018.1435316.
- [245] Zhang S, Ding Y, Liu B, Chang C. Supply and demand of some critical metals and present status of their recycling in WEEE. *Waste Manag* 2017;65:113–27. doi:10.1016/J.WASMAN.2017.04.003.
- [246] Singerling SA. Minerals Yearbook of Platinum-group metals. US Geol Surv 2019.
- [247] U.S. Geological Survey. Mineral Commodity Summaries 2019. US Geol Surv

2019:124–5.

- [248] Kim JG. Material flow and industrial demand for palladium in Korea. *Resour Conserv Recycl* 2013;77:22–8.
doi:<http://dx.doi.org/10.1016/j.resconrec.2013.04.009>.
- [249] Wilburn DR. Global Exploration and Production Capacity for Platinum-Group Metals From 1995 Through 2015. n.d.
- [250] Roa F, Way JD, McCormick RL, Paglieri SN. Preparation and characterization of Pd–Cu composite membranes for hydrogen separation. *Chem Eng J* 2003;93:11–22. doi:10.1016/S1385-8947(02)00106-7.
- [251] Tennison S. Current hurdles in the commercial development of inorganic membrane reactors. *Membr Technol* 2000;2000:4–9. doi:10.1016/S0958-2118(01)80001-X.
- [252] Scholes CA, Smith KH, Kentish SE, Stevens GW. CO₂ capture from pre-combustion processes—Strategies for membrane gas separation. *Int J Greenh Gas Control* 2010;4:739–55. doi:10.1016/j.ijggc.2010.04.001.
- [253] Wiesner MR, Chellam S. The promise of membrane technology. *Environ Sci Technol* 1999;33:360A-366A.
- [254] Damen K, van Troost M, Faaij A, Turkenburg W. A comparison of electricity and hydrogen production systems with CO₂ capture and storage—Part B: Chain analysis of promising CCS options. *Prog Energy Combust Sci* 2007;33:580–609. doi:10.1016/j.pecs.2007.02.002.
- [255] Rubin ES, Chen C, Rao AB. Cost and performance of fossil fuel power plants with CO₂ capture and storage. *Energy Policy* 2007;35:4444–54. doi:10.1016/j.enpol.2007.03.009.
- [256] Singh D, Croiset E, Douglas P., Douglas M. Techno-economic study of CO₂ capture from an existing coal-fired power plant: MEA scrubbing vs. O₂/CO₂ recycle combustion. *Energy Convers Manag* 2003;44:3073–91. doi:10.1016/S0196-8904(03)00040-2.
- [257] Chen C, Rubin ES. CO₂ control technology effects on IGCC plant performance and cost. *Energy Policy* 2009;37:915–24. doi:10.1016/j.enpol.2008.09.093.
- [258] DAVISON J. Performance and costs of power plants with capture and storage of

- CO₂. *Energy* 2007;32:1163–76. doi:10.1016/j.energy.2006.07.039.
- [259] Ordorica-Garcia G, Douglas P, Croiset E, Zheng L. Technoeconomic evaluation of IGCC power plants for CO₂ avoidance. *Energy Convers Manag* 2006;47:2250–9. doi:10.1016/j.enconman.2005.11.020.
- [260] Iaquaniello G, De Falco M, Salladini A. Palladium-based selective membranes for hydrogen production. In: Drioli E, Barbieri G, editors. *Membr. Eng. Treat. Gases, Vol. 2 Gas-separation Probl. Comb. with Membr. React.*, Cambridge, UK, UK: The Royal Society of Chemistry; 2011.
- [261] U.S. Geological Survey. Global mine production of palladium from 2014 to 2018, by country (in metric tons). Stat - Stat Portal n.d. <https://prd-wret.s3-us-west-2.amazonaws.com/assets/palladium/production/atoms/files/mcs-2019-plati.pdf> (accessed May 9, 2019).
- [262] Kirk-Othmer, editor. *Concise Encyclopedia of Chemical Technology*. vol. 12. 4th ed., New York: Wiley; 1999, p. 950.

Chapter 3 - Experimental and Methodology

This chapter explains the major experimental equipment used and the procedures followed to study the targets discussed previously. Four main studies have been undertaken as part of this dissertation work, namely: permeation studies, SMR studies, carbon capture studies, and techno-economic analysis (TEA) studies. The methodologies, equipment, and techniques used for each phase of this research are highlighted in this chapter and explained in detail in their own appropriate chapters.

3.1 Methodology

The permeation studies are performed with pure gases including hydrogen, helium, and argon, to study the physical characteristics of the membranes and their integrity under the experimental conditions. The SMR reaction studies are undertaken to study the performance of the MR for the SMR reaction and find the optimal operating conditions at which methane conversion, hydrogen recovery, and hydrogen purity on the permeate side are maximized and also to set the initial conditions for the carbon capture experiments. The carbon capture experiments have been performed to study the potential of MR system coupled with zeolite 13X materials for separating CO₂ from the retentate stream. Finally, the TEA studies are performed to evaluate the economic attractiveness of this project. The main equipment used for the first three studies are mass flow controllers (MFCs), mass spectrometer (MS), and Autosorb iQ adsorption equipment. The method used for the TEA studies are detailed in Chapter 6. The following sections discuss the details of each equipment and method.

3.1.1 Equipment calibration

An essential element of every experimental research work is precise measurements and instrument calibration is the backbone of accurate measurements. This section explains the calibration steps for all the instruments that will be used in this work.

3.1.1.1 Mass flow controller

The flow rates of the feed gases were controlled using Aalborg GFC17 MFCs (Aalborg Instruments & Controls Inc., Orangeburg, New York, U.S) and the actual flow rate of each gas was simply measured using a bubble-flowmeter. Although the nominal accuracy of the MFCs are reported as $\pm 1\%$ of full range, the deviations from the set points were found to be significantly greater than the experimental tolerance in previous works conducted in our group.[1] Hence, external calibration of the MFCs are recommended and will be taken before the start of each reaction test.

The calibration step for each MFC is simply finding a linear relationship between the setpoint of each MFC and the actual flow rate of each gas through their designated MFC. For this purpose, the actual flow rate of a gas at each setpoint was measured using the bubble flowmeter. To minimize the human error, the experimental measurements were repeated 10 times at each set point and the average value of these 10 measurements was considered as the experimental point. An example of the calibration plot for CH₄ MFC is depicted in Figure 3-1 and the slopes and R² values for all other gases and their pertinent MFCs are presented in Table 3-1. It should be noted that for all calibrations, the intercept is forced to zero as the gas flow rate is equal to zero when the MFC is completely closed i.e. when the setpoint is equal to zero.

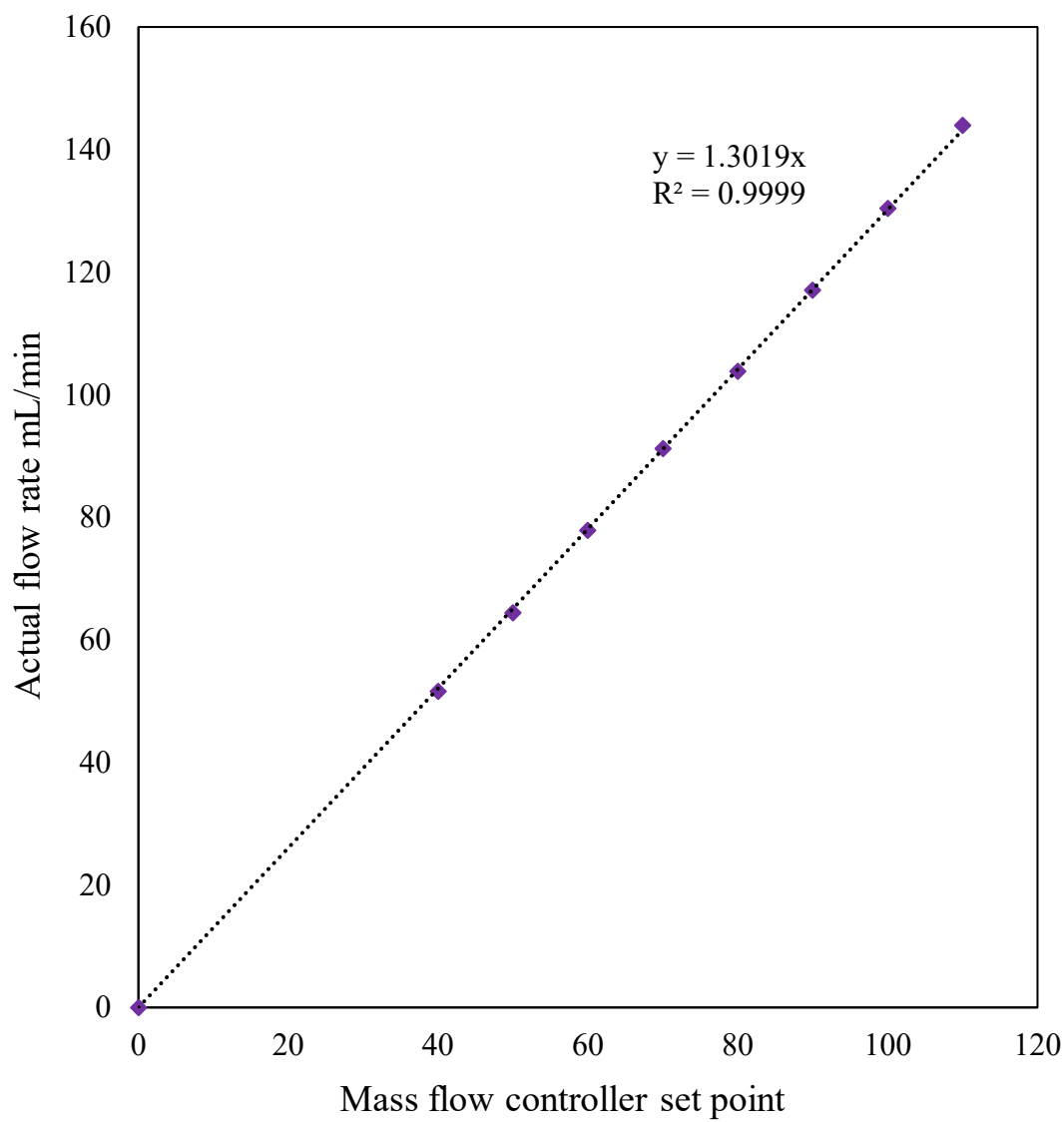


Figure 3-1. MFC calibration for CH₄

Table 3-1 Calibration parameters for various MFCs

Gas	Slope	R ²
Ar ¹	1.4095	0.9990
Ar ²	1.1166	0.9912
CH ₄	0.7627	0.9992
CO	1.4207	0.9986
CO ₂	0.9683	0.9965
H ₂	1.0750	0.9986
He	1.9900	0.9981

¹ This MFC was used to feed argon into the MS

² This MFC was used to feed argon into the MR

3.1.1.2 Mass spectrometer

One of the critical tools that has been used in this study is the Extrel MAX300-LG mass spectrometer (MS). This instrument is capable of measuring masses in the range from 1-250 atomic mass unit (amu) with the capability to monitor gases and vapors with fragment masses that fall within that range. In addition, with membrane inlet option, this instrument can detect compositions as low as 10 parts per trillion (ppt) for each component. In order to accurately measure the composition of gases in each stream one needs to precisely calibrate the MS.

In order to calibrate the MS, a fixed flow rate of argon gas was fed into the instrument and the experimental data points were recorded. Next, some arbitrary and various compositions of the gases present in the SMR reaction (H_2 , CH_4 , CO , and CO_2) were fed into the instrument. Next, the ratio of the flow rates of each gas to that of argon (Q_i/Q_{Ar}) was plotted against the intensity ratio of the same pair (I_i/I_{Ar}) to obtain a linear relationship between the parameters. The slope of each straight line is known as the response factor (RF_{ij}) for that gas pair and was recorded for each pair to perform the calculations during the reaction phase. Once all the desired RFs were recorded the calculations for determining the composition of each gas in the reaction can be calculated by simply following Eq. 3-1

$$Q_{i,rxn} = Q_{Ar} \times RF \times \left(\frac{I_{i,rxn}}{I_{Ar}} \right) \quad \text{Eq. 3-1}$$

Where, $Q_{i,rxn}$ is the flow rate of component i in the reaction; Q_{Ar} is the standard flow rate of argon gas which is held constant during all measurements; RF_{ij} is the response factor of pair i/j (j being the carrier gas which is argon in this study) obtained from the calibration step; $I_{i,rxn}$ and I_{Ar} are the intensities of component i and Ar measured during the reaction. An example of the calibration for CH_4/Ar pair is depicted in Figure 3-2.

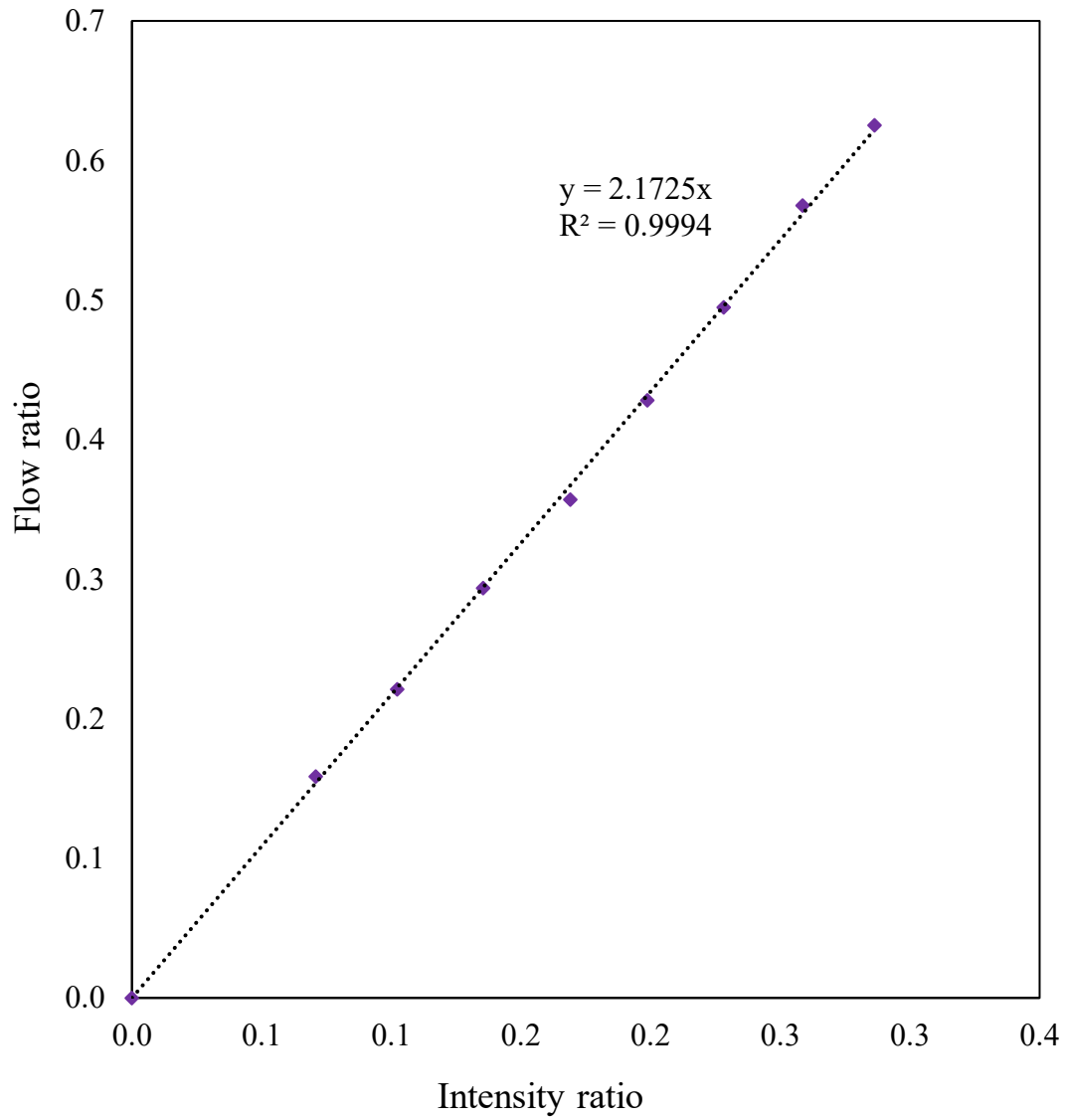


Figure 3-2. MS calibration for the CH₄/Ar pair

3.2 Experimental design

In this section the experimental setup and the operating conditions for each research target is explained in detail.

3.2.1 Permeation studies

Two different types of membranes have been used for the permeation studies in this work: composite Pd-Au and composite Pd membranes. The Pd and Pd-Au membranes were prepared by deposition of thin layers of palladium-gold on YSZ and pure Pd on asymmetric microporous Al₂O₃ substrate supports, respectively, via electroless plating. The Pd/YSZ membrane was manufactured according to the procedure developed by Ma et al. [43–45], while the Pd-Au/Al₂O₃ was manufactured in Nanjing Tech University (Nanjing, China) following the procedure developed by Collins and Way. [2]

The gravimetric method, as presented in Eq. 3-2, was used to calculate the thickness of the Pd and Pd-Au membranes as described by Anzelmo. [1]

$$\delta_{Pd} = \frac{m_{total} - m_{substrate}}{A_{active}} \times \frac{1}{\rho_{Pd}} \quad \text{Eq. 3-2}$$

Where δ_{Pd} is the thickness of the Pd layer, m_{total} is the total mass of the deposited palladium and the substrate, $m_{substrate}$ is the mass of the substrate, A_{active} is the active surface area of the MR, and ρ_{Pd} is the density of palladium. The active surface area of the membrane was calculated using Eq. 3-3:

$$A_{active} = \pi \cdot OD \cdot L_{active} \quad \text{Eq. 3-3}$$

Where OD and L_{active} are the outer diameter and the active length of the membrane, respectively. The ceramic support for preparation of the Pd membrane was provided by Praxair company with an active length of ~7.2 cm and an OD of 9.8 mm. The total active

Experimental and Methodology

surface area of the Pd membrane was calculated to be $\sim 12 \text{ cm}^2$. The Pd-Au membrane was provided by Nanjing Tech University (Nanjing, China), and had an active length of $\sim 4.5 \text{ cm}$ and an OD of 12.3 mm . The total active surface area of the Pd-Au membrane was calculated to be $\sim 17.3 \text{ cm}^2$. The thickness of the Pd and Pd-Au layers were determined to be $\sim 11 \text{ }\mu\text{m}$ and $\sim 8 \text{ }\mu\text{m}$ respectively.

Before initiating the permeation tests, the membrane was activated by flowing $\sim 30 \text{ mL/min}$ of pure H_2 at $400 \text{ }^\circ\text{C}$ and a trans-membrane pressure of 50 kPa for 2 h , as recommended by Helmi et al. to remove the organic impurities on the membrane surface.[3]

Ideal selectivity is an inherent property of the membrane and is widely used to describe the permeating characteristics of membrane and to evaluate the extent of membrane selectivity toward H_2 . Ideal selectivity can be defined as presented in Eq. 3-4 and is obtained through the pure gas permeation tests:

$$\text{Ideal Selectivity } (\alpha_{\text{H}_2/i}) = \frac{P_{\text{H}_2}}{P_i} \quad \text{Eq. 3-4}$$

where i represents either He or Ar.

The permeating flux of each pure gas is measured using a bubble-flow meter and reported as an average over 10 measurements. All experimental data are recorded 15 minutes after changing the trans-membrane pressure to ensure steady state is achieved. Hydrogen permeation through a composite Pd-based membrane can be explained by the following general equation:[4]

$$J_{\text{H}_2} = P_{\text{H}_2} \frac{(p_{\text{H}_2,ret}^n - p_{\text{H}_2,perm}^n)}{\delta} \quad \text{Eq. 3-5}$$

where J_{H_2} is the H_2 permeating flux, P_{H_2} is the H_2 permeance, and $P_{\text{H}_2,retentate}$ and $P_{\text{H}_2,permeate}$ are the partial pressures of H_2 in the retentate and permeate sides, respectively. The

Experimental and Methodology

exponent n in Eq. 3-5 is called the dependence factor, which is an indication of the dependency of H_2 permeating flux to the partial pressure of H_2 and can vary between 0.5 and 1.0. The value of n can be determined experimentally by plotting H_2 permeating flux as a function of transmembrane pressure. A value of 0.5 for n (Sieverts'-Fick's law) is an indication that the transport of H_2 through the dense metallic layer is governed by the solution-diffusion mechanism.

In order to find the correct value of n , the H_2 permeation flux as at various trans-membrane pressure will be measured at 400 °C. Next, the permeating fluxes will be plotted against the driving force for each value of n , varying between 0.5-1.0, and a linear regression analysis will be performed. The line with the highest R^2 value is selected as the appropriate dependence factor for the membrane.

The H_2 permeance is a function of temperature and its temperature dependency can be described by an Arrhenius-type equation as shown in Eq. 3-6:

$$Pe_{H_2} = Pe_{H_2}^0 \exp\left(-\frac{E_a}{RT}\right) \quad \text{Eq. 3-6}$$

Where $Pe_{H_2}^0$ is called the pre-exponential factor, E_a is the apparent activation energy, R is the universal gas constant, and T is the absolute temperature. In order to fully characterize the membranes in this study, the permeance of the membranes were measured at three different temperature; 350, 400, and 450 °C and the apparent activation energy and pre-exponential factor were determined accordingly. By plotting H_2 permeance vs. reciprocal of absolute temperature on a logarithmic scale, one can easily find the apparent activation energy and pre-exponential factor. The experimental results for phase 1 of this work are presented in detail in Chapter 4.

3.2.2 SMR reaction studies

The SMR reactions were conducted using a Pd-based composite membrane. The membrane used for the SMR experiments had an OD of 1cm, a thickness of approximately 12 μ m, and an active length of 17.5 cm. The total active surface area of the membrane is calculated to be $\sim 55.0 \text{ cm}^2$. This membrane has been prepared by deposition of thin Pd layer over a ceramic (YSZ) support. The support is purchased from Praxair, while the membrane has been fabricated by Dr. Simona Liguori in the Clean Energy Conversion (CEC) laboratory. The membrane module has an approximate length of 32cm and is custom-built by CEC.

Prior to performing the reaction experiments, the initial permeation tests with pure H₂, He, and Ar were conducted at 400 °C and pressure range of 150 to 600 kPa to find the ideal selectivity of the membrane toward hydrogen and evaluate its permeability, as explained in section 3.2.1. These permeation tests allow to understand the permeating characteristics of the membrane.

After the conclusion of the initial permeation tests and membrane characterization, the reaction tests were conducted. Experimental tests were performed at feed pressures between 100 kPa to 400 kPa in equal intervals of 50 kPa and at a fixed temperature of 400°C. This range is chosen based on the results obtained from the previous studies and in order to minimize the negative effects of concentration polarization and dilution while keeping the operating temperature fairly low and minimizing damage to the MR at higher pressures. An image of the MR and membrane module is illustrated in Figure 3-3.



Figure 3-3. Image of the Pd membrane and membrane module

Approximately 3 g of commercial Ni-based catalyst supplied by Johnson Matthey Inc. was packed inside the lumen side of the MR. Before packing, the catalyst was crushed and sieved to a particle size of $\sim 300 \mu\text{m}$, in order to increase the available surface area for the SMR reaction.

The MR system was heated using an ultra-high temperature heating tape, model STH051-080, at a rate of $\sim 1.5 \text{ }^\circ\text{C}/\text{min}$ under argon gas. The voltage for heating was controlled by a Thermolyne-type 45,500 input control. The experimental temperature was monitored via a K-type Omega HH801A thermocouple. The accuracy of the thermocouple over a range of $-100 \text{ }^\circ\text{C}$ to $1372 \text{ }^\circ\text{C}$ is reported to be $\pm (0.1\% \text{ rdg} + 1 \text{ }^\circ\text{C})$.

During the reaction experiments, industrial grade methane and superheated steam were fed into the lumen side of the MR. Methane gas was supplied into the MR via the previously calibrated MFC as described in section 3.1.1 while deionized water was supplied to the

Experimental and Methodology

MR using an Eldex Optos 1LMP pump. Deionized water was vaporized, and converted into superheated steam in the spiral pre-heating zone before entering the MR. The water vapor in the retentate side was condensed using a temperature-regulated water bath (Julabo F25-EH). The pressure on the retentate side was regulated with an Ashcroft Back Pressure Regulator. The permeate and retentate streams were connected to the Mass Spectrometer (Extrel Max300-LG) and the composition of each stream was analyzed continuously to closely monitor the reaction performance. A schematic of the MR setup is shown in Figure 3-4.

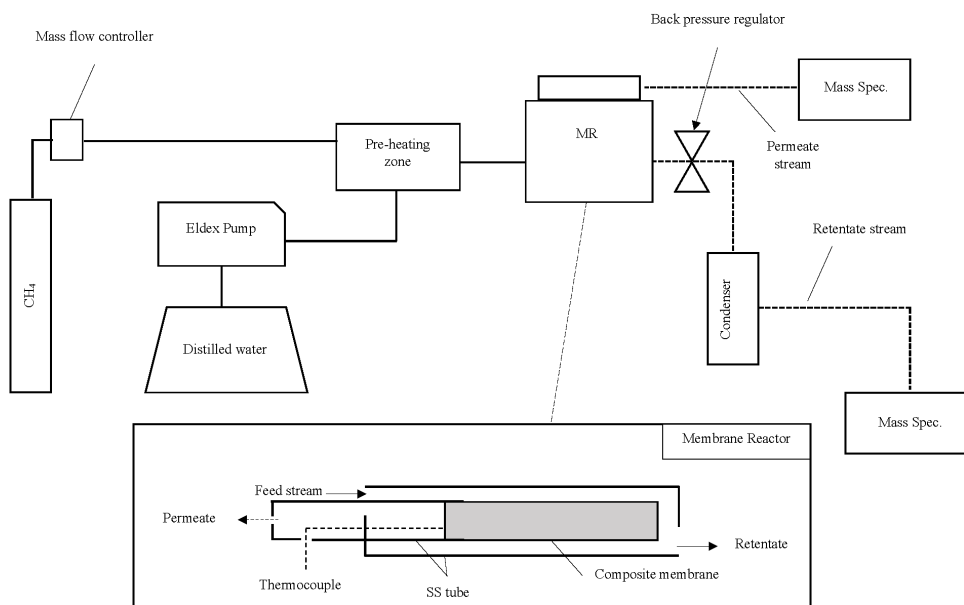


Figure 3-4. Schematic of the MR setup

The pressures on the retentate sides was gradually increased in intervals of 50 kPa, up to 400 kPa while the pressure in the permeate side was kept constant at 100 kPa. Methane conversion, hydrogen recovery, and hydrogen purity are be the major indicators used in this study to evaluate the performance of the MR. By continuously recording the compositions of permeated and retentate streams via MS, one can easily calculate the

Experimental and Methodology

methane conversion, hydrogen recovery, and hydrogen purity according to Eq. 3-7 through Eq. 3-9:

$$\text{Methane conversion } (X_{CH_4}) = \frac{Q_{CH_4}^{In} - Q_{CH_4}^{Out}}{Q_{CH_4}^{In}} \quad \text{Eq. 3-7}$$

$$\text{Hydrogen recovery } (R_{H_2}) = \frac{Q_{H_2}^{Permeate}}{Q_{H_2}^{Permeate} + Q_{H_2}^{Retentate}} \quad \text{Eq. 3-8}$$

$$\text{Hydrogen purity } (Purity_{H_2}) = \frac{Q_{H_2}^{Permeate}}{Q_{Total}^{Permeate}} \quad \text{Eq. 3-9}$$

Where $Q_{CH_4}^{in}$ is the molar flow rate of methane entering the MR, $Q_{CH_4}^{out}$ is the molar flow rate of methane exiting the MR, $Q_{H_2}^{permeate}$ is the molar flow rate of hydrogen on the permeate side, $Q_{H_2}^{retentate}$ is the molar flow rate of hydrogen on the retentate side, and $Q_{Total}^{permeate}$ is the total molar flow rate of all gaseous species on the permeate side,

At each new operating pressure (at pressure step $j+1$), the methane conversion and hydrogen purity will be recorded and compared with the previous value (at pressure step j) and the incremental changes are calculated as following:

$$\text{Incremental change in methane conversion} = \frac{X_{CH_4,j+1} - X_{CH_4,j}}{X_{CH_4,j}} \quad \text{Eq. 3-10}$$

$$\text{Incremental change in hydrogen recovery} = \frac{R_{H_2,j+1} - R_{H_2,j}}{R_{H_2,j}} \quad \text{Eq. 3-11}$$

$$\text{Incremental change in hydrogen purity} = \frac{Purity_{H_2,j+1} - Purity_{H_2,j}}{Purity_{H_2,j}} \quad \text{Eq. 3-12}$$

The operating pressure at which the incremental changes in these three performance indicators are less than 1% will be chosen as the optimum reaction pressure. The operating pressure at which the methane conversion, hydrogen recovery, and hydrogen purity are maximum are considered as the optimal operating conditions. After determining the optimal condition, the permeation tests with pure hydrogen were conducted again to ensure the integrity of the MR system was preserved.

3.2.3 Carbon capture experiments

One of the cornerstones of this work is the CO₂ capture studies. During this phase, the SMR reactions were repeated at the optimal operating conditions that were identified at the conclusion of the SMR reaction, namely p_{optimum} and 400 °C. The experimental procedures for this phase were exactly the same as described in section 3.2.2, except for the analysis of the retentate stream.

During this phase, a sorbent column packed with zeolite 13x was placed immediately after the cold trap. The retentate stream, which was fully dehydrated and directed to the zeolite 13X pack as shown in Figure 3-5.

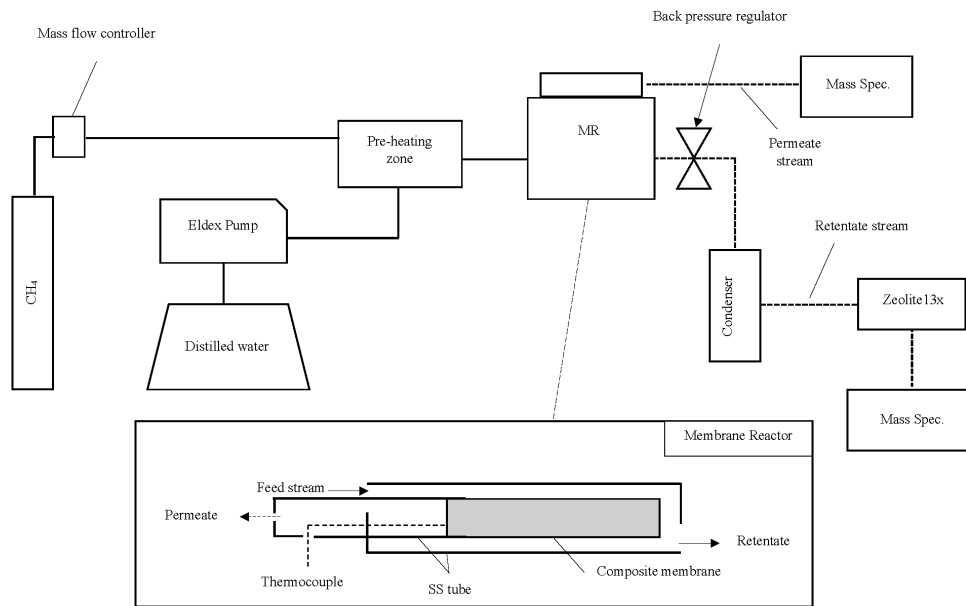


Figure 3-5. Schematic of the MR setup with inclusion of zeolite 13X for CO₂ capture

The operating condition of the zeolite pack were fixed at 25 °C and 100 kPa. The retentate stream was in constantly passing through the zeolite 13X while CO₂ being adsorbed onto the solid particles. The outgoing stream from the zeolite pack was sent to the MS where its composition was monitored continuously. By plotting the CO₂ composition versus time, one can easily obtain the maximum CO₂ uptake by the zeolite 13X. It should be noted that the initial CO₂ composition in the retentate stream ($x_{CO_2,i}$) is known from the results obtained at the conclusion of SMR studies. The composition of the retentate stream and in particular that of CO₂ in the retentate stream was closely monitored throughout all the reaction tests. The purity of CO₂ on the retentate side can be calculated using Eq. 3-13:

$$CO_2 \text{ purity } (Purity_{CO_2}) = \frac{Q_{CO_2}^{Retentate}}{Q_{Total}^{Retentate}} = x_{CO_2}^{Retentate} \quad \text{Eq. 3-13}$$

Experimental and Methodology

The reason that 13X was chosen as the adsorbent for this study is due to its significantly higher affinity for CO₂ at low pressures.[5] In addition, at 25 °C and 1bar, zeolite 13X has shown a significantly higher CO₂ uptake (>200 mg/g) compared with other adsorbents such as ZIF-8 (30 mg/g), activated carbon (99 mg/g), or Na-Zeolite β (120 mg/g).[6]

It should be noted that at time t=0, the CO₂ concentrations detected by the MS will undergo a sharp decline from $x_{CO_2,i}$ to zero followed by a gradual buildup which is expected to follow the Langmuir isotherm model as presented in Eq. 3-14:

$$\phi = \frac{Kp_{CO_2}}{1 + Kp_{CO_2}} \quad \text{Eq. 3-14}$$

Where, ϕ is the ratio of the number of occupied adsorption sites to that of the available adsorption sites, K is the equilibrium constant which is the ratio of the rate constant for adsorption (k_a) to the rate constant for desorption (k_d), p_{CO_2} is the partial pressure of CO₂ at the surface of the solid sorbent. One way to analyze the adsorption data is by performing the breakthrough analysis. In this method, the concentration of CO₂ at the outlet is constantly monitored using MS. The concentration of CO₂ over the initial CO₂ concentration is plotted against time. The time at which the CO₂ concentration at the outlet is equal to 5% of the initial concentration is considered the breakthrough time and the time after which the CO₂ concentration reaches to a plateau is considered the steady state time. A schematic of a dimensionless breakthrough curve is illustrated in Figure 3-6. The detail of this process is explained in Chapter 5.

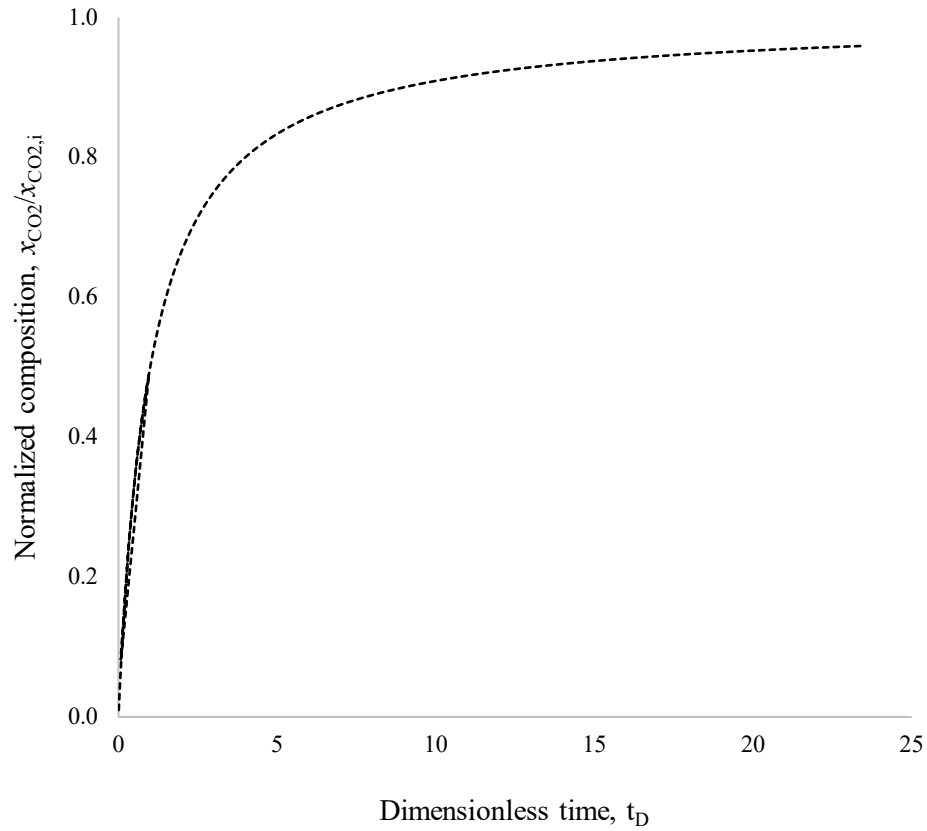


Figure 3-6. Isothermal CO₂ adsorption based on the Langmuir model

The maximum CO₂ uptake by the zeolite 13X can be calculated by subtracting the minimum CO₂ concentration ($x_{CO_2,min}$) on the graph from $x_{CO_2,i}$ and multiplying it by the mass flow rate of CO₂ at the operating condition as following:

$$CO_2 \text{ uptake} = (x_{CO_2,i} - x_{CO_2,min}) \times Q_{CO_2} \times \rho_{CO_2}(p,T) \quad \text{Eq. 3-15}$$

3.3 Material characterization

The proposed material characteristic techniques for this work include Scanning Electron Microscope (SEM), and X-ray diffraction (XRD) techniques. These techniques were used after the conclusion of the reactions to study the integrity of the Pd layer and the phase composition of the membrane. Existence of any cracks/pinholes on the surface of the Pd layer can be detected by SEM which indicates that the lattice structure of the membrane is susceptible to expansion/contraction induced by hydrogen diffusion inside the crystal structure. Furthermore, detection of any undesirable phase (such as Pd-Ag-S) by XRD is a clear indication of Pd decomposition.

References

- [1] Anzelmo B. On-board Hydrogen Production from Natural Gas Via a Metallic Pd-based Membrane Reactor. Stanford University, 2016
- [2] Collins, J.P.; Way, J.D. Preparation and Characterization of a Composite Palladium-Ceramic Membrane. *Ind. Eng. Chem. Res.* 1993, 32, 3006–3013, doi:10.1021/ie00024a008.
- [3] Helmi, A.; Fernandez, E.; Melendez, J.; Tanaka, D.A.P.; Gallucci, F.; Van Sint Annaland, M. Fluidized bed membrane reactors for ultra pure H₂ production—A step forward towards commercialization. *Molecules* 2016, 21, doi:10.3390/molecules21030376.
- [4] Ma YH, Mardilovich PP, She Y. Hydrogen gas-extraction module and method of fabrication 2000
- [5] Bezerra DP, Oliveira RS, Vieira RS, Cavalcante CL, Azevedo DCS. Adsorption of CO₂ on nitrogen-enriched activated carbon and zeolite 13X. *Adsorption* 2011;17:235–46. doi:10.1007/s10450-011-9320-z.
- [6] Chen C, Park DW, Ahn WS. CO₂ capture using zeolite 13X prepared from bentonite. *Appl Surf Sci* 2014;292:63–7. doi:10.1016/j.apsusc.2013.11.064

Chapter 4 - Hydrogen Permeation in Pd-based MRs

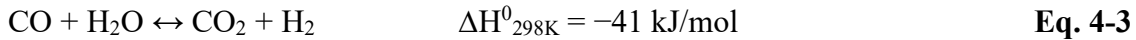
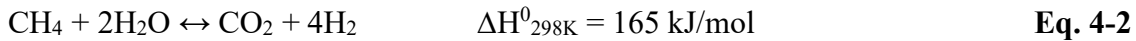
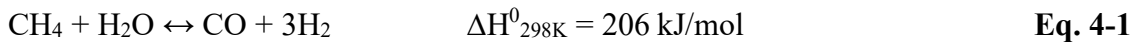
This chapter discusses the permeation and separation properties of two Pd-based composite membranes. One membrane was characterized by an approximately 8 μm -thick palladium (Pd)-gold (Au) layer deposited on an asymmetric microporous Al_2O_3 substrate; the other membrane consisted of an approximately 11 μm -thick pure palladium layer deposited on a yttria-stabilized zirconia (YSZ) support. Furthermore, the permeation tests for ternary and quaternary mixtures of H_2 , CO , CO_2 , CH_4 , and H_2O were conducted on the Pd/YSZ membrane and the details are discussed here. The effects of gas hourly space velocity (GHSV) and the steam-to-carbon (S/C) ratio on H_2 permeation were also investigated using simulated steam methane reforming mixtures. The integrity of the membranes were studied using SEM and XRD analysis techniques. The results obtained in this phase of this PhD study have been published as a peer reviewed article in the journal of “Environments” under the title “**Performance of Pd-Based Membranes and Effects of Various Gas Mixtures on H_2 Permeation**”.

4.1 Introduction

Fossil fuels comprise approximately 80% of the energy portfolio in the U.S. today [1]. The transportation sector accounts for approximately 70% of domestic petroleum consumption [2]. Light-duty vehicles emit significant amounts of CO_2 , volatile organic compounds (VOC), carbon monoxide (CO), and nitrogen oxides (NO_x) [3]. Climate change effects can be mitigated through the development of state-of-the-art carbon capture technologies, utilizing more efficient industrial processes, switching to less carbon-intensive fuels, and through the use of renewable carbon-free energy resources [4]. H_2 can be used as a replacement fuel for gasoline to help mitigate greenhouse gas (GHG) effects and improve air quality. Replacing internal combustion engine vehicles with H_2 fuel cell vehicles (HFCV) has the potential to reduce the GHG emissions by up to 40% [5]. In order for HFCVs to be commercially viable, the cost of H_2 , delivered at the pump, should be reduced to USD 2.00–3.00/gge (gallon of gasoline equivalent) for its commercial application in HFCVs [6]. Steam methane reforming (SMR) remains the most widely used industrial process for H_2 generation, which accounts for 50% of global H_2 production [7].

Hydrogen Permeation in Pd-based MRs

Conventional reactors produce H₂ via two separate reactions: steam methane reforming (1,2) and water gas shift (WGS) (3). Since the products of the SMR reaction contain high concentrations of CO (i.e., 3–10%), two WGS reactors are required to both maximize H₂ production and increase the purity of the produced H₂ stream [8,9]. SMR is composed of three reversible reactions (i.e., Eq. 4-1 through Eq. 4-3) that normally take place under very harsh operating conditions (i.e., 800–1000 °C and 1.5–2.0 MPa) due to thermodynamic constraints. Since ultra-pure H₂ (99.999%) with less than 50 ppm of CO concentration is required for proton exchange membrane fuel cells (PEMFC), further purification of H₂ is required [9,10]. Techniques such as preferential oxidation (PrOx), pressure swing adsorption (PSA), cryogenic distillation, dense Pd-membranes, etc. can be used to achieve this goal [11]. The most commonly-used technique in the industry for H₂ purification is PSA. However, approximately 20% of produced H₂ is lost in the PSA process [7].



Membrane reactor (MR) technology is still the most promising technology for the separation, purification, and production of H₂ [12]. MR technology is an alternative method that can be used to perform the SMR reaction at lower operating temperatures and pressures. In particular, Pd-based metallic membranes are the best candidates for the production of high-purity H₂ due to their ‘infinite’ selectivity towards H₂ permeation [13]. Dense Pd membranes have the potential to produce H₂ with purities greater than 99.9999% [10].

However, the fact that the permeation flux of H₂ is inversely proportional to the membrane thickness makes dense thick Pd-membranes unattractive for commercial applications due to their very small H₂ flux. One way to address the low permeating flux issue is to deposit a thin Pd layer on a porous substrate, i.e., either ceramic or porous stainless steel (PSS). A favorable membrane should maintain high selectivity toward H₂, high permeability to

operate effectively at high flow rates and restrained surfaces, and good chemical and structural stability to avoid deterioration under exertion [12]. The membrane configurations that provide these characteristics are twofold: thin Pd layer deposited on a ceramic support, and thin Pd layer deposited on metallic support covered with an intermetallic diffusion barrier. The membrane support provides the mechanical stability and usually does not exhibit any selective properties. The main characteristics of an effective membrane support are its high permeability toward gases and interconnected porous network. Such supports are usually composed of a few millimeters of sintered metallic or ceramic materials [14].

The use of ceramic supports in composite membranes is constantly increasing due to their low cost and controllable pore size. Inferior mechanical stability, poor weldability, and differing thermal expansion coefficients from Pd are the main disadvantages of ceramic supports. The prevailing ceramic supports are α -alumina, γ -alumina, and YSZ [15–17]. The main advantage of metallic supports such as PSS is that their similar thermal expansion coefficient to that of Pd minimizes disbanding which stems from different thermal expansion coefficients. Furthermore, metallic supports offer better weldability compared with ceramic-based supports [18–20]. Some common drawbacks of metallic supports are their rough surface, large pore size, and the intermetallic diffusion of Pd into the metallic support [21–24]. This problem can be avoided by employing an intermetallic diffusion barrier between the metallic support and the Pd layer [14]. Some of the intermetallic diffusion barriers reported in the literature are TiN, Ti O₂, Al₂O₃, α -Fe₂O₃, γ -Al₂O₃, and yttria-stabilized zirconia (YSZ), with TiN being reported as the most promising one.

Nevertheless, the pure Pd membrane is susceptible to poisoning when in contact with impurities such as H₂S, CO, and CO₂. In order to prevent this problem, Pd is alloyed with transition metals (e.g., Ag, Au, Cu, Mo, Ta, Y). In particular, alloying Pd with metals such as Ag and Cu can significantly decrease the fabrication cost while maintaining the features of the membrane and improve its resistivity against impurities [25]. Alloyed membranes consisting of Pd-Cu, Pd-Ag, and Pd-Au have gained significant attention, and have been studied intensively due to their high resistance against sulfur poisoning [26–28].

Although the permeating flux of H₂ is significantly improved and the fabrication cost of the membrane can be considerably lowered by using alloyed Pd membranes, the finished cost of a Pd-based membrane is still too far from the DOE target of < USD 1000/m² to be considered economically viable on a large scale [12,29]. Nonetheless, Pd-based membranes have been studied and characterized for various purposes over the past decades. Schramm & Seidel compared the mass transfer properties of a dense porous Vycor glass membrane and Pd-based membrane at 20 °C and 200 °C, respectively, and found that permeating fluxes of N₂, H₂, and Ar are reduced significantly in the Pd-modified membrane [30]. Gallucci et al. [31] and Jørgensen et al. [32] used unsupported dense Pd-Ag membranes with a thickness of 50 μm to investigate the effects of several operating conditions on the MR performance. In both of these studies, the H₂ permeating flux was significantly low, which could be attributed to the thickness of the membrane.

Liguori et al. studied the performance of a MR using a 20-μm thick Pd/PSS membrane. They concluded that both ideal selectivity and H₂ permeation remain unchanged under the WGS reaction conditions [8]. Chen et al. performed a two-dimensional numerical analysis of concentration polarization in a membrane tube and found that an increase in trans-membrane pressure or membrane permeance will enhance the H₂ permeation flux and escalate the concentration polarization effect [33]. Zhang et al. studied, both numerically and experimentally, the influences of pressure, temperature, and feed gas flow rate on the degree of concentration polarization during the ammonia cracking process, and concluded that increasing the trans-membrane pressure aggravates the negative effect of concentration polarization, while increasing the feed gas flow rate decreases the concentration polarization effect [15]. Mori et al. studied the effects of concentration polarization on CH₄ conversion and H₂ recovery in the SMR reaction, and found that the rate of SMR is reduced due to slower removal of H₂, which can be explained by the concentration polarization effect [34]. Caravella et al. investigated the effects of numerous parameters on a newly-defined variable called Concentration Polarization Coefficient (CPC) through numerical simulation, and concluded that the CPC decreases with increasing membrane thickness, downstream total pressure, Reynolds number, and H₂ mole fraction in the upstream side,

and increasing temperature increases the CPC [35]. In a later simulation study by Caravella and Sun, they found that the Effective Average Concentration Polarization Coefficient (EAC) increases by increasing temperature and total feed pressure, whereas increasing H₂ mole fraction on the permeate side and GHSV will lower EAC [36]. Hara et al. studied, both numerically and experimentally, the effects of concentration polarization and CO hindrance on H₂ permeation in a Pd-based MR using binary mixtures of Ar-H₂ and CO-H₂, and found that the presence of CO in the feed mixture causes a stronger decrease of the H₂ permeation flux [37]. Peters et al. performed a study on a thin, defect-free Pd-Ag_{23%} membrane at 400 °C and very high pressure of 2600 kPa, and investigated the effects of dilution, depletion, concentration polarization, and competitive adsorption on the H₂ permeating flux [28]. Their findings show that the permeating flux of H₂ will decrease due to the concentration polarization effect in a binary mixture of H₂-N₂. The reduction in H₂ permeating flux is more pronounced when N₂ is substituted with CO₂, while a H₂-CO binary mixture shows the lowest H₂ permeating flux.

Despite the significant research performed in the literature on the Pd-based membranes, there are few works investigating the influence of the several factors affecting the H₂ permeating flux: dilution, depletion, concentration polarization, and competitive surface adsorption at conditions satisfying the DOE target requirements (differential pressure of 20 psi, and operating temperature of 400 °C) [6,38] and using the mixtures that represent SMR process in a systematic experimental work. Numerous mathematical models and simulation studies can be found in the open literature that investigate the effects of concentration polarization on the H₂ permeating flux; however, the majority of these works lack experimental confirmation [39–42].

In this work, the effects of numerous gaseous components of the SMR reaction on the H₂ permeation flux is studied in detail. The negative effects (concentration polarization, dilution, depletion, and competitive adsorption on the Pd surface) through which each gas can reduce the H₂ permeating flux are analyzed by performing permeation tests of binary mixtures of H₂ with He, Ar, N₂, CH₄, CO, CO₂, and H₂O. Next, the study is extended to ternary and quaternary mixtures to explore the cumulative effects of SMR components on

Hydrogen Permeation in Pd-based MRs

the H₂ permeating flux. Finally, the permeation tests are performed on a simulated stream of the SMR reaction, and the aforementioned negative effects are investigated.

4.2 Materials and Methods

4.2.1 Pd-Based Membrane

The composite Pd-Au and Pd membranes were prepared by deposition of thin layers of palladium-gold on YSZ and pure Pd on asymmetric microporous Al₂O₃ substrate supports, respectively, via electroless plating. The Pd/YSZ membrane was manufactured according to the procedure developed by Ma et al. [43–45], while the Pd-Au/Al₂O₃ was manufactured in Nanjing Tech University (Nanjing, China) following the procedure developed by Collins and Way [46]. The thickness of the Pd and Pd-Au layers were determined to be ~11 μm and ~8 μm respectively using the gravimetric method according to the procedure described by Anzelmo [47].

The ceramic support for preparation of the Pd membrane was provided by Praxair company with an active length of ~7.2 cm and an OD of 9.8 mm. The total active surface area of the Pd membrane was calculated to be ~12 cm². The Pd-Au membrane was provided by Nanjing Tech University (Nanjing, China), and had an active length of ~4.5 cm and an OD of 12.3 mm. The total active surface area of the Pd-Au membrane was calculated to be ~17.3 cm². Before initiating the permeation tests, the membrane was activated by flowing ~30 mL/min of pure H₂ at 400 °C Table 4-1 and a trans-membrane pressure of 50 kPa for 2 h, as recommended by Helmi et al. to remove the organic impurities on the membrane surface [48] Permeation tests with pure gases (H₂, He, Ar) and gas mixtures, as presented in , at 400 °C and pressure range of 150 to 600 kPa, have been performed in this study.

Table 4-1 Gas mixtures fed into the Pd and Pd-Au MRs at 400 °C for permeation tests.

Gas Mixture Type	Gas Mixture Feed	Gas Mixture Composition	Total Flow Rate (mL/min)
Pd Membrane			
Binary	H ₂ /Ar	50/50	276
Binary	H ₂ /Ar	50/50	542
Binary	H ₂ /Ar	50/50	810
Binary	H ₂ /Ar	50/50	1078
Binary	H ₂ /He	50/50	276
Binary	H ₂ /CH ₄	50/50	276
Binary	H ₂ /H ₂ O	50/50	276
Binary	H ₂ /CO ₂	50/50	276
Ternary	H ₂ /CO/He	50/5/45	276
Ternary	H ₂ /CO ₂ /CH ₄	50/25/25	276
Ternary	H ₂ /CO ₂ /H ₂ O	50/25/25	276
Quaternary	H ₂ /CO ₂ /CO/He	50/25/2.5/22.5	276
Quaternary	H ₂ /H ₂ O/CO/He	50/25/2.5/22.5	276
Senary	H ₂ /CO ₂ /H ₂ O/CH ₄ /CO/He	40/20/23/7/1/9	276
Pd-Au Membrane			
Binary	H ₂ /Ar	50/50	276
Binary	H ₂ /He	50/50	276
Binary	H ₂ /N ₂	50/50	276
Binary	H ₂ /H ₂ O	50/50	276

4.2.2 Procedure

A schematic of the experimental setup is presented in Figure 4-1. As shown in Figure 4-1, the reaction gases are fed to the annular space of the MR (retentate side). The MR system was heated using an ultra-high temperature heating tape, model STH051-080. The voltage for heating was controlled by a Thermolyne-type 45,500 input control. The experimental temperature was monitored via a K-type Omega HH801A thermocouple. The accuracy of the thermocouple over a range of -100 °C to 1372 °C is $\pm (0.1\% \text{ rdg} + 1 \text{ }^\circ\text{C})$. The flow rates of the feed gases were controlled using Aalborg GFC17 mass flow controllers (Aalborg Instruments & Controls Inc., Orangeburg, New York, U.S.). Deionized water was supplied to the MR using an Eldex Optos 1LMP pump. Water was vaporized, and superheated steam was formed in a spiral pre-heating zone before entering the MR. The water vapor in the retentate side was condensed using a temperature-regulated water bath (Julabo F25-EH). The pressure on the retentate side was regulated with an Ashcroft Back Pressure Regulator. The pressure on the retentate side was measured with a Swagelok EN 837-1 pressure gauge.

Hydrogen Permeation in Pd-based MRs

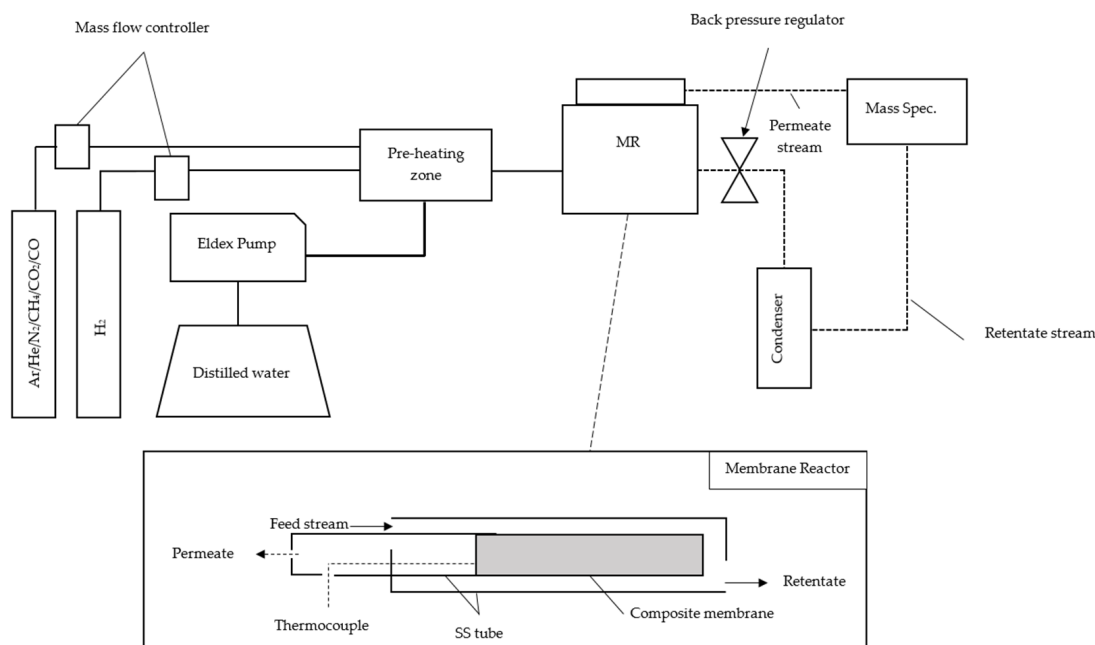


Figure 4-1 Schematic of the experimental setup.

The MR was heated up to 400 °C with a heating ramp of ~ 1.5 °C/min under Ar gas. In this study, the influences of various gaseous components of SMR reaction (CO₂, CO, CH₄, H₂O) on the H₂ permeating flux were investigated in binary, ternary, quaternary, and simulated mixtures of SMR. The negative effects of concentration polarization were investigated using equimolar binary mixtures of H₂-Ar at 400 °C and pressures ranging from 150 kPa to 600 kPa. Dilution and depletion effects were investigated using equimolar binary mixtures of H₂-N₂ and H₂-CH₄ at 400 °C and pressures ranging from 150 kPa to 600 kPa. The negative effects of competitive adsorption on the Pd surface were investigated using the equimolar binary mixtures of H₂-CO and H₂-CO₂ at 400 °C and pressures ranging from 150 kPa to 600 kPa, according to the procedures followed by Peters et al. [28]. Furthermore, ternary, quaternary and simulated SMR streams were utilized to further investigate the combined effects of the aforementioned four negative factors. In addition, the effects of operating conditions of temperature and pressure, as well as S/C ratio and GHSV on the H₂ permeating flux were explored. Trans-membrane pressure, S/C ratio, GHSV were varied between 50 to 500 kPa, 2.0 to 3.5, and 221 to 884 h⁻¹, respectively.

Hydrogen Permeation in Pd-based MRs

At the beginning of the characterization experiments, the permeation fluxes of pure gases H₂, He, and Ar were measured. The permeating flux of each pure gas was measured using a bubble-flow meter. Every experimental point represents an average value of at least 10 measurements at the same operating conditions, with an average error variation lower than 2.3%. All experimental data was recorded 15 min after changing the trans-membrane pressure to ensure a steady state was achieved. For tests involving the gas mixtures, the permeating flux of pure H₂ was measured before and after each experiment to evaluate the influence of each mixture on the permeating flux of H₂.

The H₂ permeation through a composite Pd-based membrane can be explained by the following general equation [49]

$$J_{H_2} = P_{H_2} (p_{H_2, retentate}^n - p_{H_2, permeate}^n) \quad \text{Eq. 4-4}$$

where J_{H_2} is the H₂ permeating flux, P_{H_2} is the H₂ permeance, and $P_{H_2, retentate}$ and $P_{H_2, permeate}$ are the partial pressures of H₂ in the retentate and permeate sides, respectively. The exponent n in Eq. 4-4 is called the dependence factor, which is an indication of the dependency of H₂ permeating flux to the partial pressure of H₂, and can vary between 0.5 and 1.0. The value of n can be determined experimentally by plotting H₂ permeating flux as a function of transmembrane pressure. A value of 0.5 for n (Sieverts'-Fick's law) is an indication that the transport of H₂ through the dense metallic layer is governed by the solution-diffusion mechanism. The H₂ permeance is a function of temperature, and its temperature dependency can be described by an Arrhenius-type equation:

$$P_{H_2} = P_{H_2}^0 \exp(-E_a/RT) \quad \text{Eq. 4-5}$$

where $P_{H_2}^0$ is called the pre-exponential factor, E_a is the apparent activation energy, R is the universal gas constant, and T is the absolute temperature. The ideal selectivity was used to describe the permeating characteristic of the membrane and to evaluate the extent of membrane selectivity toward H₂:

$$\text{Ideal Selectivity } (\alpha_{H_2/i}) = P_{H_2}/P_i \quad \text{Eq. 4-6}$$

where i represents either He or Ar

4.2.3 Materials

Ultra-high purity H₂ and He (99.999% purity), industrial grade Ar (99.985% purity), CH₄ (99.97% purity), CO₂ (99.9% purity), and N₂ (99.0% purity) were used for the permeation and reaction simulation experiments in this work. CO used in this study was diluted with He due to safety concerns and had a certified purity of 10.3%. All the gases were obtained from General Air Services & Supplies.

4.3 Results and Discussion

4.3.1 Membrane Permeation Tests

In this study, two different membranes, namely Pd and Pd-Au, were used to evaluate the permeation fluxes of H₂ at various operating conditions and using different mixtures. The permeation tests with pure gases of H₂, He, and Ar were conducted on both membranes to characterize the membranes and find their perm-selective properties. Further permeation tests with binary, ternary, quaternary, and simulated SMR mixtures were carried out for the Pd membrane, while for the Pd-Au membrane, the permeation tests were conducted only with the binary mixtures.

4.3.1.1 Pure Components

To fully evaluate the permeation characteristics of the membrane, permeation tests with pure gases were performed. In particular, the permeation tests with pure hydrogen were carried out to determine the membrane parameters such as Pe^0 , E_a , and n , as indicated in Eq. 4-4 and Eq. 4-5. Hence, permeation tests with pure H₂ at various temperatures and trans-membrane pressures were carried out for each membrane to estimate these parameters.

In order to find the correct value of n , the H₂ permeation flux as at various trans-membrane pressures was measured at 400 °C. Next, the permeating fluxes were plotted against the driving force for each value of n , varying between 0.5–1.0, and a linear regression analysis was performed, as shown in Figure 4-2. The line with the highest R² value was selected as the appropriate dependence factor for each membrane. The best linear regressions obtained have values of $n = 0.5$ and $n = 0.7$ for Pd-Au and Pd membranes, respectively. These calculations indicate that the H₂ transport through the Pd-Au membrane is limited by solution diffusion through the bulk of the Pd layer, while for the Pd membrane, the transport mechanism can be affected by Pd surface or bulk defects or impurities present in the Pd surface stemming from non-perfect fabrication or pinhole developments. Moreover, at 400 °C and a trans-membrane pressure of 50 kPa, the membranes showed a H₂

Hydrogen Permeation in Pd-based MRs

permeance of $8.42 \times 10^{-4} \text{ mol/m}^2 \cdot \text{s} \cdot \text{Pa}^{0.5}$ and $2.54 \times 10^{-5} \text{ mol/m}^2 \cdot \text{s} \cdot \text{Pa}^{0.7}$ for Pd-Au and Pd membranes, respectively.

Hydrogen Permeation in Pd-based MRs

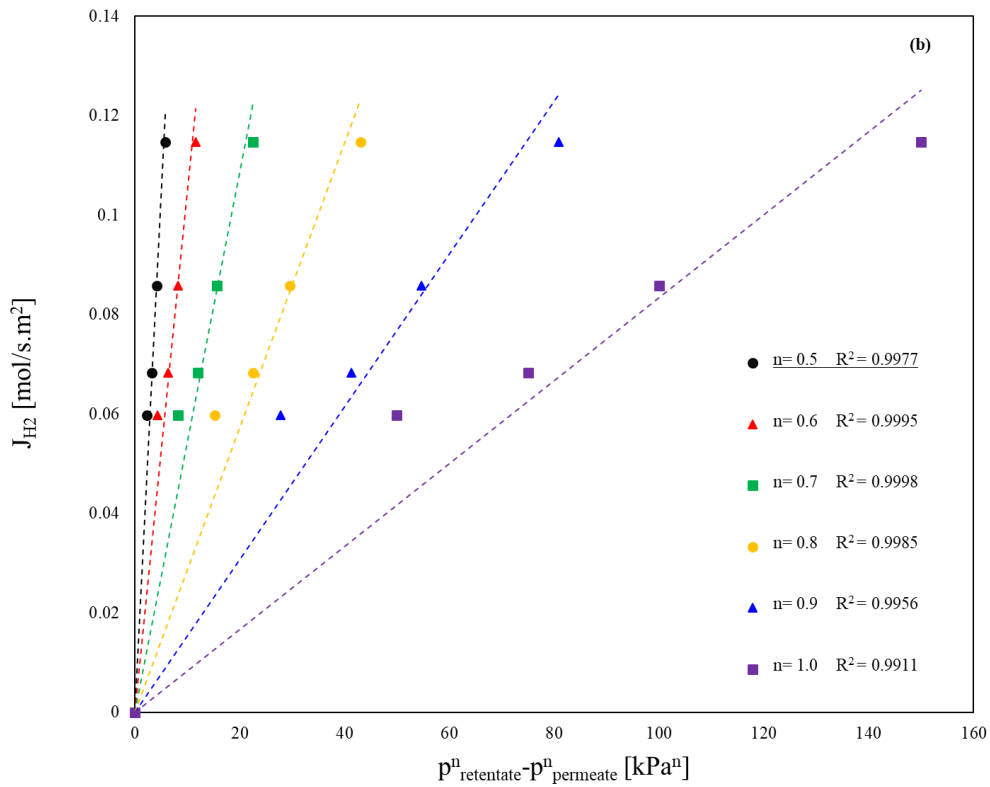
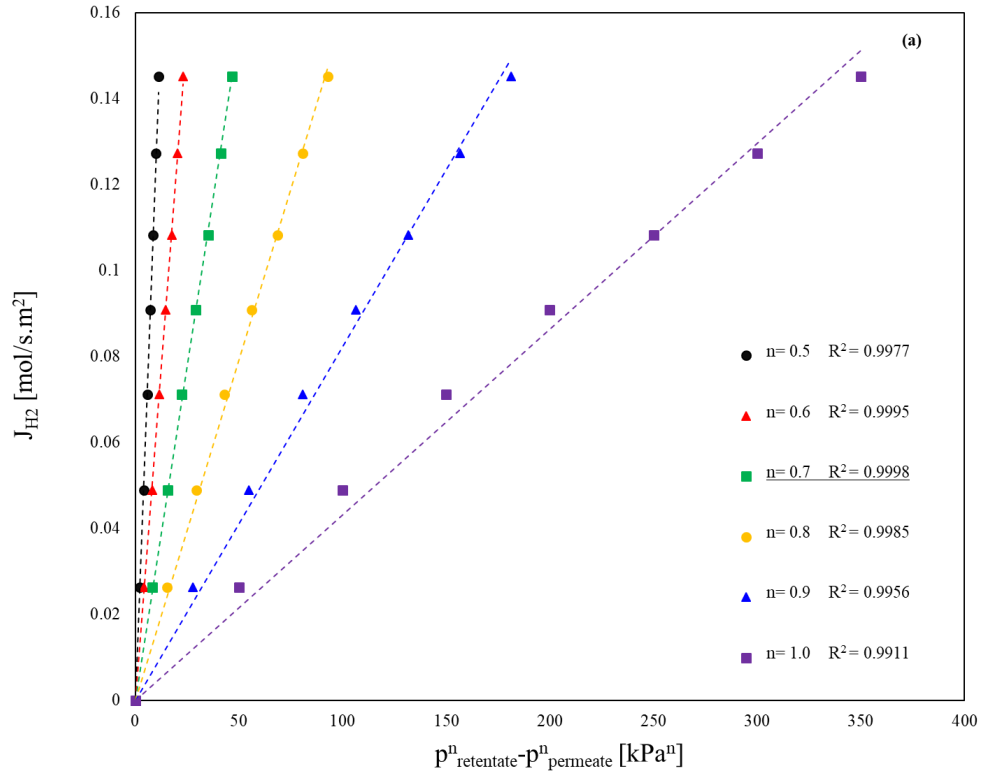


Figure 4-2 Permeating flux of H₂ vs. trans-membrane pressure at 400°C and various values of *n* for (a) Pd membrane (b) Pd-Au membrane.

Hydrogen Permeation in Pd-based MRs

In order to evaluate values of Pe^0 , and E_a , permeation tests were performed for the Pd/YSZ membrane with pure H₂ at a trans-membrane pressure of 100 kPa and at different temperatures ranging from 350 to 400 °C. Using Eq. 4-5, the H₂ permeance vs. reciprocal of absolute temperature was plotted on a logarithmic scale, as shown in Figure 4-3.

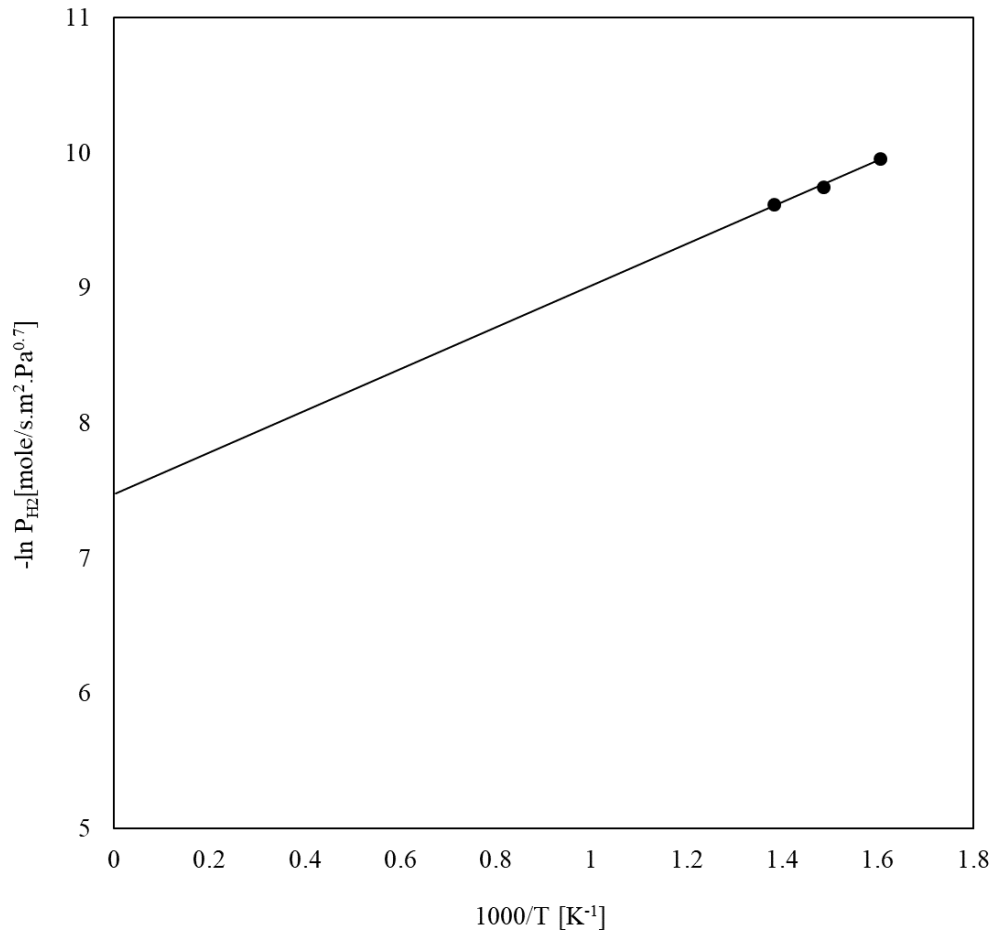


Figure 4-3 Arrhenius plot representing the permeation flux of pure H₂ in a Pd/Al₂O₃ at a trans-membrane pressure of 100 kPa.

The values for P^0 and E_a were found to be $5.66 \times 10^{-4} \text{ mol}/\text{m}^2\cdot\text{s}\cdot\text{Pa}^{0.7}$ and 12.8 kJ/mol, respectively. These values are comparable with the results obtained by other authors, as reported in Table 4-2.

Table 4-2 Gas mixtures fed into the Pd and Pd-Au MRs at 400 °C for permeation tests.

Membrane	Δp [kPa]	Pd thickness [μm]	T [°C]	E_a [kJ/mol]	P [$\text{mol}/\text{m}^2 \cdot \text{s} \cdot \text{Pa}^{0.5}$]	n	Referenc e
Pd/Al ₂ O ₃	400	5	300	NA	* 10^{-6}	0.5	[50]
Pd/SS disk	220	7.2	400	NA	* 15.6×10^{-7}	0.595	[51]
Pd/SS disk	220	9.6	400	NA	* 10.6×10^{-4}	0.595	[51]
Pd/SS disk	220	12.1	400	NA	* 9.3×10^{-4}	0.595	[51]
Pd/SS disk	220	14.6	400	NA	* 5.5×10^{-4}	0.595	[51]
Pd-Ag _{23%} /PSS	2500	2.8	400	NA	6.48×10^{-3}	0.5	[52]
Pd-Ag _{23%} /PSS	1900	2.8	400	NA	6.20×10^{-3}	0.5	[52]
Pd-Ag _{23%} /PSS	1400	2.8	400	NA	5.96×10^{-3}	0.5	[52]
Pd-Ag _{23%} /PSS	900	2.8	400	NA	5.25×10^{-3}	0.5	[52]
Pd-Ag _{23%} /PSS	500	2.8	400	NA	4.66×10^{-3}	0.5	[52]
Pd-Ag _{23%} /PSS	100	2.8	400	NA	3.67×10^{-3}	0.5	[52]
Pd/PSS	100	20	350	16.4	* 5×10^{-7}	0.5	[53]
Pd/PSS	50	10	400	14.7	* 8.7×10^{-7}	0.55	[24]
Pd/Al ₂ O ₃	200	7	400	11.7	* 2.3×10^{-6}	0.54	[24]
Pd/YSZ	50	11	400	12.8	** 2.54×10^{-5}	0.7	This work
Pd-Au/Al ₂ O ₃	50	8	400	NA	8.42×10^{-4}	0.5	This work

* Values are reported in units of $\text{mol}/\text{m}^2 \cdot \text{s} \cdot \text{Pa}^{0.5}$ which can be converted to the current units by diving over membrane thickness

** Units of $\text{mol}/\text{m}^2 \cdot \text{s} \cdot \text{Pa}^{0.7}$.

He and Ar gases were further used to inspect the presence of any defects or pinholes in the membranes, and also to calculate the ideal selectivity of H₂ with respect to He ($\alpha_{\text{H}_2/\text{He}}$) and Ar ($\alpha_{\text{H}_2/\text{Ar}}$). The ideal selectivities of each membrane as a function of trans-membrane pressure are reported in Table 4-3. As can be seen in Table 4-3, for both Pd/YSZ and Pd-Au/Al₂O₃, the ideal selectivity of H₂ with respect to both He and Ar decreases as the trans-membrane pressure increases. This behavior can be explained by the transport mechanism of each gas through the membrane. According to Mardilovich et al., at temperatures above 350 °C, the main transport mechanisms for He, Ar, N₂, CO₂, and CH₄ are Knudsen diffusion and viscous or Poiseuille flow, while the main transport mechanism for H₂ is solution-diffusion [53]. As indicated in Eq. 4-4, the permeating flux of H₂ increases linearly with $P_{\text{H}_2, \text{retentate}}^{0.7} - P_{\text{H}_2, \text{permeate}}^{0.7}$, while for other gases, the permeating flux increases linearly with $P_{\text{retentate}} - P_{\text{permeate}}$. Hence, the permeating flux of other gases will increase more than that of H₂, with an equal increase in the trans-membrane pressure. This will result in a decrease in the ideal selectivity of H₂ at higher pressures. In addition, the existence of defects such as pinholes can exacerbate the reduction in the ideal selectivity values at higher pressures. Although the values of ideal selectivities are high for both membranes, the permeation test results confirm that the Pd membrane is not defect-free

and not completely selective toward H₂, while the Pd-Au membrane shows infinite selectivity to H₂ at 400 °C and a trans-membrane pressure of 50 kPa.

Table 4-3 Ideal Selectivity of H₂ with respect to He and Ar under various pressures at 400 °C for composite Pd and Pd-Au membranes.

Δp (kPa)	$\alpha_{H_2/He}$	$\alpha_{H_2/Ar}$
Pd Membrane		
50	700	5900
100	660	4000
150	650	3800
200	640	3700
Pd-Au Membrane		
50	∞	∞
100	6700	18,200
150	4600	12,400

For both Pd and Pd-Au membranes, at each trans-membrane pressure considered, the ideal selectivity of H₂ to Ar is greater than that of H₂ to He. This behavior can also be described by the prevailing transport mechanism for these gases. As mentioned previously, He and Ar transport through the membrane via Knudsen diffusion and viscous or Poiseuille flow. For these non-absorbing gases, the total permeance can be expressed as the sum of Knudsen and viscous flows, as shown in Eq. 4-7:

$$F_{total} = F_K + F_v \cdot p_{avg} = \frac{2}{3} \sqrt{\frac{8}{\pi}} \frac{\varepsilon \mu_k r}{L \sqrt{RTM}} + \frac{1}{8} \frac{\varepsilon \mu_v r^2}{L \eta RT} \cdot p_{avg} \quad \text{Eq. 4-7}$$

The Knudsen flux is inversely proportional to the square root of the molecular weight of the gas, while viscous flux is inversely proportional to the gas viscosity at a specific temperature [53]. Since both viscosity and molecular weight of He are smaller than those of Ar, at a given temperature, the permeating flux of He is higher than that of Ar, which, in return, will result in a lower ideal selectivity of H₂ to He.

Furthermore, the permeation flux of pure H₂ and the ideal selectivity of H₂ to Ar for the Pd/YSZ membrane were studied at various temperatures between 350 °C to 450 °C. As can be seen in Figure 4-4a, at each driving force, the permeation flux of H₂ increases as temperature increases, which can be explained by Eq. 4-5. According to Eq. 4-5, the

Hydrogen Permeation in Pd-based MRs

permeance of H₂ follows an Arrhenius-type behavior, meaning that the permeance increases at elevated temperatures. Therefore, at a fixed driving force, the permeating flux of H₂ is greatest at the highest temperature and smallest at the lowest temperature. Furthermore, it can be seen in Figure 4-4b that the ideal selectivity of H₂ to Ar also increases monotonically as the temperature increases. By increasing the temperature, the permeance of H₂ grows according to an Arrhenius-type behavior, while the permeance of Ar decreases due to a different transport mechanism, i.e., Knudsen diffusion [53]. As a result, the ideal selectivity of H₂/Ar ($\alpha_{\text{H}_2/\text{Ar}}$) increases as the temperature increases.

Hydrogen Permeation in Pd-based MRs

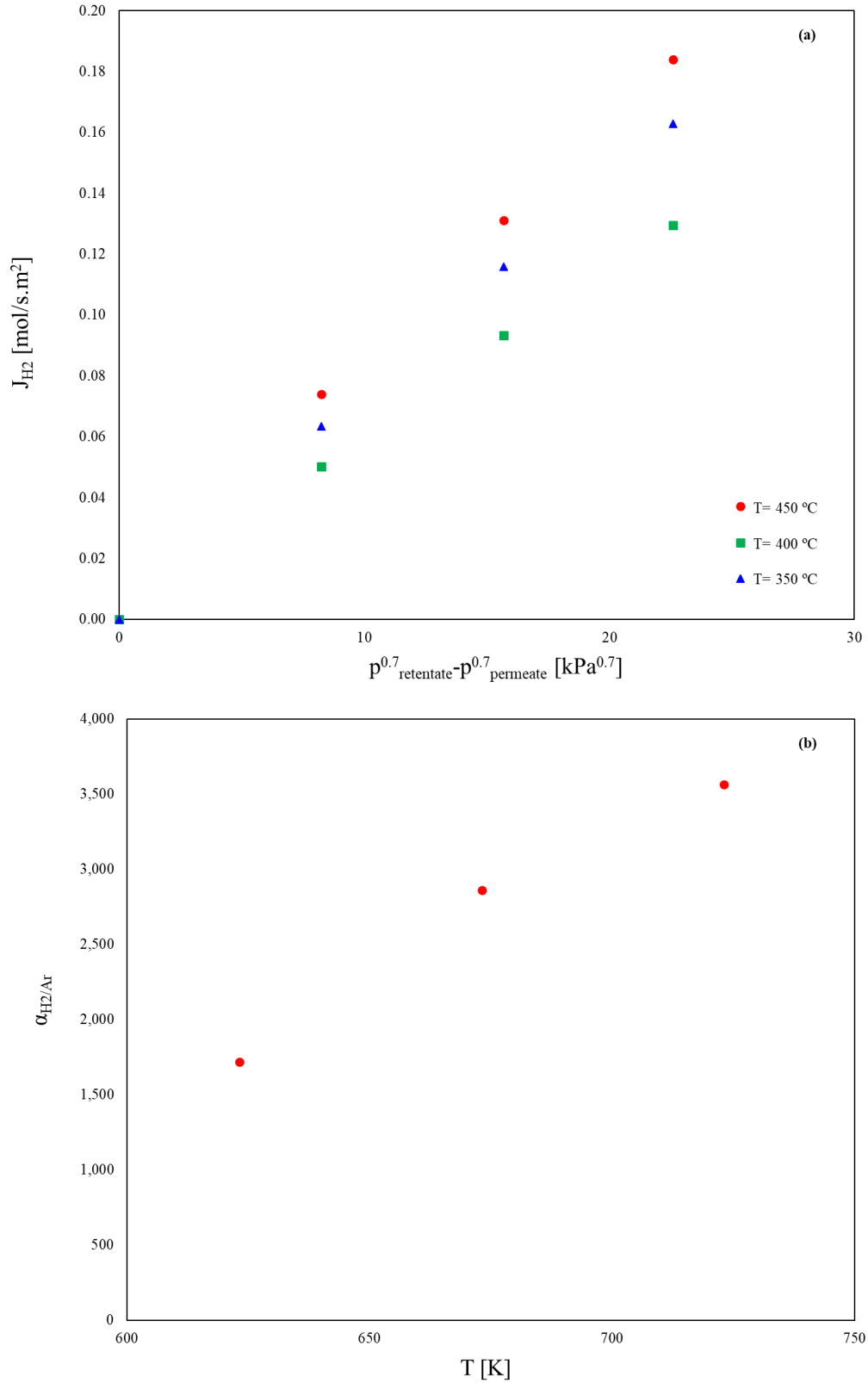


Figure 4-4 Influence of temperature on the (a) permeating flux of H₂ (b) ideal selectivity of H₂ to Ar.

4.3.1.2 Binary Mixtures

The permeating flux of H₂ in a mixture with other gases can be influenced by several mechanisms such as: (1) dilution of H₂ in the feed side as a result of the presence of other gases; (2) H₂ depletion in the bulk feed due to H₂ removal along the membrane module; (3) concentration polarization or build-up of H₂-depleted layer adjacent to the membrane surface due to gas-phase mass-transfer limitations; and (4) competitive adsorption of other gases on the membrane surface [8,28,54]. These factors can reduce the H₂ permeating flux by either reducing the partial pressure of H₂ on the retentate side, or by provoking competitive adsorption on the Pd surface by blocking the active sites [28].

4.3.1.2.1 Influence of Inert Gases on the H₂ Permeation

He, Ar, and N₂ are assumed to be inert gases that do not adsorb on the Pd and Pd-Au surface [28,53,55,56]. Permeation tests were performed with pure H₂ before and after each experiment to investigate the effects of such gases on the H₂ permeating flux. Next, permeation tests with various binary mixtures using both Pd/YSZ and Pd-Au/Al₂O₃ membranes were performed, and H₂ permeating fluxes for each gas mixture were plotted against the driving force. In the end, the permeation tests were repeated with pure H₂ and the changes in permeation flux were evaluated.

As presented in Figure 4-5a and Figure 4-5b, for both membranes, the permeation flux of H₂ in all binary mixtures decreases significantly, compared with the pure H₂ case. For instance, at 400 °C and a driving force of 8.3 kPa^{0.7}, the H₂ permeation fluxes in the binary mixtures decrease by more than 89% compared with the pure H₂ permeation flux in the Pd membrane. For the Pd-Au membrane, this drop is more than 85% at a driving force of 2.25 kPa^{0.5}. This large decrease in the H₂ permeating flux cannot be simply explained by the dilution effect. The fast rate of H₂ removal from the retentate side to the permeate side creates a H₂-depleted “concentration polarization” layer immediately next to the membrane surface. The development of this concentration polarization layer is attributed to the mass-transfer resistance in the gas phase, which, in turn, lowers the partial pressure of H₂ and

Hydrogen Permeation in Pd-based MRs

subsequently reduces its flux [28,54]. The concentration polarization effect, however, is more pronounced at lower driving forces, e.g., for a binary mixture of H₂/Ar in the Pd membrane, the decrease in the permeation flux of H₂ from 89% to 80% when the driving force is increased from 8.25 to 15.69 kPa^{0.7}. For the H₂/Ar mixture in the Pd-Au membrane, the decrease in H₂ permeation flux changes from 88% to 81% as the driving force increase from 2.2 kPa^{0.5} to 4.14 kPa^{0.5}.

Hydrogen Permeation in Pd-based MRs

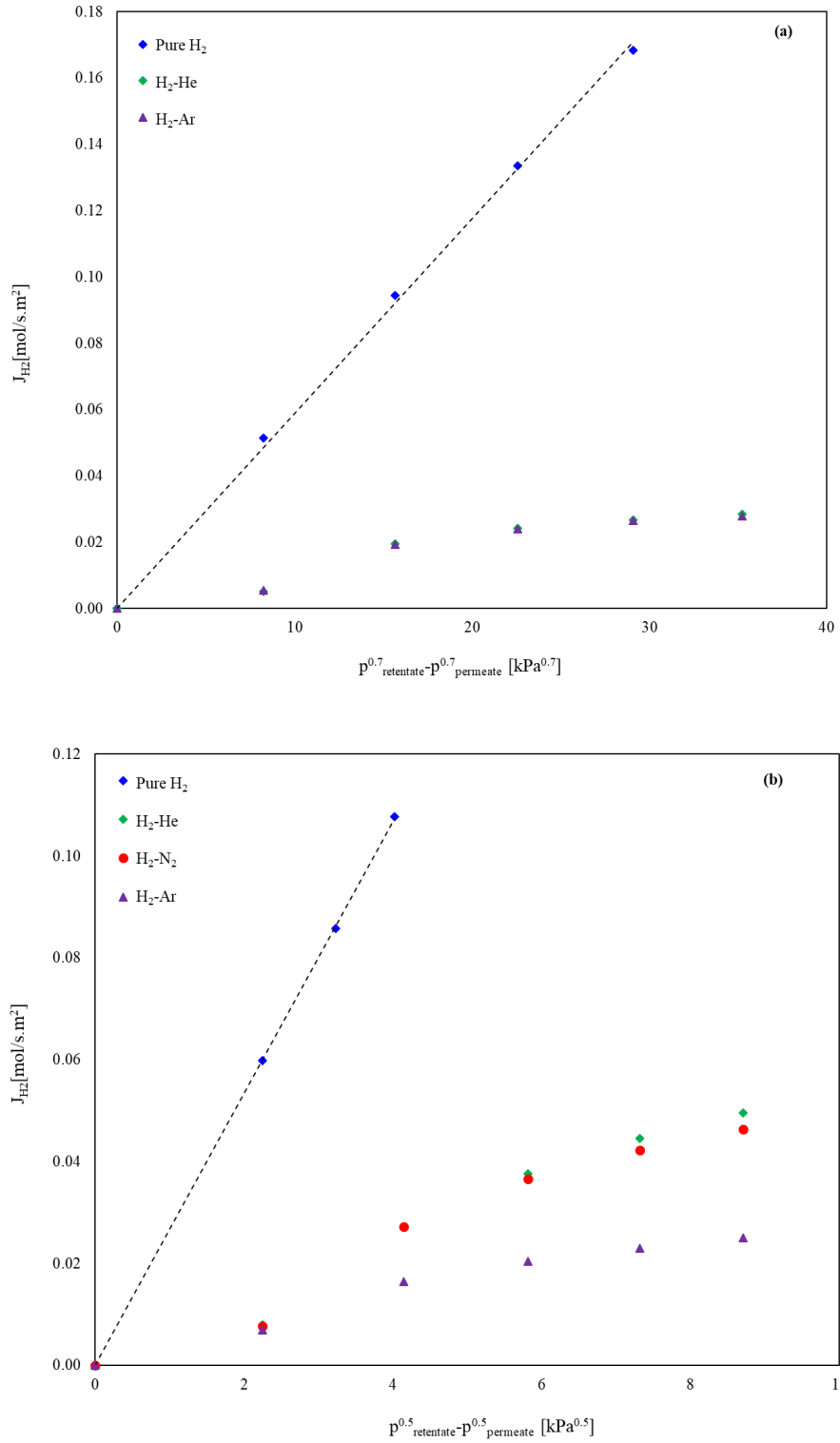


Figure 4-5 Influence of inert gases on the permeation flux of H₂ in (a) Pd/YSZ and (b) Pd-Au/Al₂O₃ membranes.

Hydrogen Permeation in Pd-based MRs

Furthermore, the influence of feed flow rate on the H₂ permeation flux of the equimolar binary mixtures of H₂ and Ar was investigated in this study. As shown in Figure 4-6, H₂ permeation flux increases in each equimolar binary mixture with feed flow rate for both membranes. This can be explained by the fact that at higher flow rates, the mass-transfer resistance is reduced, and as a result, the H₂ flux through the membrane is enhanced.

Hydrogen Permeation in Pd-based MRs

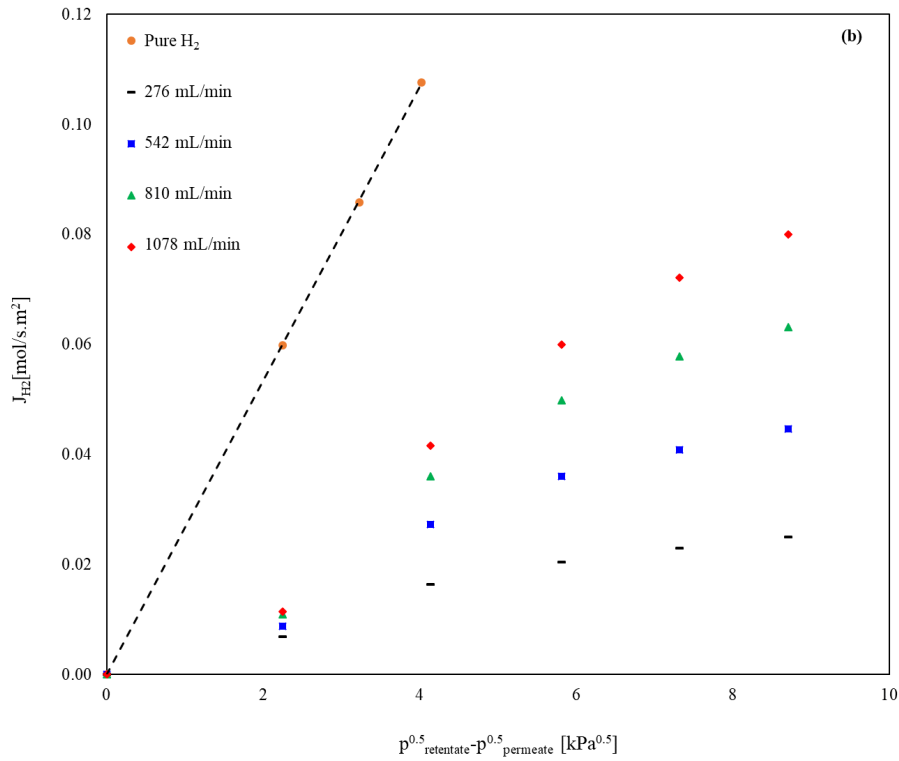
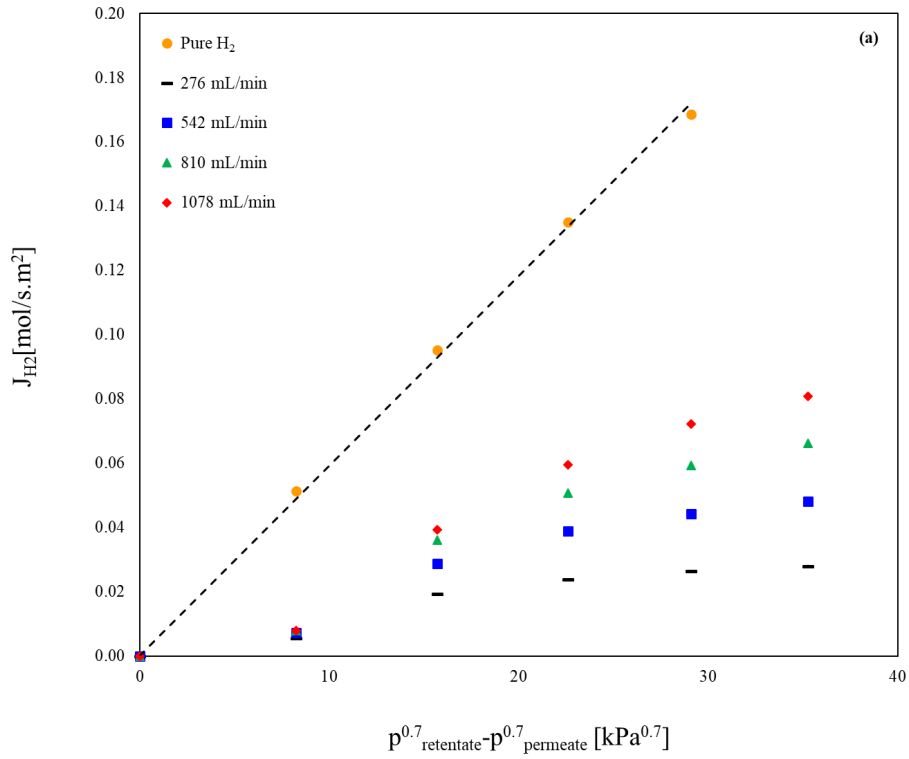


Figure 4-6 Influence of feed flow rate on the permeation flux of H₂ in (a) Pd/YSZ and (b) Pd-Au/Al₂O₃ membranes.

4.3.1.2.2 Influence of CH₄, CO₂, CO, and H₂O on the H₂ Permeation

The influence of several non-inert gases on the H₂ permeating flux was studied by feeding the binary mixture as reported in Table 4-1, and the results are shown in Figure 4-7 for both Pd/YSZ and Pd-Au/Al₂O₃. As can be seen in Figure 4-7a, at 400 °C and a driving force of 10 kPa^{0.7}, steam has the most adverse effect on the H₂ permeating flux, with 88% of flux reduction compared with pure H₂ for Pd membrane. Similarly, for Pd-Au membrane, steam shows the worst effect on the permeation flux of H₂, with an approximately 87% decrease in the permeating flux of H₂ of at a driving force of 10 kPa^{0.5}. CO has the second worst effect on the permeating flux of H₂. At the same operating conditions of pressure and temperature, the permeating flux of H₂ decreases by 80% and 85% for Pd and Pd-Au membranes, respectively. CH₄ shows the lowest decrease in H₂ permeating flux, and exhibits a similar reduction to Ar. The main reason for this behavior is that CH₄ has negligible surface adsorption on the Pd layer, while CO and CO₂ show a strong affinity toward Pd. CO, CO₂, and steam are considered as competitively-adsorbing inhibitors that show high affinity toward the Pd surface [54]. According to Amano et al., the adsorption of even small amounts of CO and CO₂ on the Pd surface causes a significant decrease in the effective surface area for the dissociation of H₂ molecules, hence causing “blanketing” effects [57]. The CO molecules in particular can block the H₂ adsorption sites and/or increase the activation barrier for dissociation and desorption of H₂ molecules [58,59]. It is worth noting that the operating conditions, as well as CO concentrations of as low as 5%, could have a significant effect on the H₂ flux.

The mechanism by which steam reduces the H₂ permeation flux is different than that of CO, however. The presence of steam molecules in the mixture could result in the formation and adsorption of oxygen atoms through H₂O decomposition/recombination, which can poison the active surface of Pd [8]. In this work, for the permeation tests using gas mixtures, the permeating flux of pure H₂ was measured before and after each experiment to evaluate the influence of each component on the permeating flux of H₂. These results show that, on average, the H₂ permeating fluxes immediately after the permeation tests decreased by 0.5%, 3.7%, 5.5%, and 8.7% compared with the H₂ permeating fluxes immediately before

Hydrogen Permeation in Pd-based MRs

the permeation tests for H₂-CH₄, H₂-CO₂, H₂-CO, and H₂-H₂O binary mixtures respectively. These reductions, however, were reversible, and the permeation fluxes of H₂ were restored to the initial values after approximately 7 hours for H₂-H₂O mixtures, and approximately less than 3 hours for H₂-CO₂, H₂-He, and H₂-CO mixtures.

Hydrogen Permeation in Pd-based MRs

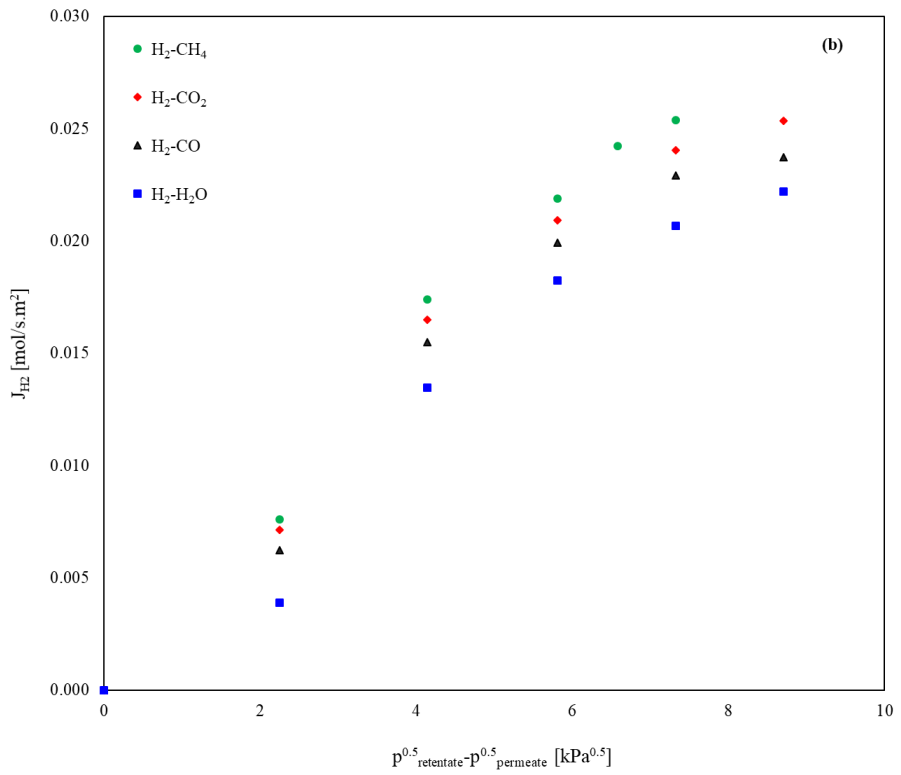
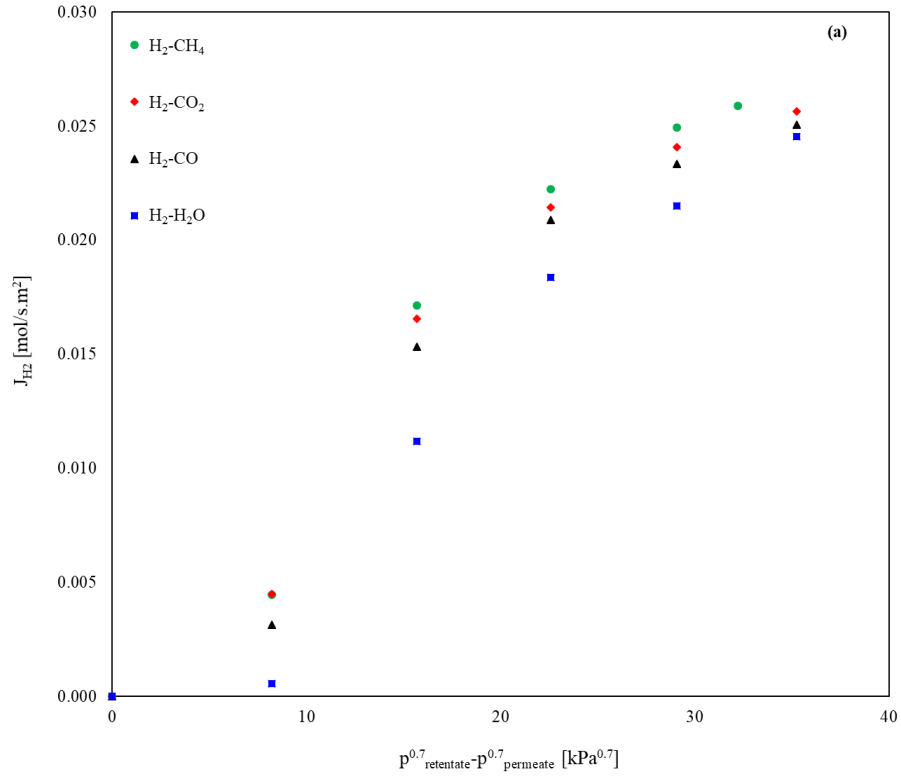


Figure 4-7. Influence of impurities on the permeation flux of H₂ in (a) Pd/YSZ and (b) Pd-Au/Al₂O₃ membranes.

4.3.1.3 Ternary Mixtures

Throughout the ternary mixture investigations, the molar concentration of H_2 in all experiments was held constant at 50%, while the other impurities/components were added to the mixtures with concentrations as reported in Table 4-1. The influence of impurities and SMR components in ternary gas mixtures is presented in Figure 4-8. As shown in this figure, the mixture of $H_2/CO/H_2O$ has the greatest adverse effect on H_2 permeating flux. This may be due to the competitive adsorption nature of CO and decomposition/recombination effect of steam combined, together leading to an increased reduction of the permeating flux of H_2 .

The mechanism by which the mixture of $H_2/CO_2/CO$ affects the H_2 flux is competitive adsorption between the CO, CO_2 , and H_2 molecules for the active sites on the Pd surfaces, while in the ternary mixture of $H_2/CO_2/CH_4$, the competitive adsorption, dilution, and concentration polarization mechanism plays an important role [28,54,57–59].

Hydrogen Permeation in Pd-based MRs

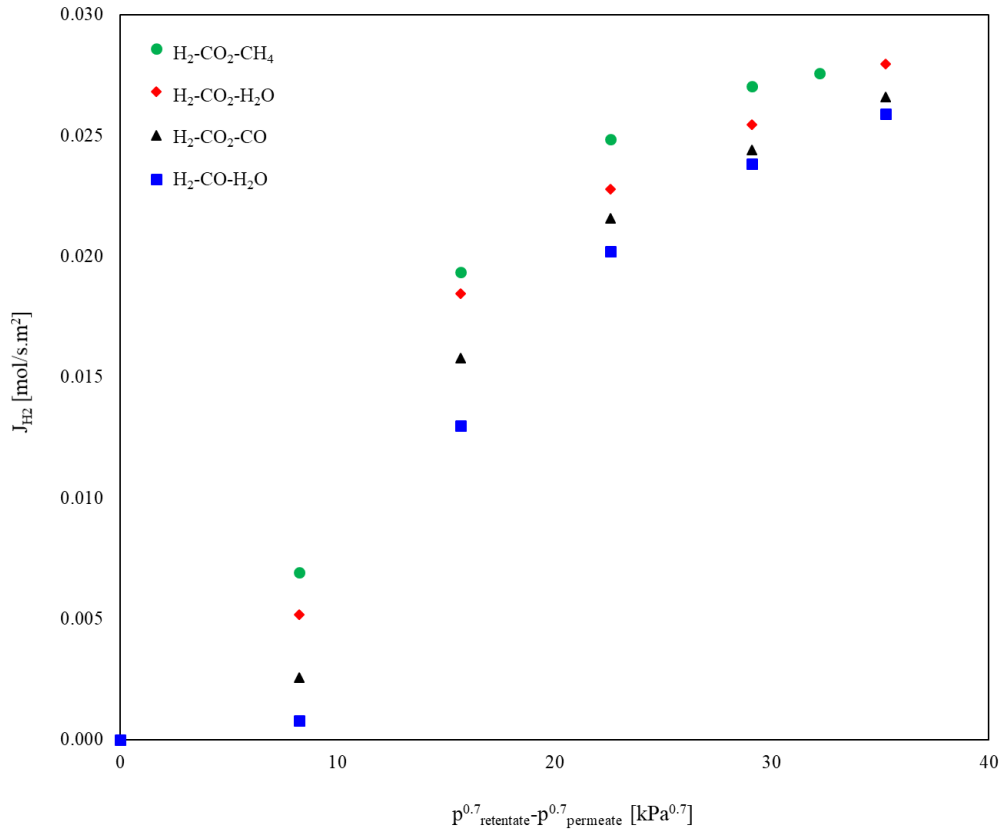


Figure 4-8 H₂ permeation flux in ternary gas mixtures using Pd/YSZ membrane.

4.3.1.4 Simulated SMR Stream

The simulated stream of the SMR reaction was prepared with the compositions reported in Table 4-1. A S/C ratio of 2.0 was used during the first set of experiments. The results of the simulated SMR stream are plotted and compared against the ternary mixture as well as the pure H₂ systems, as shown in Figure 4-9. It can be clearly concluded from this figure that when all the reformed stream components are present in the feed mixture, the H₂ permeation flux is reduced the most. In a simulated SMR stream, the negative effects of concentration polarization, dilution, and depletion of H₂ (resulting from existence of CH₄ and He in the feed stream), combined with the negative effects of competitive adsorption (due to existence of CO and CO₂ in the feed stream) and the decomposition/recombination effect of steam, will reduce the permeating flux of H₂ even more compared with the ternary mixture. From the data presented in Figure 4-9, it can be calculated that at a driving force

Hydrogen Permeation in Pd-based MRs

of $22.6 \text{ kPa}^{0.7}$, the H_2 permeating flux in the ternary mixture of $\text{H}_2\text{-CO}_2\text{-CH}_4$ decreases by 84% compared to the permeating flux of pure H_2 . This decrease is 91% for the simulated SMR stream. In other words, the H_2 permeating flux of the simulated SMR stream is 43% lower compared with the ternary mixture of $\text{H}_2\text{-CO}_2\text{-CH}_4$ at the same driving force. This result confirms the conclusion that the negative effects of concentration polarization and surface adsorption enhance the decrease in the H_2 flux.

Hydrogen Permeation in Pd-based MRs

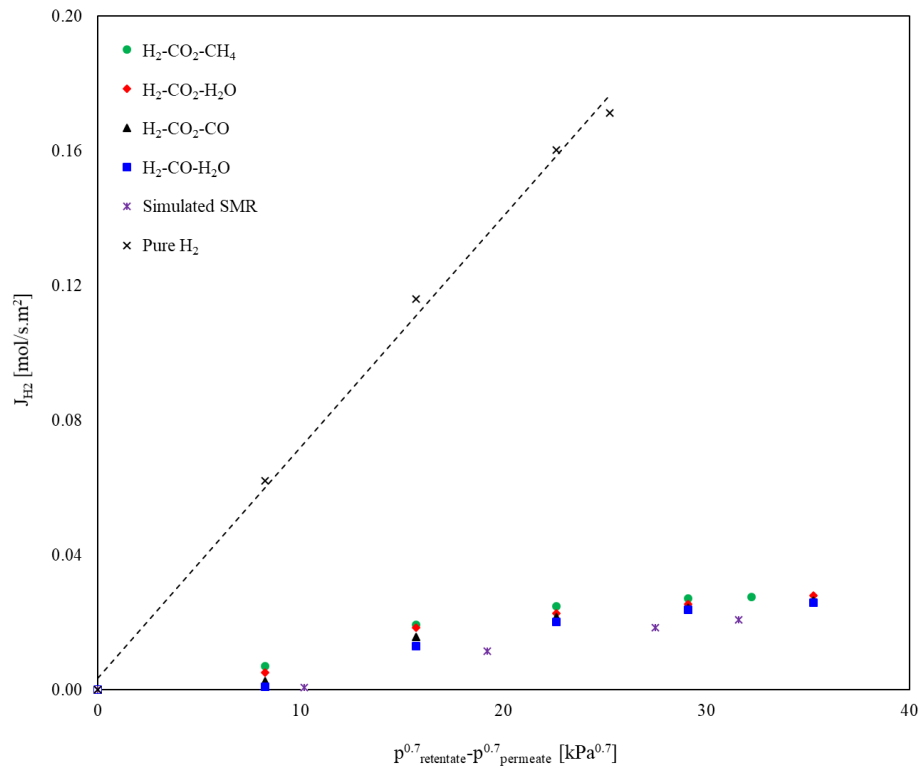
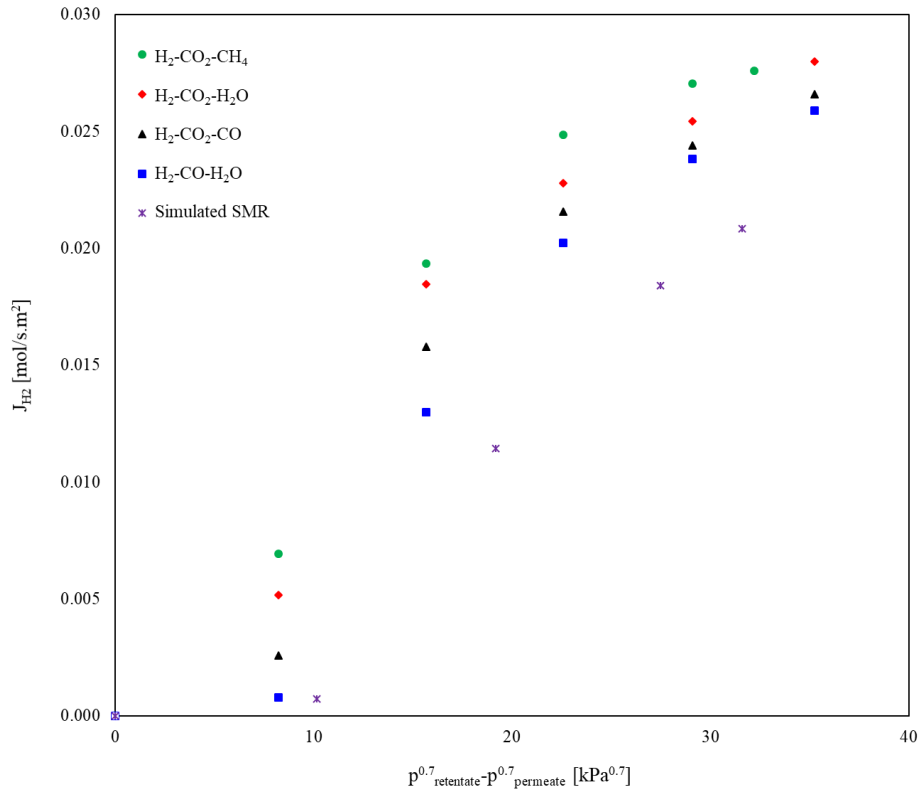


Figure 4-9 H₂ permeation flux in simulated SMR stream using Pd/YSZ membrane.

4.3.1.4.1 Influence of GHSV and S/C Ratio on the H₂ Permeation

The final set of permeation tests was performed to study the effects of GHSV and S/C ratio on the H₂ permeation flux in a simulated SMR stream. The molar concentration of all gases used in the simulation can be found in Table 4-1. In the study of GHSV, the value of S/C ratio was fixed at 3.5. The GHSV is calculated by dividing the total flow rate of gases in the membrane over the active volume of the membrane, with the GHSV initially set at 441 h⁻¹. Next, the GHSV was changed to 882 h⁻¹ (2x the initial value) and 221 h⁻¹ (half of the initial value). The permeation results for all cases are presented in Figure 4-10. As shown in this graph, there is a strong positive correlation between the GHSV and the H₂ permeating flux. In general, the H₂ permeating flux increases with GHSV. This could be attributed to the fact that at higher space velocities, the mass-transfer resistance in the gas phase decreases, leading to a reduction in the concentration polarization effect. In particular, by doubling or halving the GHSV, the H₂ permeation flux increases by a factor of 1.6, and decreases by a factor of 1.7, respectively.

Hydrogen Permeation in Pd-based MRs

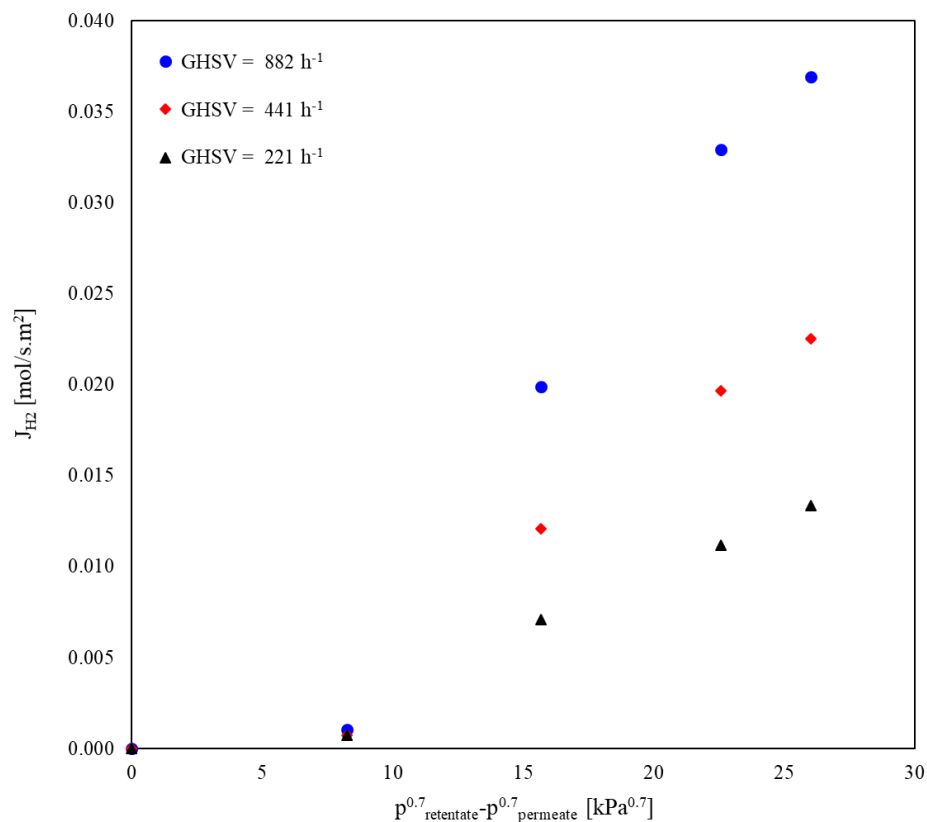


Figure 4-10 Influence of GHSV on the H₂ permeating flux using Pd/YSZ membrane.

The effect of the S/C ratio was changed between 2.0 and 3.5 while keeping the GHSV constant at 441 h⁻¹. As shown in Figure 4-11, the S/C ratio does not have any significant effect on the H₂ permeation flux. It is worth mentioning that the industrial SMR reaction is performed at S/C ratios greater than 3/1, only to maintain the catalyst activity during the reaction [60]. High S/C ratios do not change the thermodynamic conditions of the SMR reaction, and only favor the kinetics of the reaction by keeping the catalyst from deactivation, which is caused by formation of fibrous carbon on the interface of the Ni catalyst [61]. In this study, the permeation tests have been investigated by simulating SMR streams, and no real reaction is performed. Hence, the value of the S/C ratio has no effect on the permeating flux of H₂, as shown in Figure 4-11. However, the low S/C ratio can affect the performance of the MR during the reaction test through the deposition of coke on the catalyst active sites and membrane.

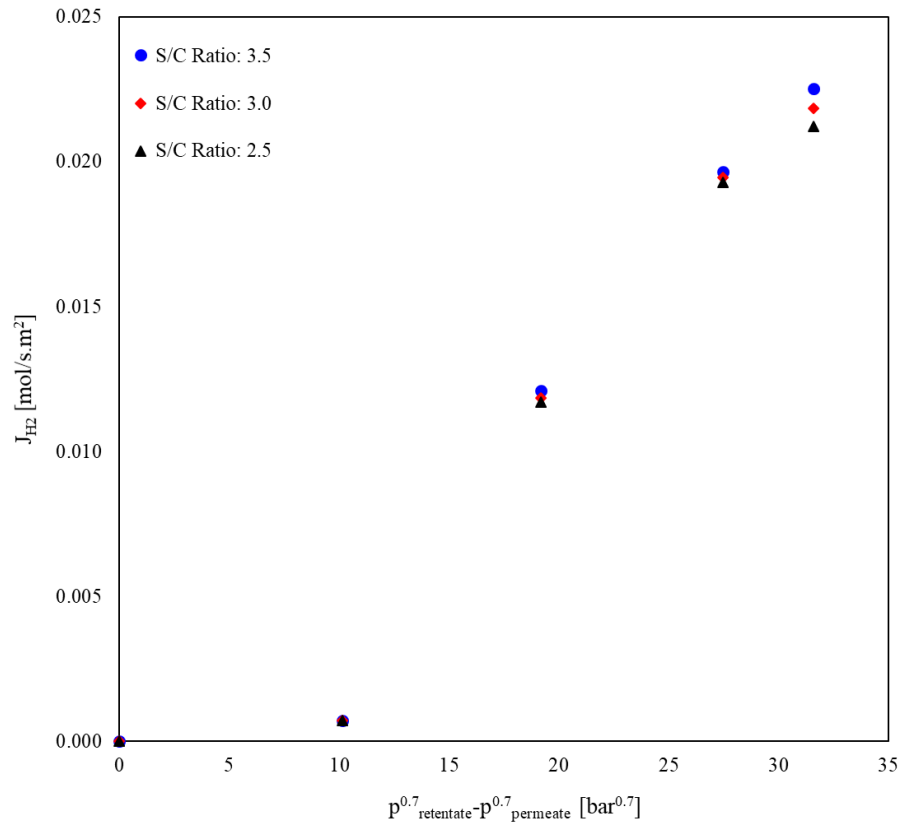


Figure 4-11 Influence of S/C ratio on the H₂ permeating flux using Pd/YSZ membrane.

4.3.2 Scanning Electron Microscope (SEM) Tests

The surface morphology was characterized by SEM and the elemental composition was studied with energy dispersive spectroscopy (EDS) using a JEOL-7000F SEM-EDS to investigate the potential interactions between the feed gas components and the membrane surface, as well as the development of any possible pinholes or cracks.

As shown in Figure 4-12a,b, the surface of the Pd-Au membrane is very uniform before the permeation tests, while the uniformity is distorted after the conclusion of the tests, as indicated in Figure 4-12c,d. Small holes can be seen on Pd-Au membrane both before and after the permeation tests. However, the number of these pinholes is much lower, and their sizes are smaller in a pristine Pd-Au membrane compared with the Pd-Au membrane that has undergone permeation tests. Fernandez et al. [62] reported that the existence of impurities during the membrane fabrication process could lead to the development of

pinholes. The existence of small pinholes in the pristine membrane confirms the fact that some impurities could exist during the electroless plating process. Suleiman et al. [63] reported that continuous exposure of the Pd surface to H_2 causes lattice dilation which, in turn, leads to the development of pinholes and cracks on the membrane surface. Baloyi et al. [64], reported that exposure of the membrane to H_2 and the diffusion of H_2 atoms through the bulk of metal results in the expansion of lattice structure. They attributed the development of pinholes after the permeation tests to the phase change from a to b-phase and the formation of Pd-hydride.

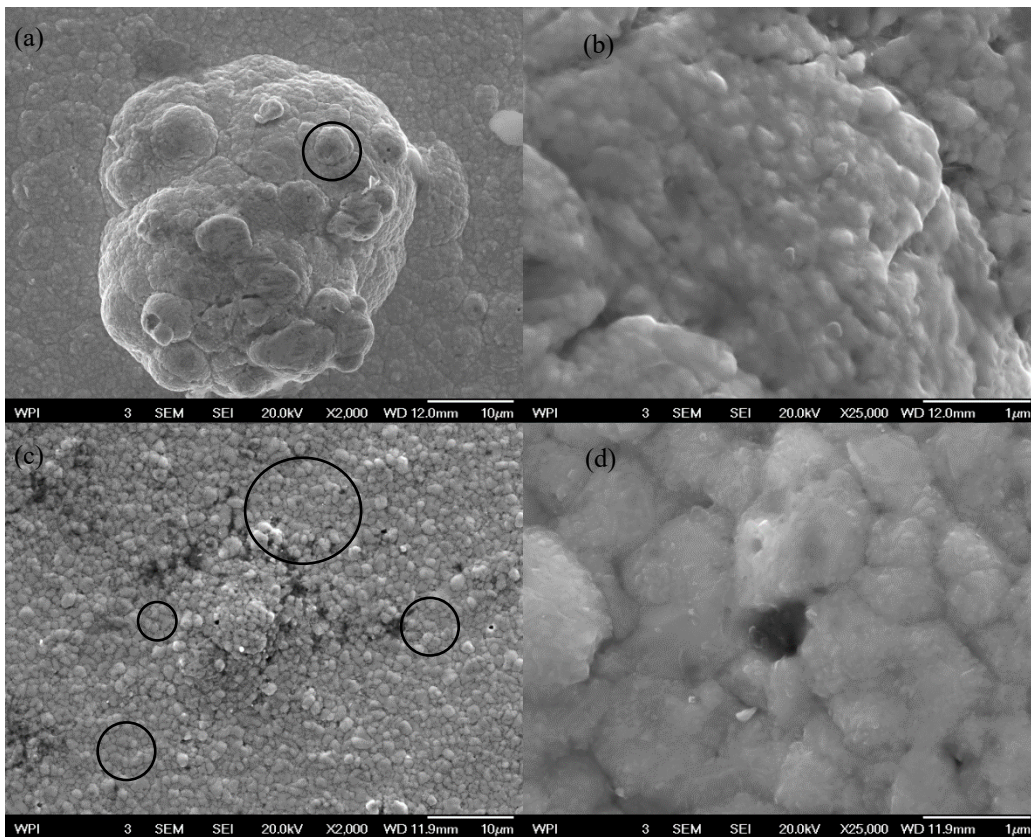


Figure 4-12 SEM image of the Pd-Au membrane before (a,b) and after the permeation tests (c,d).

For the Pd/YSZ membrane, the SEM-EDS analysis was performed on the membrane only after the reaction tests. One can see the development of several pinholes on the Pd surface in Figure 4-13. The diameter of these pinholes is approximately 200–300 nm, as can be seen in Figure 4-13c. According to Guazzone and Ma [65], incoherent sintering of small Pd clusters or Pd crystallites could result in the formation of pinholes at temperatures

between 400–450 °C. Another possible explanation for the development of pinholes could be the numerous cycles of cooling and heating that the membrane has gone through during the tests, as well as the adverse effects of the gaseous components such as CO on the membrane surface. The fact that the ideal selectivity values of H₂/He and H₂/Ar were not infinite at the beginning of the permeation tests and constantly reduced as the permeation tests continued confirms that the development of pinholes is a combination of incoherent sintering during electroless plating, numerous cycles of heating and cooling, and/or due to the bursting of gas pockets close to the membrane surface in the FCC Pd membrane [66].

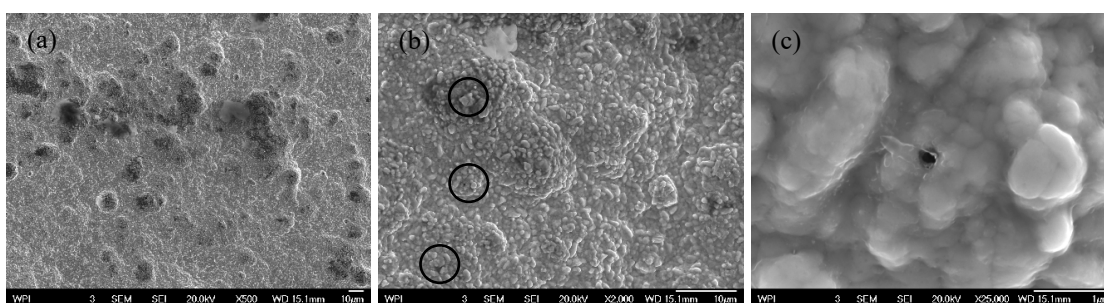


Figure 4-13 SEM image of the Pd membrane after the permeation tests at various magnifications: (a) X500 (b) X2,000 and (c) X25,000

EDS analysis were performed on both Pd and Pd-Au membranes to identify the composition of their surfaces at different spots, as shown in Figure 4-14. EDS analysis of several of the spots on the Pd membrane surface reveals that Pd is not evenly distributed over the membrane surface. The composition of Pd on different spots over the membrane surface varies from 49.2 wt% to 98.4 wt%. For the Pd-Au, a similar trend is observed. Pd and Au are not distributed evenly on the Pd-Au membrane surface. Au content inside the holes is considerably smaller compared with the Au content on the intact bulk of the membrane.

Hou and Hughes [67] reported that the continuous exposure of Pd membrane surface to CO can cause membrane deactivation due to coke formation on the membrane surface. The formation of coke on the membrane surface is confirmed by the EDS analysis, as shown in Figure 4-14c. This can explain the reduction in H₂ permeation flux that was observed during permeation tests with binary mixtures of H₂-CO. While some spots on the Pd

Hydrogen Permeation in Pd-based MRs

membrane were found to have carbon contents as high as 33 wt%, no evidence of coke formation was found on the surface of the Pd-Au membrane, as shown in Figure 4-14d. Further EDS analysis revealed the formation of oxides on the surfaces of both Pd and Pd-Au membranes. This could be a good indication of the formation of PdO on the membrane surfaces which, in turn, adversely affects the permeating flux of H₂. In addition, the intensity of the support materials (Al₂O₃) detected on the surface of the membranes is negligible, which indicates that the holes did not extend all the way to the support, and only affected the top plated layers.

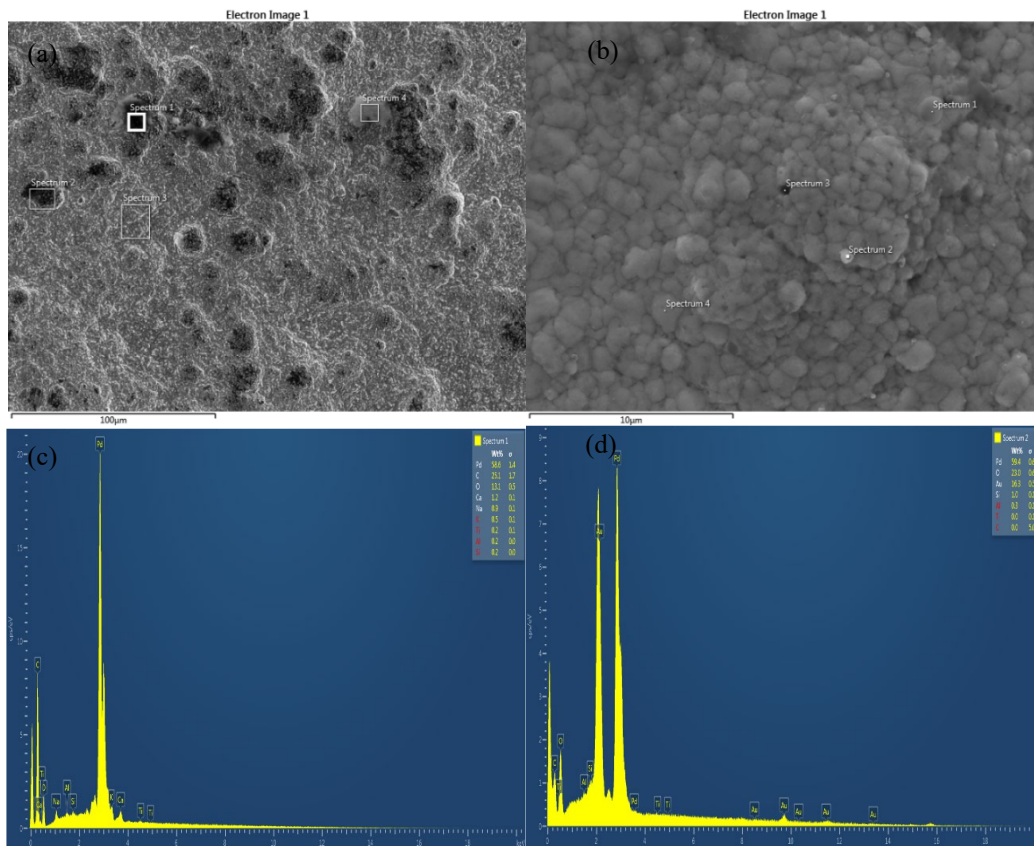


Figure 4-14 EDS analysis of the surface composition for Pd (a,c), and Pd-Au (b,d) membranes.

4.3.3 X-ray Diffraction (XRD) Tests

XRD tests were performed on the membranes after the permeation tests to investigate the development of any potential undesired phases, such as PdO. The XRD analysis were

Hydrogen Permeation in Pd-based MRs

performed using Empyrean diffractometer, and the data were analyzed using Highscore Plus software (Version 4.7, PANalytical, Almelo, The Netherlands).

For Pd membrane five major peaks were identified with their corresponding Miller indices, as reported in Table 4-4 and shown in Figure 4-15. These peaks were in good agreement with the results reported by King and Manchester [68]. As shown in Table 4-4, the lattice structure of Pd at a diffraction angle of 40.1307° has slightly expanded from 2.244°A to 2.247°A . This lattice expansion can be explained by the diffusion of H_2 through the bulk of the metal [64].

For the Pd-Au membrane, five major peaks were detected, as reported in Table 4-4 and shown in Figure 4-15. The composition of the surface material was determined to be $\text{Au}_{0.4}\text{Pd}_{3.6}$. Since the composition is mainly Pd, one expects to see the locations of these peaks close to those of pure Pd. These peaks are in agreement with the results reported by Baba et al. [69].

Baloyi et al. reported that long-term exposure of the Pd-based membranes to H_2 could result in peak shifting, reduction in peak intensity, broadening of peaks, and the formation of new peaks [64]. According to Ungar [70], the shifting of peaks could be attributed to internal stresses, twinning, and/or planar faults that are caused by the diffusion of H atoms through the membrane, while the reduction in peak intensity could stem from point defects, stacking faults, and crystallite smallness. The existence of pinholes and internal stresses could explain the shift of peaks, as well as the reduction in their intensity in the Pd-Au membrane compared with the Pd membrane.

Hydrogen Permeation in Pd-based MRs

Table 4-4 XRD analysis for Pd and Pd-Au MRs at 400 °C.

2θ (°)	d (°Å)	d ^{lit} (°Å)	Rel. Int. (%)	h	k	l
Pd Membrane						
40.1307	2.24703	2.24439	100	1	1	1
46.7137	1.94457	1.94370	16.81	2	0	0
68.1775	1.37436	1.37440	16.55	2	2	0
82.2012	1.17177	1.17210	9.46	3	1	1
86.6651	1.12251	1.12220	4.27	2	2	2
Pd-Au Membrane						
39.8528	2.26018	2.25802	100.00	1	1	1
46.4581	1.95305	1.95550	47.66	0	0	2
67.7534	1.38193	1.38275	15.56	0	2	2
81.7610	1.17696	1.17921	15.33	1	1	3
86.1299	1.12810	1.12901	4.26	2	2	2

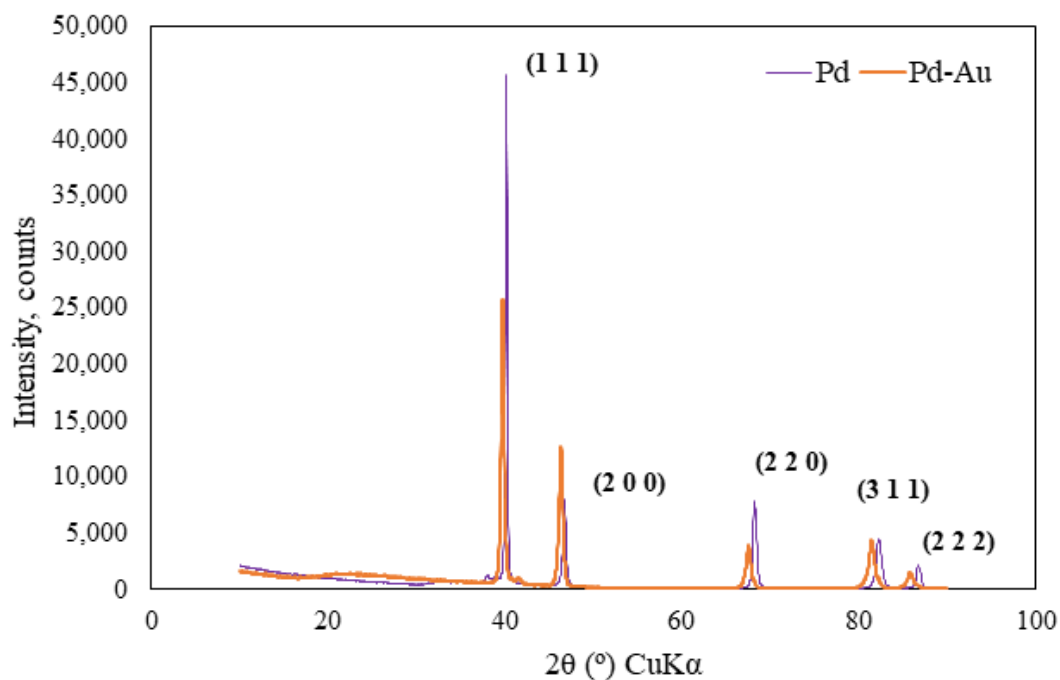


Figure 4-15 XRD analysis of Pd/YSZ and Pd membranes after the permeation tests.

References

- [1] EIA Annual Energy Outlook, Energy Information Administration (EIA); U.S. Department of Energy: Washington, DC, USA, 2014.
- [2] U.S. Energy Information Administration. *Monthly Energy Review*; EIA: Washington, DC, USA, 2018.
- [3] Holladay, J.D.; Hu, J.; King, D.L.; Wang, Y. An overview of hydrogen production technologies. *Catal. Today* **2009**, *139*, 244–260, doi:10.1016/j.cattod.2008.08.039.
- [4] Plasynski, S.I.; Litynski, J.T.; McIlvried, H.G.; Srivastava, R.D. Progress and new developments in carbon capture and storage. *CRC. Crit. Rev. Plant Sci.* **2009**, *28*, 123–138, doi:10.1080/07352680902776440.
- [5] Lattin, W.C.; Utgikar, V.P. Transition to hydrogen economy in the United States: A 2006 status report. *Int. J. Hydrogen Energy* **2007**, *32*, 3230–3237, doi:10.1016/j.ijhydene.2007.02.004.
- [6] U.S. Department of Energy Hydrogen, Fuel Cells and Infrastructure Technologies Program, Multi-Year Research, Development and Demonstration Plan: Planned program activities for 2005–2015; US Department Of Energy Washington, DC, 2007
- [7] Iulianelli, A.; Liguori, S.; Wilcox, J.; Basile, A. Advances on methane steam reforming to produce hydrogen through membrane reactors technology: A review. *Catal. Rev. Sci. Eng.* **2016**, *58*, 1–35, doi:10.1080/01614940.2015.1099882.
- [8] Liguori, S.; Pinacci, K.P.; Seelam; R; Keiski, F.; Drago, V.; Calabrò, V.; Basile, A.; Iulianelli, A. Performance of a Pd/PSS membrane reactor to produce high purity hydrogen via WGS reaction. *Catal. Today* **2012**, *193*, 87–94, doi:10.1016/j.cattod.2012.02.005.
- [9] Ghenciu, A.F. Review of fuel processing catalysts for hydrogen production in PEM fuel cell systems. *Curr. Opin. Solid State Mater. Sci.* **2002**, *6*, 389–399, doi:10.1016/S1359-0286(02)00108-0.
- [10] Al-Mufachi, N.A.; Rees, N.V.; Steinberger-Wilkens, R. Hydrogen selective membranes: A review of palladium-based dense metal membranes. *Renew. Sustain. Energy Rev.* **2015**, *47*, 540–551, doi:10.1016/j.rser.2015.03.026.

- [11] Ohi, J.M.; Vanderborgh, N.; Voecks, G. Hydrogen Fuel Quality Specifications for Polymer Electrolyte Fuel Cells in Road Vehicles; US DOE EERE: Washington, DC, USA, **2016**.
- [12] De Falco, M.D.; Marrelli, L.; Iaquaniello, G. *Membrane Reactors for Hydrogen Production Processes*; Springer: London, UK, 2011; ISBN 9780857291509.
- [13] Burkhanov, G.S.; Gorina, N.B.; Kolchugina, N.B.; Roshan, N.R.; Slovetsky, D.I.; Chistov, E.M. Palladium-based alloy membranes for separation of high purity hydrogen from hydrogen-containing gas mixtures. *Platin. Met. Rev.* **2011**, *55*, 3–12, doi:10.1595/147106711X540346.
- [14] Li, A.; Grace, J.R.; Lim, C.J. Preparation of thin Pd-based composite membrane on planar metallic substrate. Part II. Preparation of membranes by electroless plating and characterization. *J. Memb. Sci.* **2007**, *306*, 159–165, doi:10.1016/j.memsci.2007.08.042.
- [15] Zhang, J.; Liu, D.; He, M.; Xu, H.; Li, W. Experimental and simulation studies on concentration polarization in H₂ enrichment by highly permeable and selective Pd membranes. *J. Memb. Sci.* **2006**, *274*, 83–91, doi:10.1016/j.memsci.2005.07.047.
- [16] Zhang, D.; Fan, Y.; Xu, N.; He, Y. Effect of intermetallic diffusion between Pd and Ti-Al alloy on the performance of Pd/Ti-Al alloy composite membranes. *J. Memb. Sci.* **2011**, *377*, 221–230, doi:10.1016/j.memsci.2011.04.052.
- [17] Yan, S.; Maeda, H.; Kusakabe, K.; Morooka, S. Thin Palladium Membrane Formed in Support Pores by Metal-Organic Chemical Vapor Deposition Method and Application to Hydrogen Separation. *Ind. Eng. Chem. Res.* **1994**, *33*, 616–622, doi:10.1021/ie00027a019.
- [18] Tong, J.; Kashima, Y.; Shirai, R.; Suda, H.; Matsumura, Y. Thin defect-free Pd membrane deposited on asymmetric porous stainless steel substrate. *Ind. Eng. Chem. Res.* **2005**, *44*, 8025–8032, doi:10.1021/ie050534e.
- [19] Li, A.; Grace, J.R.; Lim, C.J. Preparation of thin Pd-based composite membrane on planar metallic substrate: Part I: Pre-treatment of porous stainless steel substrate. *J. Memb. Sci.* **2007**, *298*, 175–181, doi:10.1016/J.MEMSCI.2007.04.016.

- [20] Mardilovich, I.P.; Engwall, E.; Ma, Y.H. Dependence of hydrogen flux on the pore size and plating surface topology of asymmetric Pd-porous stainless steel membranes. *Desalination* **2002**, *144*, 85–89, doi:10.1016/S0011-9164(02)00293-X.
- [21] Yepes, D.; Cornaglia, L.M.; Irusta, S.; Lombardo, E.A. Different oxides used as diffusion barriers in composite hydrogen permeable membranes. *J. Memb. Sci.* **2006**, *274*, 92–101, doi:10.1016/j.memsci.2005.08.003.
- [22] Wang, J.; Luo, J.; Feng, S.; Li, H.; Wan, Y.; Zhang, X. Recent development of ionic liquid membranes. *Green Energy Environ.* **2016**, *1*, 43–61, doi:10.1016/j.gee.2016.05.002.
- [23] Shu, J.; Adnot, A.; Grandjean, B.P.A.; Kaliaguine, S. Structurally stable composite Pd-Ag alloy membranes: Introduction of a diffusion barrier. *Thin Solid Films* **1996**, *286*, 72–79, doi:10.1016/S0040-6090(96)08544-6.
- [24] Liguori, S.; Iulianelli, A.; Dalena, F.; Pinacci, P.; Drago, F.; Broglia, M.; Huang, Y.; Basile, A. Performance and long-term stability of Pd/PSS and Pd/Al₂O₃ membranes for hydrogen separation. *Membranes* **2014**, *4*, 143–162, doi:10.3390/membranes4010143.
- [25] Dolan, M.D. Non-Pd BCC alloy membranes for industrial hydrogen separation. *J. Memb. Sci.* **2010**, *362*, 12–28, doi:10.1016/j.memsci.2010.06.068.
- [26] Borgognoni, F.; Tosti, S.; Vadrucci, M.; Santucci, A. Pure hydrogen production in a Pd-Ag multi-membranes module by methane steam reforming. *Int. J. Hydrogen Energy* **2011**, *36*, 7550–7558, doi:10.1016/j.ijhydene.2011.03.120.
- [27] Brunetti, A.; Caravella, A.; Drioli, E.; Barbieri, G. Process Intensification by Membrane Reactors: High-Temperature Water Gas Shift Reaction as Single Stage for Syngas Upgrading. *Chem. Eng. Technol.* **2012**, *35*, 1238–1248, doi:10.1002/ceat.201100641.
- [28] Peters, T.A.; Stange, M.; Klette, H.; Bredesen, R. High pressure performance of thin Pd-23%Ag/stainless steel composite membranes in water gas shift gas mixtures; influence of dilution, mass transfer and surface effects on the hydrogen flux. *J. Memb. Sci.* **2008**, *316*, 119–127, doi:10.1016/j.memsci.2007.08.056.

- [29] Dolan, M.D.; Donelson, R.; Dave, N.C. Performance and economics of a Pd-based planar WGS membrane reactor for coal gasification. *Int. J. Hydrogen Energy* **2010**, *35*, 10994–11003, doi:10.1016/j.ijhydene.2010.07.039.
- [30] Schramm, O.; Seidel-Morgenstern, A. Comparing porous and dense membranes for the application in membrane reactors. *Chem. Eng. Sci.* **1999**, *54*, 1447–1453, doi:10.1016/S0009-2509(99)00062-7.
- [31] Gallucci, F.; Paturzo, L.; Famà, A.; Basile, A. Experimental Study of the Methane Steam Reforming Reaction in a Dense Pd/Ag Membrane Reactor. *Ind. Eng. Chem. Res.* **2004**, *43*, 928–933, doi:10.1021/ie030485a.
- [32] Jørgensen, S.L.; Nielsen, P.E.H.; Lehrmann, P.E. Steam reforming of methane in a membrane reactor. *Catal. Today* **1995**, *25*, 303–307, doi:10.1016/0920-5861(95)00074-P.
- [33] Chen, W.H.; Syu, W.Z.; Hung, C.I. Numerical characterization on concentration polarization of hydrogen permeation in a Pd-based membrane tube. *Int. J. Hydrogen Energy* **2011**, *36*, 14734–14744, doi:10.1016/j.ijhydene.2011.08.043.
- [34] Mori, N.; Nakamura, T.; Noda, K.-I.I.; Sakai, O.; Takahashi, A.; Ogawa, N.; Sakai, H.; Iwamoto, Y.; Hattori, T. Reactor Configuration and Concentration Polarization in Methane Steam Reforming by a Membrane Reactor with a Highly Hydrogen-Permeable Membrane. *Ind. Eng. Chem. Res.* **2007**, *46*, 1952–1958, doi:10.1021/ie060989j.
- [35] Caravella, A.; Barbieri, G.; Drioli, E. Concentration polarization analysis in self-supported Pd-based membranes. *Sep. Purif. Technol.* **2009**, *66*, 613–624, doi:10.1016/j.seppur.2009.01.008.
- [36] Caravella, A.; Sun, Y. Correct evaluation of the effective concentration polarization influence in membrane-assisted devices. Case study: H₂ production by Water Gas Shift in Pd-membrane reactors. *Int. J. Hydrogen Energy* **2016**, *41*, 11653–11659, doi:10.1016/j.ijhydene.2015.12.068.
- [37] Hara, S.; Sakaki, K.; Itoh, N. Decline in hydrogen permeation due to concentration polarization and CO hindrance in a palladium membrane reactor. *Ind. Eng. Chem. Res.* **1999**, *38*, 4913–4918, doi:10.1021/ie990200n.

- [38] Thoen, P.M.; Roa, F.; Way, J.D. High flux palladium-copper composite membranes for hydrogen separations. *Desalination* **2006**, *193*, 224–229, doi:10.1016/j.desal.2005.09.025.
- [39] Coroneo, M.; Montante, G.; Catalano, J.; Paglianti, A. Modelling the effect of operating conditions on hydrodynamics and mass transfer in a Pd-Ag membrane module for H₂ purification. *J. Memb. Sci.* **2009**, *343*, 34–41, doi:10.1016/j.memsci.2009.07.008.
- [40] He, G.; Mi, Y.; Lock Yue, P.; Chen, G. Theoretical study on concentration polarization in gas separation membrane processes. *J. Memb. Sci.* **1999**, *153*, 243–258, doi:10.1016/S0376-7388(98)00257-9.
- [41] Mourgues, A.; Sanchez, J. Theoretical analysis of concentration polarization in membrane modules for gas separation with feed inside the hollow-fibers. *J. Memb. Sci.* **2005**, *252*, 133–144, doi:10.1016/j.memsci.2004.11.024.
- [42] Takaba, H.; Nakao, S. Computational fluid dynamics study on concentration polarization in H₂/CO separation membranes. *J. Memb. Sci.* **2005**, *249*, 83–88, doi:10.1016/J.MEMSCI.2004.09.038.
- [43] Ma, Y.H.; Mardilovich, I.P. Composite Structures with Porous Anodic Oxide Layers and Methods of Fabrication. U.S. Patent No 8,366,805, 5 February 2013.
- [44] Ma, Y.H.; Mardilovich, I.P.; Engwall, E.E. Composite Gas Separation Modules Having High Tamman Temperature Intermediate Layers. U.S. Patent No 7,255,726, 14 August 2007.
- [45] Ma, Y.H.; Mardilovich, P.P.; She, Y. Hydrogen Gas-Extraction Module and Method of Fabrication. U.S. Patent No 6,152,987, 28 November 2000.
- [46] Collins, J.P.; Way, J.D. Preparation and Characterization of a Composite Palladium-Ceramic Membrane. *Ind. Eng. Chem. Res.* **1993**, *32*, 3006–3013, doi:10.1021/ie00024a008.
- [47] Anzelmo, B. On-Board Hydrogen Production from Natural Gas via a Metallic Pd-Based Membrane Reactor. Ph.D. Dissertation, Stanford University, Stanford, CA, USA, 2016.
- [48] Helmi, A.; Fernandez, E.; Melendez, J.; Tanaka, D.A.P.; Gallucci, F.; Van Sint Annaland, M. Fluidized bed membrane reactors for ultra pure H₂ production—A step

- forward towards commercialization. *Molecules* **2016**, *21*, doi:10.3390/molecules21030376.
- [49] Iulianelli, A.; Liguori, S.; Huang, Y.; Basile, A. Model biogas steam reforming in a thin Pd-supported membrane reactor to generate clean hydrogen for fuel cells. *J. Power Sources* **2015**, *273*, 25–32, doi:10.1016/j.jpowsour.2014.09.058.
- [50] Pacheco Tanaka, D.A.; Llosa Tanco, M.A.; Nagase, T.; Okazaki, J.; Wakui, Y.; Mizukami, F.; Suzuki, T.M. Fabrication of hydrogen-permeable composite membranes packed with palladium nanoparticles. *Adv. Mater.* **2006**, *18*, 630–632, doi:10.1002/adma.200501900.
- [51] Gade, S.K.; Thoen, P.M.; Way, J.D. Unsupported palladium alloy foil membranes fabricated by electroless plating. *J. Memb. Sci.* **2008**, *316*, 112–118, doi:10.1016/j.memsci.2007.08.022.
- [52] Peters, T.A.; Stange, M.; Bredesen, R. On the high pressure performance of thin supported Pd–23%Ag membranes—Evidence of ultrahigh hydrogen flux after air treatment. *J. Memb. Sci.* **2011**, *378*, 28–34, doi:10.1016/J.MEMSCI.2010.11.022.
- [53] Mardilovich, P.P.; She, Y.; Ma, Y.H.; Rei, M.H. Defect-Free Palladium Membranes on Porous Stainless-Steel Support. *AIChE J.* **1998**, *44*, 310–322, doi:10.1002/aic.690440209.
- [54] Mejdell, A.L.; Jøndahl, M.; Peters, T.A.; Bredesen, R.; Venvik, H.J. Effects of CO and CO₂ on hydrogen permeation through a ~3 μm Pd/Ag 23 wt.% membrane employed in a microchannel membrane configuration. *Sep. Purif. Technol.* **2009**, *68*, 178–184, doi:10.1016/j.seppur.2009.04.025.
- [55] Amandusson, H.; Ekedahl, L.G.; Dannetun, H. Hydrogen permeation through surface modified Pd and PdAg membranes. *J. Memb. Sci.* **2001**, *193*, 35–47, doi:10.1016/S0376-7388(01)00414-8.
- [56] Li, A.; Liang, W.; Hughes, R. The effect of carbon monoxide and steam on the hydrogen permeability of a Pd/stainless steel membrane. *J. Memb. Sci.* **2000**, *165*, 135–141, doi:10.1016/S0376-7388(99)00223-9.
- [57] Amano, M.; Nishimura, C.; Komaki, M. Effects of High Concentration CO and CO₂ on Hydrogen Permeation through the Palladium Membrane. *Mater. Trans. JIM* **1990**, *31*, 404–408.

- [58] Eriksson, M.; Ekedahl, L.-G.G. Real time measurements of hydrogen desorption and absorption during CO exposures of Pd: Hydrogen sticking and dissolution. *Appl. Surf. Sci.* **1998**, *133*, 89–97, doi:10.1016/S0169-4332(98)00185-8.
- [59] Gallucci, F.; Chiaravalloti, F.; Tosti, S.; Drioli, E.; Basile, A. The effect of mixture gas on hydrogen permeation through a palladium membrane: Experimental study and theoretical approach. *Int. J. Hydrogen Energy* **2007**, *32*, 1837–1845, doi:10.1016/j.ijhydene.2006.09.034.
- [60] Yamazaki, O.; Tomishige, K.; Fujimoto, K. Development of highly stable nickel catalyst for methane-steam reaction under low steam to carbon ratio. *Appl. Catal. A Gen.* **1996**, *136*, 49–56, doi:10.1016/0926-860X(95)00268-5.
- [61] Rostrup-Nielsen, J.; Trimm, D.L. Mechanisms of carbon formation on nickel-containing catalysts. *J. Catal.* **1977**, *48*, 155–165, doi:10.1016/0021-9517(77)90087-2.
- [62] Fernandez, E.; Coenen, K.; Helmi, A.; Melendez, J.; Zuñiga, J.; Pacheco Tanaka, D.A.; Van Sint Annaland, M.; Gallucci, F. Preparation and characterization of thin-film Pd-Ag supported membranes for high-temperature applications. *Int. J. Hydrogen Energy* **2015**, *40*, 13463–13478, doi:10.1016/j.ijhydene.2015.08.050.
- [63] Suleiman, M.; Jisrawi, N.M.; Dankert, O.; Reetz, M.T.; Bähz, C.; Kirchheim, R.; Pundt, A. Phase transition and lattice expansion during hydrogen loading of nanometer sized palladium clusters. *J. Alloys Compd.* **2003**, *356–357*, 644–648, doi:10.1016/S0925-8388(02)01286-0.
- [64] Baloyi, L.N.; North, B.C.; Langmi, H.W.; Bladergroen, B.J.; Ojumu, T.V. The production of hydrogen through the use of a 77 wt% Pd 23 wt% Ag membrane water gas shift reactor. *S. Afr. J. Chem. Eng.* **2016**, *22*, 44–54, doi:10.1016/j.sajce.2016.11.001.
- [65] Guazzone, F.; Ma, Y.H. Leak growth mechanism in composite Pd membranes prepared by the electroless deposition method. *AIChE J.* **2008**, *54*, 487–494, doi:10.1002/aic.11397.
- [66] Goldbach, A.; Yuan, L.; Xu, H. Impact of the fcc/bcc phase transition on the homogeneity and behavior of PdCu membranes. *Sep. Purif. Technol.* **2010**, *73*, 65–70, doi:10.1016/j.seppur.2010.01.007.

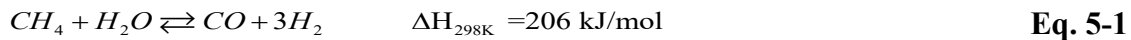
- [67] Hou, K.; Hughes, R. The effect of external mass transfer, competitive adsorption and coking on hydrogen permeation through thin Pd/Ag membranes. *J. Memb. Sci.* **2002**, *206*, 119–130, doi:10.1016/S0376-7388(01)00770-0.
- [68] King, H.W.; Manchester, F.D. A low-temperature X-ray diffraction study of Pd and some Pd-H alloys. *J. Phys. F Met. Phys.* **1978**, *8*, 15–26, doi:10.1088/0305-4608/8/1/007.
- [69] Baba, K.; Miyagawa, U.; Watanabe, K.; Sakamoto, Y.; Flanagan, T.B. Electrical resistivity changes due to interstitial hydrogen in palladium-rich substitutional alloys. *J. Mater. Sci.* **1990**, *25*, 3910–3916, doi:10.1007/BF00582459.
- [70] Ungár, T. Microstructural parameters from X-ray diffraction peak broadening. *Scr. Mater.* **2004**, *51*, 777–781, doi:10.1016/j.scriptamat.2004.05.007.

Chapter 5 - Carbon Capture and Hydrogen Production via MRs

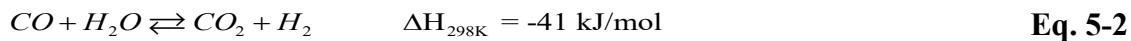
This chapter discusses the details of the SMR reaction and its performance using a Pd-based MR. The metrics that are used to measure the performance of the SMR are methane conversion, hydrogen recovery, and hydrogen purity on the permeate side. The adsorption mechanism of CO₂ on zeolite 13X surface is discussed in this chapter and the potential of MR for simultaneous production of hydrogen and separation of CO₂ is examined.

5.1 Introduction

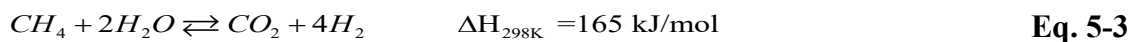
In a conventional SMR reactor, natural gas and superheated steam react over the surface of a nickel-based catalyst [1] at very harsh operating conditions (temperature and pressure ranges between 800 °C to 1000 °C and 15 to 20 bar, respectively [2]) to produce a mixture of H₂ and CO as shown in Eq. 5-1[3,4,13,5–12]



The syngas (a mixture of hydrogen and carbon monoxide) exiting the reformer contains a substantial content of carbon monoxide (generally higher than 5 vol.%),[2] which may be converted to more hydrogen via two water-gas shift (WGS) reactions (i.e., high temperature shift (HTS) and low temperature shift (LTS))WGS reaction as shown in Eq. 5-2:



The overall SMR reaction can be obtained by combining the reforming and WGS reactions (Eq. 5-1 and Eq. 5-2) as following:



Produced hydrogen is later sent to a separation and purification unit to purify hydrogen for the end use application. Pressure swing adsorption (PSA) is currently the dominant technique in the industry for purifying hydrogen.

5.1.1 Membrane reactor for SMR

As explained in details in Chapter 2, the current methods of hydrogen production, heavily depend on fossil fuels as feedstock which will exacerbate the climate change problem.[14,15] Nevertheless, alternative methods could be employed to produce hydrogen in a sustainable way while capturing CO₂. [16] It has been suggested that membrane reactor (MR) has the potential to produce hydrogen onboard while separating and storing CO₂ storage on the vehicle. [9,13]

A membrane reactor uses the same method (SMR) to produce hydrogen. However, the main difference between a MR and a conventional reactor (CR), is that the MR has the potential to combine the reforming reaction, WGS reaction, and the purification units in one single unit and hence, intensify the whole process. The process schematic of a MR is compared is presented in Figure 5-1. A MR is characterized by two separate sides, a retentate side where the SMR reaction takes place and a permeate side where the hydrogen molecules are collected. Continuous removal of the hydrogen molecules from the retentate side to the permeate side will shift the reforming reaction to the right-hand side of Eq. 5-3 according to the Le Chatelier's principle, resulting in higher methane and carbon monoxide conversion (X_{CH_4} , X_{CO}) values.[17] By using a membrane that is infinitely selective toward hydrogen such as dense Pd membranes, a very pure stream of hydrogen could be collected on the permeate side.

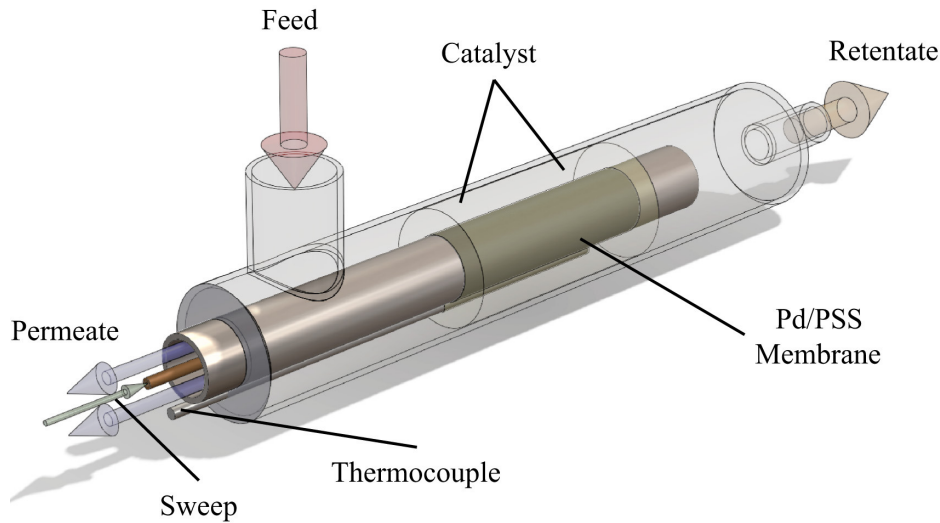


Figure 5-1. Schematic of a MR for SMR or SAR process (taken from Anzelmo et al.) [18]

5.1.2 Principles of Pd-based MR

Pd-based metallic membranes have the potential to produce hydrogen due to their “infinite perm-selectivity” toward hydrogen.[19] Hydrogen with purities as high as 99.9999% could be produced via Pd-based MRs which is ideal for use in HFCVs.[20,21] Hydrogen transport through palladium is governed by the solution-diffusion mechanism which takes place in six distinct steps: [22,23].

1. Hydrogen chemisorption on the Pd surface
2. Dissociation of molecular hydrogen into atomic hydrogen on the Pd surface
3. Dissolution of atomic hydrogen in the Pd surface
4. Diffusion of atomic hydrogen within the Pd lattice
5. Association of the hydrogen atoms
6. Desorption of hydrogen molecules from the surface

Hydrogen transport through the Pd membrane can be either surface-limited or diffusion-limited. When diffusion is the limiting step, hydrogen permeation flux can be expressed by Sieverts-Fick’s law.

$$J_{H_2} = Pe_H \frac{(p_{H_2,ret}^{0.5} - p_{H_2,perm}^{0.5})}{\delta} \quad \text{Eq. 5-4}$$

where J_{H_2} is the hydrogen permeating flux through the membrane, Pe_{H_2} is the permeability of the membrane, $p_{H_2,ret}^{0.5}$ and $p_{H_2,perm}^{0.5}$ are the partial pressure of hydrogen in the retentate and permeate sides, respectively, and δ is the membrane thickness.

Despite its simplicity, there are some shortcomings in the Sieverts-Fick's law which has made numerous scientists to recommend using a general form of this law in which the hydrogen permeating flux is proportional to the partial pressure of hydrogen to the power of n: [24–27]

$$J_{H_2} = Pe_H \frac{(p_{H_2,ret}^n - p_{H_2,perm}^n)}{\delta} \quad \text{Eq. 5-5}$$

The empirical exponent n in Eq. 5-5 is a dependent factor which determines the correlation between the hydrogen permeating flux and the driving force (partial pressure of hydrogen on the retentate and permeate sides). The value of n, varies between 0.5 and 1.0 [28], and is usually evaluated using nonlinear regression technics.[29]. Although controversial, the value of n has been used as a benchmark to determine the rate controlling steps. The deviation of n values from 0.5 may be explained by the deviation of the hydrogen solubility from the values proposed by Sieverts' law, which may result from incorrect assumptions of the rate-determining steps, non-ideality of interstitial hydrogen diffusivity, or crystallographic phase transition. [27] In addition, a deviation from 0.5 indicates that the permeation of hydrogen may be influenced by a combination of other factors such as Pd surface impurities, bulk defects, i.e., organic contaminants from fabrication or pinholes, respectively.[30,31]

5.1.3 Operating parameters of a MR

There are several operating conditions that have significant impact on the performance of the MR. These parameters could be engineered to improve the permeating flux of hydrogen, to enhance the conversion of methane, to prevent the formation of coke in the reactor, and to reduce the cost. Some of the most important operating parameters in the design of a MR are operating pressure and temperature, steam to carbon (S/C) ration, purity of the feed gas, and use of sweep gas.

As shown in Eq. 5-3, SMR reaction is an endothermic reaction hence, the thermodynamic performance of MR in terms of methane conversion will be improved at higher temperatures. Hence, SMR reaction is usually performed at temperatures above 800°C to achieve thermodynamic favorability and to avoid the formation of solid carbon.[32] However, the MR makes it possible to operate the SMR reaction at much lower temperatures (in the range of 450-600 °C) which is the greatest thermodynamic and economic improvement compared with the CR.[33]

Regarding the operating pressure, in a conventional SMR process, increasing the pressure will shift the reaction toward the left-hand side of Eq. 5-3 and hence, reducing the methane conversion, as shown by Anzelmo et al.[18] However, for MR systems the effect could be the opposite. In a MR, higher operating pressures will lead to increased flux of hydrogen through the MR. According to the Le Chatelier's principle, removal of hydrogen from the reaction zone will shift the reaction to the right had side of Eq. 5-3 and as a result will improve the methane conversion. This increase in methane hydrogen more than offsets the negative thermodynamic effect of increasing the pressure and allows the MR to operate at higher operating conditions.

One of the greatest problems in the SMR process is the deposition of carbon residues or “coke formation” on the catalyst and membrane surfaces during the reaction. One way to prevent/minimize this adverse phenomenon is using an excess amount of steam or higher S/C ratio. S/C ratios between 2.0-4.0 are common in CRs.[33]

Nevertheless, one needs to optimize all these parameters in a way to find the best compromise between lower operating cost and higher methane conversion and hydrogen purity. In a recent work, Kian et al., have studied the performance of Pd-based membranes under various operating conditions. They have shown that by increasing the trans-membrane pressure, although the permeating flux of hydrogen increases, the ideal selectivity of hydrogen with respect to helium ($\alpha_{H_2/He}$) and argon ($\alpha_{H_2/Ar}$) decreases which can be translated into more operating costs for separation and purification of hydrogen.[34] They have furthermore shown that at higher operating temperatures the permeating flux of hydrogen increases exponentially following an Arrhenius-type behavior. In addition, they have further explained that the existence of other gases in the reaction zone, i.e. CO, CO₂, H₂O, CH₄, significantly reduces the hydrogen permeation flux due to four different mechanisms of dilution, depletion, concentration polarization, and competitive adsorption. It has been shown in the literature that the existence of parts per million (ppm) levels of H₂S in the natural gas can block the active sites on the Pd surface for hydrogen dissociation by forming palladium sulfide.[35]

By using a sweep gas like nitrogen or argon, the MR can function at lower operating conditions while showing the same performance in terms of methane conversion. However, some of the greatest arguments against the use of sweep gas are the need to heat up the sweep gas to reaction temperature and extra cost of separation and purification of hydrogen after production.[36] This means that contrary to the common belief, the capital costs (for special equipment) and the operating expenses may significantly increase when a sweep gas is used.

5.1.4 CO₂ capture

Removal of carbon dioxide from the power plants and industrial processes has been one of the contributing factors in the battle against climate change in the recent decades. Today, carbonate and alkanolamine are the main solutions used in the industry to capture CO₂ on a large scale. Although effective, these processes are very energy-intensive and the

equipment used in the facilities suffer from severe corrosion, both of which will lead to higher cost of capture.[37] Due to these reasons, a lot of scientists have shifted their attention toward inorganic porous materials such as zeolites and activated carbon as alternative technologies for CO₂ capture. These materials have shown very strong selectivity toward adsorption of CO₂. [37]

Zeolites are nano porous inorganic materials with frameworks composed of [SiO₄]⁴⁻ and [AlO₄]⁵⁻ tetrahedra and can be used in various industrial applications such as catalysis and gas separation. Zeolite 13X can be synthesized from kaolinite, Al₂Si₂O₅(OH)₄ by engineering the Si/Al ratios to values above 1.5 [38] Due to their high adsorption capacities compared with other solid sorbents, 13X has gained significant interest for CO₂ capture applications in the last decade. However, one of the greatest challenges with using 13X for carbon capture purposes arises when the gaseous stream contains water. As discussed by Wilcox, zeolite 13X has a strong preference toward water compared with CO₂. This can be explained by the differences between the dipole and quadrupole moments. Although a CO₂ molecule has a strong quadrupole moment, it does not bear a dipole moment while a water molecule carries a strong dipole moment. Dipole interactions are inherently stronger than quadrupole interactions which will make water to adsorb easier on the zeolite surface compared with CO₂. [39] Hence, in order to effectively capture CO₂ using 13X, one needs to completely remove water from the gaseous stream first.

The permeate stream in a Pd-based MR is a high purity stream of hydrogen with purities as high as 99.999% which can be used directly for HFCVs. The retentate stream, however, may contain other reaction gases such as carbon monoxide, carbon dioxide, superheated steam, and some non-reacted methane. When methane conversion values are very high and close to unity, the retentate stream is mainly composed of carbon dioxide and superheated steam. Steam can be easily separated from the retentate stream by condensing it via a cold trap. Hence, the retentate stream will be highly concentrated with CO₂ which can be captured, transported, and stored with significantly lower thermodynamic work. However, the concentration of CO₂ in the retentate side is usually much less than 100%, after steam condensation. The values of methane conversion in Pd-based MRs could be as low as 19%.

Carbon Capture and Hydrogen Production via MRs

Anzelmo et al. have reported a maximum value of 84% for methane conversion in a Pd/PSS MR which operates at 400 °C and a pressure of 300 kPa, with an argon sweep flow rate of 100 mL/min.[18] This value will be significantly lower in the absence of a sweep gas.

5.2 Experimental Methodology and Materials

5.2.1 Pd-based Membrane

The Pd-based composite membrane used in this study was prepared by deposition of a thin layer of Pd on an asymmetric Al₂O₃ support via electroless plating technique. This membrane was manufactured according to the procedure developed by Collins and Way.[40] The thickness of the Pd layer was determined to be approximately 10µm using gravimetric method explained by Anzelmo.[41] The ceramic support on which the Pd was deposited can be characterized by an active length of approximately 17 cm and an OD or approximately 10 mm. The total active surface is of the membrane calculated to be approximately 20 cm².

5.2.2 Permeation tests

Before starting the reaction experiments, the system was checked for any possible leaks with helium gas and at room temperature. The experimental setup was pressurized to a pressure of 10 bar and was left under pressure for 2 hours. After two hours no significant pressure drop was observed, and the system found to be leak free.

At this point, the MR system was gradually heated up to 400 °C with a steady heat ramp of approximately 1.5 °C/min under argon gas. An ultra-high temperature heating tape, model STH051-080 was used for this purpose. The voltage for heating was controlled by a Thermolyne-type 45,500 input control. The experimental temperature was monitored via a K-type Omega HH801A thermocouple. The accuracy of the thermocouple over a range of -100 °C to 1372 °C is reported to be ± (0.1% rdg + 1 °C).

After the system reached to 400 °C and the temperature stabilized, the membrane surface was activated by flowing pure hydrogen gas at 400 °C and a trans-membrane pressure of 50 kPa for 2 hours at a constant flow rate of 30 mL/min as explained previously by Kian et al. [34] After activating the MR surface, the permeation tests were conducted with pure

Carbon Capture and Hydrogen Production via MRs

hydrogen, helium, and argon at 400 °C and pressures up to 600 kPa to find the permeance and ideal selectivity of the membrane.

The permeating flux of pure gases were measured using a bubble-flow meter. In order to minimize the human error, every experimental data point represents an average value of 10 measurements. The average error found to be less than 3.9% for all measured points. All the permeation data points reported in this work were collected at least 15 minutes after the trans-membrane pressures were changed to ensure a steady state was achieved. A schematic of the experimental setup is presented in Figure 5-2(a) and an image of the SMR system is shown in Figure 5-2(b).

Carbon Capture and Hydrogen Production via MRs

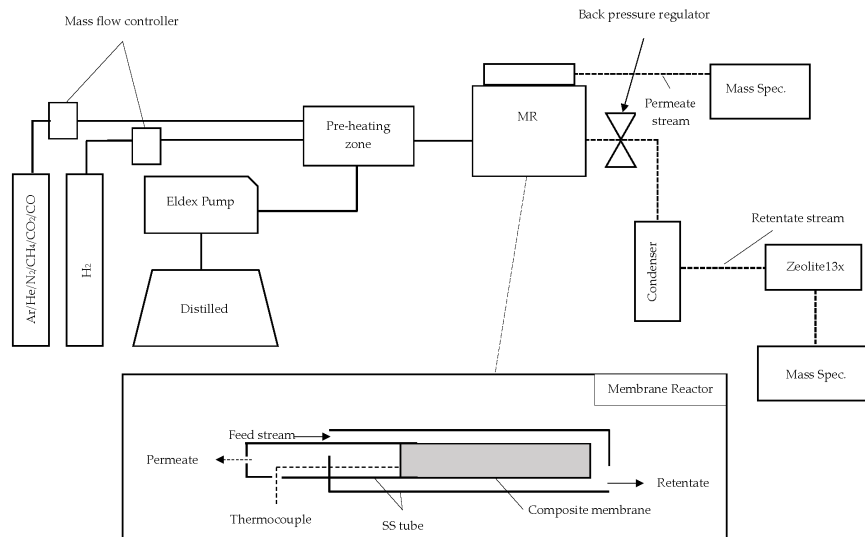


Figure 5-2. Schematic of the experimental setup (a); image of the MR used for SMR studies (b)

5.2.3 SMR reactions

After the conclusion of the permeation tests, the flow of hydrogen to the MR was stopped and argon gas was fed into the system for 2 hours. This was done to ensure that the system is completely depleted of hydrogen gas prior to the SMR reactions which could otherwise lead to erroneous interpretations of methane conversion and hydrogen recovery values.

The lumen side of the MR was filled with 3 grams of commercial grade HiFUEL[®] catalyst which was crushed and refined to 355-500 μm size. The reaction gases, methane and superheated steam, were fed into the lumen side of the MR (retentate side) while the desirable product (hydrogen) was collected on the shell side (permeate side).

Flow rate of methane was controlled using an Aalborg GFC17 mass flow controller (Aalborg Instruments & Controls Inc., Orangeburg, New York, U.S.) while an Eldex Optos 1LMP pump was used to provide deionized water to the reactor. A spiral pre-heating zone was used to ensure that water was completely vaporized, and converted to superheated steam before entering the MR. The water vapor in the retentate side was condensed using a temperature-regulated water bath (Julabo F25-EH) which was set at $-5.0\text{ }^{\circ}\text{C}$. A DRIERITE packed column was used for further dehydration of the retentate stream. The pressure on the retentate side was regulated with an Ashcroft Back Pressure Regulator. The pressure on the retentate side was measured with a Swagelok EN 837-1 pressure gauge.

An Extrel Max-300LG Mass Spectrometer (MS) was used to analyze the composition of dehydrated gaseous streams coming from both retentate and permeate sides. The MS was calibrated using various compositions of hydrogen, methane, carbon dioxide, and carbon monoxide. Argon gas was used as the background/carrier gas. Precision of the MS instrument is reported to be in the order of ppm.

Performance of the MR was investigated using three parameters, namely: methane conversion, hydrogen recovery, and permeate side hydrogen purity which are defined by Eq. 5-6 through Eq. 5-8.

$$X_{CH_4} = \frac{Q_{CH_4}^{IN} - Q_{CH_4}^{OUT}}{Q_{CH_4}^{IN}} \times 100 \quad \text{Eq. 5-6}$$

$$HR = \frac{Q_{H_2}^{Permeate}}{Q_{H_2}^{Permeate} + Q_{H_2}^{Retentate}} \times 100 \quad \text{Eq. 5-7}$$

$$HPP = \frac{Q_{H_2}^{Permeate}}{Q_{Total}^{Permeate}} \times 100 \quad \text{Eq. 5-8}$$

where $Q_{H_2}^{Permeate}$ and $Q_{H_2}^{Retentate}$ are the molar flow rates of hydrogen in the permeate and retentate sides respectively, $Q_{Total}^{Permeate}$ is the molar flow rate of all the gaseous species on the permeate side.

The SMR experiments were performed at 400 °C and various pressures up to 600 kPa. The operating conditions that result in the best performance in terms of methane conversion, hydrogen purity, and hydrogen recovery, were selected as the optimal condition for the next phase of this work, i.e. the SMR with carbon capture.

5.2.4 The use of 13X for capturing CO₂ produced by SMR reaction in the MR

After the conclusion of the SMR reactions and identifying the optimal operating conditions in terms of methane conversion, hydrogen purity, and hydrogen recovery, the retentate stream was completely dehydrated by sending the stream to a cold trap which is held at constant temperature of -5.0 °C. In order to ensure the retentate stream is completely dehydrated, the condensed stream was later passed through a DRIRITE column to adsorb any possible residual water vapor. The retentate stream was sent to the Mass Spectrometer (MS) to analyze for further analysis and to confirm that the stream is devoid of any amount of water. The carbon capture experiments were conducted at the optimal operating conditions using the solid sorbent 13X, as explained in the following sections.

5.2.4.1 Physisorption experiments

Before conducting the carbon capture experiments, the physisorption tests were conducted to figure out the adsorption characteristics of the 13X samples such as average surface area, total pore volume, and average pore diameter, to ensure the calculations in the adsorption phase studies do not violate the continuity equation. The adsorption experiments were performed using the Autosorb iQ analytical system a product of Quantachrome Corporation. Adsorption characterizations of the 13X were investigated using N₂ adsorption at 77.35K and CO₂ adsorption at 273.15K. Apparent surface area was determined using the Brunauer–Emmett–Teller (BET) method, while the pore volume was calculated using the Dubinin–Radushkevich (DR) method.

In order to accurately analyze the surface characteristics of the 13X samples, the porous material needs to be pretreated at elevated temperatures and under vacuum to remove any contaminants such as water vapor or oils. Surface cleaning was performed using the degassing stations. Before starting the calorimetry experiment, the samples were degassed at 623.15K for approximately 5 hours in glass bulbs connected to the vacuum equipment. After sealing the glass bulb and connecting it to the vacuum pump, it was introduced into the calorimetry chamber along with the liquid probe. After reaching to thermal equilibrium, the sample seal was broken, and the sample started interacting with the immersion liquid. The heat evolved during this process was continuously recorded with time.

5.2.4.2 Preparation of 13X

The zeolite 13X used in this experiment were purchased from Sigma-Aldrich. The 13X molecular sieves were used as pellets with an average pellet with an average diameter of 1.6 mm and a MW of 60.08 g/mol. In order to ensure the 13X samples are devoid of any water, the pellets were dried at 393K for 24 hours.

5.2.4.3 Gas sorption experiments

After the conclusion of the SMR reactions at the optimal operating conditions, the dehydrated retentate stream was sent to the MS to analyze its composition and ensure there is no water vapor in the retentate stream. Next, this stream was diverted into the 13X packed column and the amount of carbon dioxide adsorbed onto the zeolite 13X pellets were calculated by applying the material balance principle.

5.2.4.4 Breakthrough experiments

The CO₂ concentration through the packed bed is a function of space and time: $C_{CO_2}=f(x,t)$. The classical method for find the concentration profile of CO₂ as a function of time and space, relies on drawing the appropriate control volume (depending on the geometry of the system can be cartesian, cylindrical, or spherical control volume) and writing the continuity equation over the control volume. This will lead into a partial differential equation, second order in space and first order in time, which can be solved either analytically or numerically depending on the initial and boundary conditions. One useful method that can be employed to study the performance of the packed bed is the “breakthrough curve” studies. The breakthrough curve is used to investigate the dynamic behavior of the absorption process and gives an estimate of when the flow should be stopped, and the sorbent should be regenerated. Wilcox [39] has explained in detail how to calculate the breakthrough time, and fraction of bed that is saturated at breakthrough as presented in Eq. 5-9:

$$\varphi = \frac{2t_b}{t_b + t_{ss}} \quad \text{Eq. 5-9}$$

such that φ is the fraction of the bed volume saturated at breakthrough, t_b is the breakthrough time, and t_{ss} is called the stoichiometric or steady state time and is defined at the time at which CO₂ concentration reaches to equilibrium.

5.2.5 Membrane characterization

In order to characterize the membranes, multiple techniques have been undertaken in this study. As explained in section 2.2, at the beginning of this work and before performing the SMR reaction tests, permeation tests with pure hydrogen and inert gases i.e. helium and argon were conducted to investigate the permeation characteristics of the membrane and the existence of any possible leaks. At the conclusion of the experiments, the material characterization techniques including X-ray diffraction (XRD), scanning electron microscope (SEM) with energy dispersive spectroscopy (EDS). The details of these tests are explained in the following sections.

5.2.5.1 SEM-EDS

At the conclusion of the SMR reactions, the morphology of membrane was studied using SEM instrument. This was used to investigate the possible development of any pinholes or cracks on the Pd surface. Furthermore, EDS technique was used to analyze the elemental composition of the Pd surface. A JEOL JSM-7000F SEM-EDS instrument was used to perform the SEM-EDS analyses. AZtec 3.4 was used to collect and analyze the EDS data.

5.2.5.2 XRD

The XRD tests were performed after the conclusion of the SMR reactions, to investigate the possibility of development of any undesired phases such as palladium oxides. Empyrean diffractometer was used to perform the XRD tests, and the results were analyzed using Highscore Plus software (Version 4.7, PANalytical, Almelo, The Netherlands). In this study The Cu $K\alpha$ radiation ($\lambda = 1.540598 \text{ \AA}$) was used and Cr tubes were used as anode materials. The parameters used in the XRD analysis were the following:

Bragg angles $2\theta = 50\text{--}150^\circ$, step size = 0.033° , and time per step = 60.325 ms.

5.2.6 Materials

The materials used for this study are ultra-high purity (UHP) hydrogen and helium (99.999% purity), industrial grade argon (99.985% purity), and industrial grade methane (99.97% purity). Deionized water has been used to make superheated steam required for the SMR reaction. Commercial grade zeolite 13X pellets with an average pellet diameter of 1.6 mm and a MW of 60.08 g/mol purchased from Sigma-Aldrich were used for the CO₂ separation capture studies. The catalyst used in this study is the commercial Hifuel R110 provided by Johnson Matthey.

5.3 Results and Discussion

5.3.1 Hydrogen permeation

As explained earlier, the permeation tests with pure gases namely, hydrogen, helium, and argon were conducted to characterize the membrane and find its perm-selectivity properties such as its permeance, ideal selectivity, and exponent n as indicated in Eq. 5-5. In order to find n , the permeation fluxes of hydrogen at various trans-membrane pressures were measured at 400 °C. These permeating fluxes were plotted on a Cartesian coordinate against the driving force, $(p^n_{\text{retentate}} - p^n_{\text{permeate}})$ for various values of n changing between 0.5-1.0.

The dimensions of the membrane that was used for these SMR experiments are listed in Table 5-1.

Table 5-1. Dimensions of the MR used for SMR reactions

Dimension	Value
Outer diameter, OD [mm]	10
Active length, L_{active} [mm]	172
Thickness, δ [μm]	9.8

The active surface area was calculated to be 54.04 cm², according to Eq. 5-10:

$$A_{\text{active}} = \pi \cdot OD \cdot L_{\text{active}} \quad \text{Eq. 5-10}$$

In order to measure the permeating flux, the volumetric flow rate was measured as explained in section 2.2, as the average value of 10 data points using a bubble flow meter. The volumetric flow rate was converted into molar flux, assuming pure gases behave as ideal gases at ambient pressure ($p=101,325$ Pa) and experimental temperature ($T=673.15\text{K}$), according to Eq. 5-11:

$$J_{H_2} = \frac{pQ}{RTA_{active}}$$

Eq. 5-11

Where p is the total pressure, Q is the volumetric flow rate, R is the universal gas constant, T is the absolute temperature, A_{active} is the active surface area of the MR, and J_{H_2} is the molar permeating flux of hydrogen reported in $[\text{mol}\cdot\text{s}^{-1}\cdot\text{m}^{-2}]$.

Hydrogen permeation versus trans-membrane pressures are presented in Figure 5-3. As can be seen from this plot, the linear regression with the value of $n=0.5$ gives the highest R^2 value and is chosen as the appropriate n exponent for future calculations. It should be mentioned that a value of $n=0.5$ is an indication that the hydrogen transport through the palladium layer is governed by solution-diffusion mechanism.[34]

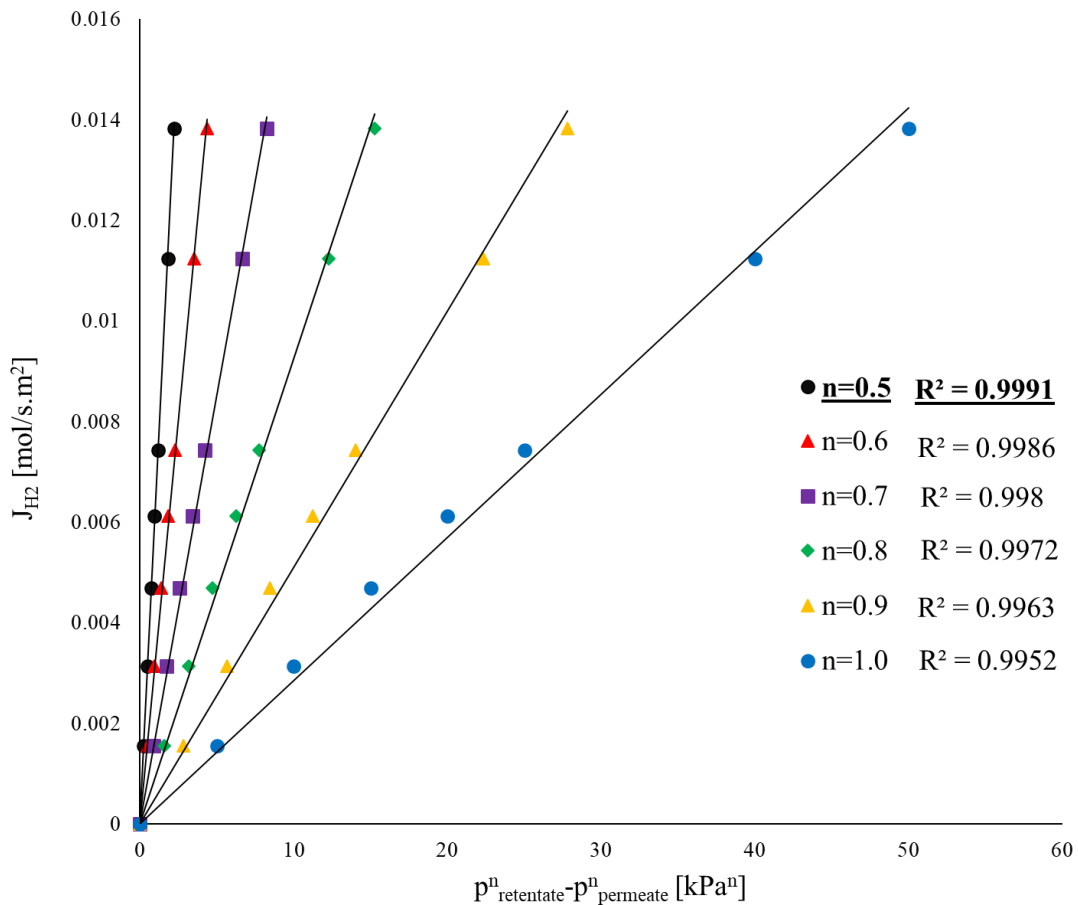


Figure 5-3. Permeation flux of H_2 vs. trans-membrane pressure at 400°C and various values of n

Before performing the SMR reaction, helium and argon gases were used to investigate the possible presence of any defects or pinholes in the membrane. As explained by Kian et al., the main transport mechanism for He and Ar gases through the MR are Knudsen diffusion and Poiseuille flow while the hydrogen transport through the MR is governed by solution-diffusion mechanism as indicated earlier. Hence, upon existence of any imperfections or pinholes on the membrane surface, He and Ar atoms are going to permeate through these imperfections. The permeating fluxes of these inert gases increase as the trans-membrane pressure increases.[34] To investigate this matter, Ar and He were used at trans-membrane pressures ranging from 5-500kPa and 400°C and the ideal selectivities were calculated according to Eq. 5-12:

$$\alpha_{H_2} = \frac{J_{H_2}}{J_i} \quad \text{Eq. 5-12}$$

Where J_{H_2} is the hydrogen permeating flux and J_i is the permeating flux of component i , either He or Ar. the ideal selectivity of hydrogen with respect to both helium and argon at the aforementioned operating pressures were found to be infinite, meaning at the operating trans-membrane pressures no detectable amount of helium or argon permeated thorough the MR which reaffirms that membrane was fabricated flawlessly and no pinholes or imperfections existed on the MR surface prior to starting the SMR experiments.

5.3.2 Steam Methane Reforming Reaction

The optimal operating conditions have been chosen as the conditions of pressure and temperature at which the hydrogen purity, hydrogen recovery, and methane conversion are the greatest. Since all the reaction tests were conducted at constant temperature, the pressure at which these variables are maximized is considered as the “optimal operating pressure” to conduct the carbon capture experiments at.

In order to find such pressure, the SMR reactions were performed at various operating pressures ranging from 1 to 15 bar and methane conversion, hydrogen recovery, and hydrogen purity, were calculated according to Eq. 5-6 through Eq. 5-8, respectively.

5.3.2.1 Methane conversion

Methane conversion is the key parameter that determines the efficiency of the SMR process. Methane conversion, X_{CH_4} , was calculated according to Eq. 5-6. As it is presented in Figure 5-4, the values of methane conversion increase steadily as the reaction pressure increases. As indicated in this figure, by increasing the reaction pressure from 100kPa to 400kPa, methane conversion increases by more than 80%. According to Eq. 5-1 and based on the Le Chatelier's principle, by increasing the operating pressure it is expected for the SMR reaction to shift to the left-hand-side of Eq. 5-1 and hence toward lower methane conversion values. This argument could be valid for a conventional reactor (CR), however, in a MR, higher operating pressures will create higher driving force which in turn leads to more hydrogen to permeate from the retentate side to the permeate side. The constant removal of hydrogen from the reaction bed will move the reaction to the right-hand-side of Eq. 5-1.[18] This constant removal of hydrogen more than offsets the shift effects due to higher pressure and the overall influence of increasing the operating pressure is higher methane conversion and hydrogen yield which is explained next.

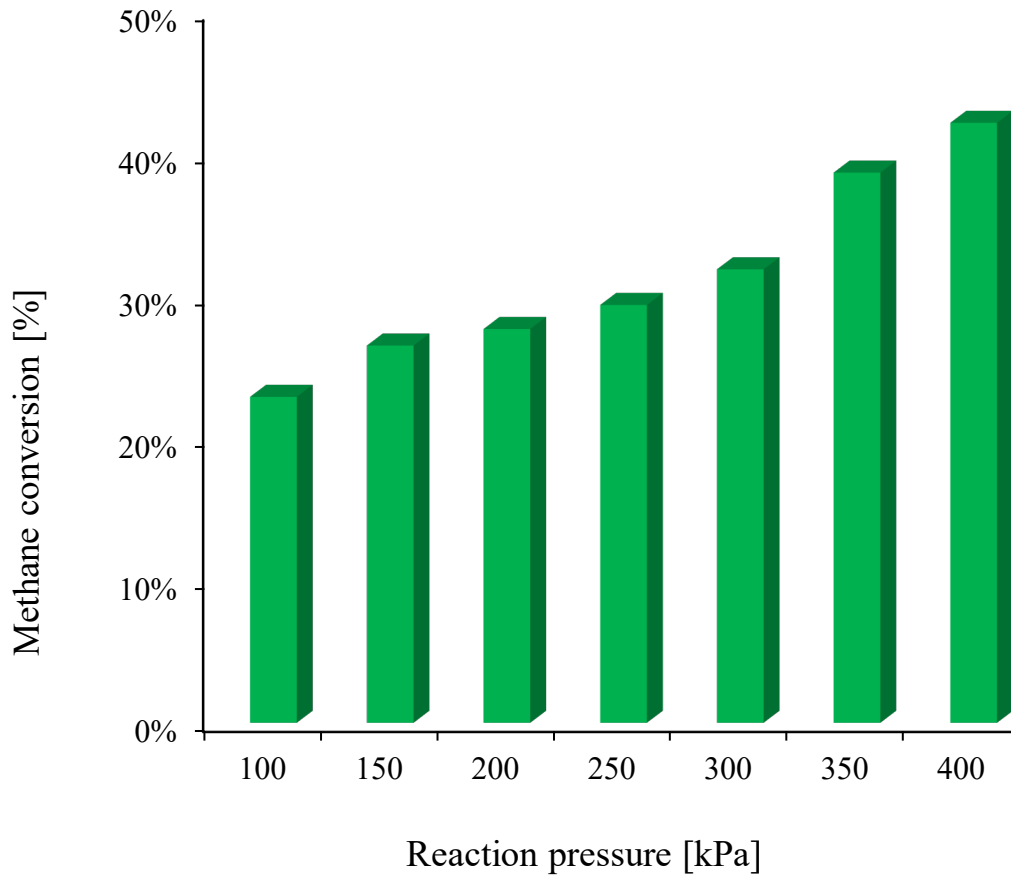


Figure 5-4. Effect of the reaction pressure on methane conversion

5.3.2.2 Hydrogen recovery

Hydrogen recovery is the other key factor in determining the optimal operating conditions of the MR. As explained earlier and indicated by Eq. 5-7, hydrogen recovery is the ratio of hydrogen collected in the permeate side over the total produced hydrogen. The values of HR versus reaction pressure are presented in Figure 5-5. As can be seen in this figure, HR shows a very similar behavior to that of methane conversion when pressure increases however, the influence of pressure on hydrogen recovery is even more pronounced due to two reasons. First, as explained earlier, increasing the reaction pressure will increase the methane conversion which means more hydrogen can be produced at higher pressures. Second, and more importantly, at higher pressures, more hydrogen permeates through the

MR (from retentate to the permeate side) which means more hydrogen can be potentially collected. One can see that the hydrogen recovery increases from almost zero percent at atmospheric pressure to more than 40% at 400kPa.

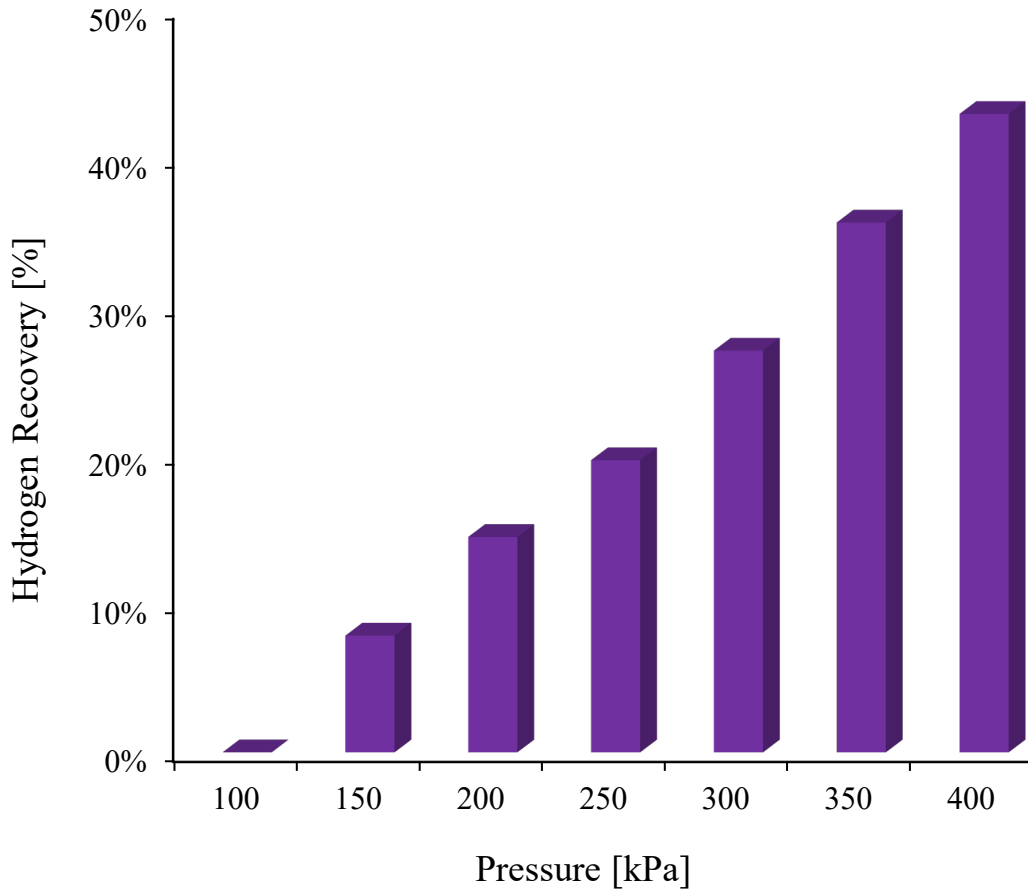


Figure 5-5. Effect of the reaction pressure on hydrogen recovery

5.3.2.3 Hydrogen purity

The permeate side hydrogen purity is of significant importance, specifically for some industrial applications such as ammonia synthesis, or for supplying fuel cells, e.g., proton exchange membrane fuel cells (PEMFCs) and hydrogen fuel cell vehicles (HFCVs) where ultrahigh purities (99.99+%) hydrogen is required.[1] Hydrogen purity was calculated according to Eq. 5-8 as described earlier. The permeate stream was constantly monitored by the MS and no evidence of any reaction gases was detected by the MS except for

hydrogen. Hence, the hydrogen purity on the permeate side was calculated to be 100% at all pressures consistently. It is worth mentioning that at very high operating pressures (>15 bar) due to the failure of the MR and creation of cracks in the membrane structure, the hydrogen purity abruptly drops to very small values. Therefore, constant monitoring of hydrogen purity could be used as a good indicator of the integrity of the MR in development or industrial applications.

5.3.2.4 Adsorption analysis experiments

Apparent surface area was determined using the BET method as following:

$$\frac{1}{W \left(\frac{p}{p_0} - 1 \right)} = \frac{1}{W_m C} + \frac{C-1}{W_m C} \left(\frac{p}{p_0} \right) \quad \text{Eq. 5-13}$$

Where W is the mass of adsorbed gas per gram of sample at a relative pressure of p/p₀, W_m is the mass of the gas adsorbed per gram of sample for complete monolayer coverage of the adsorbent surface, and C is the BET constant which is expressed as following:

$$C = \frac{p_{c1} v_1}{p_{c2} v_2} \text{Exp} \left((E_1 - E_L) / RT \right) \quad \text{Eq. 5-14}$$

Where p_{c1} and p_{c2} are the probability of fluid particles condensing upon collision with layer 1 and layer 2, respectively, v₁ and v₂ are the vibrational frequencies of the adsorbate normal to layer 1 and layer 2 respectively, E₁ is the activation energy barrier required to overcome the adsorption energy on layer 1, and E_L is the energy associated with condensation to a liquid phase.[39]

A plot of 1/W(p/p₀ - 1) vs. p/p₀ will show a linear behavior at relative pressures between 0.05 to 0.35. Using the slope (s) and intercept (i) of this line, one can calculate the value of W_m and consequently the apparent surface area (S). is required to calculate the surface area as following:

$$s = \frac{C-1}{W_m C} \quad \text{Eq. 5-15}$$

$$i = \frac{1}{W_m C} \quad \text{Eq. 5-16}$$

$$W_m = \frac{1}{s + i} \quad \text{Eq. 5-17}$$

$$S = \frac{W_m N A_{cs}}{MW} \quad \text{Eq. 5-18}$$

Where N is the Avogadro's Number (6.023×10^{23} molecules/mole), A_{cs} is the molecular cross-sectional area of the adsorbate molecules and MW is the molecular weight of the adsorbate molecules. The values of A_{cs} for nitrogen and carbon dioxide molecules are 16.200 \AA^2 and 21.000 \AA^2 , respectively. The BET parameters used to calculate the adsorption characteristics of the 13X samples along with the surface area obtained with CO_2 and N_2 are presented listed in Table 5-2. The BET adsorption data obtained using CO_2 and N_2 are presented in Table 5-3 and Table 5-4, respectively. The adsorption plots of each adsorbates are presented in Figure 5-6.

Carbon Capture and Hydrogen Production via MRs

Table 5-2. Parameters used in BET method calculations

Parameter	CO ₂	N ₂
Sample Weight [g]	0.3255	0.3242
Final Outgas Temp.[°C]	350	350
Non-ideality [1/Torr]	9.10E-06	6.58E-05
Bath temp. [K]	273.15	77.35
Molecular weight [g/mol]	44.01	28.013
Cross Section [Å ²]	21.000	16.200
Liquid Density [g/cc]	0.927	0.808
Slope [1/g]	6.824 1	6.921
Intercept [1/g]	-5.967e-02	-1.476e-01
Correlation Coefficient, r	0.997535	0.997045
C constant	-113.367	-45.888
Surface area [m ² /g]	424.778	514.133
Pore volume [cc/g]	NA ^{xiii}	0.35
Average half pore width [Å]	NA	13.59

Table 5-3. BET adsorption data for CO₂ at 273.15K

Relative Pressure P/Po	Volume @ STP cc/g	1/[W((Po/P)-1)] 1/g
4.91E-02	81.2683	3.24E-01
7.86E-02	88.691	4.90E-01
9.98E-02	92.0651	6.13E-01
1.54E-01	98.1681	9.43E-01
1.99E-01	101.5904	1.25E+00
2.52E-01	104.5575	1.64E+00
3.04E-01	106.8767	2.08E+00

Table 5-4. BET adsorption data for N₂ at 77.35K

Relative Pressure P/Po	Volume @ STP cc/g	1/[W((Po/P)-1)] 1/g
5.04E-02	164.7715	2.58E-01
8.09E-02	166.2637	4.24E-01
9.96E-02	166.8915	5.30E-01
1.49E-01	168.2864	8.32E-01
2.00E-01	169.5002	1.18E+00
2.49E-01	170.471	1.56E+00
3.00E-01	171.4338	2.00E+00

xiii The BET method cannot be applied to calculate the pore volume when CO₂ is used as an adsorbate, as CO₂ cannot exist in liquid form at atmospheric pressure regardless of its temperature.

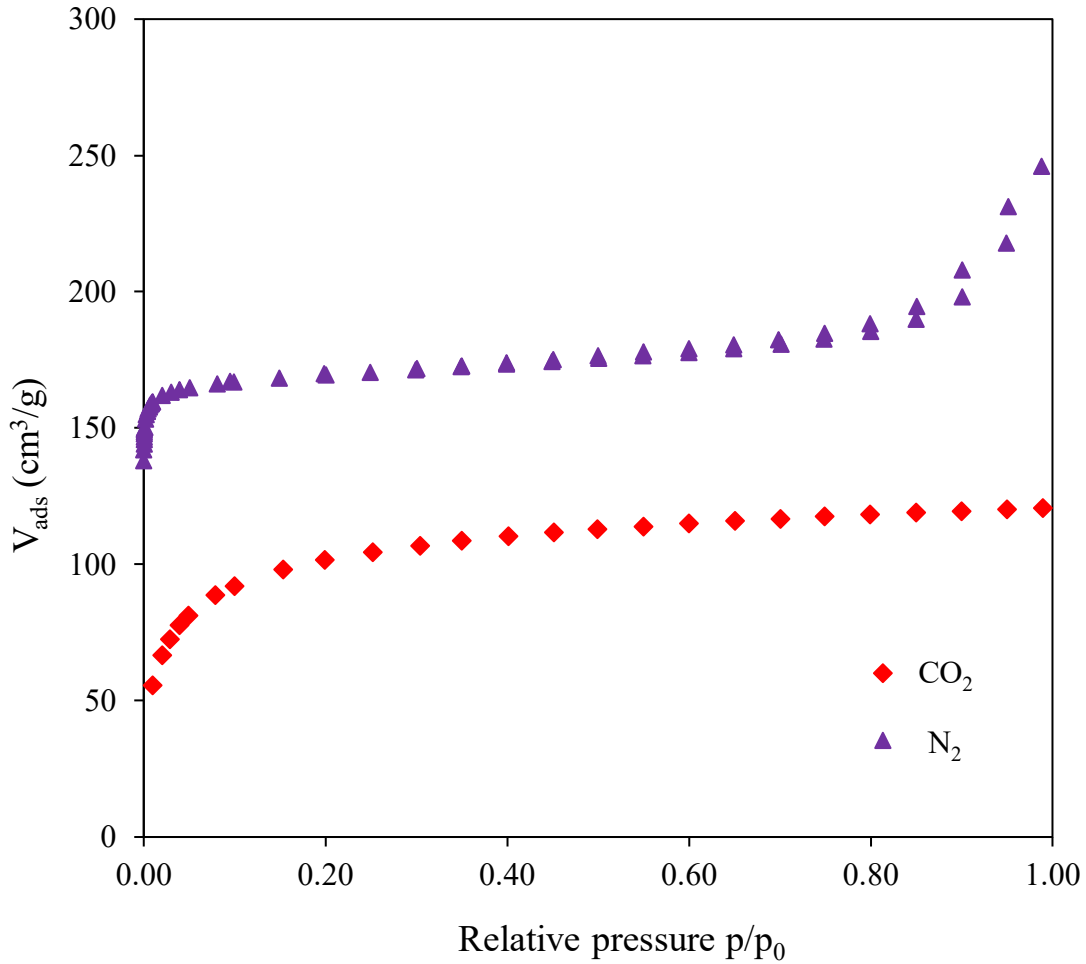


Figure 5-6. Adsorption isotherms for CO_2 (at 273.15K) and N_2 (at 77.35K)

The total pore volume can be calculated assuming the pores were completely filled with the liquid adsorbate at relative pressures close to unity. Since the pores that are not filled at relative pressures below unity do not contribute significantly to the total pore volume, this is a reliable assumption. Hence, the volume of adsorbate can be converted to the volume of liquid filling the pore space using the following formula:

$$V_{pore} = V_{liq} = nV_m \quad \text{Eq. 5-19}$$

Where n is the number of the adsorbed moles of the adsorbate at relative pressure close to unity (values of p/p_0 equal or greater than 0.99 are satisfactory), and V_m is the molar volume

of the adsorbate in liquid phase. Number of the adsorbed moles of the adsorbate, n , can be obtained from the following equation:

$$n = \frac{m_{ad}}{MW} = \frac{\rho V_{ad}}{MW} \quad \text{Eq. 5-20}$$

Where MW is the molecular weight of the gas, m_{ad} is the mass of gas molecules adsorbed, ρ is the density of the adsorbed gas, and V_{ads} is the volume of the gas adsorbed at relative pressure close to unity.

Combining Eq. 5-19 and Eq. 5-20, the pore volume can be obtained as following:

$$V_{pore} = V_{liq} = \frac{\rho V_{ad}}{MW} V_m \quad \text{Eq. 5-21}$$

Assuming the pores as perfect cylinders, the average pore diameter can be calculated as following:

$$D_{pore} = \frac{4V_{pore}}{S} = \frac{4\rho V_{ad}}{MW} V_m \quad \text{Eq. 5-22}$$

However, since the BET model does not apply to the micropores, and suffers from numerous shortcomings when dealing with microporous materials such as the assumption that the adsorbent should have a homogenous surface, molecules can be adsorbed onto the second higher layers before filling up the lower layers, and lack of lateral interaction between the molecules adsorbed onto the same layer which will make the molar adsorption energy within that layer a constant value. In addition, the negative values that are found for the BET C-constant are physically meaningless which makes it even more complicated to interpret accurately.[42] Due to these shortcomings, the Dubinin–Radushkevich (DR) method has been chosen to calculate the pore volume and average pore diameter as shown in Eq. 5-23.

$$\frac{W}{W_0} = \exp \left[- \left(\frac{RT \ln(p/p_0)}{\beta E_0} \right)^2 \right] \quad \text{Eq. 5-23}$$

Where W is the adsorbed volume, W_0 is the micropore volume, R is the universal gas constant, T is the absolute temperature, p is the pressure, p_0 is the saturation pressure, β is the affinity coefficient, and E_0 is the characteristic energy of a standard adsorbate with respect to the given solid.

According to the DR method, a plot of the logarithm of the adsorbed volume of the adsorbate, $\log(V_{ad})$, versus the squared logarithm of relative pressures, $\log^2(p_0/p)$, would give a straight line from which the micropore volume and average micropore diameter can be calculated. The details of the DR method are explained by Nguyen et al. [43]

The DR parameters used to calculate the adsorption characteristics of the 13X samples along with the micropore characteristics obtained with CO_2 and N_2 are presented in Table 5-5.

Table 5-5. Parameters used in DR method calculations

Parameter	CO_2	N_2
Sample Weight [g]	0.3255	0.3242
Final Outgas Temp.[°C]	350	350
Non-ideality [1/Torr]	9.10E-06	6.58E-05
Bath temp. [K]	273.15	77.35
Affinity coefficient (β)	0.3300	0.3300
Molecular weight	44.01	28.013
Cross Section [\AA^2]	21.000	16.200
Liquid Density [g/cc]	0.927	0.808
Critical Temperature [K]	304.100	126.200
Critical Pressure [atm]	72.900	33.500
DR. Exponent (n)	2.0000	2.0000
Slope	-7.29E-02	-5.47E-03
Intercept	6.93E-02	6.82E-02
Correlation Coefficient	1.00E+00	0.9989
Average half pore width [\AA]	3.360	3.250
Adsorption energy [kJ/mol]	38.689	40.005
Micropore volume [cc/g]	0.230	0.260
Micropore surface area [m^2/g]	612.047	732.376

Carbon Capture and Hydrogen Production via MRs

The DR adsorption data obtained using CO₂ and N₂ and CO₂ are presented in Table 5-6 and Table 5-7, respectively and the adsorption plots of each adsorbate are presented in Figure 5-7.

Table 5-6. DR adsorption data for CO₂ at 273.15 K

Log ² (P/Po)	Weight Adsorbed (g)
3.998595E+00	3.5613E-02
2.885655E+00	4.2627E-02
2.373668E+00	4.6299E-02
1.974243E+00	4.9587E-02
1.712287E+00	5.1941E-02
1.219908E+00	5.6685E-02
1.001582E+00	5.8841E-02

Table 5-7. DR adsorption data for N₂ at 77.35 K

Log ² (P/Po)	Weight Adsorbed (g)
1.60E+01	5.59E-02
1.36E+01	5.75E-02
1.23E+01	5.84E-02
1.15E+01	5.90E-02
1.09E+01	5.95E-02
1.04E+01	5.99E-02
9.87E+00	6.02E-02
9.54E+00	6.05E-02
9.26E+00	6.07E-02
8.97E+00	6.09E-02
7.23E+00	6.21E-02
6.35E+00	6.28E-02
5.74E+00	6.33E-02
5.28E+00	6.37E-02
4.92E+00	6.40E-02
4.64E+00	6.42E-02
4.37E+00	6.44E-02
4.18E+00	6.46E-02
3.99E+00	6.47E-02
2.86E+00	6.56E-02
2.32E+00	6.61E-02
1.96E+00	6.65E-02
1.68E+00	6.68E-02
1.19E+00	6.74E-02
1.00E+00	6.76E-02
6.84E-01	6.82E-02

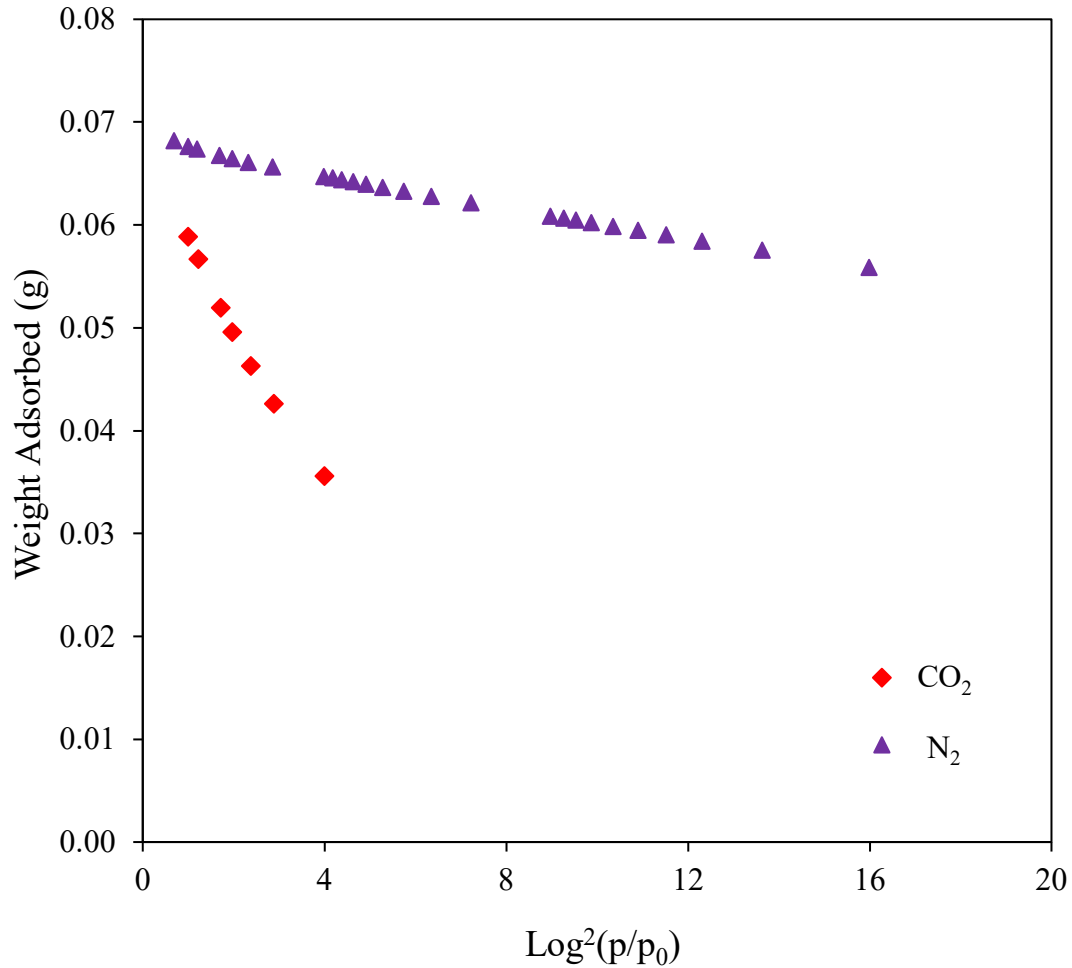


Figure 5-7. DR adsorption isotherms for CO₂ (at 273.15K) and N₂ (at 77.35K)

5.3.3 Breakthrough analysis

In order to perform the breakthrough studies, the dehydrated retentate stream was sent to the sorbent packed bed and the effluent concentration was continuously measured via the MS. The stream that was sent to the MS was mainly composed of CO₂ diluted with argon as the carrier gas. The CO₂ adsorption capacity of the bed can be calculated using the following formula as described by Qasem et al. [44]:

$$q_{CO_2} = \frac{\left(\frac{y_{CO_2} \cdot Q_F \cdot t_{ss} \cdot P_s}{RT_s} - \frac{y_{CO_2} \cdot V \cdot \epsilon \cdot P_{actual}}{RT_{actual}} \right)}{m} \quad \text{Eq. 5-24}$$

Where y_{CO_2} is the mole fraction of carbon dioxide in the retentate stream, Q_F is the volumetric flow rate of the retentate stream at standard condition, V is the bed volume, P_s is the standard pressure, T_s is the standard temperature, P is the actual pressure, T is the actual temperature, R is the universal gas constant, ϵ is the bed porosity, m is the mass of the adsorbent, and t_{ss} is the stoichiometric time which can be calculated from the breakthrough curve using the following integral:

$$t_{ss} = \int_0^{\infty} \left(1 - \frac{c(t)}{c_0} \right) dt \quad \text{Eq. 5-25}$$

It should be noted that the product of porosity and bed volume ($\epsilon \times V$) is equal to micropore volume which was obtained during the adsorption experiments and is calculated using the DR method and is reported in Table 5-5. The breakthrough curve for CO₂ adsorption is presented in Figure 5-8. As it is indicated on this plot, the time at which the outlet concentration ratio (C/C_0) is equal to 5% is considered as the breakthrough time (t_b) and is found to be approximately 30 minutes. The stoichiometric time has been calculated using the numerical integration techniques. Using trapezoidal method, the stoichiometric time is found to be approximately 44 minutes. Under standard conditions of $T=298K$ and $p=101,325$ Pa, and at the operating conditions of $T=673K$ and $p=405.3$ kPa, the CO₂ capture capacity of the packed bed is found to be 5.96 mmole CO₂ per gram of 13X (or 262.25 mg CO₂ per gram 13X). This number may be used as a reference number when designing the carbon capture systems.

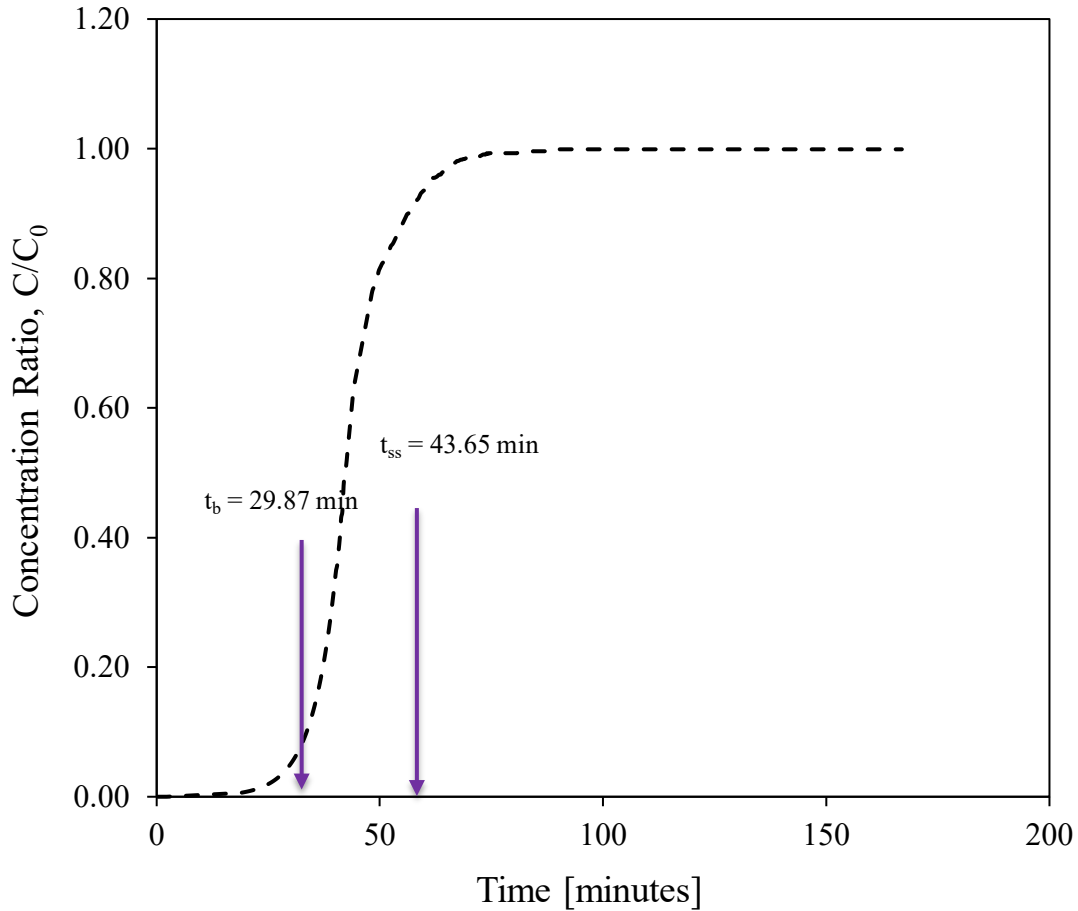


Figure 5-8. breakthrough curve for CO₂ adsorption on 13X at atmospheric pressure and 298.15K

As explained earlier, the fraction of bed volume saturated at breakthrough (ϕ) can be calculated using Eq. 5-9, and the value of ϕ is found to be 81%. This means that at breakthrough time, and only after 30 minutes, more than 80% of the bed volume is saturated with CO₂. This parameter is of critical importance in designing carbon capture systems and should be studied and determined accurately in order to have a better understanding of the time when the sorbent bed needs to be regenerated.

Once, the breakthrough and the steady state times are calculated, one can simply calculate the carbon capture capacity of the 13X packed bed using material balance as explained by Eq. 5-24.

5.3.4 Membrane integrity and characterization

After the conclusion of the SMR reaction, the MR was taken out of the membrane modules and characterization tests, namely XRD and SEM were conducted. An image of the MR at the end of the SMR experiments is presented in Figure 5-9. As it can be seen in this figure, one end of the MR has been discolored and turned into “lustrous green” while the other end of the MR remained intact. This discoloration is a good indication that the palladium layer is severely oxidized in one end and an evidence that PdO is formed on the surface of the Pd membrane.[42] This significant change was further investigated using the analytical characterization techniques.

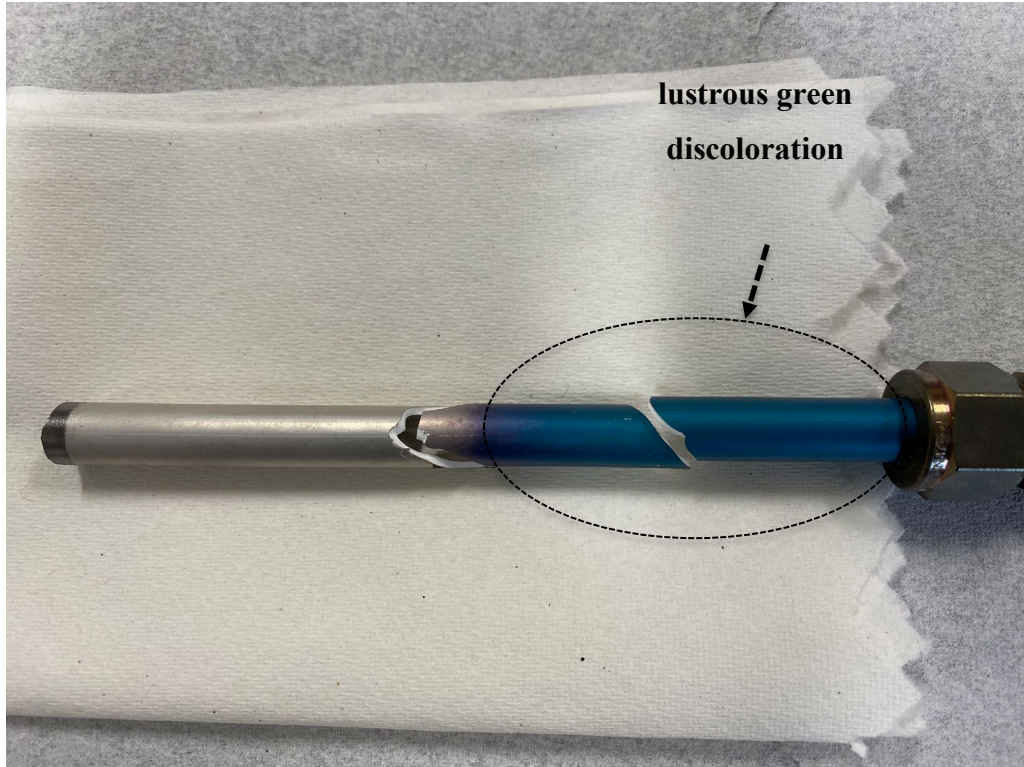


Figure 5-9. MR Pd-13 after the conclusion of the SMR reaction

5.3.4.1 SEM-EDS analysis

Surface morphology was studied using the SEM-EDS technique to evaluate the chemical interactions between the reaction gases and surface of the Pd membrane. Furthermore, the development of pinholes was scrutinized. The SEM images of an intact membrane, which had not gone through the SMR reaction, along with the images of the membrane that was used to perform the SMR reactions are presented in Figure 5-10 and Figure 5-11. As it can be seen in Figure 5-10, the surface of the intact membrane is very uniform with some sporadic cauliflower-like structures appearing on the surface which is an indication of Pd particle sintering on the ceramic support.[45,46] However, no evidence of pinholes was observed during the SEM analyses. The SEM images, along with the ideal selectivity results are good indicators that the electroless plating process was optimal and the sintering of the Pd particles on the alumina support was ideal.

However, after going through the SMR reactions, as can be seen in Figure 5-11, a high density of pinholes was observed. These pinholes were spread all over the membrane surface and their diameter could reach to as large as 1 micron. One reason for the existence of pinholes on the surface of the MR could be the incoherent sintering of Pd clusters or Pd crystallites at temperatures between 400-450 °C as proposed by Guazzone and Ma.[47] However, given the fact that no evidence of pinholes was observed on the surface of the intact membrane, along with the infinite ideal selectivity values obtained during the permeation tests, the authors believe the formation of pinholes should be attributed to numerous cycles of heating and cooling that the membrane had gone through. In addition, the adverse effects of some gaseous components such as CO, could be another major reason for the development of these pinholes as proposed by Kian et al.[34] It should be noted that the intact membrane used in this study is not the same membrane used in the SMR reactions however, it is one of the 14 membrane reactors that were fabricated in the same batch and is a very good representative of the initial conditions of the MR used to perform the reactions.

Carbon Capture and Hydrogen Production via MRs

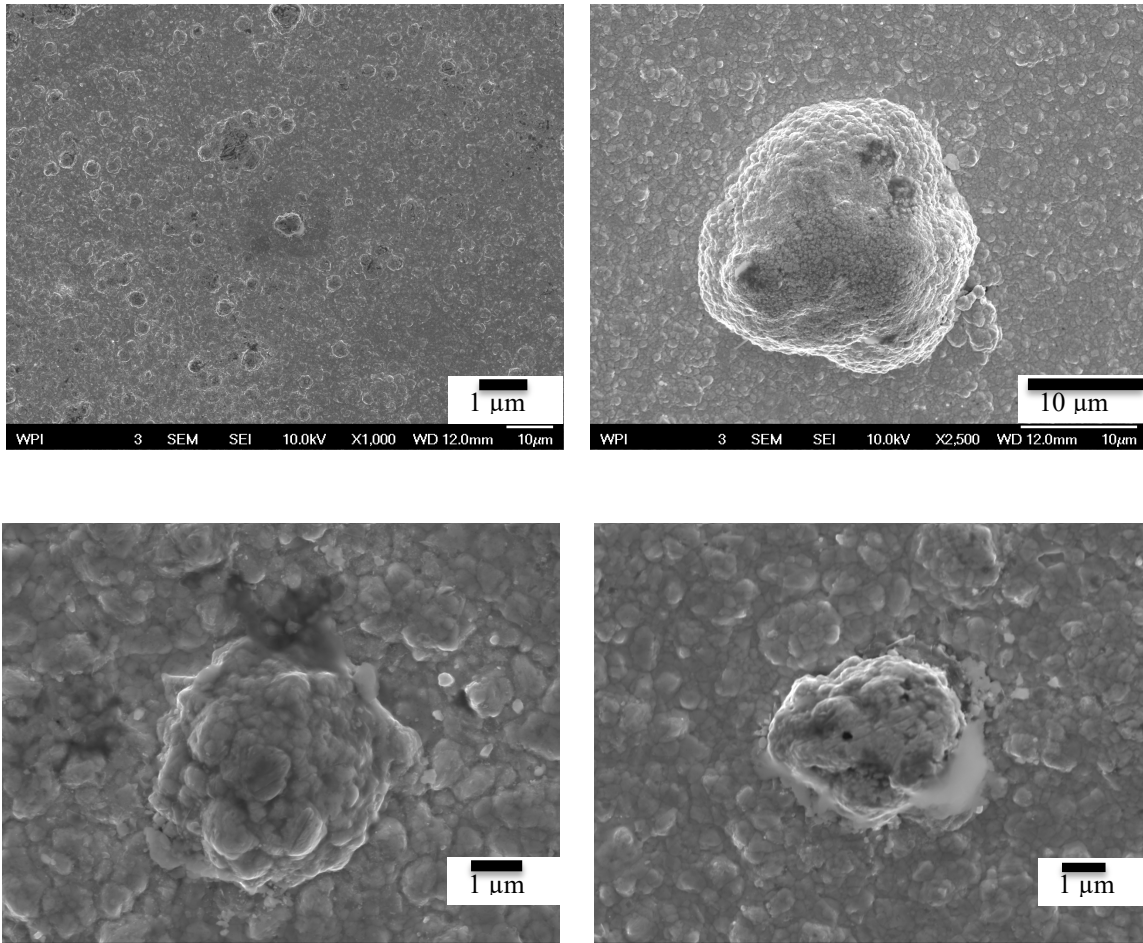


Figure 5-10. SEM images of the intact membrane MR that has not been exposed to SMR reactions

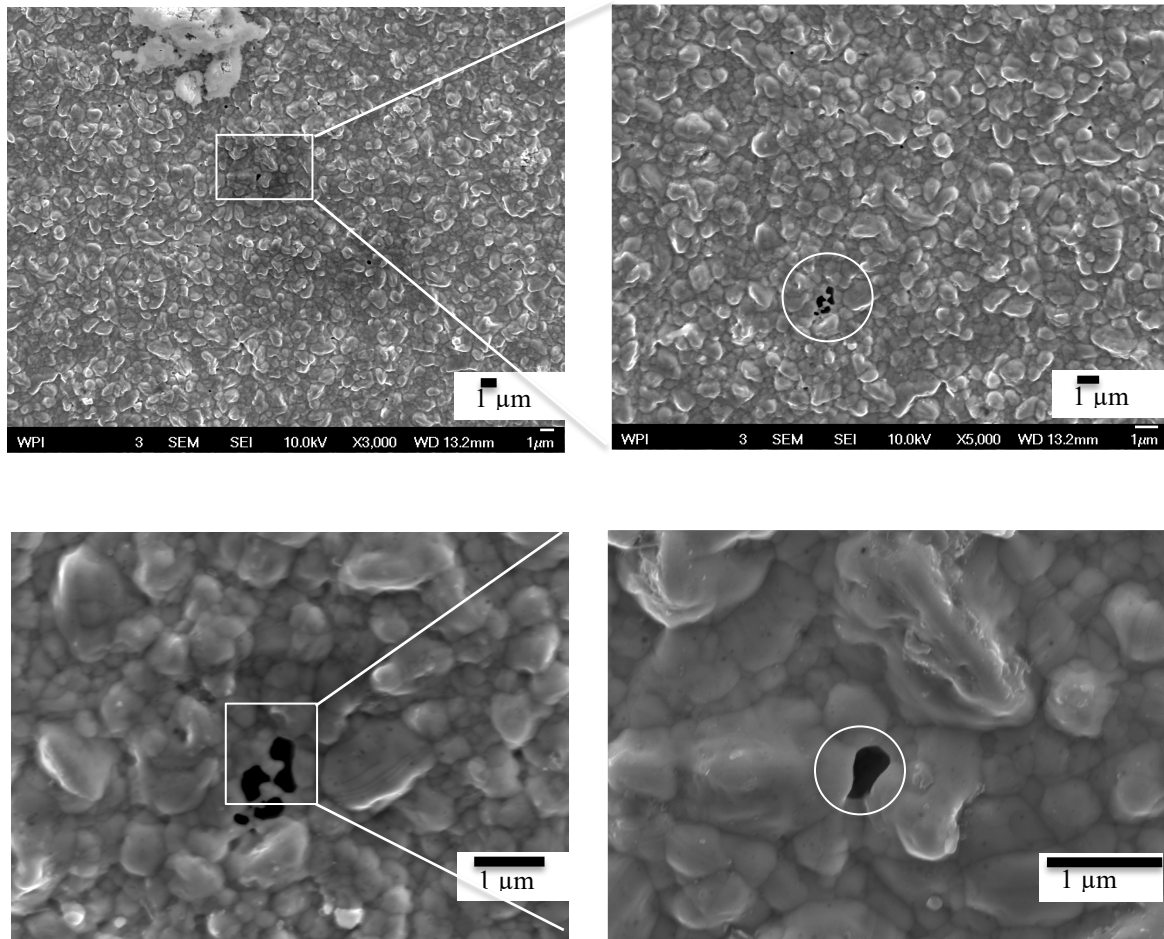


Figure 5-11. SEM images of the MR after the conclusion of the SMR reaction

The EDS analyses were employed to study the surface compositions of both intact and used membranes. In total, 13 spectrums were taken from both intact and used samples one of which was discarded as it did not meet the expected quality of this work. The EDS energy peaks along with the elements identified are listed in and graphically presented in Table 5-8.

Table 5-8. EDS peaks and compositions for intact and used membranes

Intact Membrane		Used Membrane	
EDS Peak [keV]	Element	EDS Peak [keV]	Element
0.284	Pd	0.284	Pd
2.503	Pd	0.525	O
2.66	Pd	2.503	Pd
2.839	Pd	2.66	Pd
2.99	Pd	2.839	Pd
3.553	Pd	2.99	Pd
		3.553	Pd

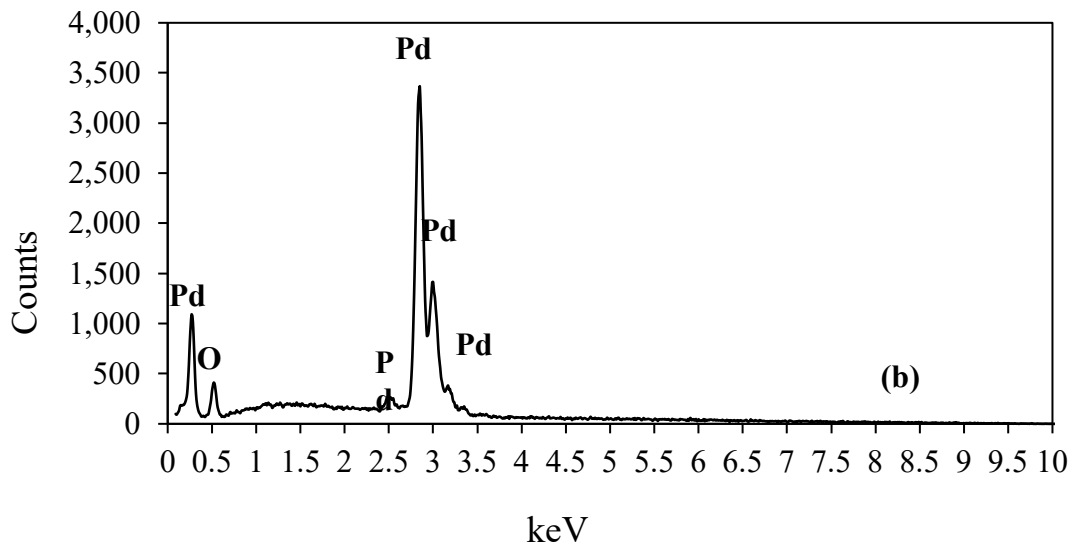
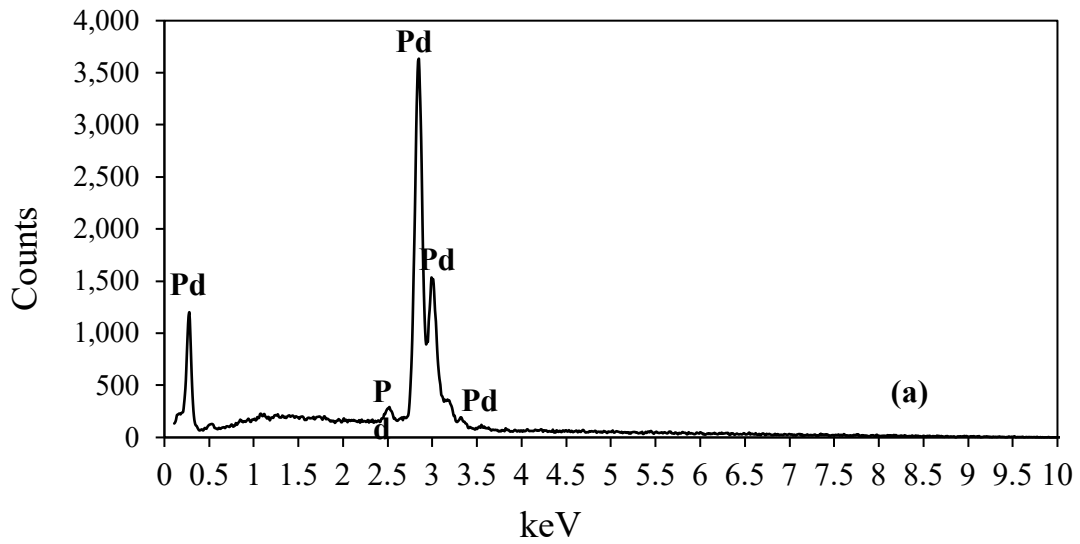


Figure 5-12. EDS analysis of the a) intact and b) used MRs

The EDS analyses show only Pd peaks for the unused membrane while some oxygen peaks were detected in the EDS results of the used membrane. The EDS analysis presented in Figure 5-12(b) belongs to the green color part of the MR which can further confirm the formation of PdO on the membrane surface.

5.3.4.2 XRD analysis

The XRD analysis is based on the famous Bragg's law which is presented by Eq. 5-26:

$$\lambda = 2d \sin(\theta) \quad \text{Eq. 5-26}$$

Where λ is the X-ray wavelength, d is the interplane spacing, and θ is the glancing angle. For a cubic crystalline system, the following relationship can be used to find the appropriate Miller indices of crystallographic planes:

$$d_{hkl} = \frac{a}{\sqrt{h^2 + k^2 + l^2}} \quad \text{Eq. 5-27}$$

Where, a is the lattice spacing (or unit cell dimension) of the cubic crystals and h , k , and l are the Miller indices of the Bragg plane. The unit cell dimension for a cubic crystal, can be simply obtained from the following geometrical relationship:

$$a = 2\sqrt{2}r \quad \text{Eq. 5-28}$$

Where r is the atomic radius which is 0.461 nm for palladium.

Combining Eq. 5-26 through Eq. 5-28, one can obtain the Miller indices from XRD analysis using the following formula:

$$d_{hkl} = \frac{\lambda}{2 \sin(\theta)} = \frac{2\sqrt{2}r}{\sqrt{h^2 + k^2 + l^2}} \quad \text{Eq. 5-29}$$

The major peaks along with the Miller indices for the MR are reported in Table 5-9.

Table 5-9. XRD analysis of the Pd-based MR

2θ (°)	d (°Å)	d^{lit} (°Å)	Rel. Int. (%)	h	k	l
Pd Membrane						
40.1307	2.24703	2.24439	100	1	1	1
46.7137	1.94457	1.94370	16.81	2	0	0
68.1775	1.37436	1.37440	16.55	2	2	0
82.2012	1.17177	1.17210	9.46	3	1	1
86.1299	1.12810	1.12901	4.26	2	2	2

The XRD plots for the intact Pd membrane and the oxidized membrane are presented in Figure 5-13 and the major peaks along with their Miller indices have been identified. As it has been discussed in detail in the previous works, the slight expansion of the lattice structure of the Pd crystallites can be explained by diffusion of hydrogen through the bulk of the membrane.[34] There has been a slight shift in the location of the Pd peaks which could result from the existence of pinholes and internal stresses. The PdO peaks cannot be clearly observed in Figure 5-13(a), and hence, the peaks of the used membrane were re-plotted again in Figure 5-13(b). Although strong evidence of palladium oxide was observed in both the SEM studies and by change of color of the MR, the XRD results show no significant indication of oxidation. This could lead the authors to conclude that the oxidation of palladium was merely limited to the surface of the MR and did not penetrate all the way to the bulk of the palladium layer. This conclusion could be reaffirmed by performing glancing incidence XRD studies.

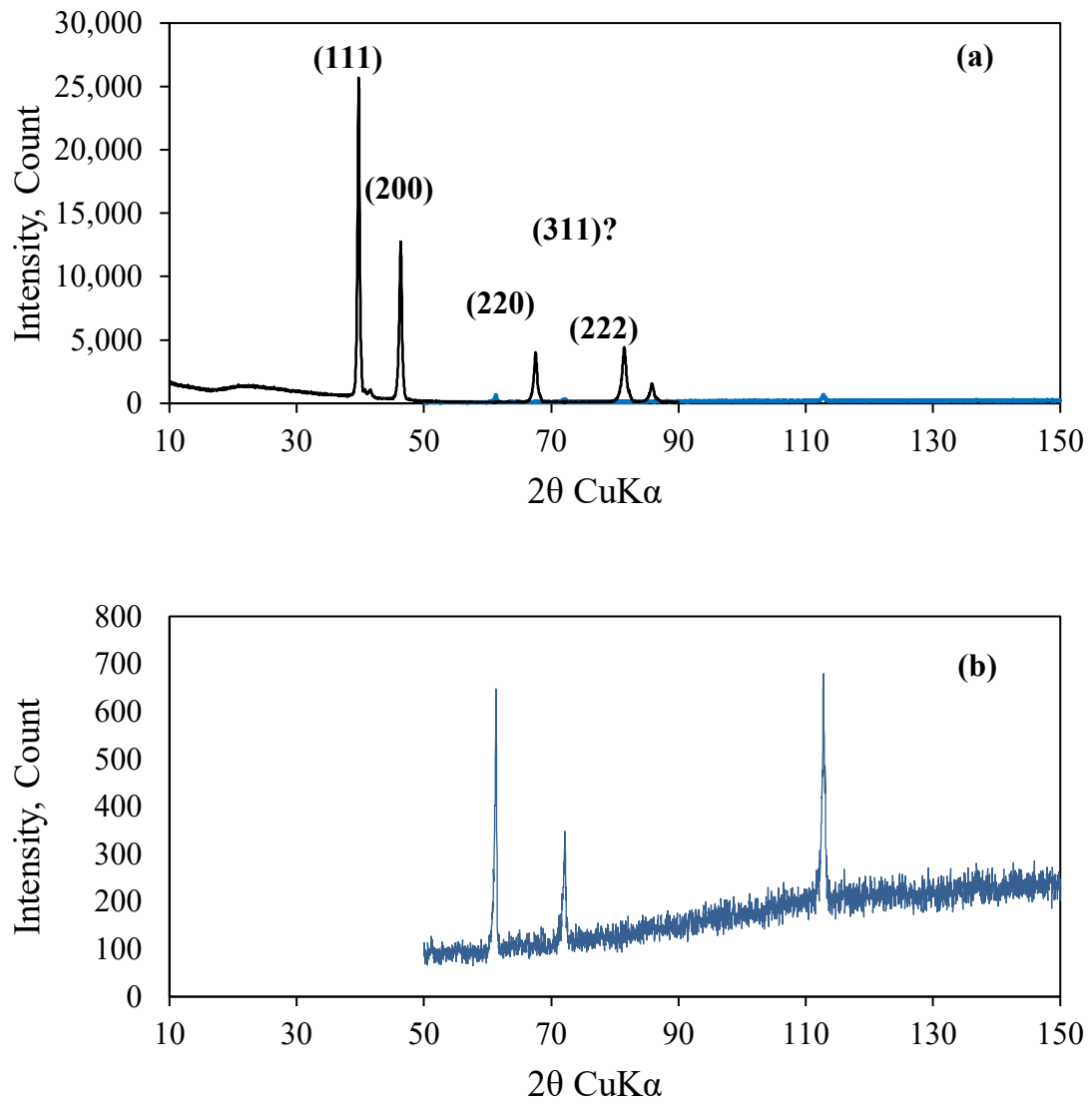


Figure 5-13. XRD analysis of the a) intact and b) used MRs

References

- [1] Sjardin M, Damen KJ, Faaij APC. Techno-economic prospects of small-scale membrane reactors in a future hydrogen-fuelled transportation sector. *Energy* 2006;31:2523–55. doi:10.1016/j.energy.2005.12.004.
- [2] Barelli L, BIDINI G, Gallorini F, SERVILI S. Hydrogen production through sorption-enhanced steam methane reforming and membrane technology: A review. *Energy* 2008;33:554–70. doi:10.1016/j.energy.2007.10.018.
- [3] Soltani R, Rosen MA, Dincer I. Assessment of CO₂ capture options from various points in steam methane reforming for hydrogen production. *Int J Hydrogen Energy* 2014;39:20266–75. doi:10.1016/j.ijhydene.2014.09.161.
- [4] Boyano A, Blanco-Marigorta AM, Morosuk T, Tsatsaronis G. Exergoenvironmental analysis of a steam methane reforming process for hydrogen production. *Energy* 2011;36:2202–14. doi:10.1016/j.energy.2010.05.020.
- [5] Johansson D, Franck P-Å åke, Berntsson T. Hydrogen production from biomass gasification in the oil refining industry - A system analysis. *Energy* 2012;38:212–27. doi:10.1016/j.energy.2011.12.011.
- [6] Maqbool W, Park SJ, Lee ES. Steam Methane Reforming of Natural Gas with Substantial Carbon Dioxide Contents–Process Optimization for Gas-to-Liquid Applications. *Appl. Mech. Mater.*, vol. 548, Trans Tech Publ; 2014, p. 316–20.
- [7] Nieva MA, Villaverde MM, Monzón A, Garetto TF, Marchi AJ. Steam-methane reforming at low temperature on nickel-based catalysts. *Chem Eng J* 2014;235:158–66. doi:10.1016/j.cej.2013.09.030.
- [8] MURADOV N, VEZIROGLU T. “Green” path from fossil-based to hydrogen economy: An overview of carbon-neutral technologies. *Int J Hydrogen Energy* 2008;33:6804–39. doi:10.1016/j.ijhydene.2008.08.054.
- [9] Muradov NZZ, Veziroğlu TNN. From hydrocarbon to hydrogen–carbon to hydrogen economy. *Int J Hydrogen Energy* 2005;30:225–37. doi:10.1016/j.ijhydene.2004.03.033.
- [10] Lee D, Cha K, Kim H-S, Park C, Kim Y. Syngas and hydrogen production via stepwise methane reforming over Cu-ferrite/YSZ. *Int J Energy Res* 2014;38:1522–

30. doi:10.1002/er.3159.
- [11] Spath PL, Mann MK. Life cycle assessment of hydrogen production via natural gas steam reforming. National Renewable Energy Laboratory Golden, CO; 2000.
- [12] Faraji S, Sotudeh-Gharebagh R, Mostoufi N. Hydrogen recovery from refinery off-gases. *J Appl Sci* 2005;5:459–64.
- [13] Kalamaras CM, Efstathiou AM. Hydrogen Production Technologies: Current State and Future Developments. *Conf Pap Energy* 2013;2013:1–9. doi:10.1155/2013/690627.
- [14] Armaroli N, Balzani V. The Hydrogen Issue. *ChemSusChem* 2011;4:21–36. doi:10.1002/cssc.201000182.
- [15] BALL M, WIETSCHEL M. The future of hydrogen – opportunities and challenges. *Int J Hydrogen Energy* 2009;34:615–27. doi:10.1016/j.ijhydene.2008.11.014.
- [16] Pacala S, Socolow R. Stabilization wedges: Solving the climate problem for the next 50 years with current technologies. *Science* (80-) 2004;305:968–72. doi:10.1126/science.1100103.
- [17] Augustine AS, Ma YH, Kazantzis NK. High pressure palladium membrane reactor for the high temperature water-gas shift reaction. *Int J Hydrogen Energy* 2011;36:5350–60. doi:10.1016/j.ijhydene.2011.01.172.
- [18] Anzelmo B, Wilcox J, Liguori S. Natural gas steam reforming reaction at low temperature and pressure conditions for hydrogen production via Pd/PSS membrane reactor. *J Memb Sci* 2017;522:343–50. doi:10.1016/j.memsci.2016.09.029.
- [19] Catalano J, Giacinti Baschetti M, Sarti GC. Influence of the gas phase resistance on hydrogen flux through thin palladium–silver membranes. *J Memb Sci* 2009;339:57–67. doi:10.1016/J.MEMSCI.2009.04.032.
- [20] Burkhanov GS, Gorina NB, Kolchugina NB, Roshan NR, Slovetsky DI, Chistov EM. Palladium-based alloy membranes for separation of high purity hydrogen from hydrogen-containing gas mixtures. *Platin Met Rev* 2011;55:3–12.
- [21] Al-Mufachi NA, Rees N V., Steinberger-Wilkens R. Hydrogen selective membranes: A review of palladium-based dense metal membranes. *Renew Sustain*

- Energy Rev 2015;47:540–51. doi:10.1016/j.rser.2015.03.026.
- [22] Yan S, Maeda H, Kusakabe K, Morooka S. Thin Palladium Membrane Formed in Support Pores by Metal-Organic Chemical Vapor Deposition Method and Application to Hydrogen Separation. vol. 33. 1994.
- [23] Rahimpour MR, Samimi F, Babapoor A, Tohidian T, Mohebi S. Palladium membranes applications in reaction systems for hydrogen separation and purification: A review. *Chem Eng Process Process Intensif* 2017;121:24–49. doi:10.1016/j.cep.2017.07.021.
- [24] Caravella A, Barbieri G, Drioli E. Concentration polarization analysis in self-supported Pd-based membranes. *Sep Purif Technol* 2009;66:613–24. doi:10.1016/j.seppur.2009.01.008.
- [25] Yun S, Ted Oyama S. Correlations in palladium membranes for hydrogen separation: A review. *J Memb Sci* 2011;375:28–45. doi:10.1016/j.memsci.2011.03.057.
- [26] Morreale BD, Ciocco M V., Enick RM, Morsi BI, Howard BH, Cugini A V., et al. The permeability of hydrogen in bulk palladium at elevated temperatures and pressures. *J Memb Sci* 2003;212:87–97. doi:10.1016/S0376-7388(02)00456-8.
- [27] Deveau ND, Ma YH, Datta R. Beyond Sieverts' law: A comprehensive microkinetic model of hydrogen permeation in dense metal membranes. *J Memb Sci* 2013;437:298–311. doi:10.1016/j.memsci.2013.02.047.
- [28] Basile A, Campanari S, Manzolini G, Iulianelli A, Longo T, Liguori S, et al. Methane steam reforming in a Pd–Ag membrane reformer: An experimental study on reaction pressure influence at middle temperature. *Int J Hydrogen Energy* 2011;36:1531–9. doi:10.1016/j.ijhydene.2010.10.101.
- [29] Caravella A, Scura F, Barbieri G, Drioli E. Sieverts law empirical exponent for PD-based membranes: Critical analysis in pure H₂ permeation. *J Phys Chem B* 2010;114:6033–47. doi:10.1021/jp1006582.
- [30] Guazzone F, Engwall EE, Ma YH. Effects of surface activity, defects and mass transfer on hydrogen permeance and n-value in composite palladium-porous stainless steel membranes. *Catal Today* 2006;118:24–31. doi:10.1016/J.CATTOD.2005.12.010.

- [31] Paglieri SN, Way JD. INNOVATIONS IN PALLADIUM MEMBRANE RESEARCH. *Sep Purif Methods* 2002;31:1–169. doi:10.1081/SPM-120006115.
- [32] Pham Minh D, Siang TJ, Vo D-VN, Phan TS, Ridart C, Nzihou A, et al. Hydrogen Production From Biogas Reforming: An Overview of Steam Reforming, Dry Reforming, Dual Reforming, and Tri-Reforming of Methane. *Hydrog. Supply Chain.*, Elsevier; 2018, p. 111–66. doi:10.1016/b978-0-12-811197-0.00004-x.
- [33] Chen Y, Wang Y, Xu H, Xiong G. Efficient production of hydrogen from natural gas steam reforming in palladium membrane reactor. *Appl Catal B Environ* 2008;81:283–94. doi:10.1016/j.apcatb.2007.10.024.
- [34] Kian K, Woodall C, Wilcox J, Liguori S. Performance of Pd-Based Membranes and Effects of Various Gas Mixtures on H₂ Permeation. *Environments* 2018;5:128. doi:10.3390/environments5120128.
- [35] Cornaglia L, Múnera J, Lombardo E. Recent advances in catalysts, palladium alloys and high temperature WGS membrane reactors: A review. *Int J Hydrogen Energy* 2015;40:3423–37. doi:10.1016/j.ijhydene.2014.10.091.
- [36] Oklany JS, Hou K, Hughes R. A simulative comparison of dense and microporous membrane reactors for the steam reforming of methane. *Appl Catal A Gen* 1998;170:13–22. doi:10.1016/S0926-860X(98)00027-1.
- [37] Chue KT, Kim JN, Yoo YJ, Cho SH, Yang RT. Comparison of Activated Carbon and Zeolite 13X for CO₂ Recovery from Flue Gas by Pressure Swing Adsorption. *Ind Eng Chem Res* 1995;34:591–8. doi:10.1021/ie00041a020.
- [38] Garshasbi V, Jahangiri M, Anbia M. Equilibrium CO₂ adsorption on zeolite 13X prepared from natural clays. *Appl Surf Sci* 2017;393:225–33. doi:10.1016/j.apsusc.2016.09.161.
- [39] Wilcox J. Carbon capture. Springer Science & Business Media; 2012.
- [40] Collins JP, Way JD. Preparation and characterization of a composite palladium-ceramic membrane. *Ind Eng Chem Res* 1993;32:3006–13. doi:10.1021/ie00024a008.
- [41] Anzelmo B. On-board Hydrogen Production from Natural Gas Via a Metallic Pd-based Membrane Reactor. Stanford University, 2016.
- [42] De Lange MF, Vlugt TJH, Gascon J, Kapteijn F. Adsorptive characterization of

- porous solids: Error analysis guides the way. *Microporous Mesoporous Mater* 2014;200:199–215. doi:10.1016/j.micromeso.2014.08.048.
- [43] Nguyen C, Do DD. The Dubinin-Radushkevich equation and the underlying microscopic adsorption description. *Carbon N Y* 2001;39:1327–36. doi:10.1016/S0008-6223(00)00265-7.
- [44] Qasem NAA, Ben-Mansour R, Habib MA. Enhancement of adsorption carbon capture capacity of 13X with optimal incorporation of carbon nanotubes. *Int J Energy Environ Eng* 2017;8:219–30. doi:10.1007/s40095-017-0235-7.
- [45] Qiao A, Zhang K, Tian Y, Xie L, Luo H, Lin YS, et al. Hydrogen separation through palladium-copper membranes on porous stainless steel with sol-gel derived ceria as diffusion barrier. *Fuel* 2010;89:1274–9. doi:10.1016/j.fuel.2009.12.006.
- [46] Brisotto M, Gelfi M, Rinaldi C, Depero LE, 154 R. Study of microstrain and stress in non-planar Palladium membranes for hydrogen separation RSE (Ricerca sul sistema Energetico) via 2014. doi:10.4028/www.scientific.net/AMR.996.27.
- [47] Guazzone F, Ma YH. Leak growth mechanism in composite Pd membranes prepared by the electroless deposition method. *AIChE J* 2008;54:487–94. doi:10.1002/aic.11397.

Chapter 6 - Technoeconomic Analysis

Hydrogen producing facilities may be categorized into three different groups based on their hydrogen production capacities: small-scale or distributed (i.e., 100-1,500 kg H₂ per day at fueling stations), medium-scale or semi-central (i.e., 1,500-50,000 kg H₂ per day on the outskirts of cities), large-scale or central (i.e., >50,000 kg of H₂ per day).[1] Conventional SMR technology is a well-developed technology and currently, the energy yield of hydrogen production is estimated at 60 gH₂/kWh. This value is equivalent to a cost of \$1.72^{xiv} per kg of H₂. The finished cost of producing one kg of hydrogen may vary significantly depending on the geographical location and the method of generating electricity. This energy yield of hydrogen production of 60 gH₂/kWh is the target value set by the U.S. DOE as the benchmark for other competitive technologies by 2020.[1] Although the 2020 target cost to produce one kg H₂ for various technologies varies from \$2.30 to \$9.20, the ultimate target cost for all technologies is set at \$1.00-2.00 per kg of H₂.

Depending on the type of electrolyte used for the electrolysis processes, the electrolyzers can be divided into three main categories, i.e., proton exchange membrane (PEM) electrolyzer, alkaline electrolyzer, and solid oxide electrolysis cell (SOEC). PEMs usually require noble catalysts which in turn increases the capital costs required for manufacturing such electrolyzers. However, the solid polymer electrolyte used in these electrolyzers provides them with significant advantages which makes these electrolyzers unique. Compact and leak-free design, high current density, low gas crossover rate, and capacity to operate at pressures as high as 350 bar are among the advantages of PEMs. This last feature makes it possible to produce hydrogen at significantly higher pressure thereby eliminating the need for compressors before delivering the hydrogen to the consumer. PEMs usually operate at intermediate voltages (1.7-2.0V) and high current densities (more than 1.0 A.cm⁻²) which lead to higher nominal efficiencies.[2]

^{xiv} Assuming the average price of 1 kWh of electricity to be \$0.1031 as reported by the U.S. Energy Information Administration as of April 2019.

The alkaline electrolyzer is the most mature and the most common type of electrolyzer which has the lowest capital cost amongst all electrolyzer types. Despite their low capital cost, alkaline electrolyzers are prone to leaking, and have lower current density both of which stem from the fact that unlike PEMs, alkaline electrolyzers use aqueous electrolytes. Alkaline electrolyzers usually operate at high voltages (1.8-2.4V) and low current densities (0.2-0.3 A.cm⁻²) which will result in lower system efficiencies.[2]

SOECs are newer technology compared to PEMs and alkaline electrolyzers. SOECs usually operate at very high temperatures (900-950°C) which translates into higher capital costs due to the need for more expensive materials such as ceramics in the manufacturing of the SOEC cells. Furthermore, a heat source is required to provide the thermal energy for SOECs. Unlike alkaline electrolyzers, SOECs do not suffer from leakage and have a more compact design. The single greatest drawback of SOECs is their long-term degradation which is actively being investigated by scientists. SOECs operate at very low voltages (i.e., less than 1.4V) and moderate current densities (0.4-0.8 A.cm⁻²) which allows them to have considerably higher electrical efficiency. Significant research is currently being conducted on the SOEC-based power-to-methane (P2M) systems to increase their technological readiness level (TRL) from TRL5 to TRL6.[3]

It is worth noting that the “thermodynamic limit” of the energy yield for SMR may be up to 105 gH₂/kWh while for water electrolysis the limit is 25.4 gH₂/kWh^{xv} at 25°C and ambient pressure. It should be noted that the current commercial electrolyzer systems have significantly high efficiencies (approximately 50 kWh/kgH₂) which are very close to the theoretical minimum energy. Nevertheless, when coupled with renewable energy resources such as PV cells, the overall efficiency of the system declines significantly (i.e., efficiencies as low as 20% for PV-SOEC are common) stemming from the very low efficiency of the PV cells (i.e., less than 17%).[2] Hence, efficiency improvements based on novel

^{xv} The theoretical minimum required electric energy to produce 1 kg of hydrogen at 25°C and atmospheric pressure is approximately 39.4 kWh (based on the higher heating value of hydrogen).

technological breakthroughs are very limited for these system.[4] High temperature electrolysis systems, however, have the potential to improve this limit and lower the cost only if the electrolyzer system is located in the proximity of a low-cost or waste heat source. Therefore, the key to success of the electrolyzer systems relies on the optimization of other key parameters such as capital cost or lifetime rather than focusing on electrical efficiency. As a result, small commercial electrolyzer systems in remote areas, due to their low capital requirements, can be very competitive against the conventional hydrogen plants.

Fuel cost is the single largest cost component in production of hydrogen by natural gas reforming accounting between 45-75% of the production cost of hydrogen. Nevertheless, low prices of natural gas in some geographical regions such as the Middle East and Russia (due to the existence of enormous conventional natural gas resources) and the U.S. (due to the existence of immense unconventional gas resources such as shale gas reserves and the availability of advanced technologies such as hydraulic fracturing and horizontal drilling), have made the production cost of hydrogen very inexpensive in these regions.

Depending on the region, retrofitting of a CCUS unit to the SMR plant could increase the capital expenditure (CAPEX), and cost of fuel by 50% and 10%, respectively. The operating expenses could be doubled on average, due to the costs associated with CO₂ capture, handling, compression, transport and storage. However, there are some promising regions where the cost of producing hydrogen from a SMR with CCUS unit could be as low as USD 1.40 per kg of hydrogen produced.

Despite technological advancements in the development of membranes and MRs, their numerous physical and technological features such as lifetime have not been realized with great certainty.[5] One of the reasons that there is not a general consensus on the lifetime of membranes is the lack of unanimity of the term “long-term test”. In the open literature the experiments ranging from 80-8640 hours have been considered as “long-term tests”. [5-8] The movement of the Pd crystallites/atoms increases at high temperature and for prolonged time periods which increases the possibility of pinhole formation and subsequent membrane failure.[9] This effect is exacerbated as the thickness of the Pd layer decreases.

Therefore, the thickness of the Pd layer can be increased to avoid the formation of pinholes. However, as shown previously in Eq. 2-22, the hydrogen permeating flux has an inverse relationship with the thickness of the Pd layer and by increasing the membrane thickness the hydrogen flux would decrease, which is not economically attractive. [10] Hence, one of the most important elements in the design of an MR is the selection of an optimized thickness for the Pd layer which will be a compromise between the lifetime and hydrogen permeating flux. The lifetime of the Pd-based membrane is usually assumed to be 5 years. [5] This means that at least four replacements are required for a plant with a lifetime of 25 years.[11] One of the major challenges for accurate economic evaluation for the Pd-based MR technology is the lack of large-scale commercial experience in this area. As a result, the majority of the economic studies reported in the literature are based on theoretical estimates. These studies adopt economic concepts such as net present value (NPV), fixed capital investment (FCI) total capital investment (TCI), and internal rate of return (IRR) to give a reliable fiscal understanding of the Pd-based MR technology. [5, 10, 12-14] The sources of uncertainties that have been integrated into these studies will result in statistical economic evaluations rather than single-point approximations which leads to inaccurate valuation assessments and improper economic decisions. These studies mainly suffer from the principle of “flaw of averages”. [5, 10, 12-15]

In order to overcome the flaw of averages, Castro et al. [5] used Monte Carlo simulation methods to study the effects of lifetime and membrane thickness on the economic performance of multiple Pd and Pd/Au membranes. Uncertainties such as sources of commodity market, and uncertainties associated with regulatory and financing make the integration of Monte Carlo simulations in economic assessments inevitable. In this study it is showed that the lifetime of a pure Pd membrane is inferior to that of the Pd/Au membrane as the gold particles act as a paste that fills and covers the pinholes and defects induced in the surface of the membrane during the permeation tests. [16] Furthermore, the purity of produced hydrogen decreases with time. More interestingly, this decrease in quality is more pronounced in membranes with thinner Pd layers. However, thicker membranes will increase the capital investment significantly. For instance, increasing the Pd layer thickness from 2.7 μm to 4.6 μm and 10.4 μm will increase the membrane lifetime

by 16% and 152%, respectively. The TCI also increases as the thickness of the Pd layer increases from 2.7 μm to 4.6 μm and 10.4 μm due to additional amounts of Pd used in membrane fabrication. This study reveals that the thinnest membrane has the best economic performance in terms of lowest FCI, TCI, and levelized cost of hydrogen (LCOH).

Collodi et. al performed a comprehensive study on the economic performance of various SMR plants. Their work compares and contrasts the performance and various cost indices of a SMR plants with and without CCUS units producing 100,000 Nm^3/h H_2 operating as a merchant plant. [17] This study evaluates five different alternative scenarios to capture CO_2 from a SMR plant and compares them with a modern SMR plant which is equipped with feedstock pretreatment, pre-reforming, HT shift, and PSA units. These alternative technologies can capture CO_2 from the shifted syngas, PSA tail gas or SMR flue gas using mono-ethanolamine (MEA), methyl-di-ethanolamine (MDEA), or cryogenic and membrane separation. In this work the discounted cash flow analysis and LCOH are used to compare various technologies. Furthermore, the cost of CO_2 avoided (CAC) is another key index which is used to compare the overall performance of these plants. The CAC may be calculated as:

$$CAC = \frac{LCOH_{CCS} - LCOH_{Reference}}{CO_2 \text{ Emissions}_{Reference} - CO_2 \text{ Emissions}_{CCS}} \quad \text{Eq. 6-1}$$

According to this study, in solvent-based CO_2 capture scenarios, the overall consumption of natural gas has increased by more than 200% only to regenerate the solvent. The electricity that is required for CO_2 capture, will result in high energy penalties in these cases. In a plant where CO_2 is captured from the PSA tail gas using low temperature CO_2 separation and membrane technology, the consumption of natural gas is reduced by approximately 7% compared to the base case. Moreover, in order to capture 90% of the CO_2 from the SMR plant, the capital cost will increase by 78% compared with the base case. Furthermore, depending on the overall CO_2 capture rate, from 53% to 90%, the LCOH may increase by 0.02 to 0.06 USD/ Nm^3 , respectively. The CO_2 avoided cost is

estimated to vary between \$51.12 and \$77.24 per tonne^{xvi}. The LCOH will increase between 18-45% depending on the CCUS technology implemented at the plant. Other similar studies show that CO₂ capture (80-85% capture from the concentrated PSA stream) will add approximately 25-30% to the cost of produced hydrogen by the SMR process.[18] The cost of hydrogen production may be reduced if a positive cash flow is generated by selling the captured CO₂ for direct usage. It should be noted that cost of hydrogen produced by SMR is very sensitive to the price of natural gas, its quality and heating value.[19] Furthermore, the capacity and efficiency of hydrogen plants must be considered when calculating the LCOH as the economy of scale play a crucial role in the industrial processes. For instance, two hydrogen production plants could be identical in all aspects except for their capacities and this can have a significant effect on the LCOH of the plants.

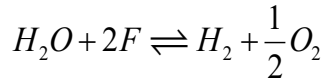
These results indicate that the production of hydrogen with CCUS units (either solvent-based or membrane-based) will add significantly to the LCOH, consumes a compelling amount of the electricity, which would otherwise be exported to the grid. Therefore, it is crucial for any hydrogen producing facility to consider these economic implications before making a decision about retrofitting their plants with CCUS units.

Hydrogen may also be produced by water electrolysis where water is dissociated into hydrogen and oxygen molecules. Water electrolysis for hydrogen production is accomplished according the following half reactions:



The overall chemical reaction for water electrolysis can be written as a combination of the two half-reactions as follows: [19,20]

^{xvi} Converted using the weighted average exchange rate of 1.106560 for EURUSD in 2016.



Eq. 6-4

such that F is the Faraday constant measuring 1 mole of electricity (96,485 °C/mol). According to Eq. 6-4, the overall cost of water electrolysis is mandated by the price of acquiring water and the cost of electricity. Cost of acquiring water can be reduced to negligible amounts by developing the electrolysis plant in appropriate geographical locations where water is abundant and cheap. In order to improve the conductivity and enhance the overall yield of hydrogen, an electrolyte, usually caustic potash (KOH), is dissolved in water. Despite the advantages of water electrolysis, such as potentially low CO₂ emissions^{xvii} associated with the electrolysis process, there are still challenges that need to be addressed: the amount of electricity consumed in commercial alkaline electrolysis systems for the production of pure hydrogen is very high (approximately 4.5-5 kWh/m_n³ H₂), [21] the cathode and anode electrodes are coated with platinum and manganese oxide respectively[19], which makes the process economically unattractive. Furthermore, compression of the produced hydrogen to pressures as high as 880 bar will add further costs.[22] According to recent studies performed by National Academies of Sciences and the U.S. DOE, the current delivered cost of one kilogram of hydrogen generated by grid-power electrolysis, wind-power electrolysis, and solar-power electrolysis are approximately \$6-7, \$7-11, and \$10-30 respectively. These numbers may be reduced to as low as \$3-4 per kilogram of hydrogen delivered with advancements in the wind turbine and solar panel technologies and with the introduction of “smart grid” in the future.[23]

As reported, the major challenges associate with water electrolysis technologies are the significant amount of electricity and large volumes of water required for the process. Producing today’s global hydrogen demand from water electrolysis requires more than

xvii It is worth noting that in 2018, 63.5% of the U.S. electricity was generated from fossil fuels. Approximately 35% of electricity was produced from natural gas while roughly 27% of electricity came from coal. Therefore, the source of electricity must be considered to calculate the accurate emission values. Furthermore, some might argue, if the electricity come from the renewable sources, it would be better to decarbonize the grid in the first place rather than spending it for water electrolysis directly.

3,600 TWh of electricity which is more than the annual electricity generation of the whole European Union. In addition, approximately 9 kg of water is required to produce 1.0 kg of hydrogen. Producing today's global energy demand from water electrolysis will require more than 617 million cubic meter of water which is equivalent to 1.3% of water consumed in the global energy sector. Using fresh water for electrolysis could be an environmental and social challenge in areas that are already dealing with water crisis. Direct use of sea water, in coastal areas, would result in corrosive damage to the equipment. Use of desalinated water could be the only short-term solution to the water problem. However, it should be noted that it requires between 3-4 kWh of electricity to desalinate 1 m³ of seawater through reverse osmosis process.

As mentioned earlier, the three main electrolyzer technologies that exist today are alkaline electrolyzers, PEMs, and SOECs. Nonetheless, another hydrogen production technology that has received significant attention in recent years is solar-driven electrolysis. Electrolysis fueled by solar energy can be divided into two major categories: photoelectrochemical (PEC) water splitting and photovoltaic electrolysis (PV-E). A PEC system is a fully integrated unit that absorbs sunlight and directly produces hydrogen while the PV-E system consists of independent photovoltaic modules that drive separate electrolyzer units and has more operational flexibility compared with the PEC system.[24]

Cost of hydrogen produced by electrolysis depends on factors such as the cost of electricity, cost of water, conversion efficiency, CAPEX, and annual operating hours. CAPEX requirements for alkaline electrolysis, PEM electrolysis, and SOEC electrolysis could be in the ranges of \$500-1,400/kW_e, \$1,100-1,800/kW_e, and \$2,800-5,600/kW_e respectively. According to a recent study by Shaner et al., the LCOH and total CAPEX for a base-case PV-E system are estimated at \$12.1 per kg H₂ and \$260 million, respectively. The LCOH and capital expenditure for the base-case PEC system is reported to be \$11.4 per kg H₂ and \$205 million, respectively. [24] In order for a PV-E system to be competitive with the PEC system, an increase in efficiency or decrease in the capital expenditure is necessary.

Solar-driven technologies are limited by low solar power density (less than 1 kWm^{-2}), low capacity factor (less than 25%), and low conversion efficiencies (less than 20%). The cost of producing hydrogen (without compression, storage, and dispensing) by SMR can be as low as \$1.43 per kg of H_2 , when the price of natural gas feedstock is assumed to remain constant at \$4 per MMBtu.[25] With the current prices of natural gas^{xviii}, in order for PV-E technologies to be at cost parity with SMR, a minimum carbon tax of \$1,200 per tonne of CO_2 would be required.[24]

Considering the challenges associated with the development of electrolysis technology, along with the economic disadvantages compared with processes such as SMR, it is expected that the scale of hydrogen produced by electrolysis will not change in the near future and will be mainly limited to small-scale and unique applications. An additional crucial aspect that one needs to keep in mind is the concept of “locked investment”. The average plant lifetime is approximately 25-30 years and once a plant is built it is expected to be operational for this timeframe. This may even further slowdown the transition toward decarbonization in the absence of appropriate legal frameworks. The only scenario in which an increase in the volume of produced hydrogen by electrolysis is plausible, is when stringent national and international climate policies are put in place that help our global society to reduce our dependence on fossil fuels. Implementation of such policies would make the finished cost of produced hydrogen significantly higher due to either carbon penalties associated with combustion of natural gas or the cost of CO_2 capture and sequestration. Therefore, under such policies, water electrolysis could be a competitive alternative.

Hydrogen can also be produced from biomass resources. However, one of the major challenges with this approach is the large-scale availability of cheap biomass. For instance, in order to produce the hydrogen demand in the U.S., roughly 100% of the nation’s biomass capacity is required while the same goal can be achieved with only 6% of the country’s wind power and 1% of its solar power potential. Nevertheless, combining biomass and

xviii The average price of natural gas in the U.S. in the year 2018 was approximately \$3.15 per MMBtu.

CCUS for hydrogen production could be a potential “negative emission” technology which will be more attractive in a scenario where climate change mitigation policies place higher penalties on CO₂ emissions.

In recent years, plasmas have gained interest for application to hydrogen production from both gaseous and liquid fuels. One of the plasma-based techniques for hydrogen production is the plasma arc decomposition technology. This method simply decomposes natural gas into carbon and hydrogen and is claimed to produce no CO₂ [26] as indicated in Eq. 6-5:



In principle, plasma reforming reactions are the same as conventional reforming reactions with the exception that the required energy and free radicals used for the reforming reaction are provided by a plasma that is usually generated by electric or thermal energy. [27] The plasma used for hydrogen production from gaseous fuels are generated by various methods such as electron beam, dielectric-barrier discharge, gliding arc, plasmatron arc, and microwave discharge.[1] Plasma reformers can generate pure hydrogen streams from an array of hydrocarbon fuels (such as gasoline, diesel, oil, natural gas, alcohols, etc.) with conversion efficiencies very close to 100%.[28] Among all the plasma methods, the plasma generated by a plasmatron arc and supported by a catalyst is the most advanced technology that is currently capable of producing hydrogen from methane with an energy yield (225 gH₂/kWh) that meets the 2020 DOE target.[1] In addition, the recent developments in the microwave plasma sources (MPSs) with catalysts have shown very promising results and have achieved energy yields as high as 62.8 gH₂/kWh.[1]

One advantage of using plasma approaches for hydrogen production is its compactness due to the high energy density of the plasma system and very short response time. Furthermore, the heavy particles (such as atoms and molecules) can reach temperatures as high as 2,000-6,000K while lighter particles (such as electrons) can reach temperatures up to 10,000K in the plasma environment. In addition, plasma matter contains reactive radicals (i.e., H, OH,

and O) and ions which significantly enhance the conversion of hydrocarbon fuels into hydrogen in the high-temperature medium.[1]

Although some plasma reforming methods such as MPS have numerous advantages over the conventional reforming processes such as better response time, the ability to produce hydrogen from heavier hydrocarbons, and hydrogen production from gaseous fuels with an energy yield close to that set by DOE target, the high amount of electricity required in addition to high electrode erosion at elevated pressures represent significant challenges.[29,30] Furthermore, plasma methods face other challenges such as low hydrogen production rates, and high investment and operating costs.[1]

Other than the methods discussed earlier, there are some other technologies that show significant potential for hydrogen production and might play a role in future hydrogen economy scenarios. Among these methods are the chemical looping combustion (CLC) and the alcohol reforming processes that show promising capacity for future carbon-free scenarios.[31]

In the recent decades a compelling amount of research has been conducted in the area of hydrogen production via alcohol reforming. One of the advantages of alcohol reforming over methane reforming is that unlike steam reforming of methane, in alcohol reforming, the hydrocarbon source is in liquid state which may eliminate the need for gaseous hydrogen storage and distribution for on-board hydrogen production in HFCVs.[32] Other advantages of alcohol reforming over steam reforming include easier handling and transport, lower cost, and alternative modes of synthesis.[33,34] For instance, methanol and ethanol can be effortlessly synthesized from both fossil fuels and biomass-based syngas. The latter method has a great potential to make alcohol reforming an attractive alternative method for conventional SMR in a low carbon intensity economy. More specifically, in a process called bioenergy with carbon capture and storage (BECCS), bioethanol can be produced from the fermentation of biomass, such as corn and sugarcane, while CO₂ is captured permanently stored in geological formations.

Technoeconomic Analysis

Steam alcohol reforming (SAR) can be carried out in an MR in an identical process to that of SMR as depicted in Figure 6-1. Gallucci et al., have conducted numerous experimental studies on the SAR process which reveal that in an MR, methanol conversions could be as high as 100% while in the same conventional reactor, the maximum ethanol conversion is reported to be only 50%.[34]

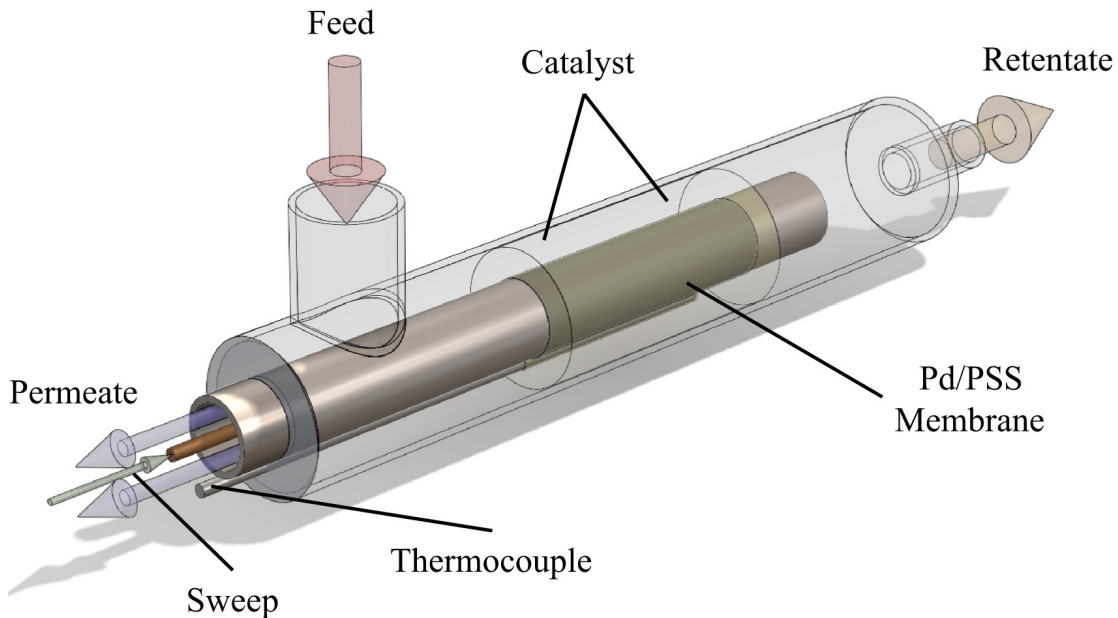
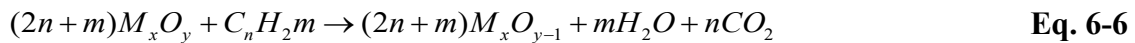


Figure 6-1. Schematic of an MR for SMR or SAR process (taken from Anzelmo et al.) [35]

Many other studies investigated the effect of several parameters on the performance of SAR in MR technology. In particular, Hedayati et al. performed a rigorous exergy analysis for the ethanol steam reforming reaction conducted in an MR [36,37]. Their exergy analyses revealed that the performance of the reforming system can be improved by eliminating/minimizing the irreversibilities and losses in the system, and that the optimal operating conditions which give the highest exergy efficiencies for the ESR reaction correspond at highest possible operating pressures and temperatures and lowest possible steam to carbo (S/C) ratios.

Nevertheless, further development in MRs performance and more stringent climate policies could make the SAR an attractive alternative to the conventional SMR.

Another technology that has gained significant attention for hydrogen production in the last two decades is the CLC process. Unlike a conventional combustion cycle system, a CLC process, employs two fluidized bed reactors, an air reactor (AR) and a fuel reactor (FR) accompanied with a circulating metal oxide (M_xO_y) which serves as an oxygen carrier for the combustion cycle. The metal oxide particles are reduced in the FR using the hydrocarbon fuel as a reducer according to Eq. 6-6. Next, the reduced particles are oxidized in the AR to regenerate the metal oxide as shown in Eq. 6-7.[31]



One of the biggest advantages of the CLC process is the separation of fuel from the air using two different reaction chambers. This CLC design will allow for using nearly pure oxygen without nitrogen which significantly eliminates NO_x formation [38] and improves the thermal efficiency of the process. [39] In addition, the only combustion products are H_2O and CO_2 which are not diluted by hydrogen. This will allow for capturing nearly pure CO_2 by simply condensing out the water vapor. Some of the common challenges associated with CLC processes are the erosion of the reformer tubes due to high temperature, the need for PSA and WGS reactors for hydrogen separation and purification, and selection of the suitable oxygen carrier with favorable reactive properties and high resistance against carbon deposition. However, the major drawback of the CLC process is the high pressure required for air compression and very high temperatures (more than 1000 °C) required to keep the conversion rates high in the FR. This can be directly translated into high operating costs associated for production of a unit mass of hydrogen. One way to address these challenges is to combine the CLC system with the membrane reactor which is called the membrane assisted chemical looping reforming (MA-CLR) as proposed by Spallina et al.[40] Their study shows that the MA-CLR can produce between 12-20% more hydrogen compared with the conventional fired tubular reforming (FTR) process while the cost of

Technoeconomic Analysis

producing hydrogen drops by more than 30%^{xix}.^[40] A summary of hydrogen production technologies along with their advantages and drawbacks is provided in Table 6-1.

xix The average production cost of hydrogen by FTR and MA-CLR technologies is reported to be 0.28 €/Nm³H₂ and 0.19 €/Nm³H₂ respectively in 2016 values.^[40] These values can be converted to 2019 inflation adjusted values of \$3.72/kgH₂ and \$2.52/kgH₂ respectively. The weighted average exchange rate in 2016 is assumed to be 1.106560 for EURUSD.

Table 6-1. Benefits, Drawbacks and Costs of different Hydrogen Production Technologies [41,42]

Technology	Benefits	Drawbacks	Status	Thermodynamic energy yield [gH ₂ /kWh]	Cost [\$/kg H ₂] ^{xx}	Reference
SMR plant with PSA (No CCUS)	High efficiency Economically attractive High H ₂ recovery (89%) High purity H ₂ (99.99+%)	GHG emissions Limited fossil fuel resources	Commercially available	60	1.00-2.14 ^{xxi}	[43,1,17,44]
SMR plant with CCUS (solvent-based)	Less CO ₂ emissions Concentrated stream of CO ₂ can be utilized or geologically sequestered	Larger volume due Additional steam requirement to regenerate the solvent High energy penalty for CO ₂ capture and compression	Pilot scale. Economic incentives required for commercial scale.	<60	1.50-3.16 ^{xxii}	[1,44,45]
SMR with CCUS (Pd-based membrane)	More compact design No solvent regeneration and energy penalties associated with it Less CO ₂ emissions Concentrated stream of CO ₂ can be sequestered or used for EOR	High cost of membrane materials and fabrication	Currently available at pilot scale. Further development required for commercial scale.	<60	~3.54 ^{xxiii}	[46]
Water electrolysis	Technologically simple Pure hydrogen and oxygen products Zero GHG emission depending on the energy source No need for installation of CCUS unit	High energy consumption Low overall efficiency ^{xxiv} Economically unattractive Available at small scale High capital cost	Available at small scale. Development of new materials and technologies required	20-40 ^{xxv}	2.80-28.75 ^{xxvi}	[43,47,1,21,44,45,48,49]
Plasma	Better response time Hydrogen production from heavy hydrocarbons Compact system High energy density High conversion of hydrocarbons	High electric power requirement Electrode erosion High operating pressures Low hydrogen production rate High investment and operating costs	Research and development phase.	0.5-225 ^{xxvii}	NA	[1,29,30]
MA-CLC	Separation of fuel from the air Elimination of NO _x Easy capture of nearly pure CO ₂	Erosion of the reformer tubes Selection of oxygen carrier Carbon deposition	Research and development phase	NA	~2.52	[40,50]

^{xx} All the reported values either belong or are inflation adjusted to the 2019 USD.

^{xxi} Costs vary based on differences in has prices, capital and operating expenditures, and geographical locations.

^{xxii} Costs vary based on differences in has prices, capital and operating expenditures, and geographical locations. The upper limit reported in 2007 USD is \$2.55

^{xxiii} The hydrogen production cost of <\$3.54 is achievable with an integrated Pd-alloy membrane reformer system when the rate of hydrogen production is at least 1,500 kg/day. The original USD value reported in the reference is \$3.10 which is in 2011 USD.

^{xxiv} The inherent efficiency of the electrolyzer systems are significantly high; however, when coupled with PV cells the overall efficiency decreases considerably.

^{xxv} Energy yield varies depending on the electrolysis method, source of electricity, and efficiency of the electrolyzer systems used.

^{xxvi} Costs vary based on the electrolysis process, hydrogen production rate, capacity factor, and electricity source. The original USD values reported in the references are \$2.27-23.27 which are in 2007 USD.

^{xxvii} Energy yield varies significantly depending on the plasma technology employed. Dielectric barrier discharge is less energy efficient (as low as 0.5 gH₂/kWh) while plasmatron with catalyst is more energy efficient (as high as 225 gH₂/kWh)

Technoeconomic Analysis

A comparison between the production cost of hydrogen using different technologies is represented in Figure 6-2. As it can be seen in this figure, natural gas without CCUS is the least expensive method of producing hydrogen while water electrolysis with the grid electricity is the most expensive method for producing the same amount of hydrogen. Furthermore, this plot shows that, except for coal, the greatest cost component is the fuel cost therefore, the future prices of hydrogen will be a strong function of fuel prices. It is also worth mentioning that the hydrogen production cost with electrolysis is not sensitive to the CO₂ price while coal without CCUS has the greatest sensitivity to CO₂ prices.

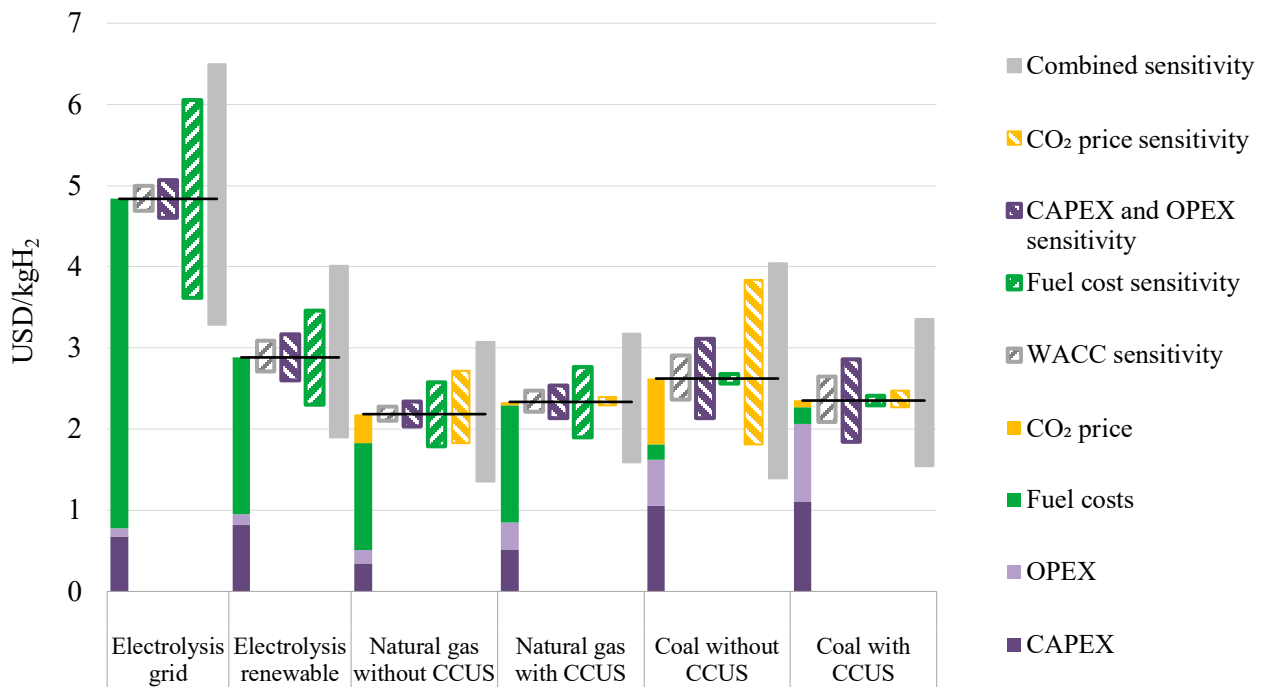


Figure 6-2. Hydrogen production cost and price sensitivity of various technologies (adapted from the 2019 IEA report: The Future of Hydrogen: Seizing today's opportunities)[44]

However, it should be noted that when discussing water electrolysis technologies, it is crucial to include the source of electricity when calculating CO₂ emissions. If the electricity for water electrolysis is provided by renewable energies or is coming from nuclear power, then one can assume CO₂ intensity of the process as negligible. Otherwise, depending on

Technoeconomic Analysis

the source of electricity (natural gas or coal) the water electrolysis could emit significant amounts of CO₂. As it is shown in Figure 6-3, approximately 40 kg of CO₂ is emitted for every kg of hydrogen produced via water electrolysis when the electricity is generated in a coal-fired power plant. As a comparison, the CO₂ emission from a natural gas steam reforming plant without CCUS is approximately 9 kgCO₂/kgH₂. This means that for water electrolysis process to have the same amount of emission as a natural gas reforming without CCUS, the CO₂ intensity of the produced electricity should be less than 185 (gCO₂/kWh). These differences arise from the fact that significant amount of energy is lost during the conversion of fossil fuels to electricity. Therefore, if the CO₂ intensity of the electricity is not reduced to the above-mentioned limits, it would be more environmentally attractive to just burn the natural gas in a reforming reaction to produce hydrogen rather than converting it to electricity and later produce hydrogen via electrolysis. Hence, it is very clear that electrolysis for hydrogen production makes sense from a greenhouse gas emissions reduction perspective only if the electricity is generated from non-fossil fuel sources.

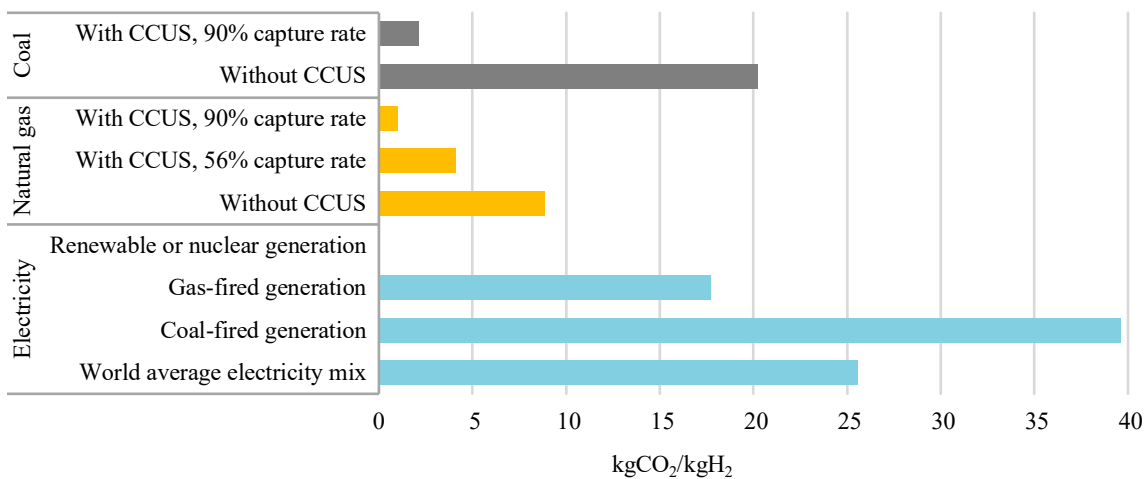


Figure 6-3. CO₂ emissions associated with various technologies for hydrogen production (adapted from the 2019 IEA report: The Future of Hydrogen: Seizing today's opportunities)[44]

References

- [1] Mizeraczyk J, Urashima K, Jasiński M, Dors M. Hydrogen production from gaseous fuels by plasmas—A review. *Int J Plasma Env Sci Technol* 2014;8:89–97.
- [2] Mohammadi A, Mehrpooya M. A comprehensive review on coupling different types of electrolyzer to renewable energy sources. *Energy* 2018;158:632–55. doi:10.1016/j.energy.2018.06.073.
- [3] Wang L, Pérez-Fortes M, Madi H, Diethelm S, herle J Van, Maréchal F. Optimal design of solid-oxide electrolyzer based power-to-methane systems: A comprehensive comparison between steam electrolysis and co-electrolysis. *Appl Energy* 2018;211:1060–79. doi:10.1016/j.apenergy.2017.11.050.
- [4] Bertuccioli L, Chan A, Hart D, Lehner F, Madden B, Standen E. Study on development of water electrolysis in the EU. *Fuel Cells Hydrog Jt Undert* 2014.
- [5] Castro-Dominguez B, Ma LC, Mardilovich IP, Kazantzis NK, Ma YH. Integrated Experimental-Technoeconomic Analysis of the Lifetime of Pd-Au Membranes. *Ind Eng Chem Res* 2016;55:10160–71. doi:10.1021/acs.iecr.6b01898.
- [6] Wu LQ, Xu N, Shi J. Preparation of a palladium composite membrane by an improved electroless plating technique. *Ind Eng Chem Res* 2000;39:342–8. doi:10.1021/ie9904697.
- [7] Lin YM, Rei MH. Study on the hydrogen production from methanol steam reforming in supported palladium membrane reactor. *Catal. Today*, vol. 67, Elsevier; 2001, p. 77–84. doi:10.1016/S0920-5861(01)00267-X.
- [8] Pomerantz N, Ma YH. Effect of H₂S on the Performance and Long-Term Stability of Pd/Cu Membranes. *Ind Eng Chem Res* 2009;48:4030–9. doi:10.1021/ie801947a.
- [9] Guazzone F, Ma YH. Leak growth mechanism in composite Pd membranes prepared by the electroless deposition method. *AIChE J* 2008;54:487–94. doi:10.1002/aic.11397.
- [10] Ma L-C, Kazantzis NK, Ma YH. Natural gas in hydrogen production: a cost study. *Proc Inst Civ Eng - Energy* 2015;168:61–73. doi:10.1680/ener.14.00017.
- [11] Gazzani M, Manzolini G. Using palladium membranes for carbon capture in integrated gasification combined cycle (IGCC) power plants. *Palladium Membr. Technol.*

Hydrog. Prod. Carbon Capture Other Appl. Princ. Energy Prod. Other Appl., Elsevier; 2014, p. 221–46. doi:10.1533/9781782422419.2.221.

[12] Koc R, Kazantzis NK, Nuttall WJ, Ma YH. An economic evaluation framework for membrane reactor modules in the presence of uncertainty: The case for process safety investment and risk reduction. *J Loss Prev Process Ind* 2013;26:468–77. doi:10.1016/j.jlp.2012.07.012.

[13] Ma LC, Castro-Dominguez B, Kazantzis NK, Ma YH. Integration of membrane technology into hydrogen production plants with CO₂ capture: An economic performance assessment study. *Int J Greenh Gas Control* 2015;42:424–38. doi:10.1016/j.ijggc.2015.08.019.

[14] Koc R, Kazantzis NK, Ma YH. Membrane technology embedded into IGCC plants with CO₂ capture: An economic performance evaluation under uncertainty. *Int J Greenh Gas Control* 2014;26:22–38. doi:10.1016/J.IJGGC.2014.04.004.

[15] Ma LC, Castro-Dominguez B, Kazantzis NK, Ma YH. A cost assessment study for a large-scale water gas shift catalytic membrane reactor module in the presence of uncertainty. *Sep Purif Technol* 2016;166:205–12. doi:10.1016/j.seppur.2016.04.019.

[16] Mardilovich IP, Castro-Dominguez B, Kazantzis NK, Wu T, Ma YH. A comprehensive performance assessment study of pilot-scale Pd and Pd/alloy membranes under extended coal-derived syngas atmosphere testing. *Int J Hydrogen Energy* 2015;40:6107–17. doi:10.1016/j.ijhydene.2015.03.001.

[17] Collodi G, Azzaro G, Ferrari N, Santos S. Techno-economic Evaluation of Deploying CCS in SMR Based Merchant H₂ Production with NG as Feedstock and Fuel. *Energy Procedia*, vol. 114, Elsevier; 2017, p. 2690–712. doi:10.1016/j.egypro.2017.03.1533.

[18] MURADOV N, VEZIROLU T. From hydrocarbon to hydrogen-carbon to hydrogen economy. *Int J Hydrogen Energy* 2005;30:225–37. doi:10.1016/j.ijhydene.2004.03.033.

- [19] Hosseini SE, Wahid MA. Hydrogen production from renewable and sustainable energy resources: Promising green energy carrier for clean development. *Renew Sustain Energy Rev* 2016;57:850–66. doi:10.1016/j.rser.2015.12.112.
- [20] Zeng K, Zhang D. Recent progress in alkaline water electrolysis for hydrogen production and applications. *Prog Energy Combust Sci* 2010;36:307–26. doi:10.1016/j.pecs.2009.11.002.
- [21] Stojić DL, Marčeta MP, Sovilj SP, Miljanić ŠS. Hydrogen generation from water electrolysis—possibilities of energy saving. *J Power Sources* 2003;118:315–9. doi:10.1016/S0378-7753(03)00077-6.
- [22] Körner A, Tam C, Bennett S, Gagné JF. Technology roadmap-hydrogen and fuel cells. Int Energy Agency Paris, Fr 2015.
- [23] Sharma S, Ghoshal SK. Hydrogen the future transportation fuel: From production to applications. *Renew Sustain Energy Rev* 2015;43:1151–8. doi:10.1016/j.rser.2014.11.093.
- [24] Shaner MR, Atwater HA, Lewis NS, McFarland EW. A comparative technoeconomic analysis of renewable hydrogen production using solar energy. *Energy Environ Sci* 2016;9:2354–71. doi:10.1039/C5EE02573G.
- [25] Dillich S, Ramsden T, Melaina M. DOE Hydrogen and Fuel Cells Program Record Title: Hydrogen Production Cost Using Low-Cost Natural Gas. 2012.
- [26] Press RJ, Santhanam KS V, Miri MJ, Bailey A V, Takacs GA. Introduction to hydrogen technology. John Wiley & Sons, Incorporated; 2017.
- [27] Holladay JD, Hu J, King DL, Wang Y. An overview of hydrogen production technologies. *Catal Today* 2009;139:244–60. doi:10.1016/j.cattod.2008.08.039.
- [28] Bromberg L, Cohn DR, Rabinovich A, Alexeev N, Samokhin A, Ramprasad R, et al. System optimization and cost analysis of plasma catalytic reforming of natural gas. *Int J Hydrogen Energy* 2000;25:1157–61. doi:10.1016/S0360-3199(00)00048-3.
- [29] Biniwale RB, Mizuno A, Ichikawa M. Hydrogen production by reforming of iso-octane using spray-pulsed injection and effect of non-thermal plasma. *Appl Catal A Gen* 2004;276:169–77. doi:10.1016/J.APCATA.2004.08.003.
- [30] Bromberg L, Cohn D., Rabinovich A, Alexeev N. Plasma catalytic reforming of methane. *Int J Hydrogen Energy* 1999;24:1131–7. doi:10.1016/S0360-3199(98)00178-5.

- [31] Luo M, Yi Y, Wang S, Wang Z, Du M, Pan J, et al. Review of hydrogen production using chemical-looping technology. *Renew Sustain Energy Rev* 2018;81:3186–214. doi:10.1016/j.rser.2017.07.007.
- [32] Cuttillo A, Specchia S, Antonini M, Saracco G, Specchia V. Diesel fuel processor for PEM fuel cells: Two possible alternatives (ATR versus SR). *J Power Sources* 2006;154:379–85. doi:10.1016/j.jpowsour.2005.10.065.
- [33] Lorenzuti B, Montini T, De Rogatis L, Canton P, Benedetti A, Fornasiero P. Hydrogen production through alcohol steam reforming on Cu/ZnO-based catalysts. *Appl Catal B Environ* 2011;101:397–408. doi:10.1016/j.apcatb.2010.10.009.
- [34] Gallucci F, Basile A, Tosti S, Iulianelli A, Drioli E. Methanol and ethanol steam reforming in membrane reactors: An experimental study. *Int J Hydrogen Energy* 2007;32:1201–10. doi:10.1016/j.ijhydene.2006.11.019.
- [35] Anzelmo B, Wilcox J, Liguori S. Natural gas steam reforming reaction at low temperature and pressure conditions for hydrogen production via Pd/PSS membrane reactor. *J Memb Sci* 2017;522:343–50. doi:10.1016/j.memsci.2016.09.029.
- [36] Hedayati A, Le Corre O, Lacarrière B, Llorca J. Experimental and exergy evaluation of ethanol catalytic steam reforming in a membrane reactor. *Catal. Today*, vol. 268, Elsevier; 2016, p. 68–78. doi:10.1016/j.cattod.2016.01.058.
- [37] Hedayati A, Le Corre O, Lacarrière B, Llorca J. Exergetic study of catalytic steam reforming of bio-ethanol over Pd-Rh/CeO₂ with hydrogen purification in a membrane reactor. *Int J Hydrogen Energy* 2015;40:3574–81. doi:10.1016/j.ijhydene.2014.09.016.
- [38] Ryu HJ, Jin GT, Yi CK. Demonstration of inherent CO₂ separation and no NO_x emission in a 50kW chemical-looping combustor: Continuous reduction and oxidation experiment. *Greenh. Gas Control Technol.*, Elsevier Ltd; 2005, p. 1907–10. doi:10.1016/B978-008044704-9/50238-X.
- [39] Ishida M, Jin H. A novel chemical-looping combustor without NO_x formation. *Ind Eng Chem Res* 1996;35:2469–72. doi:10.1021/ie950680s.
- [40] Spallina V, Pandolfo D, Battistella A, Romano MC, Van Sint Annaland M, Gallucci F. Techno-economic assessment of membrane assisted fluidized bed reactors for pure H₂ production with CO₂ capture. *Energy Convers Manag* 2016;120:257–73. doi:10.1016/j.enconman.2016.04.073.

- [41] Iulianelli A, Liguori S, Wilcox J, Basile A. Advances on methane steam reforming to produce hydrogen through membrane reactors technology: A review. *Catal Rev - Sci Eng* 2016;58:1–35. doi:10.1080/01614940.2015.1099882.
- [42] Grashoff GJ, Pilkington CE, Corti CW. The purification of hydrogen. *Platin Met Rev* 1983;27:157–69.
- [43] Dincer I, Acar C. Innovation in hydrogen production. vol. 42. Elsevier Ltd; 2017. doi:10.1016/j.ijhydene.2017.04.107.
- [44] International Energy Agency (IEA). The Future of Hydrogen. OECD; 2019. doi:10.1787/1e0514c4-en.
- [45] Bartels JR, Pate MB, Olson NK. An economic survey of hydrogen production from conventional and alternative energy sources. *Int J Hydrogen Energy* 2010;35:8371–84. doi:10.1016/j.ijhydene.2010.04.035.
- [46] Hopkins S. High-performance palladium based membrane for hydrogen separation and purification. Pall Corporation; 2012.
- [47] Dougherty W, Kartha S, Rajan C, Lazarus M, Bailie A, Runkle B, et al. Greenhouse gas reduction benefits and costs of a large-scale transition to hydrogen in the USA. *Energy Policy* 2009;37:56–67. doi:10.1016/J.ENPOL.2008.06.039.
- [48] Nikolaidis P, Poullikkas A. A comparative overview of hydrogen production processes. *Renew Sustain Energy Rev* 2017;67:597–611. doi:10.1016/j.rser.2016.09.044.
- [49] Dincer I. Green methods for hydrogen production. *Int. J. Hydrogen Energy*, vol. 37, Elsevier Ltd; 2012, p. 1954–71. doi:10.1016/j.ijhydene.2011.03.173.
- [50] Medrano JA, Spallina V, Van Sint Annaland M, Gallucci F. Thermodynamic analysis of a membrane-assisted chemical looping reforming reactor concept for combined H₂ production and CO₂ capture. *Int. J. Hydrogen Energy*, vol. 39, 2014, p. 4725–38. doi:10.1016/j.ijhydene.2013.11.126.

Chapter 7 - Conclusions and Recommendations

Composite membrane reactors, i.e., Pd/YSZ and Pd-Au/Al₂O₃, were fabricated by the electroless plating technique. The permeation experiments for pure gases such as H₂, He, and Ar and mixtures of H₂ with other reaction gases were performed. At 400 °C and at a trans-membrane pressure of 50 kPa, the ideal selectivity of H₂/Ar was found to be 6000 for the Pd membrane, while the Pd-Au membrane showed near-infinite selectivity towards H₂ permeation. This is an indication that the transport mechanism in the Pd-Au membrane is governed by solution diffusion, while in the Pd membrane, the transport mechanism can be affected by the Pd surface or bulk defects.

Permeation studies with pure H₂ and pure Ar show that both the H₂ permeating flux and the ideal selectivity of H₂/Ar ($\alpha_{H_2/Ar}$) increase as the operating temperature increases. Permeation tests of binary mixtures of H₂-Ar, H₂-He, and H₂-N₂, performed on both Pd/YSZ and Pd-Au/Al₂O₃, indicate a significant decrease in the permeation flux of H₂ in these binary mixtures compared with the pure H₂ case, which can be explained by the concentration polarization effect.

Permeation tests of binary mixtures of H₂-CH₄, H₂-CO₂, and H₂-CO, and H₂-H₂O were performed on both Pd/YSZ and Pd-Au/Al₂O₃. These studies show that steam has the worst effect on the H₂ permeating flux, followed by CO, CO₂, and CH₄. While CH₄ has negligible surface adsorption on the Pd layer, CO and CO₂ show strong affinity toward Pd. The existence of steam molecules in the feed mixture could result in the adsorption of oxygen atoms through H₂O decomposition/recombination, which can poison the active surface of Pd.

Permeation tests of the simulated SMR stream prove that the H₂ permeation flux is reduced even more compared with the ternary mixtures. In a simulated SMR stream, the negative effects of concentration polarization, dilution, and depletion of H₂, combined with the negative effects of competitive adsorption and the decomposition/recombination effect of steam will reduce the permeating flux of H₂ even more compared with the ternary mixture.

Conclusions and Recommendations

The concentration polarization effect is more pronounced at lower trans-membrane pressures and lower GHSVs. By increasing the trans-membrane pressure or GHSV, the negative effect of concentration polarization will be abated.

Concentration polarization, dilution, depletion, and competitive adsorption on the Pd surface are the major phenomena that are detrimental to H₂ generation and purification. Hence, it is crucial to know the mechanism by which these phenomena affect the SMR performance and how their effects can be mitigated. The negative effects by which the permeating flux of H₂ can be affected was investigated in this work, and the gases associated with each of these effects were identified. This work is one of the few that systematically addresses all four negative effects in an experimental setting and at operating conditions that satisfy the DOE target requirements. The next step that is complementary to this work would be performing the H₂ permeation tests in a MR while carrying out the SMR with industrial-grade CH₄ with impurities such as CO, CO₂, and H₂S.

In the SMR experiments, the permeation tests with pure hydrogen and inert gases namely helium and argon were also performed at 400 °C. The permeation studies show that the Pd-based membrane reactor is infinitely selective toward hydrogen and the permeation of small molecules such as helium through the Pd layer is negligible. The SMR reactions at 400°C and various operating pressures have been conducted and the performance of the SMR reaction in terms of methane conversion, hydrogen recovery, and permeate side hydrogen purity have been studied. It is found that hydrogen produced on the permeate side has ultra-high purity which is suitable for direct use in HFCVs. The methane conversion is constantly increasing with increasing operating pressure and reached to 42.2% at 400 kPa. Hydrogen recovery at lower operating pressures is almost negligible while this value increased to 43% at 400 kPa.

The carbon capture experiments were performed at the optimal operating conditions, 400°C and 400 kPa. The amount of CO₂ captured is found to be 262.25 mg CO₂ per gram of 13X. Breakthrough studies reveal that after approximately 30 minutes, more than 80% of the bed volume is saturated with CO₂. The equilibrium time is found to be approximately

Conclusions and Recommendations

44 minutes after which the 13X needs to be regenerated and the retentate stream should be redirected to a fresh packed bed.

The SEM images confirm the existence of pinholes and defects in the structure of the Pd/YSZ membrane, which could have resulted from poor fabrication or bursts of gas near the Pd surface. XRD images show a slight shift in the position of Pd peaks, which can be explained by formation of PdO after the permeation tests.

For the membrane that was used for SMR and carbon capture experiments however, the surface has gone through some oxidation which has led to discoloration of the membrane surface. Although this oxidation phenomenon is evident on the membrane and was detected in the EDS studies, the XRD results do not show any evidence of palladium oxide which could be inferred that this oxidation is only a surface phenomenon and does not extend into the bulk of the membrane. In order to better understand the oxidation state of the palladium it is recommended to perform XPS experiments.

Advantages of hydrogen energy in terms of production, conversion, transportation, storage, along with its environmental benignity will make it a very promising solution to address both ever-increasing global energy needs and adverse climate change effects. However, it should be noted that replacing one energy source with another requires technology and infrastructure development. Transition from one dominant fuel to another has taken 50 to 60 years historically. The world energy markets are currently observing the transition from oil to natural gas and this transition has occurred at the beginning years of the 21st century with the advancement of technology in horizontal drilling and hydraulic fracturing which made it possible to recover the previously inaccessible resources called “shale gas”. Therefore, despite the significant growth of the renewable energy in the global energy portfolio, it is expected that natural gas will remain a significant component of the energy market in the foreseeable future.

Fossil fuels have been the number one source for world hydrogen production (*ca.* 95%) with the current industrial process of SMR combined with PSA leading the hydrogen

Conclusions and Recommendations

production market. The price of natural gas plays an important role in the future of hydrogen production by SMR. The cost of hydrogen is largely dependent on the cost of natural gas, the required purity, and the logistics between production and point of use. Increasing prices of natural gas in the coming decades could potentially make coal gasification with CCUS a better economic alternative unless environmental regulations and policies prevent using coal or make its utilization very costly.

Currently, the main industrial uses of hydrogen are ammonia synthesis and petroleum refining. However, it is expected that novel economies such as HFCVs will be rapidly expanding as hydrogen technology develops in the coming decades. While not able to meet the high production rates associated with the world's hydrogen demand, metallic membranes have potential in applications requiring high-purity hydrogen of 99.99+% and small niche applications, where membrane costs are less of a concern than performance, such as in fuel cells and semiconductor manufacturing.

In a future carbon-constrained world, “clean” hydrogen production should take place with the implementation of CO₂ capture units. In such a scenario, using metallic membranes for hydrogen production and purification may become economically feasible, provided that a carbon tax or other incentives are levied. Compact metallic MRs could be suitable for distributed and/or mobile hydrogen production and enable CO₂ capture from these sources. Power generation from IGCC using metallic membranes for pre-combustion carbon capture may be competitive with other separation technologies (e.g., polymer membranes and physical absorption) but the large-scale use of metallic membranes will remain a theoretical concept until it is proven by sufficient experimental studies under actual industrial conditions.

Although Pd is a limited resource where the majority (*ca.* 75%) of mined supply comes from two countries, Russia and South Africa, Pd-based membrane materials play a major role in metallic membrane research. The demand for Pd has increased in the past several years, mostly from the automobile industry, while the market of mined supply has declined. Therefore, it is reasonable to minimize the use of Pd in metallic membranes. In fact, since

Conclusions and Recommendations

pure-Pd membranes have limited use due to sulfur intolerance, thermal instability, and high cost, it has been of interest in the research community to improve such membrane material properties. Alloying of Pd membranes with other metals has provided enhanced sulfur resistance and thermal stability. Membranes based on non-precious metals also have proven enhanced thermal stability while decreasing the material cost. Computational approaches for material screening could provide an efficient way to enhance new membrane developments. The ongoing research to improve metallic membrane materials or develop new materials is fairly new and has yet to be fully explored.

Moving to a hydrogen economy may be achieved through various paths such as SMR, coal gasification, geothermal, nuclear, renewable energy resources (e.g., wind and solar), etc. Each of these paths have their own benefits and drawbacks. There are numerous factors that must be investigated thoroughly before choosing the best path toward hydrogen economy. Renewability, cost, efficiency, GHG emissions, multigeneration, size reduction (land footprint), reliability and durability, purity of the produced hydrogen are some key factors that the decision makers need to consider in their selection criteria. In addition, challenges for hydrogen delivery such as high delivery cost, low efficiency, purity, leakage and safety issues need to be addressed. Finally, in hydrogen production with CCUS units, the costs associated with CO₂ sequestration, monitoring, and safe handling need to be studied with great precision as they might change the fate of the project.

Although SMR is the dominant industrial process for hydrogen production, environmental concerns associated with CO₂ emissions along with the process intensification and energy optimization are the areas that still can be improved significantly. Metallic MRs have the potential to address both challenges. MRs inherently operate at significantly lower operating pressures and temperatures while achieving similar performance to that of conventional reactors which require higher operating pressures and temperatures. Hence, the capital and operating expenses could be considerably lower compared with the conventional reactors.

Conclusions and Recommendations

The benchmark for economic production of hydrogen by the year 2020 has been determined and set in place by the U.S. DOE. The key factors set by the DOE are the energy yield of 60 gH₂/kWh which is equivalent to less than \$2.00 per kg of produced hydrogen in 2020. While established industrial processes such as SMR can easily meet the set limit by the DOE, it seems that the other processes such as water electrolysis, electron beam radiolysis, and gliding arc technologies do not meet this requirement presently. Among these methods water electrolysis has attracted significant attention due to the low CO₂ emissions associated with the electrolysis process. However, it should be noted that electricity is one of the most important components of water electrolysis process and depending on the sources of electricity, hydrogen cost could vary significantly. Therefore, only reporting the CO₂ emissions associated with the water electrolysis process itself and not mentioning the emissions associated with the electricity used in the process could be misleading. In order to realize the true emissions associated with the water electrolysis a careful life-cycle-assessment, from cradle to grave, is necessary. Furthermore, it is still a matter of disagreement if it is the best way to use water in remote areas where access to water is challenging and costly.

Among the methods that use plasma technology for hydrogen production, plasmatron method could be very efficient in terms of performance, energy yield, and production rate. However, all these methods suffer from the extremely high capital and operating expenditures.

Finally, considering the currently low gas prices, and the lenient regulations on GHG emissions, it seems that SMR process will stay the dominant process for hydrogen production in the industry. However, it needs to be emphasized that in the wake of our changing climate and the subsequent existential threats to human civilization, governments and their policy makers will need to respond more proactively by adopting policies that advocate for more sustainable, low-carbon solutions to meeting our global energy needs, which will bridge us toward a future that is less dependent on fossil fuels. Nevertheless, due to their modular characteristics, MRs show great potential to be used for smaller-scale

Conclusions and Recommendations

hydrogen production while optimizing the energy consumption associated with the process.